# Determination of cell shape in *Staphylococcus aureus*

Andreia Filipa Campos Tavares

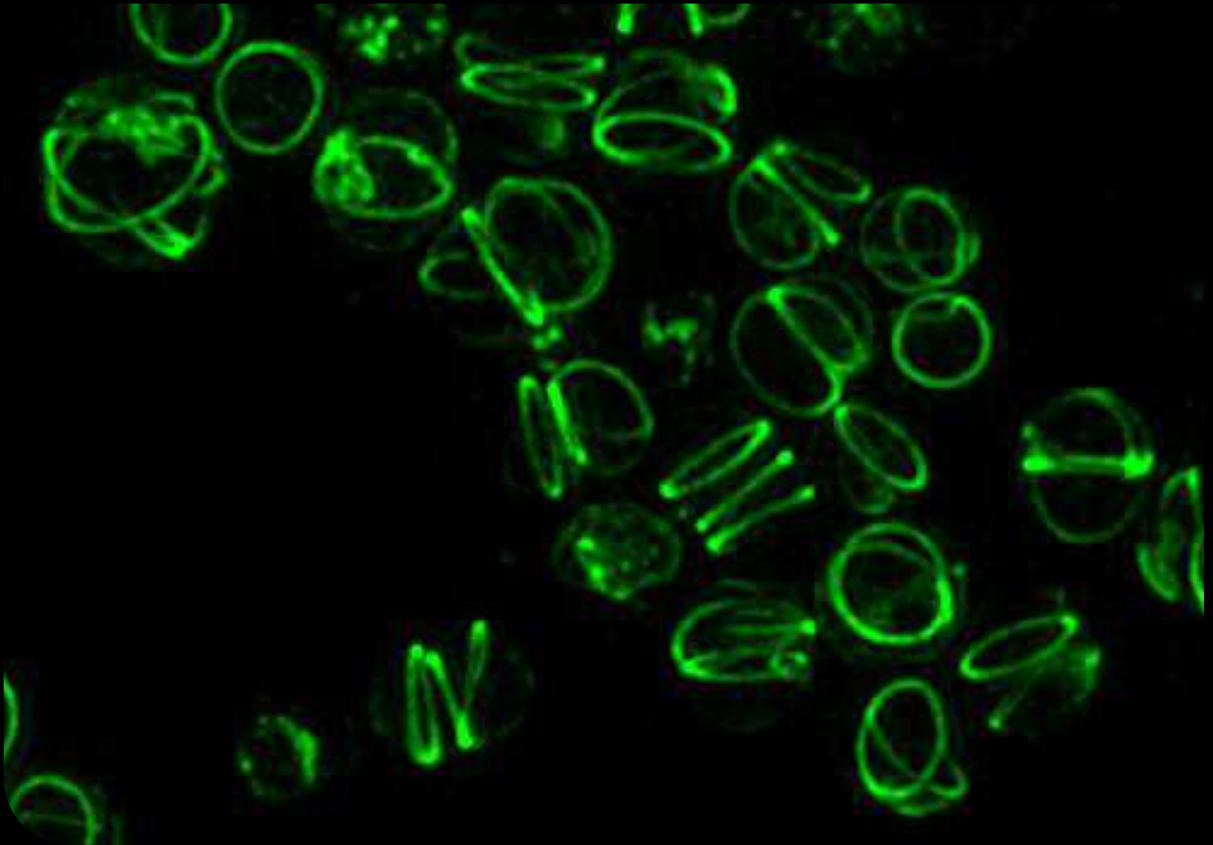Oeiras,
May, 2019

iTQB

UNIVERSIDADE
NOVA
DE LISBOA

# Determination of cell shape in *Staphylococcus aureus*

Andreia Filipa Campos Tavares

## Dissertation presented to obtain the Ph.D degree in Biology

Instituto de Tecnologia Química e Biológica António Xavier | Universidade Nova de Lisboa

Oeiras, May, 2019

## ACKNOWLEDGMENTS

All the work presented here would not be possible without the support of many people.

I would like to start by thanking to Professor Mariana Pinho, my thesis supervisor and a brilliant scientist that I had the pleasure to learn from. Thank you for believing in me from the beginning, for never preventing me from trying "just one more thing" and for giving me the chance to participate is so many different and interesting stories. I also want to thank you for the opportunity you gave me to spend some time abroad and to meet so many brilliant people, from whom I learned a lot. Very importantly, you taught me that the experimental work has its ups and downs, that negative results are always results and that not publishing those results would not be good for science. And for me, this was the first of many examples you gave me that science is the most important thing and that no matter what results I have, they mean something. You told me that as long as I keep searching I will find something, because there is always an answer to find. And you were right.

I also want to thank to Professor Sérgio Filipe for all the great discussions that made me look to the results with different eyes. In every lab meeting you contributed with ideas and hypothesis that were rarely expected, and although some of those ideas didn't make sense to me at the time, they turned out to be right. This showed me how important it is to think outside the box, to question everything and to consider all the options, even the "craziest" ones.

I want to specially acknowledge Dr. Rut Carballido-López for receiving me in her lab in France and for being part of my thesis committee. You are one of the most inspiring people I know. Your

excitement about science is contagious and your ability to look at any result, even the negative ones, as an open door to new discoveries was truly important to me and gave me a lot of motivation, especially after two years without any positive result. You showed me that with each experiment, I was one step closer to the answer and that that answer exists, it might just be difficult to find. Thank you for all the support you gave me, for welcoming me in your lab the way you did and for totally trust me since day one.

I thank to Nathalie Reichmann, with whom I worked closely for approximately 2 years. You take the definition of "hard worker" to a whole new level and working with you was the most exhausting, demanding, rewarding and fulfilling experience I had during my PhD. Thank you for all you taught me, for all the discussions, for all the extra hours of work, for showing me that even when we think that the work is good, there is always something else that we can test. This work could not have been done without you, so thank you.

During these past years I had the privilege to meet and work with amazing people, from different nationalities and with different cultures, but mainly with a huge passion for science. No matter the differences, this group of people always gave 100% of themselves to help each other, working together to produce great results. A very special thanks to Ambre, a real friend and my bench neighbour for over 4 years. Thank you for sharing so many good and bad moments with me and for always being there, even if it is just for a good (or less good…) joke. Also, a special thanks to Gonçalo, with whom I worked closely and who can never say no to help a colleague, even if it implies putting his own work on hold. To Bruno, who facilitates everyone's lives by building new informatics tools for everything we ask for and who is always ready to help, even outside his comfort zone. To Pedrinho, the leader of our

4

Democratic Republic, who helped me on one of my most stressful scientific moments, and worked hours and hours at night so that we could finish everything on time. Thank you for that and for present us every lunch with some of the worst jokes I have ever heard (sorry). To Raquel, my roommate in scientific meetings, who is always available for discussing results or ideas and with whom I shared many funny and less funny moments. To Helena, who once told me to always compare myself to the best and who taught me so many important lessons. To Marta for her help in the lab and for introducing me to Poland. To Ana Jorge, my "supervisor" when I did my first internship in the lab while I was still in the university, for introducing me to the laboratory work and for teaching me how to properly work at the bench. I also want to thank to Trish, Mário, Moritz, Andreia D., Simon, Lúcia, João, Rita, Joana and Denise, for all the scientific and non-scientific input. Thank you so much Teresa Baptista for facilitating our lives in the laboratory, you are definitely an essential part of our lab.

To everyone at the ProCeD laboratory in France, thank you for welcoming me so well and for treating me like family. A special thanks to Céline for guiding me in the lab and to introduce me to *B. subtilis*. It was a pleasure to meet everyone and to be part of such a cohesive and supportive group. Every time I use that raclette machine I think about you all! Besides the team, I also have to acknowledge other people from INRA, including Ludovica, Transi, Edgar and Setha, who explored Paris with me and contributed so much for my great time in there.

I want to thank ITQB-NOVA for the opportunity of developing my work in an institute with such great conditions and with an amazing environment. I know ITQB for many years and I am really proud of being part of its community. I also thank MolBioS PhD program for selecting

.

# TABLE OF CONTENTS

**CHAPTER V**

# ABBREVIATIONS AND ACRONYMS

| | |
|---|---|
| Amp | Ampicillin |
| ATP | Adenosine triphosphate |
| BCA | Bicinchoninic acid assay |
| bp | DNA base pairs |
| CFU | Colony forming unit |
| Cam | Chloramphenicol |
| D-Ala-D-Ala | D-alanyl-D-alanine |
| DIC | Differential interference contrast |
| DMPI | 3-{1-[(2,3-Dimethylphenyl)methyl]piperidin-4-yl}-1-methyl-2-pyridin-4-yl-1H-indole |
| DMSO | Dimethyl sulfoxide |
| ECDC | European centre for disease control |
| Ery | Erythromycin |
| FDAA | Fluorescent D-amino acid |
| FR | Fluorescence ratio |
| GFP | Green fluorescent protein |
| GlcNAc | N-acetylglucosamine |
| HADA | Hydroxycoumarin-amino-D-alanine |
| HPLC | High-performance liquid chromatography |
| IPTG | Isopropyl β-D-1-thiogalactopyranoside |
| Kan | Kanamycin |
| LA | Luria-Bertani agar |
| LB | Luria-Bertani broth |
| MATE | Multidrug and toxic extrusion protein |
| mCh | mCherry fluorescent protein |
| MIC | Minimum inhibitory concentration |
| MOP | Multidrug/oligosaccharidyl-lipid/polysaccharide protein |
| MRSA | Methicillin-resistant *Staphylococcus aureus* |
| MSSA | Methicillin-susceptible *Staphylococcus aureus* |
| MurNAc | N-acetylmuramic acid |

| | |
|---|---|
| NADA | Nitrobenzofurazan-amino-D-alanine |
| NBD | 7-nitro-2,1,3-benzoxadiazol-4-yl |
| OD | Optical density |
| P1 | Phase 1 of the *S. aureus* cell cycle |
| P2 | Phase 2 of the *S. aureus* cell cycle |
| P3 | Phase 3 of the *S. aureus* cell cycle |
| PBP | Penicillin-binding protein |
| PBS | Phosphate buffer saline |
| PCC | Pearson's correlation coefficient |
| PGN | Peptidoglycan |
| RBS | Ribosome binding site |
| SDS-PAGE | Sodium dodecyl sulfate polyacrylamide gel electrophoresis |
| SEDS | Shape, elongation, division and sporulation protein |
| SEM | Scanning electron microscopy |
| STK | Serine/threonine kinase |
| STP | Serine/threonine phosphatase |
| sGFP | Superfast-folding GFP |
| SIM | Structured illumination microscopy |
| TDL | TAMRA-D-lysine |
| TEM | Transmission electron microscopy |
| TG | Transglycosylation |
| TGase | Transglycosylase |
| TP | Transpeptidation |
| TPase | Transpeptidase |
| TSA | Tryptic soy agar |
| TSB | Tryptic soy broth |
| Tun | Tunicamycin |
| UDP | Uridine diphosphate |
| Van | Vancomycin |
| WTA | Wall teichoic acid |
| X-Gal | 5-bromo-4-chloro-3-indolyl-β-D-galactopyranoside |
| YFP | Yellow fluorescent protein |

## ABSTRACT

Cell size and morphology are two extremely important characteristics in the adaptation of bacteria to the external environment and are often associated to bacterial survival and growth. In *Staphylococcus aureus*, a common colonizer of human skin and mucus membranes, the small spherical shape of cells may be an advantage during colonization, helping this pathogen to evade host immune system. The fact that cell shape is maintained over consecutive generations evidences the existence of tightly regulated underlying mechanisms. Bacterial shape is maintained by the existence of an external cell wall mainly composed of peptidoglycan (PGN), a mesh-like molecule made by glycan chains cross-linked by short peptide bridges. Localization of PGN synthesis is dependent on the action of cytoskeletal proteins, which direct the activity of proteins involved in this synthesis, including Penicillin-Binding Proteins (PBPs) and proteins from the shape, elongation, division and sporulation (SEDS) family, to specific regions of the cells. The connection between cytoskeletal proteins and PGN synthases is thought to occur through interaction with intermediate morphogenetic elements that can act as scaffolds or stabilizers of the protein complexes. Association of all these proteins form large PGN synthesis complexes involved in the incorporation of PGN at the division site (divisome) or at the peripheral cell wall (elongasome). The coordinated activity of these complexes is the main determinant of bacterial cell morphology.

The mechanisms driving elongation and the identity of proteins of the elongasome complexes have been studied for many years in rod-shaped and ovococcoid bacteria. However, only very recently the ability of coccoid *S. aureus* cells to elongate was identified. *S. aureus* only possesses 4 native PBPs, a reduced number when compared to the 16

13

PBPs of *Bacillus subtilis*, the best well-studied gram-positive model organism, and can be considered a minimalist model, ideal for studies on bacterial cell division.

In this work, we aimed to identify which proteins are involved in *S. aureus* elongation and what is the mechanism behind it. For that, we studied several proteins known to be involved in the elongation process of rods and ovococci, including morphogenetic elements MreC and MreD and proteins belonging to PBPs and SEDS families. In *B. subtilis* and *Escherichia coli,* MreC and MreD are essential proteins believed to couple the internal cytoskeleton with the PGN synthesizing machinery. In *S. aureus*, however *mreC* and *mreD* are not essential for cell viability since null mutants retain a normal cell growth. Absence of both proteins has no effect on PGN architecture or synthesis nor on cell size, although both MreC and MreD localize mainly to the division septum, where most of the PGN synthesis occurs.

The last steps of PGN synthesis involve transglycosylation and transpeptidation reactions, responsible for PGN polymerization and cross-linking, respectively. Both reactions can be catalyzed by class A PBPs. Additionally, proteins from the SEDS family have been shown to possess transglycosylase (TGase) activity and to interact with class B PBPs (bPBPs), which have transpeptidase (TPase) activity, forming functional TGase-TPase pairs involved in septal and peripheral PGN synthesis. *S. aureus* has two bPBPs, PBP1 and PBP3, and two SEDS proteins, FtsW and RodA. In this work we show that RodA-PBP3 and FtsW-PBP1 form two cognate pairs of interacting proteins. RodA and PBP3 both localize to the division septum and the presence of PBP3 is required for the correct localization and TGase activity of RodA. Absence of both proteins does not affect cell viability or growth but leads to a decrease in side-wall PGN incorporation, resulting in rounder cells.

On the other hand, both FtsW and PBP1 are essential for *S. aureus* viability and their absence prevents the synthesis of septal PGN, arresting the normal cell cycle progression. Depletion of these proteins leads to delocalization of several members of the divisome, which forms multiple rings or arcs able to incorporate PGN in the lateral wall, resulting in cell elongation. For this reason, we propose a role for FtsW-PBP1 pair in the stabilization of the divisome at midcell. Identification of RodA-PBP3 and FtsW-PBP1 pairs is the first evidence for the existence of two PGN synthesis complexes in *S. aureus*, responsible for lateral and septal PGN incorporation, respectively.

Transglycosylation and transpeptidation reactions require the presence of lipid II, a lipid-linked PGN precursor composed by an *N*-acetylglucosamine-*N*-acetylmuramic acid-pentapeptide unit linked to the lipid carrier bactoprenol. Lipid II is synthesized in the inner leaflet of the cytoplasmic membrane and needs to be translocated across this membrane to be available on the outer leaflet of the membrane. FtsW and MurJ are two candidates proposed to be responsible for this flipping activity in *E. coli* cells. In *S. aureus*, MurJ is the main cue that directs PGN incorporation from the periphery to the division septum. Our results show that MurJ is an essential protein, whose absence leads to an accumulation of lipid II precursors at the cytoplasmic membrane and to a decrease of PGN incorporation due to a reduction of lipid II pool on the outer leaflet of the membrane. These results suggest that after MurJ depletion, lipid II accumulates on the inner surface of the cell membrane, probably due to impaired translocation, supporting a role for this protein in the process of lipid II flipping.

# RESUMO

O tamanho e morfologia são duas caraterísticas extremamente importantes na adaptação das bactérias ao meio ambiente. As células de *Staphylococcus aureus*, que coloniza frequentemente a pele e mucosas humanas, são pequenas e esféricas, trazendo-lhes vantagens durante o processo de colonização ao facilitar a evasão ao sistema imunitário do hospedeiro. O facto da morfologia celular se manter ao longo de várias gerações evidencia a existência de mecanismos de regulação para manutenção da forma bacteriana. A forma das bactérias é mantida através da existência de uma parede celular composta principalmente por peptidoglicano (PGN), que consiste numa estrutura complexa constituída por cadeias de glicanos ligadas por pequenas pontes de aminoácidos. A síntese de PGN está dependente de proteínas do citoesqueleto, que direcionam a atividade de proteínas envolvidas nesta síntese, incluindo proteínas de ligação à penicilina (Penicillin-Binding Proteins, PBPs) e proteínas envolvidas na morfologia, alongamento, divisão e esporulação (shape, elongation, division and sporulation, SEDS), para regiões específicas das células. Pensa-se que a interação entre as proteínas do citoesqueleto e as sintases do PGN ocorra através de elementos morfogenéticos que atuam como suportes ou estabilizadores dos complexos proteicos. A associação destas proteínas resulta na formação de complexos de síntese de PGN, envolvidos na incorporação de PGN no septo (divisoma) e na parede celular periférica (elongassoma). A atividade coordenada destes dois sistemas é o principal fator que determina a morfologia da bactéria.

Apesar de os mecanismos responsáveis pelos processos de alongamento de uma célula bacteriana e a identidade das proteínas que constituem o elongassoma serem bem estudados em bastonetes e

ovococos, apenas recentemente foi identificada a capacidade das células esféricas de *S. aureus* alongarem. *S. aureus* pode ser considerado um modelo minimalista para estudos de divisão celular uma vez que possui apenas 4 PBPs nativas, um número reduzido quando comparado com as 16 PBPs de *Bacillus subtilis,* o organismo modelo de bactérias gram-positivas mais estudado.

Neste estudo, tivemos como objetivo identificar quais as proteínas envolvidas no alongamento de *S. aureus* e perceber qual o mecanismo responsável por esse processo. Para tal, estudámos várias proteínas associadas ao processo de alongamento em bastonetes e ovococos, nomeadamente os elementos morfogenéticos MreC e MreD e proteínas pertencentes às famílias de PBPs e SEDS. Em *B. subtilis* e *Escherichia coli*, MreC e MreD são proteínas essenciais que se pensa fazerem a ligação entre o citoesqueleto interno e a maquinaria de síntese de PGN. No entanto, em *S. aureus*, *mreC* e *mreD* não são essenciais à viabilidade da célula, visto mutantes nulos de ambos os genes manterem um crescimento celular normal. A ausência de ambas as proteínas também não afeta a estrutura ou síntese do PGN nem o tamanho da célula, apesar de MreC e MreD se localizarem principalmente no septo, onde ocorre a maioria da síntese de PGN.

Os últimos passos da síntese de PGN resultam na sua polimerização através de reações de transglicosilação e de transpeptidação. Ambas as reações podem ser catalisadas por PBPs de classe A. Adicionalmente, proteínas da família SEDS foram identificadas como tendo atividade de transglicosilase (TGase) e como sendo capazes de interagir com PBPs de classe B (bPBPs), que têm atividade de transpeptidase (TPase), formando pares funcionais TGase-TPase envolvidos na síntese septal e periférica de PGN. *S. aureus* tem duas bPBPs, PBP1 e PBP3, e duas proteínas SEDS, FtsW

e RodA. Neste estudo mostramos que RodA-PBP3 e FtsW-PBP1 interagem entre si formando pares funcionais. RodA e PBP3 localizam-se no septo e a presença da PBP3 é necessária para a correta localização e atividade TGase de RodA. A ausência de ambas as proteínas não afeta a viabilidade ou crescimento celular, mas leva a um decréscimo da incorporação de PGN na parede lateral, resultando em células mais esféricas. Por outro lado, tanto FtsW como PBP1 são essenciais à viabilidade de *S. aureus* e a sua ausência inibe a síntese de PGN no septo, levando a uma paragem do ciclo celular. Esta ausência provoca também uma deslocalização de vários elementos do divisoma, formando múltiplos anéis ou arcos capazes de incorporar PGN na parede lateral, resultando em células mais alongadas. Com base nestes resultados propomos que o par FtsW-PBP1 tem uma função de estabilização do divisoma na região central da célula. A identificação dos pares RodA-PBP3 e FtsW-PBP1 constitui a primeira evidência da existência de dois complexos de síntese de PGN em *S. aureus*, responsáveis pela incorporação lateral e septal de PGN, respetivamente.

As reações de transglicosilação e transpeptidação requerem a presença de lípido II, um precursor lipídico do PGN composto por uma unidade de *N*-acetilglucosamina-ácido *N*-acetilmuramico-pentapeptido ligada a bactoprenol. O lípido II é sintetizado na face interna da membrana citoplasmática, sendo depois translocado para a face externa desta membrana, de forma a ficar disponível para posterior incorporação nas cadeias de PGN. Dois candidatos propostos para desempenhar esta função de translocação em *E. coli* são FtsW e MurJ. Em *S. aureus*, MurJ é o principal elemento a direcionar a síntese de PGN da periferia para o septo. Os nossos resultados mostram que o MurJ é uma proteína essencial em *S. aureus*, cuja ausência causa uma acumulação de precursores lipídicos na membrana citoplasmática e

uma diminuição da incorporação de PGN, devido a uma redução da quantidade de lípido II disponível na face externa da membrana. Estes resultados sugerem que na falta de MurJ, o lípido II acumula na face interna da membrana celular, provavelmente devido a problemas na sua translocação, contribuindo para a ideia de que esta proteína desempenha funções de translocação do lípido II em *S. aureus*.

# CHAPTER I

**General Introduction**

## Bacterial division and morphogenesis

Bacteria are the earliest form of life that appeared on Earth and, over billions of years, they were able to colonize the vast majority of its habitats. In order to survive and proliferate, bacteria have to adapt to diverse environments, many times with less favorable conditions.
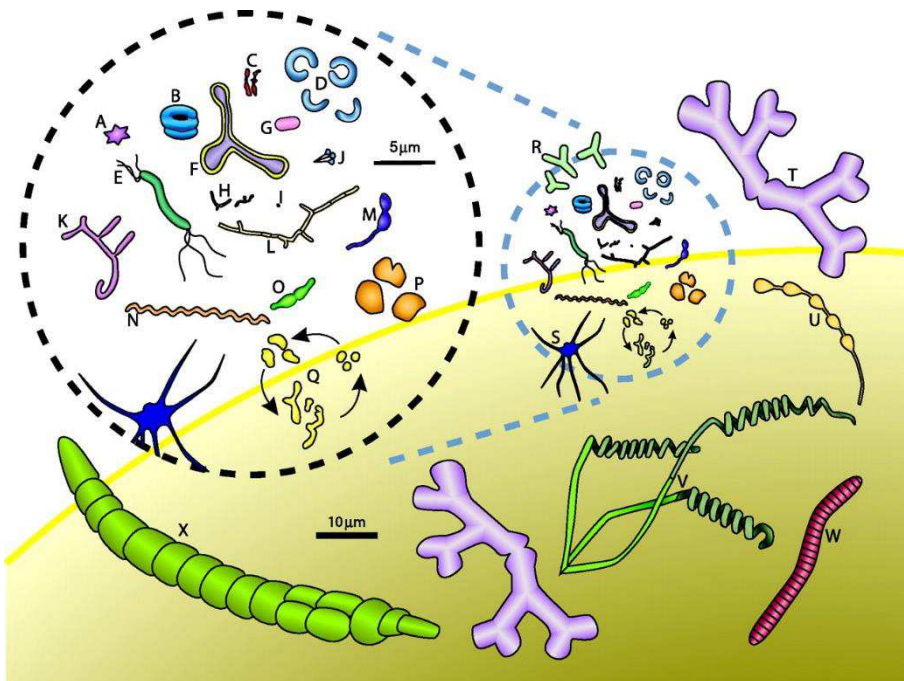


**Figure 1. Variety of prokaryotic shape.** Cell morphology varies greatly, not only among different prokaryotes but also within the same species, during different stages of the cell cycle or in response to environmental pressures. The cells are drawn to scale. (A) *Stella strain* IFAM1312; (B) *Ancylobacter flavus*; (C) *Bifidobacterium bifidum*; (D) *Clostridium cocleatum*; (E) *Aquaspirillum autotrophicum*; (F) *Pyroditium abyssi*; (G) *Escherichia coli*; (H) *Bifidobacterium* sp.; (I) transverse section of ratoon stunt-associated bacterium; (J) *Planctomyces* sp.; (K) *Nocardia opaca*; (L) Chain of ratoon stunt-associated bacteria; (M) *Caulobacter* sp.; (N) *Spirochaeta halophila*; (O) *Prosthecobacter fusiformis*; (P) *Methanogenium cariaci*; (Q) *Arthrobacter globiformis* growth

cycle; (R) *Alphaproteobacteria* from marine sponges; (S) *Ancalomicrobium* sp.; (T) *Nevskia ramosa*; (U) *Rhodomicrobium vanniellii*; (V) *Streptomyces* sp.; (W) *Caryophanon latum*; (X) *Calothrix* sp. The yellow-lined background orb represents a slice of the giant bacterium *Thiomargarita namibiensis*. Reproduced from [1].

Two key factors essential for successful environmental adaptation are cell size and morphology. Bacterial cells can adopt a wide variety of shapes, from near spherical (cocci), to rods (bacilli) or to more complex shapes like helices, stars or squares (Fig. 1). Each of these morphologies have functional consequences that allow bacteria to better respond to selective pressures like adherence to biotic or abiotic surfaces, nutrient access, predation avoidance, diffusion and motility or multiple stress conditions (reviewed extensively in [1]). The rod shape, for example, is believed to promote more robust swimming motility, to facilitate adherence to surfaces and to increase nutrient uptake[1]. On the other hand, spherical cells disseminate faster than nonmotile rod-shaped cells and are usually smaller targets, reducing the probability of being recognized and killed by the host immune system[1,2]. For this reason, several mucosa-associated bacteria minimize their size, adopting a cocci morphology[2].

Bacterial size and morphology are not static, as they can vary throughout the cell cycle, during pathogenesis or in response to environmental stress[3–5]. This evidences how important cell shape is for bacteria, responding not only to the bacterial internal needs, but also to changes in the environment. For a long time, the presence of a cell wall outside the cytoplasmic membrane was thought to be the only determinant of bacterial shape. However, two important facts indicate that this is not totally correct. The first observation is the ability of wall-less organisms, namely bacteria from the *Mollicutes* class, to adopt a

wide variety of shapes, including complex morphologies like helical cells from *Spiroplasmas* or polarized cells with membrane protrusions at the poles from some *Mycoplasmas*[6,7]. In *Haloplasma contractile,* one or two protrusions are connected to a central coccoid cell and can actively alternate between straight and corkscrew-like forms within 5 to 10 seconds, evidencing the versatility of these structures[8]. The second fact indicating that the cell wall is not the only determinant of bacterial morphology is that bacteria with different shapes share cell walls with very similar composition, contributing to the idea that some other mechanism is involved in shape determination. A new vision about cell morphogenesis emerged with the discovery of the bacterial cytoskeleton. Bacterial homologues of the three main eukaryotic cytoskeletal elements (actin, tubulin and intermediate filaments) have been identified and shown to be involved in the regulation of different cellular processes, including cell morphology, cell division, chromosome segregation or cell polarity[9]. The current theoretical model for bacterial morphogenesis establishes that cytoskeletal proteins act as a scaffold for enzymes involved in the synthesis of peptidoglycan (PGN), the major component of cell wall, directing their activity to specific regions of the cell and leading to asymmetric cell wall synthesis[10]. This asymmetric synthesis, together with alterations in peptidoglycan cross-linking, are thought to be the key for establishing the shape of the bacterial cell[2].

## Peptidoglycan maintains cell morphology

PGN is a strong but flexible mesh-like molecule, made of glycan chains cross-linked by short peptide bridges, that surrounds the cell and sustains the high osmotic pressure exerted by the cytoplasm[10]. It is therefore a major factor contributing for the maintenance of cell shape. In fact, purified PGN retains the shape of the organism it was isolated

from[11–13] and rod-shaped cells whose PGN was digested lose their shape and become wall-less spheroplasts[14,15].

### Peptidoglycan structure

In gram-negative bacteria the PGN layer is very thin, from 1 to 3 layers thick and is located between two lipid membranes, the inner and the outer membranes[10,16]. On the contrary, gram-positive bacteria like *Staphylococcus aureus* only have one cytoplasmic membrane, protected by a larger PGN layer exposed to the environment, which is 10 to 20 layers thick[10].

PGN structure is generally similar amongst eubacteria, with glycan chains built up of alternating β-1,4-linked *N*-acetylglucosamine (GlcNAc) and *N*-acetylmuramic acid (MurNAc) subunits. The length of these chains is variable, with an average length of 25-35 disaccharide units in rod-shaped *Escherichia coli*[17] and 3-10 units in spherical *S. aureus*[18]. Linked to the MurNAc subunit is a pentapeptide commonly known as stem peptide, composed by L- and D-amino acids and one dibasic amino acid, which normally is *meso*diamoinopimelic acid (*m*-A2pm) in most gram-negative bacteria and some gram-positive bacteria or L-lysine in most gram-positive bacteria[10]. This dibasic amino acid allows the cross-linking between two stem peptides, directly or through a peptide cross bridge linking the dibasic amino acid in one stem peptide to the D-Ala$_{(4)}$ of a second stem peptide. The stem peptide found in *S. aureus* is L-Ala$_{(1)}$–D-Glu$_{(2)}$–L-Lys$_{(3)}$–D-Ala$_{(4)}$–D-Ala$_{(5)}$ and its cross-linking occurs via an amino acid bridge composed of five glycines (Fig. 2)[10]. The disaccharides in *S. aureus* PGN adopt a 4-fold screw helical symmetry, resulting in stem peptides with 90º angles to one another, allowing cross-linking in all directions[19]. Moreover, long bridge structures, like the pentaglycine bridge, increase cross-linking density,

which justifies the high percentage of cross-linking observed in *S. aureus* strains in comparison with other gram-positive bacteria such as *Bacillus subtilis* or *Streptococcus pneumoniae*[19], and can probably compensate for *S. aureus* shorter glycan strains.
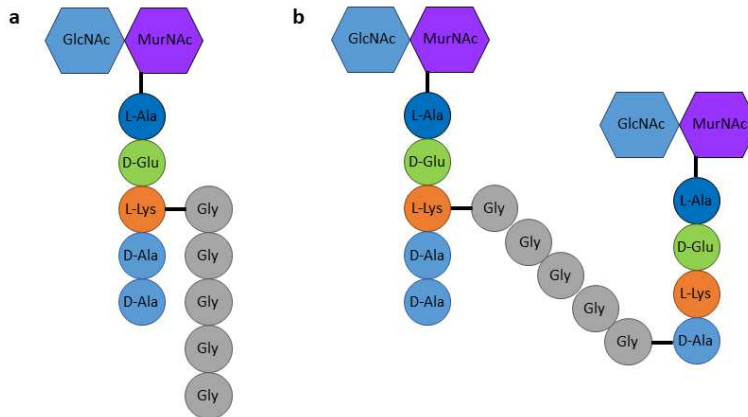


**Figure 2. Building block and structure of *S. aureus* peptidoglycan**. **a,** *S. aureus* PGN basic unit consists on *N*-acetylglucosamine(GlcNAc)-*N*-acetylmuramic acid(MurNAc)-pentapeptide with L-Lys on the third position, connected to a pentaglycine cross bridge. **b,** Cross-linking between PGN glycan strands occurs through a transpeptidation reaction in which the D-Lys$_{(3)}$ of one stem peptide is connected to the D-Ala$_{(4)}$ of a second stem peptide through a pentaglycine bridge.

PGN synthesis occurs in three stages that take place in three different cellular locations: the cytoplasm, the cytoplasmic membrane and the extracellular space (Fig. 3). This process culminates with the polymerization of the newly synthesized disaccharide-peptide units into growing PGN chains.
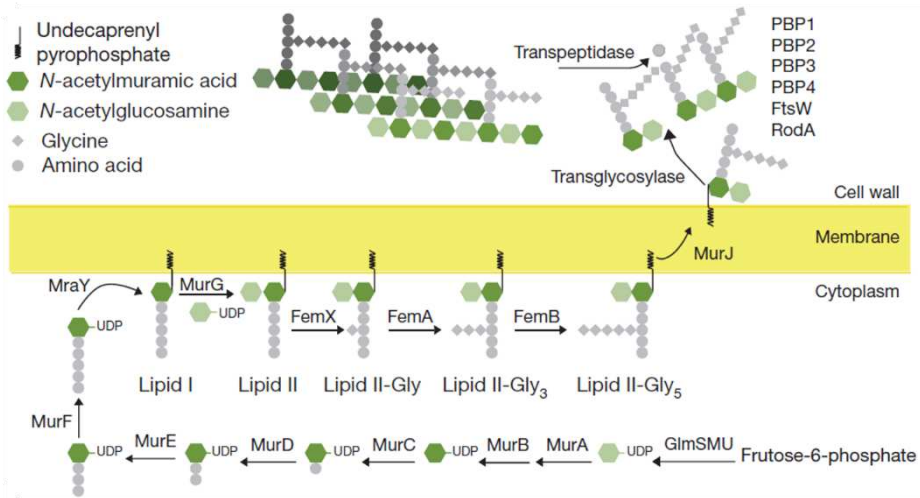
**Figure 3. Synthesis of PGN in *S. aureus.*** PGN is synthesized in three stages that occur in three different locations. The first stage is the synthesis of UDP-*N*-acetylglucosamine (UDP-GlcNAc) and UDP-*N*-acetylmuramic acid (UDP-MurNAc)-pentapeptide precursors, in the cytoplasm. The second stage comprises the synthesis of lipid I and lipid II precursors at the inner leaflet of the cytoplasmic membrane and the flipping of lipid II across the membrane to the outer leaflet. The final stage is the incorporation of the disaccharide-peptide moiety of lipid II into nascent PGN chains through reactions of transglycosylation and transpeptidation, leading to polymerization and cross-linking of the glycan strains, respectively. Reproduced from [20].

## Cytoplasmic steps of peptidoglycan synthesis

In *S. aureus*, the first stage of PGN synthesis is the synthesis of the uridine diphosphate-GlcNAc (UDP-GlcNAc) and uridine diphosphate-MurNAc (UDP-MurNAc)-pentapeptide precursors in the cytoplasm. Conversion of fructose-6-phosphate into UDP-GlnNAc occurs in four successive steps, catalyzed by the GlmSMU enzymes[21–23]. Following these reactions, a two-step process catalyzed by MurA and MurB leads to UDP-GlnNAc conversion into UDP-MurNAc[24]. Five amino acids are then added to the D-lactoyl group of UDP-MurNAc, resulting

in UDP-MurNAc-pentapeptide. Amino acids L-Ala, D-Glu, L-Lys and the dipeptide D-Ala-D-Ala are added in a sequential manner by MurC, MurD, MurE and MurF, respectively, elements of the Mur-ligase family which are believed to have a common mechanism of catalysis[25–27]. For these reactions to occur it is necessary to maintain appropriate levels of D-amino acids in the cell, controlled by the specific racemases MurI and Alr, which convert L-Glu to D-Glu and L-Ala to D-Ala, respectively[28,29]. The D-Ala-D-Ala dipeptide is then formed by the Ddl ligase, prior to incorporation by MurF[30].

### Lipid II synthesis and flipping across the membrane

In the second stage of *S. aureus* PGN synthesis, UDP-MurNAc-pentapeptide is connected to lipid-carrier undecaprenyl phosphate, or bactoprenol. Bactoprenol is a 55-carbon long-chain isoprene lipid that, because of its lipophilic nature, allows the transport of hydrophilic precursors like sugar intermediates from the cytoplasm to the extracellular space, across the plasma membrane[31]. The transfer reaction is catalyzed by MraY in the inner leaflet of the membrane, with the formation of lipid I[28,32]. The coupling of UDP-GlnNAc to lipid I by MurG with elimination of UDP and formation of a β-1,4 glycosidic bond originates lipid II [GlcNAc-β-(1,4)-MurNAc-(pentapeptide)-pyrophosphoryl-undecaprenol][24,33]. In *S. aureus*, lipid II is further altered by the peptidyltransferases FemX, FemA and FemB, which sequentially add five glycines to the L-Lys amino acid in the third position of the stem peptide[34]. During this membrane associated stage, D-Glu on the second position of the stem peptide is amidated by the GatD/MurT enzyme-complex[35,36]. In *S. aureus*, this amidation reaction is necessary to maintain a high degree of PGN cross-linking, and occurs in vitro with all bactoprenol-linked PGN precursors, including lipid I and lipid II with or

without the five glycines bridge, suggesting that GatD/MurT complex might have different substrates in vivo[35].

The percentage of lipid II in gram-positive bacteria is predicted to be less than 1% of the total amount of phospholipids in the cytoplasmic membrane[37]. At the end of the second stage, lipid II has to be flipped from the inner to the outer side of the membrane, where polymerization of new PGN strands occurs. In protein-free artificial membranes, no spontaneous translocation of fluorescently 7-nitro-2,1,3-benzoxadiazol-4-yl (NBD)-labelled lipid II is observed, but it does occur in *E. coli* membrane vesicles[38], indicating that this flipping process is performed by an enzyme. In the last decade there has been a debate regarding which enzyme was responsible for this step, with the two strongest candidates being FtsW and MurJ. FtsW is a membrane protein with 10 transmembrane domains[39] belonging to the SEDS (shape, elongation, division and sporulation) family[40]. The activity of *E. coli* FtsW as the lipid II flippase was shown using in vitro biochemical studies[41], although it was later observed that this activity was not specific for lipid II[42]. Contrary to the biochemical evidence, in vivo studies were never able to show FtsW flipping activity[43]. Moreover, recent studies in the gram-positive bacteria *B. subtilis*, *S. aureus* and *Streptococcus thermophilus*, and in the gram-negative bacteria *Pseudomonas aeruginosa,* have identified SEDS proteins as a new class of transglycosylases able to work in complexes with other peptidoglycan synthases, as will be discussed in the next section[44–46].

MurJ is a protein mostly embedded in the membrane, with 14 transmembrane domains, and belongs to the MOP (multidrug/oligosaccharidyl-lipid/polysaccharide) exporter superfamily[47]. This family of transporters include other putative flippases, homologous to MurJ, capable of translocating undecaprenyl diphosphate-linked oligosaccharides across the cytoplasmic membranes of bacteria[48–50]. A

29

reductionist bioinformatics study has identified MurJ as the best candidate for lipid II flipping in *E. coli*[51]. This prediction has been corroborated by several in vivo studies in *E. coli*, *B. subtilis* and *S. aureus,* showing that MurJ is essential for cell viability, for PGN biogenesis and for the maintenance of cellular shape and integrity[51–54]. It was also shown that in the absence of MurJ, synthesis of PGN was reduced and lipid-linked PGN precursors were accumulated in the cytoplasmic side of the membrane[43,51–53]. These results strongly support the idea that MurJ is the flippase of lipid II, although in vitro data in *E. coli* failed to support the in vivo observations[41]. Last year however, biochemical assays showed that *E. coli* MurJ has a much higher affinity for lipid II binding than FtsW, forming a complex that is relatively stable[55].

A recent study by Liu and collegues showed that in *E. coli,* FtsW presence and activity was necessary for MurJ to be correctly localized at midcell, suggesting an interdependence between these two proteins and the possibility that they may work together during cell division[56]. Because of these conflicting data, and despite the fact that MurJ is currently mostly accepted by the scientific community as the lipid II flippase, some doubts remain and further work is necessary.

## Peptidoglycan polymerization and cross-linking steps

Once lipid II is translocated to the outer leaflet of the cytoplasmic membrane, the third and final stage of PGN synthesis starts. Here, the newly synthesized disaccharide-peptide hydrophilic precursors are polymerized and cross-linked into new PGN by transglycosylation (TG) and transpeptidation (TP) reactions, respectively. In the TG reaction, the reducing end of the MurNAc present in the nascent PGN strain is linked to the C-4 carbon of the GlnNAc in the lipid-linked precursor[57]. This reaction releases undecaprenyl-pyrophosphate, which upon

dephosphorylation restores the bactoprenol molecule that can be re-used in another round of lipid II transport. In *S. aureus*, the TG reaction is performed by the transglycosylase (TGase) domain of PBP2[58,59], by the monofunctional transglycosylases MGT and SgtA[58,60–62] and by the SEDS protein FtsW, whose TGase activity was recently identified[46]. In recent studies in *B. subtilis*, RodA, another member of the SEDS family, has also been shown to have TG activity[44,45].

The TP reaction first cleaves the bond between the two last amino acids of one stem peptide (D-Ala-D-Ala). In *S. aureus*, the released energy is then used to link the D-Ala on the fourth position to the last glycine of the pentaglycine bridge on a second stem peptide. In bacteria that do not possess a pentaglycine bridge, like *E. coli* or *B. subtilis*, a direct cross-link is performed between the D-Ala on the fourth position of the first stem peptide and the dibasic amino acid *m*-A2pm on the third position of the second stem peptide[24]. This reaction is performed by the transpeptidase (TPase) domain of penicillin-binding proteins (PBPs)[58].

PBPs are the most well studied family of proteins involved in last stages of PGN synthesis, as they are the target of β-lactam antibiotics, such as penicillin. These proteins can be divided into high-molecular-weight (HMW) PBPs and low-molecular-weight (LMW) PBPs. HMW PBPs are attached to the cytoplasmic membrane by an N-terminal transmembrane anchor and have two domains on the outer surface of the cytoplasmic membrane[10]. The C-terminal domain possesses TPase activity and is inhibited in the presence of penicillin, due to structural similarities between this β-lactam antibiotic and the D-Ala-D-Ala end of the stem pentapeptide precursor, the natural substrate of this domain[63]. HMW PBPs can be divided into class A or class B depending on the structure and catalytic activity of their N-terminal domain. In class A HMW PBPs (aPBPs), the N-terminal domain has TGase activity, making

these PBPs capable of performing both TG and TP reactions[10]. PBP-like TG active sites are inhibited by the antibiotic moenomycin[64]. Class B HMW PBPs (bPBPs) only possess TPase activity and their N-terminal domain is believed to establish protein-protein interactions with cell division proteins, contributing for cell morphogenesis[58,65]. The LMW PBPs are monofunctional enzymes that can have different activities including DD-carboxypeptidase or transpeptidase, leading to a reduction or increase in the degree of PGN cross-linking, respectively[58,66].

*S. aureus* has only 4 native PBPs, of which PBP2 is the only aPBP. PBP1 and PBP3 are bPBPs and PBP4 is a LMW PBP with TPase activity. In methicillin-resistant *S. aureus* (MRSA) strains, a fifth bPBP, PBP2a, from an extra-species source, is present[67,68]. PBP1 primary amino acid structure is highly similar to PBP2b from *B. subtilis*, PBP2x from *S. pneumoniae*, and PBP3 from *E. coli*[69], enzymes shown to be involved in cell division[70–72]. PBP1 localizes to the division site and is an essential enzyme for the viability of *S. aureus* cells. In its absence the population of bacteria becomes morphologically heterogeneous, with larger and more elongated cells showing difficulties in completing septum synthesis, and eventually dying[69,73]. Inactivation of PBP1 TPase domain results in problems in cell separation and decreased PGN cross-linking, but does not impair bacterial growth or septal localization, suggesting a second essential function for this enzyme, independent of its TPase activity[74]. PBP2 is a bifunctional PBP responsible for both TG and TP reactions. Its TPase domain is essential in methicillin-sensitive *S. aureus* (MSSA) strains but not in MRSA strains, due to the presence of PBP2a[75,76]. It has been suggested that PBP2 TPase domain is responsible for the production of the initial cross-linked muropeptides, up to pentamers, with progressively decreasing efficiency[77]. PBP2 localizes to the septum through a mechanism dependent on its TPase

substrates in MSSA strains or on a possible interaction with PBP2a in MRSA strains[78,79]. PBP3 primary amino acid structure is similar to PBP2a from *B. subtilis*, PBP2b from *S. pneumoniae* and PBP2 from *E. coli*, proteins involved in cell elongation[80–82]. Little is known about the role of this protein in *S. aureus* since it is not essential for cell viability or growth and its absence does not affect PGN muropeptides composition or resistance to β-lactam antibiotics[83]. The only minor alterations observed in the absence of PBP3 were a small decrease in the autolysis rate and the appearance of cells with abnormal size and shape and disoriented septa in the presence of sublethal concentrations of methicillin[83]. PBP4 is the only LMW PBP in *S. aureus* and although it localizes mainly to the septum it can also be found in the cell periphery[84,85]. PBP4 is not essential for cells survival but its TPase activity is responsible for most of the peripheral incorporation of PGN precursors and for the high degree of PGN cross-linking observed in *S. aureus*[77,85]. PBP2a has a TPase domain with very low affinity to β-lactam antibiotics, which allows its function when the TPase domains of the remaining PBPs are inactive[86,87]. In the presence of β-lactams, the TPase domain of PBP2a and the TGase domain of PBP2 can work together in a possible complex for the synthesis of PGN[76].

Besides aPBPs and monofunctional transglycosylases, a new class of TGases has been suggested based on the fact that bacteria lacking these enzymes were able to survive. *B. subtilis* encodes four aPBPs and does not encode other enzymes with similar TGase domains. However, cells lacking all four aPBPs are viable and are able to synthesize PGN and to maintain a rod morphology[88]. These cells have a reduced growth rate when compared to cells lacking only 3 aPBPs and display some morphological defects, like an increased cell length, and division problems, with mislocalization of the division septa[88]. In the presence of moenomycin, cells from the parental strain

show similar alterations but the quadruple mutant cells are not affected[88]. Analogous observations were performed in *Enterococcus faecalis*, in which deletion of all 3 aPBPs resulted in viable cells with reduced growth rate and PGN cross-linking level, and resistant to moenomycin[89]. These studies, performed over a decade ago, suggested the existence of a different class of TGase proteins, not sensitive to moenomycin and able to synthesize PGN in the absence or upon inactivation of all aPBPs.

As referred above, the SEDS family has been recently identified as a new class of TGases, remotely similar to the O-antigen ligase from gram-negative bacteria, which is a membrane TGase that also uses lipid-linked precursors as substrates[44]. RodA is a member of the SEDS family involved in cell elongation. In rod-shaped bacteria like *E. coli* or *B. subtilis*, RodA is essential for viability and its depletion results in defects in the elongation process with the formation of round cells that eventually lyse[40,90]. Overexpression of RodA can lessen the growth defect of the *B. subtilis* strain lacking all four aPBPs, and almost suppress its morphological defects and high levels of lysis[44]. Additionally, RodA shows TGase activity in vitro and is responsible for moenomycin resistance in the four aPBPs mutant, confirming that its TGase domain is different from the one of aPBPs which is inhibited by this antibiotic[44,45]. A similar role was proposed for the SEDS protein FtsW in the divisome[44] and its TGase activity has been recently identified in vitro for the *B. subtilis*, *S. aureus, S. thermophilus* and *P. aeruginosa* proteins and shown to be dependent on the interaction with a cognate bPBP[46]. SEDS proteins and bPBPs have been shown to interact and to form complexes involved in cell growth and division[91–93]. In many bacteria, members of these two families are genetically linked and are often found in the context of the *mreBCD* operon (cell elongation) or in the cluster of cell wall synthesis and cell division[44,94].

With the discovery of SEDS TGase activity, the hypothesis that these proteins formed functional TGase-TPase pairs with bPBPs was postulated (Fig. 4)[44,45,95].
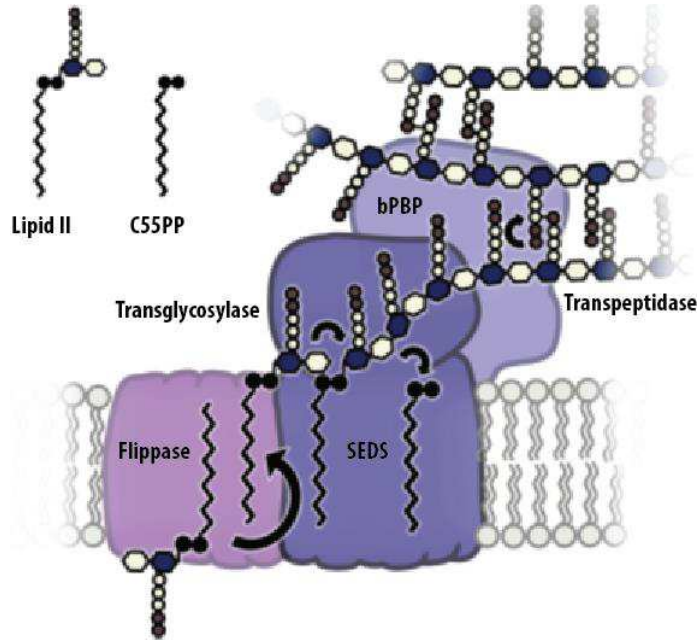


**Figure 4. SEDS proteins and class B PBPs (bPBPs) can work together in a TGase-TPase functional complex**. Lipid II precursor is flipped across the cytoplasmic membrane by a lipid II flippase, probably MurJ, polymerized into nascent PGN strains by a newly identified transglycosylase SEDS protein and cross-linked by its bPBP cognate pair. Adapted from [96].

FtsW was shown to be part of the division machinery together with PBP3 in *E. coli*, PBP2b in *B. subtilis* or PBP2x in *S. pneumoniae* [71,97–99]. In *E. coli*, localization of FtsW is necessary for the recruitment of PBP3[100], while in *B. subtilis,* FtsW and PBP2b require the presence of each other for proper localization at the division site, evidencing the interdependency between them[101]. These localization dependencies suggested the existence of a pre-formed complex between FtsW and bPBPs involved in cell division. The existence of this complex was later

proved by the identification of direct interactions between FtsW and PBP3 in *E. coli,* both in vivo and in vitro by Förster resonance energy transfer (FRET) and co-immunoprecipitation experiments[91]. Similarly, co-immunoprecipitation assays were used to show interactions between FtsW and PBP2x in *S. pneumoniae,* PBP1 in *S. aureus* and PBP3 in *P. aeruginosa*[46,99].

The second SEDS protein, RodA, is part of the elongation machinery in rod-shaped and ovococcoid bacteria[102–104]. In *B. subtilis*, proteins from the elongation complex organize in patches that move processively along the lateral cell wall, perpendicularly to the longer cell axis[104,105]. RodA and PBP2a/PbpH in *B. subtilis* or PBP2 in *E. coli* show a similar movement pattern, moving slowly and directionally around the cell circumference[102,104] and contributing to the idea of a functional connection between SEDS and bPBPs. Additionally, in *E. coli* cells lacking PBP1b, the main PGN synthesizing enzyme in normal *E. coli* membranes, high levels of both RodA and PBP2 are necessary to perform TGase and TPase reactions essential to PGN synthesis, with RodA being required for the proper function of PBP2[106]. Besides the functional association, a direct physical interaction between RodA and PBP2b was identified in vitro in *S. pneumoniae,* by two-step pull-down and bacterial two-hybrid assays, confirming the formation of RodA-PBP2b complex[103,107].

Although only one PGN synthetic machinery has been identified in *S. aureus*, this species possesses two SEDS proteins, FtsW and RodA and two bPBPs, PBP1 and PBP3. Previous work by Monteiro and Fernandes et al. has shown that *S. aureus* cells slightly elongate during specific phases of the cell cycle[85]. This raised the hypothesis of the existence of two functional TGase-TPase pairs, involved in PGN incorporation, similar to what was observed in other species, a question addressed in chapter 3 of this thesis.

## Bacterial Divisome

Most bacteria divide by binary fission, a process in which the mother cell divides in two equal and genetically identical halves. In this process, DNA is replicated and segregated into opposing cell poles followed by synthesis of a division septum at the equatorial plane, that upon constriction and splitting originates two daughter cells. The formation of the division septum involves the cooperation of over 30 proteins, collectively known as the divisome, which are responsible for coordinating chromosome segregation, membrane invagination and PGN synthesis and hydrolysis[108]. In most bacteria, divisome assembly depends on FtsZ, a cytoskeletal protein homologue to tubulin[109]. In terms of structure the two cytoskeletal proteins are very similar, containing two domains connected by a central helix[110,111]. FtsZ also contains a C-terminal tail responsible for its interaction with other divisome proteins[112–115]. FtsZ polymerizes into protofilaments in a GTP-dependent reaction and assembles into a ring-shaped structure (Z-ring) next to the inner side of the cytoplasmic membrane at the future division site[116]. This structure functions as a scaffold for the other members of the divisome that are subsequently recruited. The assembly of Z-ring is very accurate, both in time and space, guaranteeing a precise division of the mother cell and avoiding bisection of bacterial genetic material[117,118].

### Positioning of FtsZ ring

The location of the new division site is determined by the positioning of FtsZ ring, which can be regulated by both negative and positive mechanisms. The negative mechanisms prevent FtsZ polymerization away from midcell and include the Min system and nucleoid occlusion proteins. The Min system was initially identified in *E.*

*coli* and *B. subtilis* and is based on the inhibition of FtsZ polymerization by the MinCD protein complex. MinC binds and disrupts FtsZ polymers and is recruited and activated by MinD, which binds to the membrane in an ATP dependent manner[119]. In *E. coli*, MinCD oscillates between cell poles resulting in a protein gradient where higher concentrations are present at the poles and lower concentrations at midcell[120]. On the other hand, no oscillatory movement is observed in *B. subtilis*, and MinCD complex is recruited to both cell poles by DivIVA[119]. DivIVA senses regions of high membrane curvature, localizing to the cell poles and to the nascent division septum (future cell pole) during membrane invagination[119,121]. This localization at midcell prevents the formation of further Z-rings on both sides of the division septum. After cell division, the division septum becomes the new cell pole and DivIVA localization changes from midcell rings into polar patches[121], recruiting Min proteins[119]. In both Min systems, MinC and MinD are concentrated on cell poles and the midcell becomes the preferential location for Z-ring assembly.

Nucleoid occlusion proteins bind specific DNA sequences scattered throughout the chromosome, but essentially absent from the terminus region, and inhibit the formation of the Z-ring in the proximity of the nucleoid[122–125]. This effect is mediated by different proteins like SlmA in *E. coli*[123] or Noc in *B. subtilis*[122,125] and *S. aureus*[124]. After binding to the nucleoid, SlmA affinity for FtsZ filaments increases, leading to filament disruption near the nucleoid[126]. On the contrary, no interaction has been identified between Noc and FtsZ in *B. subtilis* and Noc is believed to physically inhibit the assembly of the division machinery by binding directly to the cytoplasmic membrane and recruiting the DNA sequences to the periphery[125]. In both *E. coli* and *B. subtilis*, the combination of nucleoid occlusion and the Min system leads to the establishment of the Z-ring at midcell. In *S. aureus*, Noc is the

only mechanism identified for determining Z-ring positioning[124] and is also involved in the control of DNA replication initiation[127]. In the absence of Noc, a small percentage of *S. aureus* cells form multiple FtsZ rings that are placed over the nucleoid[124]. The fact that Noc depleted *S. aureus* cells are viable, and that *E. coli* and *B. subtilis* cells without both nucleoid occlusion and Min system, despite having several septation problems and aberrant FtsZ structures, can still correctly position FtsZ, suggests that additional regulators are likely to exist[128,129].

Positive mechanisms controlling Z-ring positioning were identified more recently and include proteins that localize at midcell and recruit FtsZ to that localization. One example is MapZ in *S. pneumoniae*, which can interact with newly synthesized PGN on the extracellular space and with FtsZ on the cytoplasm, functioning as a physical anchor and stabilizer of the Z-ring at midcell[130]. Other examples of positive regulators are PomZ in *Myxococcus xanthus*[131] or SsgAB complex in Streptomyces[132].

### Assembly of FtsZ ring

In *E. coli* and *B. subtilis*, divisome assembly can be temporally divided in two stages and was proposed to follow a two-step assembly model. The first step consists on the formation of the Z-ring at midcell, and the second on the recruitment of downstream division proteins[98,133]. In *E. coli*, formation of the Z-ring occurs without visible cell constriction and coincides with preseptal elongation[134,135], a phase when cells elongate at midcell in an FtsZ-dependent manner[136]. Although FtsZ does not possess any membrane-binding domain, FtsZ filaments attach to the inner side of the cellular membrane via FtsA and ZipA[137,138]. These are two essential proteins that localize to midcell through interaction with FtsZ[138–140] and anchor it to the membrane. Although each of these

proteins alone is able to support the formation of Z-rings, both of them are necessary for the recruitment of later division proteins[137]. Moreover, the equilibrium between FtsZ, FtsA and ZipA is of extreme importance for proper cell division, since alteration of the proportions of these proteins, mainly FtsZ and FtsA, can lead to problems in Z-ring formation and septation[141]. In *S. aureus*, FtsA can also associate with FtsZ and this interaction enhances FtsZ GTPase activity[113,142]. While FtsA is widely conserved among bacteria, ZipA can only be found in γ-proteobacteria[143]. An alternative membrane anchor for FtsZ, found in gram-positive bacteria is SepF, originally named YlmF. In *B. subtilis* cells, FtsA depleted cells are viable but display severe cell division problems. Overexpression of SepF can compensate for the lack of FtsA in *ftsA*-null mutants and the two genes are synthetic lethal[144].

An important regulator of FtsZ polymerization is EzrA, an FtsZ inhibitor which controls the frequency and location of Z-rings. Depletion of EzrA leads to abnormal FtsZ polymerization away from midcell in rod-shaped cells like *B. subtilis*[110] or its mislocalization in *S. aureus* with occasional formation of multiple complete FtsZ rings[145,146]. EzrA localizes to the division site in an FtsZ-dependent manner[110,146], interacts with several division proteins and its absence leads to a mislocalization of PBPs in *S. aureus*[145,146]. EzrA structure is similar to that of proteins of the eukaryotic spectrin family[147]. Spectrins act as a scaffold connecting actin filaments to the membrane and coordinate membrane proteins interactions[148]. However, if EzrA can perform a similar function in bacteria is still an open question.

### Recruitment of late division proteins

The second step of divisome assembly occurs after FtsZ ring assembly, with a time delay corresponding to 20% of the cell cycle in *B.*

*subtilis*[98] or 15% to 34% in *E. coli*[133]. This step is characterized by the recruitment of a variety of proteins, called "late" division proteins, including SEDS protein FtsW, PGN synthases like *E. coli* PBP3 (FtsI) or *B. subtilis* PBP2b, DNA-binding proteins FtsK and SpoIIIE, and the structural and regulatory proteins FtsN and complexes FtsB/FtsL/FtsQ (FtsBLQ) in *E. coli* or equivalent DivIC/FtsL/DivIB in *B. subtilis*[143,149]. DivIC, FtsL and DivIB are bitopic membrane proteins with one transmembrane segment and a C-terminal extracellular region. The three proteins interact to form a ternary complex, stabilizing each other against proteolysis, and localize to the division septum in an interdependent manner[150–152]. In *E. coli*, the equivalent FtsBLQ complex has been identified by immunoprecipitation experiments and was shown to preassemble prior to septal localization[153]. Localization of DivIC/FtsL/DivIB and PBP2b are interdependent in *B. subtilis*[72] and a strong interaction between DivIB and PBP2b has been identified[154]. More recently, FtsW localization was also shown to be necessary for the localization of FtsL and PBP2b, and to require these two proteins for its own localization, evidencing an interdependent interaction[101]. These observations evidence a cooperative assembly of late division proteins in *B. subtilis*, since DivIB, FtsL, DivIC, PBP2b and FtsW assemble interdependently and the absence of any of these proteins prevents the localization of all the others[101,150,155].

Contrary to what is observed in *B. subtilis*, the localization of the different division proteins in *E. coli* seems to occur in a linear sequential manner, as the presence of each protein is necessary for the recruitment of the following one[156]. However, the fact that FtsQ, FtsL and FtsB form a complex before they localize to the Z-ring[153], that late proteins can back-recruit upstream proteins[93,157] and that some essential division proteins can be bypassed by overexpression or mutations of other divisome members[108] point to a non-sequential assembly of the

divisome in *E. coli* and demand a careful interpretation of the hierarchical assembly pathway model. Also, both early and late division proteins contribute to the regulation of divisome assembly, since the cooperative assembly of divisome proteins was suggested to depend on interactions between the early protein FtsA and the late protein FtsN[158,159]. In these studies, a model was proposed in which at low FtsN concentrations both FtsA and FtsBLQ subcomplex are in an "off" conformation, suppressing PGN synthesis. Once FtsN concentration increases, it changes FtsA into an "on" conformation, which will in turn activate FtsBLQ subcomplex that may stimulate PGN synthesis[158,159]. Despite the important role of FtsN in *E. coli*, this protein is poorly conserved in bacteria[160] and no homologues have been found in gram-positive bacteria, implying a different regulatory mechanism to initiate PGN synthesis. One possible regulatory mechanism, proposed for *B. subtilis,* is through FtsL, due to its high instability and rapid protein degradation upon repression of gene transcription. FtsL depletion prevents DivIB and DivIC septal localization, leading to the degradation of DivIC protein and to a rapid arrest of cell division[150,161].

In *S. aureus*, it was recently shown that divisome assembly occurs in a progressive way, with FtsZ being recruited earlier, followed by DivIB, FtsW and PBP1, approximately at the same time, and later by MurJ, the putative lipid II flippase[20]. MurJ localization to midcell, but not FtsW or PBP1 localization, is dependent on the presence of the complex DivIB-DivIC-FtsL[20]. *S. aureus* DivIB is capable of binding PGN through its extracellular domain and is essential for cell growth, since its depletion inhibits the completion, but not initiation, of septum synthesis[162].

FtsW has been suggested to play a role in Z-ring stabilization in *E. coli*, since its absence leads to a reduction in septation frequency[163], with a twofold decrease in the number of FtsZ rings[100], and consequent

formation of long filamentous cells. In *B. subtilis*, the assembly of Z-ring is dependent on the presence of FtsW[101,164] and in *Streptomyces coelicolor,* disruption of *ftsW* or *ftsI* (bPBP) genes inhibits Z-ring formation in aerial hyphae and prevents reorganization of spiral polymers of FtsZ into rings[165]. This indicates an early role for SEDS proteins and their cognate bPBPs in cell division. Also, a triple interaction between FtsW, PBP3 and FtsZ was identified in *Mycobacterium tuberculosis*, where FtsW silencing prevents PBP3 localization and cell septation, contributing to the idea that these proteins are involved in the regulation of septal PGN biogenesis[166,167].

## Coordination of different peptidoglycan synthesis machineries

A wide number of proteins involved in the processes of PGN synthesis and cell division organize in functional machineries that allow cells to grow and divide, while maintaining their characteristic morphology. The number, identity and function of these machineries varies according to the shape of the bacterial cells and the mechanisms that control these multi-protein complexes are not fully understood.

### The Rod shape

The majority of rod-shaped bacteria combine PGN synthesis at the septum with elongation of the lateral sidewall, along the longitudinal cell axis (Fig. 5, top panel). Septal PGN synthesis is responsible for generating the new cell poles of the daughter cells during cytokinesis, whereas lateral PGN insertion allows the establishment and propagation of the rod shape. While septal growth is dependent on the activity of the

divisome machinery directed by FtsZ, lateral wall elongation is mainly oriented by MreB.
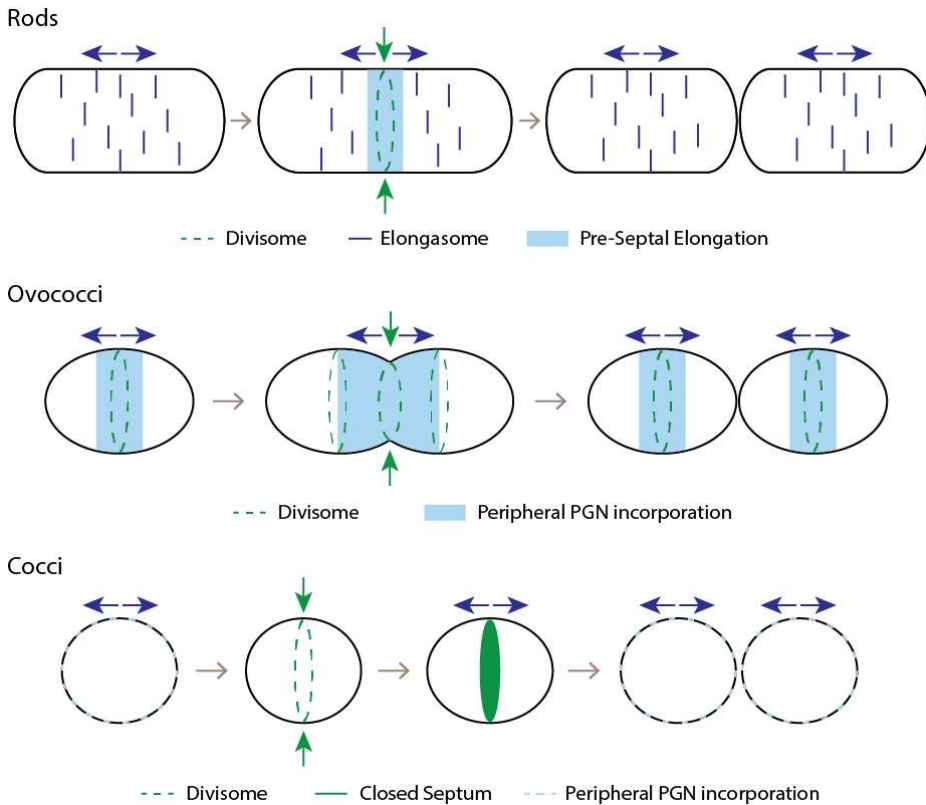


**Figure 5. PGN incorporation during growth and cell division in different bacteria.** Rod-shaped bacteria (top panel) divide by septal PGN synthesis performed by the divisome complex at midcell. Elongation results from insertion of new PGN along the lateral wall by the MreB-dependent elongasome and from FtsZ-dependent pre-septal PGN incorporation at midcell. Ovococcoid cells (middle panel) combine septal and peripheral PGN incorporation, performed by the divisome and elongasome, respectively. Both machineries are probably dependent on and coordinated by FtsZ. Coccoid cells (bottom panel) divide by PGN incorporation at midcell by the divisome complex. Slight cell growth and elongation occurs before and after septum synthesis.

Proteins from the MreB family are bacterial actin homologues, widespread in elongated bacteria but generally absent in spherical cells[168]. Consistently, MreB proteins were early identified as shape determinants, since mutations in their genes lead to alterations in cell morphology[169–171]. *E. coli* possesses only one MreB homologue and in its absence, cells lose their rod shape, becoming round and enlarged, and finally lysing[170–172]. In *B. subtilis*, three MreB homologues have been identified, MreB, MreBH, and Mbl, and the absence of any of them causes defects in cell morphology[173]. Depletion of MreB leads to cell rounding and general loss of viability, similarly to what is observed in *E. coli*[168,173]. Depletion of Mbl results in distorted cells, often bloated and with an increased and more irregular diameter[168,169,173] and absence of MreBH also leads to wider, bent cells[173].

Interactions between different MreB subunits allow MreB polymerization into filaments, in an ATP-dependent manner[174,175]. MreB binds directly to the inner side of the cytoplasmic membrane through a hydrophobic loop and, in some gram-negative bacteria, including *E. coli*, also via an N-terminus amphipathic helix[176,177]. This membrane association is related to MreB polymerization and, under the right conditions, can originate extended antiparallel filaments in vitro[176]. Initial localization studies suggested that MreB subunits polymerize into helical filaments along the longitudinal axis of the cell[168,178]. However, later studies using functional MreB fluorescent fusions and better resolution microscopy techniques, showed that MreB actually organizes into short, dynamic patches distributed along the cytoplasmic membrane[104,105,179]. These patches move independently around the cell circumference, almost perpendicularly to the longitudinal axis[104,105,179] and co-localize with the insertion of new PGN[180,181]. MreB localization is affected by the geometry of the cell and tends to prefer regions with inward indentations and to avoid bulging areas, like the cell poles[181–183].

MreB can then direct PGN synthesis into those regions of negative curvature and actively straighten them, contributing to the propagation of the rod shape. This co-localization of MreB with PGN insertion sites raised the hypothesis that the MreB cytoskeleton may control cell wall synthesis by spatially regulating enzymes involved in this process. Agreeing with this idea, several proteins known to be involved in determination of cell shape in *B. subtilis* move in a similar manner and co-localize with MreB/Mbl/MreBH motile patches[104,105]. These include *B. subtilis* PBP2a and PbpH, which play redundant roles in the synthesis of sidewall PGN[184], RodA, MreC and MreD. Together, these proteins are part of a cell wall elongation complex, or elongasome, with circumferential processive motility.

In rod-shaped cells like *B. subtilis* or *E. coli*, *mreC and mreD* genes belong to an operon together with *mreB* and are essential for cell viability[187]. Similarly to *mreB*, deletion of any of these genes leads to severe morphologic alterations, as the cells become round, swelled or twisted, culminating in cell lysis[172,188]. In most organisms, MreC has one transmembrane domain near its N-terminus and two extracellular C-terminal domains[189], while MreD is almost completely embedded in the cell membrane with four to six transmembrane spans[190]. In *E. coli*, MreC can interact with both MreD and MreB but MreB does not seem capable of interacting with MreD[172]. These interactions, together with the fact that MreC and MreD are necessary for proper MreB localization, suggest the existence of a multiprotein complex with MreC localized between MreB and MreD[172]. Besides interacting with each other, MreC and MreD can also interact with different elements of the elongasome. Affinity chromatography assays in *C. crescentus* showed that MreC has the capacity to interact with 5 PBPs and some outer membrane proteins[191] and bacterial-two-hybrid (BTH) experiments evidenced interactions with 9 class A and class B PBPs in *B. subtilis*[189]. On the other hand, BTH

experiments in *C. crescentus* have shown that MreD could interact with MurG and MraY, which are cytosolic PGN biosynthesizing enzymes[192]. In *B. subtilis,* MreC and MreD are also necessary for MreB correct localization[193] and for PGN lateral incorporation[188]. Additionally, the structure of an MreC-PBP2 complex in *Helicobacter pylori* was recently resolved, and MreC was shown to induce a significant conformational change in PBP2[194]. This suggests that MreC and MreD can act not only as a scaffold, coupling the internal cytoskeleton with the PGN synthesizing machinery, but also as regulators of this elongation multi-protein complex.

As referred above, RodA and a bPBP can form a TGase-TPase enzymatic pair suggested as the core system for lateral PGN synthesis[44,102]. Although the mechanisms coordinating TGase and TPase activities are not fully understood, a recent study in *E. coli* has identified a PBP2 variant capable of hyperactivating cell wall synthesis by stimulating RodA PGN polymerization activity[80]. This PBP2 variant was also shown to suppress the growth defects of cells lacking other morphogenetic elements like MreCD and RodZ, and to regulate MreB polymerization[80]. Considering the structural information from the resolved MreC-PBP2 complex in *H. pylori*, a model was proposed in *E. coli* in which MreC association with PBP2 leads to a conformational alteration responsible for the activation of RodA and, consequently, of PGN polymerization. This activated complex can then promote the formation of MreB filaments, which will direct PGN synthesis[80]. According to this model, PGN synthesis can only occur after elongasome assembly, providing a spatial and temporal regulation of this synthetic process. Inhibition of *E. coli* PBP2 TPase activity by β-lactam antibiotic mecillinam has been shown to induce the turnover of nascent PGN synthesized by the elongation machinery. This turnover of uncross-linked glycan chains is toxic to the cell, since it contributes to

the depletion of cell PGN precursors, affecting all PGN synthesis mechanisms and leading to cell death[195]. RodA activation by PBP2, can be a way of coordinating both TGase and TPase activities to avoid the generation of uncross-linked glycan chains and the consequent cytotoxic futile cycle of PGN synthesis and degradation[80].

Although MreB-dependent elongation is the most common in rod-shaped bacteria, some elongated bacteria, particularly within the Actinomycetales and Rhizobiales orders, do not have *mreB* genes and developed mechanisms for polar elongation[180,196,197]. In Actinomycetales, including *Mycobacterium*, *Corynebacterium* and *Streptomyces,* DivIVA plays an important role in the establishment and maintenance of polar growth, possibly cooperating with several accessory polar growth structural proteins[198–200]. On the other hand, Rhizobiales, like *Agrobacterium*, lack DivIVA homologues as well as other Actinomycetales structural proteins, and polar growth probably involves cell division proteins. In fact, FtsZ and FtsA localize to the *Agrobacterium tumefaciens* growing pole during cell elongation and to the Z-ring during cell division[201,202]. However, the mechanisms controlling this localization pattern are still unknown.

Besides cell elongation and division some elongated bacteria like *E. coli* and *C. crescentus* display a pre-septal elongation step, in which new PGN is inserted into a circumferential ring at midcell (Fig. 5, top panel) in an FtsZ-dependent manner, leading to cell envelope growth[13,135,136]. Although the mechanism behind this mode of elongation is not clear yet, in *E. coli* it requires the activity of FtsZ and ZipA and is not dependent on other divisome members, MreB-related elongasome proteins, alternate PGN synthases, the main PGN amidases nor LMW-PBPs[135].

Both preseptal elongation and *Agrobacterium* polar growth show that the importance of FtsZ is not restricted to the divisome and evidence a role for this cytoskeletal protein in cell elongation and morphology.

### The Ovococcoid shape

Cells with an ovococcoid morphology, including from *Streptococcus*, *Enterococcus*, and *Lactococcus* genus, display a combination of septal and peripheral PGN synthesis, responsible for both cell division and elongation, respectively[203] (Fig. 5, middle panel). In ovococcoid cells, MreB-like proteins have not been identified[204], indicating an organizational mechanism different from that of Rod-shaped bacteria. Septal PGN is synthesized at the division site by divisome proteins coordinated by FtsZ. Contrary to sidewall elongation in rod-shaped bacteria that is observed along the lateral wall, peripheral PGN synthesis occurs in a band between the current and the future division sites, called the equatorial rings[204,205]. This elongation mode is possibly coordinated by FtsZ, resembling pre-septal growth in rod-shaped bacteria.

Although both septal and peripheral synthesis co-exist at midcell, it is possible to inhibit each of these processes separately. In different species, including *S. pneumoniae* and *Lactococcus lactis*, depletion or antibiotic inactivation of PBP2x, involved in septal synthesis, results in elongated and enlarged cells[82,206,207] while depletion of PBP2b, involved in peripheral synthesis leads to chains of round cells[82,207,208]. Similar chains of round cells are observed after inactivation of RodA in *S. thermophilus*[208] or in the absence of MreC and MreD in *S. pneumoniae*[209], suggesting a role for these three proteins in ovococcoid cell elongation, similar to what happens in rod-shaped bacteria. However, since ovococcoid cells lack MreB proteins, the role of MreCD

as scaffolding proteins might not be their only function. These observations strongly support the proposed two-state model in which septal and peripheral growth are performed by two independent machineries, both localized at the division site[203,210]. In this model, peripheral PGN is inserted at midcell by the elongation machinery, originating longitudinal elongation, while the division machinery builds the septal cross-wall[210]. Peripheral PGN synthesis may start slightly earlier than septal synthesis but both processes are believed to occur simultaneously during most of the ovococcoid cell cycle[211]. Additionally, proteins from both complexes spatially co-localize in *S. pneumoniae*[206,210,212,213], although PBP2x may separate from the other PBPs in later stages of cell division, localizing to the center of constricting septa[212]. It was recently shown that the TPase activity of *S. pneumoniae* PBP2b is involved in septum positioning, evidencing a coordination between septal and peripheral growth[214]. Although the mechanism regulating both processes remains elusive, one possibility is through serine/threonine kinases (STKs). These proteins are involved in the control of cell elongation in bacteria lacking MreB cytoskeleton and were proposed to act as molecular switches between the two types of PGN synthesis[215–217]. STKs localization to the division site depends on the interaction of their PASTA domains with PGN[217,218]. In *S. pneumoniae*, the regulatory activity of StkP is thought to occur via DivIVA, a cell division protein highly conserved among gram-positive bacteria, whose absence leads to problems in divisome assembly and to elongated cells[217,218].

### The Coccoid shape

In coccoid bacteria, like *S. aureus,* only one PGN synthesis machinery was identified, the divisome complex, indicating that the

ability of these bacteria to grow and divide is dependent on PGN insertion mostly at the division site. In recent years, *S. aureus* cell cycle has been described in three distinct phases: phase 1 starts just after cell division prior to initiation of division septum formation, phase 2 comprises the synthesis of the division septum and phase 3 occurs between septum closure and splitting of the two daughter cells[85] (Fig. 6). Cell growth occurs gradually during the cell cycle and PBPs activity is observed across the entire cell surface[85]. This PGN peripheral synthesis is mainly due to PBP4 activity, although the contribution of other PGN synthases can not be excluded[85,219], and was the first indication that PGN incorporation in *S. aureus* was not restricted to the division septum (Fig. 5, bottom panel). A second line of evidence was that cell growth is accompanied by a slight elongation, raising the possibility that more than one synthesis machinery may exist in spherical bacteria, responsible for either cell division or peripheral elongation, similarly to what is observed in other cell morphologies. Contributing to this idea is the fact that *S. aureus* genome encodes proteins previously associated with lateral or peripheral elongation, including RodA, MreC and MreD. Although their role in spherical cells has not been identified yet, they are not essential for cell survival[220,221].
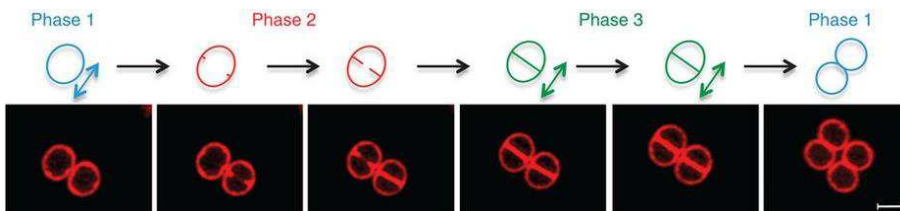


**Figure 6. *S. aureus* cell cycle occurs in three phases**. Phase 1 starts after cell division and consists of cell elongation prior septum synthesis. During Phase 2 cells synthesize division septum without obvious elongation. In Phase

3 septum is complete and cells elongate before splitting into two daughter cells. Scale bar, 1 µm. Reproduced from [85].

## *S. aureus* as a model to study morphogenesis of coccoid bacteria

Many important findings in bacterial molecular and cellular biology come from studies on classic model organisms like *B. subtilis* or *E. coli*. *B. subtilis* has several advantages as a model organism for gram-positive bacteria, namely the easiness of genetic manipulation, the large amount of available information resulting from the early sequencing of its whole genome, the possibility of studying the sporulation process and its non-pathogenic nature. However, the study of this organism is not sufficient to understand the large variety of cellular processes in gram-positive bacteria. It is therefore essential to extend research to other organisms, including species with different cell morphologies and different modes of division and elongation, as well as to pathogenic bacteria.

Several reasons make *S. aureus* a good pathogen to study. First, it is clinically relevant, since *S. aureus* strains are commonly found in human skin and mucus membranes, mainly in the nose, colonizing approximately 30% of healthy human population[222,223]. Although most people are asymptomatic carriers, the occurrence of infections is frequent, both in community as well as in hospital settings. These infections happen after bacteria cross human barriers, entering the bloodstream or internal tissues and can evolve into serious conditions, from skin, soft tissue, pleuropulmonary and osteoarticular infections, to bacteremia and infective endocarditis[222,224]. MSSA strains can be effectively treated with the more commonly used antibiotics, usually from the β-lactam class such as cephalosporins or methicillin-relatives

oxacillin or nafcillin[225]. However, the emergence of MRSA strains has increased the difficulties in the treatment of *S. aureus* infections. The 2017 report on the surveillance of antimicrobial resistance in Europe from the European Centre for Disease Prevention and Control (ECDC) indicated that the percentage of MRSA in *S. aureus* isolates was 16.9% in EU/EEA countries, with 9 out of 28 countries showing percentages between 25% and 50%, including Portugal with 39.2%[226]. MRSA strains are consequently considered an important public health problem.

MRSA strains are resistant to nearly all β-lactam antibiotics due to the presence of the staphylococcal cassette chromosome *mec*, called SCC*mec*, a mobile genetic element carrying *mecA* gene, encoding PBP2a, a PBP with low affinity for β-lactams and necessary for MRSA antibiotic resistance[227]. Due to this widespread β-lactam resistance, the need for alternative antibiotics has increased. Vancomycin, a glycopeptide antibiotic, is currently one of the few therapeutic options for MRSA infections and the isolation of vancomycin resistant strains in various countries around the world is a major concern[228–230]. To effectively fight drug-resistant bacteria it is necessary to know their weaknesses. It is therefore essential not only to evaluate how *S. aureus* spreads and causes infections, but also to understand the molecular biology and the mechanisms behind the cellular processes essential for its survival. Knowing that the presence of a cell wall is of critical importance for bacterial pathogens, studying the events that lead to its construction is imperative.

Besides its importance as a pathogen, a second reason for studying *S. aureus* is the fact that its cells display a coccoid morphology, different from the rod shape of the model organism *B. subtilis.* While the elongation process of rod-shaped cells has been widely studied, the mechanisms behind the establishment of a round shape are still relatively unknown. The fact that *S. aureus* cells do not encode MreB

homologues but are still able to slightly elongate, suggests the existence of a different mechanism determining cell shape in this organism. To understand that mechanism and how it affects cell viability, proliferation and virulence is important for the development of future clinical therapies.

Another advantage of working with *S. aureus* is its minimal PGN synthesis machinery, which makes it a good model organism to study essential processes like bacterial cell division and cell wall synthesis. It contains only 4 PBPs in MSSA strains, or 5 PBPs in MRSA strains, less than the ovococcoid *S. pneumoniae* (6 PBPs) and a very reduced number when compared to the most studied gram-positive and gram-negative model organisms *B. subtilis* (16 PBPs) or *E. coli* (12 PBPs)[10]. It is therefore interesting to understand how this reduced number of proteins is able to perform and coordinate distinct cellular processes, like cell division and cell elongation, and how each of these elements influence bacteria viability and morphology.

Finally, the almost spherical morphology of *S. aureus* enables the cells to lay in the microscopy slide in different orientations, allowing the visualization of the divisome ring in multiple angles on the same image. One important advantage is the possibility of imaging the divisome on a plane parallel to the microscopy slide, facilitating the analysis of the progression of inward PGN synthesis and cell division. This, coupled with the emergence of new powerful imaging techniques, allows the study of essential processes in this important pathogen, contributing to the search for new ways to fight *S. aureus* infections.

# REFERENCES

1.      Young, K. D. The selective value of bacterial shape. *Microbiol. Mol. Biol. Rev.* **70**, 660–703 (2006).

2.      Yang, D. C., Blair, K. M. & Salama, N. R. Staying in Shape: the Impact of Cell Shape on Bacterial Survival in Diverse Environments. *Microbiol. Mol. Biol. Rev.* **80**, 187–203 (2016).

3.      Lange, R. & Hengge-Aronis, R. Growth phase-regulated expression of *bolA* and morphology of stationary-phase *Escherichia coli* cells are controlled by the novel sigma factor sigma S. *J. Bacteriol.* **173**, 4474–81 (1991).

4.      Fawcett, P. T., Gibney, K. M. & Vinette, K. M. *Helicobacter pylori* can be induced to assume the morphology of *Helicobacter heilmannii*. *J. Clin. Microbiol.* **37**, 1045–8 (1999).

5.      Justice, S. S. *et al.* Differentiation and developmental pathways of uropathogenic *Escherichia coli* in urinary tract pathogenesis. *Proc. Natl. Acad. Sci.* **101**, 1333–1338 (2004).

6.      Miyata, M. & Ogaki, H. Cytoskeleton of mollicutes. *J. Mol. Microbiol. Biotechnol.* **11**, 256–264 (2006).

7.      Trachtenberg, S. Mollicutes-Wall-less Bacteria with Internal Cytoskeletons. *J. Struct. Biol.* **124**, 244–256 (1998).

8.      Antunes, A. *et al.* A new lineage of halophilic, wall-less, contractile bacteria from a brine-filled deep of the Red Sea. *J. Bacteriol.* **190**, 3580–7 (2008).

9.      Shih, Y. L. & Rothfield, L. The bacterial cytoskeleton. *Microbiol. Mol. Biol. Rev.* **70**, 729–54 (2006).

10.     Scheffers, D. J. & Pinho, M. G. Bacterial Cell Wall Synthesis : New Insights from Localization Studies. *Microbiol Mol Biol Rev.* **69**, 585–607 (2005).

11.     Goodwin, D. & Shedlarski, G. Purification of Cell Wall Peptidoglycan of the Dimorphic Bacterium *Caulobacter crescentus*. *Arch. Biochem. Biophys.* **170**, 23–36 (1975).

12.     Sycuro, L. K. *et al.* Peptidoglycan cross-linking relaxation promotes *Helicobacter pylori*'s helical shape and stomach colonization. *Cell* **141**, 822–33 (2010).

13.     de Pedro, M. A., Quintela, J. C., Höltje, J. V & Schwarz, H. Murein segregation in *Escherichia coli*. *J. Bacteriol.* **179**, 2823–34 (1997).

14.     Weibull, C. The isolation of protoplasts from *Bacillus megaterium* by controlled treatment with lysozyme. *J. Bacteriol.* **66**, 688–95 (1953).

15.     Gilpin, R. W., Young, F. E. & Chatterjee, A. N. Characterization of a stable L-form of *Bacillus subtilis* 168. *J. Bacteriol.* **113**, 486–99 (1973).

16.     Labischinski, H., Goodell, E. W., Goodell, A. & Hochberg, M. L. Direct proof of a 'more-than-single-layered' peptidoglycan architecture of *Escherichia coli* W7: a neutron small-angle scattering study. *J. Bacteriol.* **173**, 751–6 (1991).

17.     Harz, H., Burgdorf, K. & Höltje, J. V. Isolation and separation of the glycan strands from murein of *Escherichia coli* by reversed-phase high-performance liquid chromatography. *Anal. Biochem.* **190**, 120–8 (1990).

18.  Boneca, I. G., Huang, Z. H., Gage, D. A. & Tomasz, A. Characterization of *Staphylococcus aureus* cell wall glycan strands, evidence for a new beta-N-acetylglucosaminidase activity. *J. Biol. Chem.* **275**, 9910–8 (2000).

19.  Kim, S. J., Chang, J. & Singh, M. Peptidoglycan architecture of Gram-positive bacteria by solid-state NMR. *Biochim. Biophys. Acta* **1848**, 350–62 (2015).

20.  Monteiro, J. M. *et al.* Peptidoglycan synthesis drives an FtsZ-treadmilling-independent step of cytokinesis. *Nature* **554**, 528–532 (2018).

21.  Dutka-Malen, S., Mazodier, P. & Badet, B. Molecular cloning and overexpression of the glucosamine synthetase gene from *Escherichia coli*. *Biochimie* **70**, 287–90 (1988).

22.  Mengin-Lecreulx, D. & van Heijenoort, J. Characterization of the essential gene glmM encoding phosphoglucosamine mutase in *Escherichia coli*. *J. Biol. Chem.* **271**, 32–9 (1996).

23.  Mengin-Lecreulx, D. & van Heijenoort, J. Identification of the *glmU* gene encoding N-acetylglucosamine-1-phosphate uridyltransferase in *Escherichia coli*. *J. Bacteriol.* **175**, 6150–7 (1993).

24.  Kotnik, M., Anderluh, P. S. & Prezelj, A. Development of novel inhibitors targeting intracellular steps of peptidoglycan biosynthesis. *Curr. Pharm. Des.* **13**, 2283–309 (2007).

25.  Bertrand, J. A. *et al.* Determination of the MurD mechanism through crystallographic analysis of enzyme complexes. *J. Mol. Biol.* **289**, 579–590 (1999).

26.  Emanuele, J. J. *et al.* Kinetic and crystallographic studies of *Escherichia coli* UDP-N-acetylmuramate:L-alanine ligase. *Protein Sci.* **5**, 2566–2574 (1996).

27.  Anderson, M. S., Eveland, S. S., Onishi, H. R. & Pompliano, D. L. Kinetic Mechanism of the *Escherichia coli* UDPMurNAc-Tripeptide d-Alanyl-d-alanine-Adding Enzyme: Use of a Glutathione S-Transferase Fusion. (1996). doi:10.1021/BI961872+

28.  Doublet, P., van Heijenoort, J., Bohin, J. P. & Mengin-Lecreulx, D. The *murI* gene of *Escherichia coli* is an essential gene that encodes a glutamate racemase activity. *J. Bacteriol.* **175**, 2970–9 (1993).

29.  Scaletti, E. R., Luckner, S. R. & Krause, K. L. Structural features and kinetic characterization of alanine racemase from *Staphylococcus aureus* (Mu50). *Acta Crystallogr. Sect. D Biol. Crystallogr.* **68**, 82–92 (2012).

30.  Al-Bar, O. A., O'Connor, C. D., Giles, I. G. & Akhtar, M. D-alanine: D-alanine ligase of *Escherichia coli*. Expression, purification and inhibitory studies on the cloned enzyme. *Biochem. J.* **282 ( Pt 3**, 747–52 (1992).

31.  TouzÉ, T. & Mengin-Lecreulx, D. Undecaprenyl Phosphate Synthesis. *EcoSal Plus* **1**, 1–20 (2013).

32.  Neuhaus, F. C. Initial Translocation Reaction in the Biosynthesis of Peptidoglycan by Bacterial Membranes. *Acc. Chem. Res.* **4**, 297–303 (1971).

33.  Mengin-Lecreulx, D., Texier, L., Rousseau, M. & van Heijenoort, J. The *murG* gene of *Escherichia coli* codes for the UDP-N-acetylglucosamine: N-acetylmuramyl-(pentapeptide) pyrophosphoryl-undecaprenol N-acetylglucosamine transferase involved in the membrane steps of

peptidoglycan synthesis. *J. Bacteriol.* **173**, 4625–36 (1991).

34. Schneider, T. *et al.* In vitro assembly of a complete, pentaglycine interpeptide bridge containing cell wall precursor (lipid II-Gly5) of *Staphylococcus aureus*. *Mol. Microbiol.* **53**, 675–685 (2004).

35. Münch, D. *et al.* Identification and in vitro Analysis of the GatD/MurT Enzyme-Complex Catalyzing Lipid II Amidation in *Staphylococcus aureus*. *PLoS Pathog.* **8**, e1002509 (2012).

36. Figueiredo, T. A. *et al.* Identification of Genetic Determinants and Enzymes Involved with the Amidation of Glutamic Acid Residues in the Peptidoglycan of *Staphylococcus aureus*. *PLoS Pathog.* **8**, e1002508 (2012).

37. Kramer, N. E. *et al.* Resistance of Gram-positive bacteria to nisin is not determined by Lipid II levels. *FEMS Microbiol. Lett.* **239**, 157–161 (2004).

38. van Dam, V. *et al.* Transmembrane transport of peptidoglycan precursors across model and bacterial membranes. *Mol. Microbiol.* **64**, 1105–1114 (2007).

39. Lara, B. & Ayala, J. A. Topological characterization of the essential *Escherichia coli* cell division protein FtsW. *FEMS Microbiol. Lett.* **216**, 23–32 (2002).

40. Henriques, A. O., Glaser, P., Piggot, P. J. & Moran, C. P. Control of cell shape and elongation by the *rodA* gene in *Bacillus subtilis*. *Mol. Microbiol.* **28**, 235–247 (1998).

41. Mohammadi, T. *et al.* Identification of FtsW as a transporter of lipid-linked cell wall precursors across the membrane. *EMBO J.* **30**, 1425–1432 (2011).

42. Mohammadi, T. *et al.* Specificity of the transport of lipid II by FtsW in *Escherichia coli*. *J. Biol. Chem.* **289**, 14707–14718 (2014).

43. Sham, L. T. *et al.* MurJ is the flippase of lipid-linked precursors for peptidoglycan biogenesis. *Science* **345**, 220–222 (2014).

44. Meeske, A. J. *et al.* SEDS proteins are a widespread family of bacterial cell wall polymerases. *Nature* **537**, 634–638 (2016).

45. Emami, K. *et al.* RodA as the missing glycosyltransferase in *Bacillus subtilis* and antibiotic discovery for the peptidoglycan polymerase pathway. *Nat. Microbiol.* **2**, 1–8 (2017).

46. Taguchi, A. *et al.* FtsW is a peptidoglycan polymerase that is functional only in complex with its cognate penicillin-binding protein. *Nat. Microbiol.* (2019). doi:10.1038/s41564-018-0345-x

47. Butler, E. K., Davis, R. M., Bari, V., Nicholson, P. A. & Ruiz, N. Structure-function analysis of MurJ reveals a solvent-exposed cavity containing residues essential for peptidoglycan biogenesis in *Escherichia coli*. *J. Bacteriol.* **195**, 4639–4649 (2013).

48. Long, F., Rouquette-Loughlin, C., Shafer, W. M. & Yu, E. W. Functional Cloning and Characterization of the Multidrug Efflux Pumps NorM from *Neisseria gonorrhoeae* and YdhE from *Escherichia coli*. *Antimicrob. Agents Chemother.* **52**, 3052–3060 (2008).

49. Stevenson, G., Andrianopoulos, K., Hobbs, M. & Reeves, P. R. Organization of the *Escherichia coli* K-12 gene cluster responsible for production of the extracellular polysaccharide colanic acid. *J. Bacteriol.* **178**, 4885–93 (1996).

50. Liu, D., Cole, R. A. & Reeves, P. R. An O-antigen processing function

for Wzx (RfbX): a promising candidate for O-unit flippase. *J. Bacteriol.* **178**, 2102–7 (1996).

51. Ruiz, N. Bioinformatics identification of MurJ (MviN) as the peptidoglycan lipid II flippase in *Escherichia coli*. *Proc. Natl. Acad. Sci.* **105**, 15553–15557 (2008).

52. Inoue, A. *et al.* Involvement of an essential gene, *mviN*, in murein synthesis in *Escherichia coli*. *J. Bacteriol.* **190**, 7298–7301 (2008).

53. Meeske, A. J. *et al.* MurJ and a novel lipid II flippase are required for cell wall biogenesis in *Bacillus subtilis*. *Proc. Natl. Acad. Sci.* **112**, 6437–6442 (2015).

54. Huber, J. *et al.* Chemical Genetic Identification of Peptidoglycan Inhibitors Potentiating Carbapenem Activity against Methicillin-Resistant *Staphylococcus aureus*. *Chem. Biol.* **16**, 837–848 (2009).

55. Bolla, J. R. *et al.* Direct observation of the influence of cardiolipin and antibiotics on lipid II binding to MurJ. *Nat. Chem.* **10**, 363–371 (2018).

56. Liu, X., Meiresonne, N. Y., Bouhss, A. & den Blaauwen, T. FtsW activity and lipid II synthesis are required for recruitment of MurJ to midcell during cell division in *Escherichia coli*. *Mol. Microbiol.* **109**, 855–884 (2018).

57. Lovering, A. L., Castro, L. H. De, Lim, D. & Strynadka, N. C. J. Structural Insight into the Transglycosylation Step of Bacterial Cell-Wall Biosynthesis. *Science* **315**, 1402–1405 (2007).

58. Sauvage, E., Kerff, F., Terrak, M., Ayala, J. A. & Charlier, P. The penicillin-binding proteins: Structure and role in peptidoglycan biosynthesis. *FEMS Microbiol. Rev.* **32**, 234–258 (2008).

59. Barrett, D. *et al.* Kinetic Characterization of the Glycosyltransferase Module of *Staphylococcus aureus* PBP2. *J. Bacteriol.* **187**, 2215–2217 (2005).

60. Heaslet, H., Shaw, B., Mistry, A. & Miller, A. A. Characterization of the active site of *S. aureus* monofunctional glycosyltransferase (Mtg) by site-directed mutation and structural analysis of the protein complexed with moenomycin. *J. Struct. Biol.* **167**, 129–135 (2009).

61. Terrak, M. & Nguyen-Distèche, M. Kinetic characterization of the monofunctional glycosyltransferase from *Staphylococcus aureus*. *J. Bacteriol.* **188**, 2528–32 (2006).

62. Reed, P., Veiga, H., Jorge, A. M., Terrak, M. & Pinho, M. G. Monofunctional transglycosylases are not essential for *Staphylococcus aureus* cell wall synthesis. *J. Bacteriol.* **193**, 2549–2556 (2011).

63. Tipper, D. J. & Strominger, J. L. Mechanism of action of penicillins: a proposal based on their structural similarity to acyl-D-alanyl-D-alanine. *Proc. Natl. Acad. Sci. U. S. A.* **54**, 1133–41 (1965).

64. Huber, G. & Nesemann, G. Moenomycin, an inhibitor of cell wall synthesis. *Biochem. Biophys. Res. Commun.* **30**, 7–13 (1968).

65. Nguyen-Distèche, M., Fraipont, C., Buddelmeijer, N. & Nanninga, N. The structure and function of *Escherichia coli* penicillin-binding protein 3. *Cell. Mol. Life Sci. C.* **54**, 309–316 (1998).

66. Wyke, A. W., Ward, J. B., Hayes, M. V & Curtis, N. A. A role *in vivo* for penicillin-binding protein-4 of *Staphylococcus aureus*. *Eur. J. Biochem.* **119**, 389–93 (1981).

67. Hartman, B. J. & Tomasz, A. Low-affinity penicillin-binding protein associated with beta-lactam resistance in *Staphylococcus aureus*. *J.*

*Bacteriol.* **158**, 513–6 (1984).

68. Couto, I. *et al.* Ubiquitous Presence of a *mecA* Homologue in Natural Isolates of *Staphylococcus sciuri*. *Microb. Drug Resist.* **2**, 377–391 (1996).

69. Wada, A. & Watanabe, H. Penicillin-binding protein 1 of *Staphylococcus aureus* is essential for growth. *J. Bacteriol.* **180**, 2759–65 (1998).

70. Land, A. D. *et al.* Requirement of essential Pbp2x and GpsB for septal ring closure in *Streptococcus pneumoniae* D39. *Mol. Microbiol.* **90**, 939–955 (2013).

71. Weiss, D. S. *et al.* Localization of the *Escherichia coli* cell division protein FtsI (PBP3) to the division site and cell pole. *Mol. Microbiol.* **25**, 671–81 (1997).

72. Daniel, R. A., Harry, E. J. & Errington, J. Role of penicillin-binding protein PBP2B in assembly and functioning of the division machinery of *Bacillus subtilis*. *Mol. Microbiol.* **35**, 299–311 (2000).

73. Pereira, S. F. F., Henriques, A. O., Pinho, M. G., de Lencastre, H. & Tomasz, A. Role of PBP1 in cell division of *Staphylococcus aureus*. *J. Bacteriol.* **189**, 3525–31 (2007).

74. Pereira, S. F. F., Henriques, A. O., Pinho, M. G., de Lencastre, H. & Tomasz, A. Evidence for a dual role of PBP1 in the cell division and cell separation of *Staphylococcus aureus*. *Mol. Microbiol.* **72**, 895–904 (2009).

75. Pinho, M. G., Filipe, S. R., de Lencastre, H. & Tomasz, A. Complementation of the essential peptidoglycan transpeptidase function of Penicillin-Binding Protein 2 (PBP2) by the drug resistance protein PBP2A in *Staphylococcus aureus*. *J. Bacteriol.* **183**, 6525–31 (2001).

76. Pinho, M. G., de Lencastre, H. & Tomasz, A. An acquired and a native penicillin-binding protein cooperate in building the cell wall of drug-resistant staphylococci. *Proc. Natl. Acad. Sci.* **98**, 10886–10891 (2001).

77. Leski, T. A. & Tomasz, A. Role of Penicillin-Binding Protein 2 (PBP2) in the Antibiotic Susceptibility and Cell Wall Cross-Linking of *Staphylococcus aureus*: Evidence for the Cooperative Functioning of PBP2, PBP4, and PBP2A. *J. Bacteriol.* **187**, 1815–1824 (2005).

78. Pinho, M. G. & Errington, J. Dispersed mode of *Staphylococcus aureus* cell wall synthesis in the absence of the division machinery. *Mol. Microbiol.* **50**, 871–881 (2003).

79. Pinho, M. G. & Errington, J. Recruitment of penicillin-binding protein PBP2 to the division site of *Staphylococcus aureus* is dependent on its transpeptidation substrates. *Mol. Microbiol.* **55**, 799–807 (2005).

80. Rohs, P. D. A. *et al.* A central role for PBP2 in the activation of peptidoglycan polymerization by the bacterial cell elongation machinery. *PLoS Genet.* **14**, e1007726 (2018).

81. Murray, T., Popham, D. L. & Setlow, P. Identification and characterization of *pbpA* encoding *Bacillus subtilis* penicillin-binding protein 2A. *J. Bacteriol.* **179**, 3021–9 (1997).

82. Berg, K. H., Stamsas, G. A., Straume, D. & Havarstein, L. S. Effects of Low PBP2b Levels on Cell Morphology and Peptidoglycan Composition in *Streptococcus pneumoniae* R6. *J. Bacteriol.* **195**, 4342–4354 (2013).

83. Pinho, M. G., de Lencastre, H. & Tomasz, A. Cloning, characterization, and inactivation of the gene *pbpC*, encoding penicillin-binding protein 3

of *Staphylococcus aureus*. *J. Bacteriol.* **182**, 1074–9 (2000).

84. Atilano, M. L. *et al.* Teichoic acids are temporal and spatial regulators of peptidoglycan cross-linking in *Staphylococcus aureus*. *Proc. Nati. Acad. Sci. U S A* **107**, (2010).

85. Monteiro, J. M. *et al.* Cell shape dynamics during the staphylococcal cell cycle. *Nat. Commun.* **6**, 8055 (2015).

86. Lu, W. P. *et al.* Penicillin-Binding Protein 2a from Methicillin-Resistant *Staphylococcus aureus* : Kinetic Characterization of Its Interactions with β-Lactams Using Electrospray Mass Spectrometry. *Biochemistry* **38**, 6537–6546 (1999).

87. Fuda, C., Suvorov, M., Vakulenko, S. B. & Mobashery, S. The Basis for Resistance to β-Lactam Antibiotics by Penicillin-binding Protein 2a of Methicillin-resistant *Staphylococcus aureus*. *J. Biol. Chem.* **279**, 40802–40806 (2004).

88. McPherson, D. C. & Popham, D. L. Peptidoglycan synthesis in the absence of class A penicillin-binding proteins in *Bacillus subtilis*. *J. Bacteriol.* **185**, 1423–31 (2003).

89. Arbeloa, A. *et al.* Role of class A penicillin-binding proteins in PBP5-mediated beta-lactam resistance in *Enterococcus faecalis*. *J. Bacteriol.* **186**, 1221–8 (2004).

90. Matsuzawa, H., Hayakawa, K., Sato, T. & Imahori, K. Characterization and genetic analysis of a mutant of *Escherichia coli* K-12 with rounded morphology. *J. Bacteriol.* **115**, 436–42 (1973).

91. Fraipont, C. *et al.* The integral membrane FtsW protein and peptidoglycan synthase PBP3 form a subcomplex in *Escherichia coli*. *Microbiology* **157**, 251–259 (2011).

92. Leclercq, S. *et al.* Interplay between Penicillin-binding proteins and SEDS proteins promotes bacterial cell wall synthesis. *Sci. Rep.* **7**, 1–13 (2017).

93. Goehring, N. W., Gonzalez, M. D. & Beckwith, J. Premature targeting of cell division proteins to midcell reveals hierarchies of protein interactions involved in divisome assembly. *Mol. Microbiol.* **61**, 33–45 (2006).

94. Matsuzawa, H. *et al.* Nucleotide sequence of the *rodA* gene, responsible for the rod shape of *Escherichia coli*: *rodA* and the *pbpA* gene, encoding penicillin-binding protein 2, constitute the *rodA* operon. *J. Bacteriol.* **171**, 558–60 (1989).

95. Sjodt, M. *et al.* Structure of the peptidoglycan polymerase RodA resolved by evolutionary coupling analysis. *Nature* **556**, 118–121 (2018).

96. Henrichfreise, B., Brunke, M. & Viollier, P. H. Dispatches Bacterial Surfaces : The Wall that SEDS Built. *Curr. Biol.* **26**, R1158–R1160 (2016).

97. Daniel, R. A., Williams, A. M. & Errington, J. A complex four-gene operon containing essential cell division gene *pbpB* in *Bacillus subtilis*. *J. Bacteriol.* **178**, 2343–50 (1996).

98. Gamba, P., Veening, J. W., Saunders, N. J., Hamoen, L. W. & Daniel, R. A. Two-Step Assembly Dynamics of the *Bacillus subtilis* Divisome. *J. Bacteriol.* **191**, 4186–4194 (2009).

99. Perez, A. J. *et al.* Movement dynamics of divisome proteins and PBP2x:FtsW in cells of *Streptococcus pneumoniae*. *Proc. Natl. Acad. Sci. U. S. A.* 201816018 (2019). doi:10.1073/pnas.1816018116

100. Mercer, K. L. N. & Weiss, D. S. The *Escherichia coli* cell division protein FtsW is required to recruit its cognate transpeptidase, FtsI (PBP3), to the division site. *J. Bacteriol.* **184**, 904–12 (2002).
101. Gamba, P., Hamoen, L. W. & Daniel, R. A. Cooperative Recruitment of FtsW to the Division Site of *Bacillus subtilis*. *Front. Microbiol.* **7**, (2016).
102. Cho, H. *et al.* Bacterial cell wall biogenesis is mediated by SEDS and PBP polymerase families functioning semi-autonomously. *Nat. Microbiol.* **1**, 1–8 (2016).
103. Philippe, J., Vernet, T. & Zapun, A. The Elongation of Ovococci. *Microb. Drug Resist.* **20**, 215–221 (2014).
104. Domínguez-Escobar, J. *et al.* Processive movement of MreB-associated cell wall biosynthetic complexes in bacteria. *Science* **333**, 225–8 (2011).
105. Garner, E. C. *et al.* Coupled, circumferential motions of the cell wall synthesis machinery and MreB filaments in *B. subtilis*. *Science* **333**, 222–225 (2011).
106. Ishino, F. *et al.* Peptidoglycan synthetic activities in membranes of *Escherichia coli* caused by overproduction of Penicillin-binding protein 2 and RodA protein. *J. Biol. Chem.* **261**, 7024–31 (1986).
107. Straume, D., Stamsås, G. A., Berg, K. H., Salehian, Z. & Håvarstein, L. S. Identification of pneumococcal proteins that are functionally linked to penicillin-binding protein 2b (PBP2b). *Mol. Microbiol.* **103**, 99–116 (2017).
108. Du, S. & Lutkenhaus, J. Assembly and activation of the *Escherichia coli* divisome. *Mol. Microbiol.* **105**, 177–187 (2017).
109. Löwe, J. & Amos, L. A. Crystal structure of the bacterial cell-division protein FtsZ. *Nature* **391**, 203–206 (1998).
110. Levin, P. A., Kurtser, I. G. & Grossman, A. D. Identification and characterization of a negative regulator of FtsZ ring formation in *Bacillus subtilis*. *Proc. Natl. Acad. Sci. U. S. A.* **96**, 9642–7 (1999).
111. Nogales, E., Downing, K. H., Amos, L. A. & Lowe, J. Tubulin and FtsZ form a distinct family of GTPases. *Nat. Struct. Biol.* **5**, 451–458 (1998).
112. Ma, X. & Margolin, W. Genetic and functional analyses of the conserved C-terminal core domain of *Escherichia coli* FtsZ. *J. Bacteriol.* **181**, 7531–44 (1999).
113. Yan, K., Pearce, K. H. & Payne, D. J. A Conserved Residue at the Extreme C-Terminus of FtsZ Is Critical for the FtsA-FtsZ Interaction in *Staphylococcus aureus*. *Biochem. Biophys. Res. Commun.* **270**, 387–392 (2000).
114. Król, E. *et al. Bacillus subtilis* SepF Binds to the C-Terminus of FtsZ. *PLoS One* **7**, e43293 (2012).
115. Son, S. H. & Lee, H. H. The N-terminal domain of EzrA binds to the C terminus of FtsZ to inhibit *Staphylococcus aureus* FtsZ polymerization. *Biochem. Biophys. Res. Commun.* **433**, 108–114 (2013).
116. Mukherjee, A. & Lutkenhaus, J. Guanine nucleotide-dependent assembly of FtsZ into filaments. *J. Bacteriol.* **176**, 2754–8 (1994).
117. Bi, E. & Lutkenhaus, J. FtsZ ring structure associated with division in *Escherichia coli*. *Nature* **354**, 161–164 (1991).
118. Mannik, J. *et al.* Robustness and accuracy of cell division in *Escherichia coli* in diverse cell shapes. *Proc. Natl. Acad. Sci.* **109**, 6957–6962 (2012).

119. Rowlett, V. W. & Margolin, W. The bacterial Min system. *Curr. Biol.* **23**, R553–R556 (2013).

120. Raskin, D. M. & de Boer, P. A. Rapid pole-to-pole oscillation of a protein required for directing division to the middle of *Escherichia coli*. *Proc. Natl. Acad. Sci. U. S. A.* **96**, 4971–6 (1999).

121. Eswaramoorthy, P. *et al.* Cellular architecture mediates DivIVA ultrastructure and regulates Min activity in *Bacillus subtilis*. *MBio* **2**, e00257-11 (2011).

122. Wu, L. J. & Errington, J. Coordination of Cell Division and Chromosome Segregation by a Nucleoid Occlusion Protein in *Bacillus subtilis*. *Cell* **117**, 915–925 (2004).

123. Bernhardt, T. G. & de Boer, P. A. J. SlmA, a Nucleoid-Associated, FtsZ Binding Protein Required for Blocking Septal Ring Assembly over Chromosomes in *E. coli*. *Mol. Cell* **18**, 555–564 (2005).

124. Veiga, H., Jorge, A. M. & Pinho, M. G. Absence of nucleoid occlusion effector Noc impairs formation of orthogonal FtsZ rings during *Staphylococcus aureus* cell division. *Mol. Microbiol.* **80**, 1366–1380 (2011).

125. Adams, D. W., Wu, L. J. & Errington, J. Nucleoid occlusion protein Noc recruits DNA to the bacterial cell membrane. *EMBO J.* **34**, 491–501 (2015).

126. Cho, H., McManus, H. R., Dove, S. L. & Bernhardt, T. G. Nucleoid occlusion factor SlmA is a DNA-activated FtsZ polymerization antagonist. *Proc. Natl. Acad. Sci.* **108**, 3773–3778 (2011).

127. Pang, T., Wang, X., Lim, H. C., Bernhardt, T. G. & Rudner, D. Z. The nucleoid occlusion factor Noc controls DNA replication initiation in *Staphylococcus aureus*. *PLoS Genet.* **13**, e1006908 (2017).

128. Bailey, M. W., Bisicchia, P., Warren, B. T., Sherratt, D. J. & Männik, J. Evidence for Divisome Localization Mechanisms Independent of the Min System and SlmA in *Escherichia coli*. *PLoS Genet.* **10**, e1004504 (2014).

129. Rodrigues, C. D. A. & Harry, E. J. The Min System and Nucleoid Occlusion Are Not Required for Identifying the Division Site in *Bacillus subtilis* but Ensure Its Efficient Utilization. *PLoS Genet.* **8**, e1002561 (2012).

130. Fleurie, A. *et al.* MapZ marks the division sites and positions FtsZ rings in *Streptococcus pneumoniae*. *Nature* **516**, 259–262 (2014).

131. Treuner-Lange, A. *et al.* PomZ, a ParA-like protein, regulates Z-ring formation and cell division in *Myxococcus xanthus*. *Mol. Microbiol.* **87**, 235–253 (2013).

132. Willemse, J., Borst, J. W., de Waal, E., Bisseling, T. & van Wezel, G. P. Positive control of cell division: FtsZ is recruited by SsgB during sporulation of *Streptomyces*. *Genes Dev.* **25**, 89–99 (2011).

133. Aarsman, M. E. G. *et al.* Maturation of the *Escherichia coli* divisome occurs in two steps. *Mol. Microbiol.* **55**, 1631–1645 (2005).

134. Egan, A. J. F. & Vollmer, W. The physiology of bacterial cell division. *Ann. N. Y. Acad. Sci.* **1277**, 8–28 (2013).

135. Potluri, L. P., Kannan, S. & Young, K. D. ZipA Is Required for FtsZ-Dependent Preseptal Peptidoglycan Synthesis prior to Invagination during Cell Division. *J. Bacteriol.* **194**, 5334–5342 (2012).

136. Aaron, M. *et al.* The tubulin homologue FtsZ contributes to cell

elongation by guiding cell wall precursor synthesis in *Caulobacter crescentus*. *Mol. Microbiol.* **64**, 938–952 (2007).

137. Pichoff, S. & Lutkenhaus, J. Unique and overlapping roles for ZipA and FtsA in septal ring assembly in *Escherichia coli*. *EMBO J.* **21**, 685–93 (2002).

138. Hale, C. A. & de Boer, P. A. Direct binding of FtsZ to ZipA, an essential component of the septal ring structure that mediates cell division in *E. coli*. *Cell* **88**, 175–85 (1997).

139. Addinall, S. G. & Lutkenhaus, J. FtsA is localized to the septum in an FtsZ-dependent manner. *J. Bacteriol.* **178**, 7167–72 (1996).

140. Hale, C. A. & de Boer, P. A. Recruitment of ZipA to the septal ring of *Escherichia coli* is dependent on FtsZ and independent of FtsA. *J. Bacteriol.* **181**, 167–76 (1999).

141. Dai, K. & Lutkenhaus, J. The proper ratio of FtsZ to FtsA is required for cell division to occur in *Escherichia coli*. *J. Bacteriol.* **174**, 6145–51 (1992).

142. Fujita, J. *et al.* Crystal structure of FtsA from *Staphylococcus aureus*. *FEBS Lett.* **588**, 1879–1885 (2014).

143. Haeusser, D. P. & Margolin, W. Splitsville: structural and functional insights into the dynamic bacterial Z ring. *Nat. Rev. Microbiol.* **14**, 305–19 (2016).

144. Ishikawa, S., Kawai, Y., Hiramatsu, K., Kuwano, M. & Ogasawara, N. A new FtsZ-interacting protein, YlmF, complements the activity of FtsA during progression of cell division in *Bacillus subtilis*. *Mol. Microbiol.* **60**, 1364–1380 (2006).

145. Jorge, A. M., Hoiczyk, E., Gomes, J. P. & Pinho, M. G. EzrA contributes to the regulation of cell size in *Staphylococcus aureus*. *PLoS One* **6**, (2011).

146. Steele, V. R., Bottomley, A. L., Garcia-Lara, J., Kasturiarachchi, J. & Foster, S. J. Multiple essential roles for EzrA in cell division of *Staphylococcus aureus*. *Mol. Microbiol.* **80**, 542–555 (2011).

147. Cleverley, R. M. *et al.* Structure and function of a spectrin-like regulator of bacterial cytokinesis. *Nat. Commun.* **5**, 5421 (2014).

148. Machnicka, B. *et al.* Spectrins: A structural platform for stabilization and activation of membrane channels, receptors and transporters. *Biochim. Biophys. Acta* **1838**, 620–634 (2014).

149. den Blaauwen, T., Hamoen, L. W. & Levin, P. A. The divisome at 25: the road ahead. *Curr. Opin. Microbiol.* **36**, 85–94 (2017).

150. Daniel, R. A., Noirot-Gros, M. F., Noirot, P. & Errington, J. Multiple interactions between the transmembrane division proteins of *Bacillus subtilis* and the role of FtsL instability in divisome assembly. *J. Bacteriol.* **188**, 7396–404 (2006).

151. Daniel, R. A. & Errington, J. Intrinsic instability of the essential cell division protein FtsL of *Bacillus subtilis* and a role for DivIB protein in FtsL turnover. *Mol. Microbiol.* **36**, 278–89 (2000).

152. Robson, S. A., Michie, K. A., Mackay, J. P., Harry, E. & King, G. F. The *Bacillus subtilis* cell division proteins FtsL and DivIC are intrinsically unstable and do not interact with one another in the absence of other septasomal components. *Mol. Microbiol.* **44**, 663–74 (2002).

153. Buddelmeijer, N. & Beckwith, J. A complex of the *Escherichia coli* cell division proteins FtsL, FtsB and FtsQ forms independently of its

localization to the septal region. *Mol. Microbiol.* **52**, 1315–1327 (2004).

154. Rowland, S. L. *et al.* Evidence from Artificial Septal Targeting and Site-Directed Mutagenesis that Residues in the Extracytoplasmic Domain of DivIB Mediate Its Interaction with the Divisomal Transpeptidase PBP 2B. *J. Bacteriol.* **192**, 6116–6125 (2010).

155. Errington, J., Daniel, R. A. & Scheffers, D. J. Cytokinesis in bacteria. *Microbiol. Mol. Biol. Rev.* **67**, 52–65, table of contents (2003).

156. Buddelmeijer, N. & Beckwith, J. Assembly of cell division proteins at the *E. coli* cell center. *Curr. Opin. Microbiol.* **5**, 553–557 (2002).

157. Goehring, N. W., Gueiros-Filho, F. & Beckwith, J. Premature targeting of a cell division protein to midcell allows dissection of divisome assembly in *Escherichia coli*. *Genes Dev.* **19**, 127–137 (2005).

158. Busiek, K. K. & Margolin, W. A role for FtsA in SPOR-independent localization of the essential *Escherichia coli* cell division protein FtsN. *Mol. Microbiol.* **92**, 1212–1226 (2014).

159. Liu, B., Persons, L., Lee, L. & de Boer, P. A. J. Roles for both FtsA and the FtsBLQ subcomplex in FtsN-stimulated cell constriction in *Escherichia coli*. *Mol. Microbiol.* **95**, 945–970 (2015).

160. Möll, A. & Thanbichler, M. FtsN-like proteins are conserved components of the cell division machinery in proteobacteria. *Mol. Microbiol.* **72**, 1037–1053 (2009).

161. Daniel, R. A., Harry, E. J., Katis, V. L., Wake, R. G. & Errington, J. Characterization of the essential cell division gene *ftsL*(*yIID*) of *Bacillus subtilis* and its role in the assembly of the division apparatus. *Mol. Microbiol.* **29**, 593–604 (1998).

162. Bottomley, A. L. *et al.* *Staphylococcus aureus* DivIB is a peptidoglycan-binding protein that is required for a morphological checkpoint in cell division. *Mol. Microbiol.* **94**, 1041–1064 (2014).

163. Boyle, D. S., Khattar, M. M., Addinall, S. G., Lutkenhaus, J. & Donachie, W. D. *ftsW* is an essential cell-division gene in *Escherichia coli*. *Mol. Microbiol.* **24**, 1263–1273 (1997).

164. Süel, G. M., Kulkarni, R. P., Dworkin, J., Garcia-Ojalvo, J. & Elowitz, M. B. Tunability and noise dependence in differentiation dynamics. *Science* **315**, 1716–9 (2007).

165. Mistry, B. V, Del Sol, R., Wright, C., Findlay, K. & Dyson, P. FtsW is a dispensable cell division protein required for Z-ring stabilization during sporulation septation in *Streptomyces coelicolor*. *J. Bacteriol.* **190**, 5555–66 (2008).

166. Datta, P. *et al.* Interaction between FtsW and penicillin-binding protein 3 (PBP3) directs PBP3 to mid-cell, controls cell septation and mediates the formation of a trimeric complex involving FtsZ, FtsW and PBP3 in mycobacteria. *Mol. Microbiol.* **62**, 1655–73 (2006).

167. Datta, P., Dasgupta, A., Bhakta, S. & Basu, J. Interaction between FtsZ and FtsW of *Mycobacterium tuberculosis*. *J. Biol. Chem.* **277**, 24983–7 (2002).

168. Jones, L. J., Carballido-López, R. & Errington, J. Control of cell shape in bacteria: helical, actin-like filaments in *Bacillus subtilis*. *Cell* **104**, 913–22 (2001).

169. Abhayawardhane, Y. & Stewart, G. C. *Bacillus subtilis* possesses a second determinant with extensive sequence similarity to the *Escherichia coli mreB* morphogene. *J. Bacteriol.* **177**, 765–73 (1995).

170. Normark, S. Mutation in *Escherichia coli* K-12 mediating spherelike envelopes and changes tolerance to ultraviolet irradiation and some antibiotics. *J. Bacteriol.* **98**, 1274–7 (1969).

171. Wachi, M. *et al.* Mutant isolation and molecular cloning of mre genes, which determine cell shape, sensitivity to mecillinam, and amount of penicillin-binding proteins in *Escherichia coli*. *J. Bacteriol.* **169**, 4935–40 (1987).

172. Kruse, T., Bork-Jensen, J. & Gerdes, K. The morphogenetic MreBCD proteins of *Escherichia coli* form an essential membrane-bound complex. *Mol. Microbiol.* **55**, 78–89 (2005).

173. Soufo, H. J. D. & Graumann, P. L. Actin-like Proteins MreB and Mbl from *Bacillus subtilis* Are Required for Bipolar Positioning of Replication Origins. *Curr. Biol.* **13**, 1916–1920 (2003).

174. van den Ent, F., Amos, L. A. & Löwe, J. Prokaryotic origin of the actin cytoskeleton. *Nature* **413**, 39–44 (2001).

175. Esue, O., Cordero, M., Wirtz, D. & Tseng, Y. The assembly of MreB, a prokaryotic homolog of actin. *J. Biol. Chem.* **280**, 2628–35 (2005).

176. van den Ent, F., Izoré, T., Bharat, T. A., Johnson, C. M. & Löwe, J. Bacterial actin MreB forms antiparallel double filaments. *Elife* **3**, e02634 (2014).

177. Salje, J., van den Ent, F., de Boer, P. & Löwe, J. Direct membrane binding by bacterial actin MreB. *Mol. Cell* **43**, 478–87 (2011).

178. Shih, Y. L., Le, T. & Rothfield, L. Division site selection in *Escherichia coli* involves dynamic redistribution of Min proteins within coiled structures that extend between the two cell poles. *Proc. Natl. Acad. Sci. U. S. A.* **100**, 7865–70 (2003).

179. van Teeffelen, S. *et al.* The bacterial actin MreB rotates, and rotation depends on cell-wall assembly. *Proc. Natl. Acad. Sci.* **108**, 15822–15827 (2011).

180. Daniel, R. A. & Errington, J. Control of cell morphogenesis in bacteria: two distinct ways to make a rod-shaped cell. *Cell* **113**, 767–76 (2003).

181. Ursell, T. S. *et al.* Rod-like bacterial shape is maintained by feedback between cell curvature and cytoskeletal localization. *Proc. Natl. Acad. Sci.* **111**, E1025–E1034 (2014).

182. Billings, G. *et al.* De novo morphogenesis in L-forms via geometric control of cell growth. *Mol. Microbiol.* **93**, 883–96 (2014).

183. Hussain, S. *et al.* MreB filaments align along greatest principal membrane curvature to orient cell wall synthesis. *Elife* **7**, 1–45 (2018).

184. Wei, Y., Havasy, T., McPherson, D. C. & Popham, D. L. Rod shape determination by the *Bacillus subtilis* class B penicillin-binding proteins encoded by *pbpA* and *pbpH*. *J. Bacteriol.* **185**, 4717–26 (2003).

185. Kawai, Y., Daniel, R. A. & Errington, J. Regulation of cell wall morphogenesis in *Bacillus subtilis* by recruitment of PBP1 to the MreB helix. *Mol. Microbiol.* **71**, 1131–1144 (2009).

186. Kawai, Y., Asai, K. & Errington, J. Partial functional redundancy of MreB isoforms, MreB, Mbl and MreBH, in cell morphogenesis of *Bacillus subtilis*. *Mol. Microbiol.* **73**, 719–731 (2009).

187. Stewart, G. C. Taking shape: control of bacterial cell wall biosynthesis. *Mol. Microbiol.* **57**, 1177–1181 (2005).

188. Leaver, M. & Errington, J. Roles for MreC and MreD proteins in helical growth of the cylindrical cell wall in *Bacillus subtilis*. *Mol. Microbiol.* **57**,

1196–209 (2005).

189. Van Den Ent, F. *et al.* Dimeric structure of the cell shape protein MreC and its functional implications. *Mol. Microbiol.* **62**, 1631–1642 (2006).

190. Chastanet, A. & Carballido-Lopez, R. The actin-like MreB proteins in *Bacillus subtilis*: a new turn. *Front. Biosci. (Schol. Ed).* **4**, 1582–606 (2012).

191. Divakaruni, A. V, Loo, R. R. O., Xie, Y., Loo, J. A. & Gober, J. W. The cell-shape protein MreC interacts with extracytoplasmic proteins including cell wall assembly complexes in *Caulobacter crescentus*. *Proc. Nati. Acad. Sci. U S A* **102**, 18602–7 (2005).

192. White, C. L., Kitich, A. & Gober, J. W. Positioning cell wall synthetic complexes by the bacterial morphogenetic proteins MreB and MreD. *Mol. Microbiol.* **76**, 616–33 (2010).

193. Defeu Soufo, H. J. & Graumann, P. L. *Bacillus subtilis* actin-like protein MreB influences the positioning of the replication machinery and requires membrane proteins MreC/D and other actin-like proteins for proper localization. *BMC Cell Biol.* **6**, 10 (2005).

194. Contreras-Martel, C. *et al.* Molecular architecture of the PBP2-MreC core bacterial cell wall synthesis complex. *Nat. Commun.* **8**, 776 (2017).

195. Cho, H., Uehara, T. & Bernhardt, T. G. Beta-lactam antibiotics induce a lethal malfunctioning of the bacterial cell wall synthesis machinery. *Cell* **159**, 1300–11 (2014).

196. Brown, P. J. B. *et al.* Polar growth in the Alphaproteobacterial order Rhizobiales. *Proc. Natl. Acad. Sci.* **109**, 1697–1701 (2012).

197. Howell, M. & Brown, P. J. Building the bacterial cell wall at the pole. *Curr. Opin. Microbiol.* **34**, 53–59 (2016).

198. Kang, C. M., Nyayapathy, S., Lee, J. Y., Suh, J. W. & Husson, R. N. Wag31, a homologue of the cell division protein DivIVA, regulates growth, morphology and polar cell wall synthesis in mycobacteria. *Microbiology* **154**, 725–735 (2008).

199. Letek, M. *et al.* DivIVA is required for polar growth in the MreB-lacking rod-shaped actinomycete *Corynebacterium glutamicum*. *J. Bacteriol.* **190**, 3283–92 (2008).

200. Hempel, A. M., Wang, S., Letek, M., Gil, J. A. & Flärdh, K. Assemblies of DivIVA mark sites for hyphal branching and can establish new zones of cell wall growth in *Streptomyces coelicolor*. *J. Bacteriol.* **190**, 7579–83 (2008).

201. Zupan, J. R., Cameron, T. A., Anderson-Furgeson, J. & Zambryski, P. C. Dynamic FtsA and FtsZ localization and outer membrane alterations during polar growth and cell division in *Agrobacterium tumefaciens*. *Proc. Natl. Acad. Sci.* **110**, 9060–9065 (2013).

202. Cameron, T. A., Anderson-Furgeson, J., Zupan, J. R., Zik, J. J. & Zambryski, P. C. Peptidoglycan Synthesis Machinery in *Agrobacterium tumefaciens* During Unipolar Growth and Cell Division. *MBio* **5**, e01219-14 (2014).

203. Higgins, M. L. & Shockman, G. D. Study of cycle of cell wall assembly in *Streptococcus faecalis* by three-dimensional reconstructions of thin sections of cells. *J. Bacteriol.* **127**, 1346–58 (1976).

204. Pinho, M. G., Kjos, M. & Veening, J. W. How to get (a)round: mechanisms controlling growth and division of coccoid bacteria. *Nat. Rev. Microbiol.* **11**, 601–14 (2013).

205. Massidda, O., Nováková, L. & Vollmer, W. From models to pathogens: how much have we learned about *Streptococcus pneumoniae* cell division? *Environ. Microbiol.* **15**, 3133–3157 (2013).

206. Peters, K. *et al. Streptococcus pneumoniae* PBP2x mid-cell localization requires the C-terminal PASTA domains and is essential for cell shape maintenance. *Mol. Microbiol.* **92**, 733–755 (2014).

207. Pérez-Núñez, D. *et al.* A new morphogenesis pathway in bacteria: unbalanced activity of cell wall synthesis machineries leads to coccus-to-rod transition and filamentation in ovococci. *Mol. Microbiol.* **79**, 759–771 (2011).

208. Thibessard, A., Fernandez, A., Gintz, B., Leblond-Bourget, N. & Decaris, B. Effects of *rodA* and *pbp2b* disruption on cell morphology and oxidative stress response of *Streptococcus thermophilus* CNRZ368. *J. Bacteriol.* **184**, 2821–6 (2002).

209. Land, A. D. & Winkler, M. E. The requirement for pneumococcal MreC and MreD is relieved by inactivation of the gene encoding PBP1a. *J. Bacteriol.* **193**, 4166–79 (2011).

210. Zapun, A., Vernet, T. & Pinho, M. G. The different shapes of cocci. *FEMS Microbiol. Rev.* **32**, 345–60 (2008).

211. Wheeler, R., Mesnage, S., Boneca, I. G., Hobbs, J. K. & Foster, S. J. Super-resolution microscopy reveals cell wall dynamics and peptidoglycan architecture in ovococcal bacteria. *Mol. Microbiol.* **82**, 1096–1109 (2011).

212. Tsui, H. C. T. *et al.* Pbp2x localizes separately from Pbp2b and other peptidoglycan synthesis proteins during later stages of cell division of *Streptococcus pneumoniae* D39. *Mol. Microbiol.* **94**, 21–40 (2014).

213. Fleurie, A. *et al.* Interplay of the Serine/Threonine-Kinase StkP and the Paralogs DivIVA and GpsB in Pneumococcal Cell Elongation and Division. *PLoS Genet.* **10**, e1004275 (2014).

214. David, B. *et al.* PBP2b plays a key role in both peripheral growth and septum positioning in *Lactococcus lactis*. *PLoS One* **13**, e0198014 (2018).

215. Fiuza, M. *et al.* From the characterization of the four serine/threonine protein kinases (PknA/B/G/L) of *Corynebacterium glutamicum* toward the role of PknA and PknB in cell division. *J. Biol. Chem.* **283**, 18099–112 (2008).

216. Kang, C. M. *et al.* The Mycobacterium tuberculosis serine/threonine kinases PknA and PknB: substrate identification and regulation of cell shape. *Genes Dev.* **19**, 1692–704 (2005).

217. Beilharz, K. *et al.* Control of cell division in *Streptococcus pneumoniae* by the conserved Ser/Thr protein kinase StkP. *Proc. Natl. Acad. Sci.* **109**, E905–E913 (2012).

218. Nováková, L. *et al.* Identification of multiple substrates of the StkP Ser/Thr protein kinase in *Streptococcus pneumoniae*. *J. Bacteriol.* **192**, 3629–38 (2010).

219. Gautam, S., Kim, T. & Spiegel, D. A. Chemical Probes Reveal an Extraseptal Mode of Cross-Linking in *Staphylococcus aureus*. *J. Am. Chem. Soc.* **137**, 7441–7447 (2015).

220. Chaudhuri, R. R. *et al.* Comprehensive identification of essential *Staphylococcus aureus* genes using Transposon-Mediated Differential Hybridisation (TMDH). *BMC Genomics* **10**, 291 (2009).

221. Widhelm, T. J. *et al.* A Genetic Resource for Rapid and Comprehensive Phenotype Screening of Nonessential *Staphylococcus aureus* Genes. *MBio* **4**, 1–8 (2014).

222. Wertheim, H. *et al.* The role of nasal carriage in *Staphylococcus aureus* infections. *Lancet Infect. Dis.* **5**, 751–762 (2005).

223. Kluytmans, J., van Belkum, A. & Verbrugh, H. Nasal carriage of *Staphylococcus aureus*: epidemiology, underlying mechanisms, and associated risks. *Clin. Microbiol. Rev.* **10**, 505–20 (1997).

224. Tong, S. Y. C., Davis, J. S., Eichenberger, E., Holland, T. L. & Fowler, V. G. *Staphylococcus aureus* Infections: Epidemiology, Pathophysiology, Clinical Manifestations, and Management. *Clin. Microbiol. Rev.* **28**, 603–661 (2015).

225. David, M. Z. & Daum, R. S. Treatment of *Staphylococcus aureus* Infections. in *Current topics in microbiology and immunology* **409**, 325–383 (2017).

226. European Centre for Disease Prevention and Control. Surveillance of antimicrobial resistance in Europe – Annual report of the European Antimicrobial Resistance Surveillance Network (EARS-Net) 2017. *Stockholm: ECDC* (2018). doi:10.2900/296939

227. International Working Group on the Classification of Staphylococcal Cassette Chromosome Elements (IWG-SCC). Classification of Staphylococcal Cassette Chromosome *mec* (SCC*mec*): Guidelines for Reporting Novel SCC*mec* Elements. *Antimicrob. Agents Chemother.* **53**, 4961–4967 (2009).

228. Centers for Disease Control and Prevention (CDC). *Staphylococcus aureus* resistant to vancomycin-United States, 2002. *MMWR. Morb. Mortal. Wkly. Rep.* **51**, 565–7 (2002).

229. Emaneini, M. *et al.* Isolation of vancomycin-resistant *Staphylococcus aureus* in a teaching hospital in Tehran. *J. Hosp. Infect.* **66**, 92–3 (2007).

230. Liaqat, F. *et al.* Report-Isolation identification and control of vancomycin resistant *Staphylococcus aureus*. *Pak. J. Pharm. Sci.* **28**, 997–1004 (2015).

# CHAPTER II

**MreC and MreD proteins are not required for growth of *Staphylococcus aureus***

**Author contributions**

A. C. Tavares performed all experiments, except data analysis on *S. aureus* volume and NADA incorporation performed by P. B. Fernandes.

**Data contained in this chapter was published in:**

**Tavares, A. C.**, Fernandes, P. B., Carballido-López, R. & Pinho, M. G. MreC and MreD proteins are not required for growth of *Staphylococcus aureus*. *PLoS One* **10**(10): e0140523 (2015).

## ABSTRACT

The transmembrane proteins MreC and MreD are present in a wide variety of bacteria and are thought to be involved in cell shape determination. Together with the actin homologue MreB and other morphological elements, they play an essential role in the synthesis of the lateral cell wall in rod-shaped bacteria. In ovococcus, which lack MreB homologues, *mreCD* are also essential and have been implicated in peripheral cell wall synthesis. In this work we addressed the possible roles of MreC and MreD in the spherical pathogen *Staphylococcus aureus*. We show that MreC and MreD are not essential for cell viability and do not seem to affect cell morphology, cell volume or cell cycle control. MreC and MreD localize preferentially to the division septa, but do not appear to influence peptidoglycan composition, nor the susceptibility to different antibiotics and to oxidative and osmotic stress agents. Our results suggest that the function of MreCD in *S. aureus* is not critical for cell division and cell shape determination.

## INTRODUCTION

*Staphylococcus aureus* is a gram-positive pathogen responsible for many antibiotic-resistant hospital-acquired infections worldwide. It is well known for its capacity to cause various severe diseases such as bacteremia, pneumonia, endocarditis or osteomyelitis and for its increasing spread into the community[1]. Besides its clinical importance, *S. aureus* is also an excellent organism to study fundamental biological questions such as cell division and other cell cycle processes, given its simple shape and genetic tractability. Unlike the widely studied *Escherichia coli* and *Bacillus subtilis*, two rod-shaped model organisms, *S. aureus* is spherical and is therefore a good model to study morphogenesis of coccoid bacteria.

In most bacteria, a major factor contributing to the maintenance of cell shape is the presence of a cell wall outside the cytoplasmic membrane. The bacterial cell wall is generally composed of peptidoglycan, a mesh-like macromolecule made of glycan chains cross-linked by short peptide bridges. In gram-positive bacteria the peptidoglycan layer is thick (typically 30–100 nm), with proteins and anionic polymers embedded in it[2]. For bacterial cells to maintain a constant shape during growth and division, the activity of penicillin-binding proteins (PBPs), enzymes responsible for peptidoglycan synthesis, must be coordinated with the action of autolysins, which cleave peptidoglycan to allow cell wall expansion and splitting of the two daughter cells.

In rod-shaped bacteria, a second factor essential for the determination of cell shape is the presence of the MreB cytoskeleton. MreB-like proteins are structural homologues of eukaryotic actin that play an essential role in sidewall cylindrical elongation. These proteins have also been involved in other cellular processes like cell polarity and

chromosome dynamics (reviewed in [3]). MreB homologues were proposed to associate in elongation-specific peptidoglycan-synthesizing complexes involved in lateral cell wall synthesis, together with other morphogenetic determinants, namely the transmembrane MreC and MreD proteins, as well as the SEDS protein RodA, PBPs and peptidoglycan hydrolases[4–7]. Recently, total internal reflection fluorescence microscopy (TIRFM) and high-precision particle tracking were used to show that, in *B. subtilis*, MreB isoforms co-localize with MreC, MreD, RodA and the co-essential transpeptidases PBPH and PBP2a, exhibiting circumferential processive motility[8,9]. Movement of these cell elongation machineries is driven by peptidoglycan synthesis itself, and is thought to be restricted and oriented by the underlying MreB filaments[3,8,9].

The roles of MreC and MreD on cell shape determination have been evidenced in different bacterial species. In elongated bacteria, like *B. subtilis*, *E. coli* and *Caulobacter crescentus*, absence of MreC and MreD results in growth arrest and severe morphological defects, as the cells become round, swelled or twisted, and eventually lyse[5,6,10–12]. Additionally, these membrane proteins were found to localize along the sidewall in a pattern similar to MreB[8–10,13] and to interact with peptidoglycan synthesizing enzymes. MreC was shown to interact not only with different PBPs[7,13,14] but also with the lytic transglycosylase MltA, the scaffolding protein MipA and some outer membrane proteins in *C. crescentus*[6,13]. Furthermore, MreD can interact with peptidoglycan biosynthesizing enzymes like MurG and MraY, and its presence is necessary for the correct localization of these proteins[6]. Although a specific function is not yet attributed to MreC and MreD, in rod-shaped bacteria these proteins are therefore thought to couple the internal bacterial cytoskeleton (MreB-like proteins) to the extracellular cell wall synthesizing complexes, coordinating sidewall elongation [7,10,11,13].

MreC is usually composed of one transmembrane domain near its N-terminal and a large C-terminal extracellular domain. In *C. crescentus*, however, this protein seems to be periplasmic[13]. MreD is a polytopic membrane protein predicted to have four to six transmembrane spans.

In coccoid cells, either spherical cocci (e.g staphylococci), or ovococci, with ellipsoid shape (e.g. streptococci), MreB proteins are in general absent but MreC and MreD are still present. Ovoccocci have not only septal peptidoglycan synthesis, but also peripheral peptidoglycan synthesis, responsible for the elongation of these cells, in which MreC and MreD are likely to play a role[15,16]. This is based on the fact that MreC and MreD localize to the equators and division septa of dividing *S. pneumoniae* cells and that MreCD-depletion in this organism leads to arrest of growth, cell rounding and lysis[15]. Interestingly, although MreC and MreD are essential for cell viability and cell shape maintenance in virulent strains D39 or TIGR4[15,17], *mreCD* deletion mutants are viable and display normal growth and morphology in the *S. pneumoniae* laboratory strain R6[15,18], which contains a suppressor mutation in *pbp1a* gene, encoding a PBP that influences the diameter of pneumococcal cells.

In spherical bacteria, such as *S. aureus*, cell wall synthesis occurs mainly at the division septa where the majority of PBPs are localized (reviewed in [19]), although some peptidoglycan synthesis activity is also detectable in the periphery of the cells, mediated mostly by PBP4[20,21]. It is therefore intriguing why these organisms have retained MreC and MreD proteins, despite the lack of an MreB homologue and of a dedicated elongation machinery. While in *B. subtilis mreCD* genes are found immediately downstream of, and are co-transcribed with, *mreB*[22,23] and in *S. pneumoniae*, *mreCD* are found upstream of *pcsB*, a gene important for cell division in ovococcus, but

apparently transcribed independently[18], in *S. aureus*, *mreCD* are not near any gene encoding identified division or morphology-related proteins.

In this work we show that MreC and MreD are not essential for the viability of *S. aureus* cells as no growth, cell morphology or peptidoglycan synthesis defects were found in the absence of these proteins.

## MATERIALS AND METHODS

### Bacterial strains, plasmids and growth conditions

The plasmids and bacterial strains used in this study are described in Tables 1 and 2. *S. aureus* strains were grown at 37°C in tryptic soy broth (TSB; Difco), tryptic soy agar (TSA; Difco) or in SSM9PR minimal media[24] containing 1 x M9 salts ($Na_2HPO_4$ 12.8 g $L^{-1}$, $KH_2PO_4$ 3 g $L^{-1}$, NaCl 5 g $L^{-1}$, $NH_4Cl$ 1 g $L^{-1}$), $MgSO_4$ 2 mM, $CaCl_2$ 0.1 mM, glucose 1%, casaminoacids 1%, Thiamine-HCl 1 mM and nicotinamide 0.05 mM. Culture medium was supplemented with appropriate antibiotics (erythromycin 10 µg $ml^{-1}$, chloramphenicol 10 µg $ml^{-1}$ or kanamycin 150 µg $ml^{-1}$; Sigma-Aldrich), with 100 µg $ml^{-1}$ 5-bromo-4-chloro-3-indolyl-β-D-galactopyranoside (X-Gal; VWR), with isopropyl-β-D-thiogalactopyranoside (IPTG; VWR) or with 0.5 mM $CdCl_2$, when required. *E. coli* strains were grown at 37°C in Luria-Bertani broth (LB; Difco) or in LB agar (Difco) supplemented with ampicillin 100 µg $ml^{-1}$ (Sigma-Aldrich) when necessary.

**Table 1 – Plasmids used in this study.**

| Plasmids | Description | Source or Ref. |
|---|---|---|
| pMAD | *E. coli - S. aureus* shuttle vector with a thermosensitive origin of replication for Gram-positive bacteria, Amp$^R$, Ery$^R$; *lacZ* | 25 |
| pBCB13 | pMAD derivative with up- and downsteam regions of *spa* locus and P*spac-lacI,* Amp$^R$, Ery$^R$; *lacZ* | 26 |
| pMGPII | *S. aureus* replicative plasmid containing *lacI* gene, Amp$^R$, Cam$^R$ | 27 |
| pMutin4 | *E. coli - S. aureus* shuttle vector; integrative in *S. aureus*, IPTG-inducible P*spac* promoter, Amp$^R$, Ery$^R$ | 28 |
| pCNX | Shuttle vector containing a cadmium inducible P*cad* promoter; Amp$^R$ Kan$^R$ | 20 |

| | | |
|---|---|---|
| pET30a | Cloning vector for producing His tag fusions, Kan[R] | Novagen |
| pTRC99a-P7 | Vector containing *p7superfastgfp*, Amp[R] | [29] |
| pSG5082 | *S. aureus* integrative vector for C-terminal GFP fusions. Amp[R], Ery[R] | [30] |
| pFAST2 | pSG5082 derivative for C-terminal fusions with *p7superfastgfp* in the native locus; integrative in *S. aureus*; Amp[R], Ery[R] | This study |
| pMutin4MreCt | pMUTIN4 with putative ribosome binding site and 463 first nucleotides of *mreC* under control of the P*spac* promoter, Amp[R], Ery[R] | This study |
| pΔ*mreC* | pMAD with *mreC* upstream and downstream regions for constructing a null mutant, Amp[R], Ery[R]; *lacZ* | This study |
| pΔ*mreD* | pMAD with *mreD* upstream and downstream regions for constructing a null mutant, Amp[R], Ery[R]; *lacZ* | This study |
| pΔ*mreCD* | pMAD with *mreCD* upstream and downstream regions for constructing a double null mutant, Amp[R], Ery[R]; *lacZ* | This study |
| p*mreCD* | pCNX encoding *mreCD* under the control of P*cad* | This study |
| pETMreCt | pET30a expressing His-MreC | This study |
| psGFPMreC | pBCB13 with s*gfp-mreC* fusion under control of the P*spac* promoter,  Amp[R], Ery[R]; *lacZ* | This study |
| psGFPMreD | pBCB13 with s*gfp-mreD* fusion under control of the P*spac* promoter,  Amp[R], Ery[R]; *lacZ* | This study |
| pFAST2MreDsGFP | pFAST2 with the 483 final nucleotides of *mreD* without the stop codon cloned upstream and in frame with *sgfp;*  Amp[R], Ery[R] | This study |

Abbreviations: Kan[R] – kanamycin resistance; Amp[R] – ampicillin resistance; Cam[R] – Chloramphenicol resistance; Ery[R] – erythromycin resistance.

## Table 2 – Strains used in this study.

| Strains | Description | Source or Ref. |
|---|---|---|
| *E. coli* | | |
| DC10B | *dam*[+] *dcm*[+] *ΔhsdRMS endA1 recA1* | [31] |
| BL21 (DE3) | B F- *dcm ompT hsdS (r$_B$-m$_B$-) gal* λ (DE3) | Stratagene |

**S. aureus**

| | | |
|---|---|---|
| RN4220 | Restriction deficient derivative of NCTC8325-4 | R. Novick |
| NCTC8325-4 | MSSA strain | R. Novick |
| COL | MRSA strain | [32] |
| COL*mreCD*i | COL with *mreCD* operon controlled by P*spac* promoter and transformed with pMGPII plasmid; Ery^R, Cam^R | This study |
| COLΔ*mreC* | COL *mreC* deletion mutant | This study |
| COLΔ*mreD* | COL lacking nucleotides 7-380 of *mreD* | This study |
| COLΔ*mreCD* | COL lacking *mreC* and nucleotides 7-380 of *mreD* | This study |
| NCTCΔ*mreC* | NCTC8325-4 *mreC* deletion mutant | This study |
| NCTCΔ*mreD* | NCTC8325-4 lacking nucleotides 7-380 of *mreD* | This study |
| NCTCΔ*mreCD* | NCTC8325-4 lacking *mreC* and nucleotides 7-380 of *mreD* | This study |
| COLpCNX | COL transformed with pCNX empy vector | This study |
| COLp*mreCD* | COL transformed with p*mreCD*oe plasmid with *mreCD* operon under the control of P*cad* promoter; Kan^R | This study |
| COLsGFPMreC | COL *spa*::P*spac-sgfp-mreC* | This study |
| COLsGFPMreD | COL *spa*::P*spac-sgfp-mreD* | This study |
| COLpFAST2MreDsGFP | COL *mreD*::*mreD-sgfp* fusion, Ery^R | This study |

Abbreviations: Ery^R – erythromycin resistance; Cam^R – chloramphenicol resistance.


## Construction of S. *aureus* strains

Primers used in this study are listed in Table 3. The *mreCD* inducible mutant containing the *mreCD* operon under the control of IPTG-inducible P*spac* promoter was constructed using the integrative vector pMUTIN4[28]. A fragment containing the putative RBS and the first 463 bp of *mreC* gene was amplified by PCR from *S. aureus* COL genomic DNA using primers MreCt-P1 and MreCt-P2. The fragment was digested with *Hind*III and *Bam*HI restriction enzymes, cloned into pMUTIN4 vector in *E. coli*, sequenced, electroporated into *S. aureus*

RN4220 strain at 30°C, using erythromycin selection, and transduced into *S. aureus* COL using phage 80α[33]. The *mreCD* operon was placed under the control of the P*spac* promoter through a single crossover event. To increase the level of repression of the P*spac* promoter, the pMGPII multi-copy plasmid[27] encoding an extra *lacI* gene was also transduced into this strain. All procedures were performed in the presence of 0.5 mM IPTG. The integration of the plasmid into the *mreC* chromosomal locus of the final strain COL*mreCD*i strain was confirmed by PCR amplification.

**Table 3 – Primers used in this study.**

| Primer | Sequence 5' - 3' |
|---|---|
| MreCt-P1 | CCCAAGCTTGACATAATAGAGGTGTTC |
| MreCt-P2 | CGGGATCCCTTTAGTAACTCTTCCAAC |
| dMreC-P1 | CCCCCCGGGATGAACGTGCATCAGTCCTAAG |
| dMreC-P2 | TATCCCTGCTCACCCAGAACACCTCTATTATG |
| dMreC-P3 | GTTCTGGGTGAGCAGGGATAAATAATGCG |
| dMreC-P4 | CGGGATCCAGTGTATGGTTGACGATG |
| dMreD-P1 | CCCCCCGGGCTGGAATGTTTGCTAGTAG |
| dMreD-P2 | CAAATTGAATGACGCATTATTTATCCCTGC |
| dMreD-P3 | AATAATGCGTCATTCAATTTGATATTATTC |
| dMreD-P4 | CGGGATCCGTTTTTTGTAGAACTTACC |
| dMreCD-P2 | CAAATTGAATGCACCCAGAACACCTCTATTATG |
| dMreCD-P3 | GTTCTGGGTGCATTCAATTTGATATTATTC |
| MreC_*Sma*I_P1 | TCCCCCGGGGACATAATAGAGGTGTTCTG |
| MreD_*Eco*RI_P2 | CGGAATTCTTACCATTGACGACGTTTC |
| sGFP-*Eco*RV-P1 | CGCGGATATCAGGAAACAGACCATGGAATTCGAGCTCGGTACACGG |
| sGFP-*Not*I-P2 | GCTTAGCGGCCGCTTAATGGTGATGATGGTGATGGTCGACTTTGTATAG |

| | |
|---|---|
| sGFP-*Sma*I-P1 | TCCCCCGGGGGCCAATAAAACTAGGAGGAAATTTAAATGAGTAAAGGAGAAGAACTTTTC |
| sGFPMreC-P2 | ACTTAAGCACGGAGGCGCCGCAGGATTTGTATAGTTCATCCATG |
| sGFPMreC-P3 | ACTATACAAATCCTGCGGCGCCTCCGTGCTTAAGTTTTTTAAAAATAAC |
| sGFPMreC-*Xho*I-P4 | CCGCTCGAGTTATTTATCCCTGCTTTC |
| sGFPMreD-P2 | GTGTACGCATGGAGGCGCCGCAGGATTTGTATAGTTCATCCATG |
| sGFPMreD-P3 | ACTATACAAATCCTGCGGCGCCTCCATGCGTACACTGTATTATTTTTTG |
| sGFPMreD-*Xho*I-P4 | CCGCTCGAGTTACCATTGACGACGTTTC |
| MreDsGFP-*Hind*III-P1 | CCCAAGCTTATAGATACTGCAATTGGGC |
| MreD-sGFP-*Bam*HI-P2 | CGGGATCCCCATTGACGACGTTTCATG |
| MreCprot-P1 | CGGGATCCCGTTCACAATCTCAATCAC |
| MreCprot-P2 | CCGCTCGAGTTATTTATCCCTGCTTTCATC |

Deletion of *mreC*, *mreD* and *mreCD* from the genome was performed using the thermosensitive plasmid pMAD[34]. The deletion mutants were constructed by PCR amplification, from *S. aureus* COL genomic DNA, of the upstream and downstream regions of *mreC* (dMreC-P1/dMreC-P2 and dMreC-P3/dMreC-P4), *mreD* (dMreD-P1/dMreD-P2 and dMreD-P3/dMreD-P4) and *mreCD* (dMreC-P1/dMreCD-P2 and dMreCD-P3/dMreD-P4). The upstream and downstream fragments of *mreC*, *mreD* and *mreCD* were joined by overlap PCR using primers dMreC-P1/dMreC-P4, dMreD-P1/dMreD-P4 and dMreC-P1/dMreD-P4, respectively. The resulting fragments were digested with *Xma*I and *Bam*HI restriction enzymes and cloned into pMAD vector producing the plasmids pΔ*mreC*, pΔ*mreD* and pΔ*mreCD*. The inserts were sequenced and the plasmids were then electroporated into *S. aureus* RN4220 strain at 30°C, using erythromycin and X-gal selection, and transduced into *S. aureus* COL and NCTC8325-4 using phage 80α. Integration and excision of the plasmids into the

chromosome was performed as previously described[34], resulting in strains COLΔ*mreC*, COLΔ*mreD*, COLΔ*mreCD*, NCTCΔ*mreC*, NCTCΔ*mreD* and NCTCΔ*mreCD*. Gene deletions were confirmed by PCR and sequencing.

For the overexpression of MreC and MreD, a fragment containing the entire *mreCD* operon was amplified using primers MreC_*Sma*I_P1 and MreD_*Eco*RI_P2. The fragment was digested with *Sma*I and *Eco*RI restriction enzymes and cloned into pCNX vector[20] in *E. coli*. After sequencing, the plasmid was electroporated into *S. aureus* RN4220 strain at 37°C, using kanamycin selection, and transduced into *S. aureus* COL using phage 80α resulting in strain COLp*mreCD*. As a control, empty vector pCNX was transduced into *S. aureus* COL strain resulting in strain COLpCNX.

To localize MreC and MreD proteins, N-terminal fusions with the P7 variant of superfast GFP[29] (sGFP) were constructed. A fragment containing a functional RBS sequence, the 714 bp *sgfp* gene excluding the stop codon and a sequence encoding a 5 amino acid linker was amplified by PCR from pTRC99a-P7 plasmid[29] using the primers sGFP-*Sma*I-P1 / sGFPMreC-P2 (*mreC* fusion) and sGFP-*Sma*I-P1/ sGFPMreD-P2 (*mreD* fusion). Primers sGFPMreC-P3 / sGFPMreC-*Xho*I-P4 and sGFPMreD_P3 / sGFPMreD-*Xho*I-P4 were used to amplify *mreC* and *mreD* genes, respectively. The fragments were joined by overlap PCR using the primers sGFP-*Sma*I-P1 / sGFPMreC-*Xho*I-P4 and sGFP-*Sma*I-P1 / sGFPMreD-*Xho*I-P4. The resulting fragments were digested with *Sma*I and *Xho*I restriction enzymes and cloned into the pBCB13 vector[26]. The plasmids were electroporated into *S. aureus* RN4220 at 30°C using erythromycin and X-gal selection and then transduced into *S. aureus* strains COL using phage 80α. By consecutive integration and excision, the *sgfp* fusions were introduced in the *spa* locus by replacement of the *spa* gene, giving rise to the final strains

COLsGFPMreC and COLsGFPMreD. The localization of MreD was also achieved by replacement of the native *mreD* gene by a *mreD-sgfp* fusion in the native locus. For this purpose, integrative plasmid pFAST2 was constructed by amplifying a 809 bp fragment encompassing the coding region of *sgfp* from pTRC99a-P7 using the primers sGFP-EcoRV-P1 and sGFP-NotI-P2, digested with *Eco*RV and *Not*I (Fermentas), and used to replace the *gfpmut*P2 gene in pSG5082[30]. Subsequently, the 483 final nucleotides of *mreD* excluding the stop codon, were amplified by PCR using the primers MreDsGFP-*Hind*III-P1 and MreDsGFP-*Bam*HI-P2 and cloned into pFAST2, in frame with the *sgfp* gene. The final plasmid pFAST2MreDsGFP was electroporated into *S. aureus* RN4220 and then transduced into *S. aureus* COL. The integration of this plasmid in the native *mreD* locus occurred through a single crossover event and was confirmed by PCR. The final strains were named COLpFAST2MreDsGFP.

## Genome sequencing

Genomic DNA was extracted from COL parental strain and *mreCD* deletion mutants and sequenced using the Illumina MiSeq system (Instituto Gulbenkian de Ciência, Oeiras, Portugal). 250-bp paired end reads with 100x average coverage were generated. Sequence reads were then assembled and analyzed with SeqMan NGen® and SeqMan Pro® (Version 12.0. DNASTAR. Madison, WI) software. COL genome (NCBI Accession NC_002951.2) was used as a reference template. The specific variations of the deletion mutants were identified by comparison with the respective parental strain. Low quality variations with read frequencies below 50% were removed from the dataset.

## Growth curves of *S. aureus* strains.

Growth of *mreCD* inducible mutants was analyzed by growing the cells overnight at 37°C in TSB medium supplemented with appropriate antibiotics and 0.5 mM IPTG. The overnight culture was washed four times with TSB and diluted 1/500 into fresh TSB medium with (control) or without 0.5 mM IPTG. When the culture without IPTG reached an $OD_{600nm}$ of approximately 1, a 1 ml sample was taken, washed four times and diluted 1/500 into fresh TSB medium with and without 0.5 mM IPTG. All cultures were incubated at 37°C with agitation and the $OD_{600nm}$ was recorded. For the growth of the deletion mutants the TSB overnight cultures were diluted to an initial $OD_{600nm}$ of 0.02 in fresh TSB or 0.002 in SSM9PR minimal medium, in triplicate. Cultures were incubated at 37°C with shaking and $OD_{600nm}$ was monitored.

## Protein purification and antibody production

The truncated *mreC* gene lacking the DNA fragment encoding the N-terminal transmembrane region was amplified by PCR from COL genomic DNA using primers MreCprot-P1 and MreCprot-P2. The resulting fragment was digested with *Bam*HI and *Xho*I restriction enzymes and cloned into the pET30a vector. The resulting plasmid, pETMreCt, encodes a combined $His_6$-tag and S-tag N-terminal fusion of the truncated MreC. pETMreCt was introduced into *E. coli* BL21 (DE3) by heat-shock transformation. The transformants were grown at 37°C in LB medium containing kanamycin 50 µg $ml^{-1}$. At $OD_{600nm}$ of approximately 1, the cultures were supplemented with 1 mM IPTG and grown for 3 additional hours. Cells were harvested by centrifugation and re-suspended in buffer A (50 mM sodium phosphate buffer pH 8 containing 150 mM NaCl, and complete-EDTA-free protease inhibitors

[Roche]). The cells were incubated at 4°C for 15 min in the presence of DNase (10 µg ml$^{-1}$), RNase (20 µg ml$^{-1}$) and lysozyme (0.4 µg ml$^{-1}$) and then disrupted by sonication. The samples were centrifuged at 16000 rpm at 4°C. As most of the protein was in the pellet (confirmed by 12% SDS-PAGE), the pellet was resuspended in buffer B (50 mM sodium phosphate buffer pH 8 containing 300 mM NaCl and 0.1% Brij) supplemented with 8 M Urea. The suspension was applied to pre-equilibrated Talon$^{TM}$ (Clontech) resin and incubated at 4°C for 48h. The same volume of buffer B without urea was added to the sample, to reduce the concentration of urea to 4 M, and the suspension was incubated at 4°C overnight. Bound protein was washed once with buffer B with 4 M urea followed by two washes without urea. Two sequential elutions with elution buffer (50 mM sodium phosphate buffer pH 8, 300 mM NaCl) containing 100 mM and 150 mM imidazole respectively were performed. Eluted fractions were mixed and dialyzed in three consecutive steps against 50 mM sodium phosphate buffer (pH 8) containing 500 mM, 300 mM and 150 mM NaCl, respectively. The purified protein was digested with enterokinase (New England Biolabs) to cleave His$_6$-tag and S-tag and separated on a 12% SDS-PAGE. The band corresponding to the truncated MreC was cut from the gel and sent to Eurogentec (Belgium) for polyclonal antibody production.


## Western blotting

*S. aureus* strains were grown overnight, diluted 1/500 in fresh medium and incubated at 37°C. When necessary, cultures were supplemented with 0.5 mM IPTG or 0.5 mM CdCl$_2$. At OD$_{600nm}$ of approximately 0.6 cells were harvested and broken with glass beads in a FastPrep FP120 cell disrupter (Thermo Electro Corporation). Samples were centrifuged to remove unbroken cells and debris and total protein

content of the clarified lysates was determined using Pierce™ BCA Protein Assay Kit (Thermo Scientific). Equal amounts of total protein from each sample were separated on 12% SDS-PAGE at 120V and then transferred to Hybond-P 0.45 PVDF membrane (GE Healthcare) using a BioRad Semi-dry transfer cell, according to standard western blotting techniques. MreC and PBP2 proteins were detected using specific polyclonal antibodies.

## Scanning electron microscopy

Exponentially growing *S. aureus* cells were harvested by centrifugation, resuspended in fixative solution (2.5% glutaraldehyde in 0.2 M sodium cacodylate buffer, pH 7.4), deposited on glass discs (Marienfeld) and kept for 1 week at 4°C. The fixative solution was subsequently removed and the cells were washed three times with the sodium cacodylate solution. The sample was progressively dehydrated by immersion in a graded series of ethanol (50% - 100%) and then mounted on aluminum stubs with carbon adhesive discs (Agarscientific). The sample was critical-point dried under $CO_2$ and sputter coated with gold-palladium (Polaron SC7640) for 200s at 10mA. SEM observations were performed using secondary electron images (2 kV) with a Hitachi S4500 instrument at the Microscopy and Imaging Platform (Micalis, Massy, France) of the INRA research center of Jouy-en-Josas (France).

## Transmission electron microscopy

Exponentially growing *S. aureus* cells were harvested by centrifugation and fixed with 2% glutaraldehyde in 0.1 M Na cacodylate buffer pH 7.2, for 3 hours at room temperature. Cells were then

contrasted with Oolong Tea Extract (OTE) 0.5% in cacodylate buffer and postfixed with 1% osmium tetroxide containing 1.5% potassium cyanoferrate. Samples were gradually dehydrated in ethanol (30% to 100%), substituted progressively in a mix of propylene oxyde-epon and embedded in Epon (Delta microscopie—Labège France). Thin sections (70 nm) were collected onto 200 mesh cooper grids, and counterstained with lead citrate. Grids were examined with Hitachi HT7700 electron microscope operated at 80kV and images were acquired with a charge-coupled device camera (AMT). Electron microscopy has benefited from the facilities and expertise of MIMA2 MET, INRA (France).

## Determination of the susceptibility to stress agents

The minimum inhibitory concentrations (MICs) of *S. aureus* strains to antibiotics, to oxidative stress agent hydrogen peroxide ($H_2O_2$) and to osmotic stress agent sodium chloride (NaCl) were determined by microdilution in 96-well plates. The wells contained serial two fold dilutions of each compound in a total volume of 100 µl of TSB. For the antibiotic susceptibility assay each well was individually inoculated with 5 µl of a $10^{-3}$ dilution of an overnight culture. For the oxidative and osmotic susceptibility assays TSB medium was inoculated to a final $OD_{600nm}$ of 0.02. A sterility control was performed with only TSB. Plates were incubated at 37°C without shaking for 24h or 48h and the MICs were recorded as the lowest concentration of compound that inhibited bacterial growth. Higher acidic pH value which inhibits cell growth was determined in a similar way using hydrochloric acid (HCl).

## Peptidoglycan purification and analysis

*S. aureus* parental and mutant strains were grown in TSB until $OD_{600nm}$ of 0.9 and peptidoglycan was purified as previously described[35]. Muropeptides were prepared by digestion with mutanolysin and analyzed by reverse phase HPLC using a Hypersil ODS (C18) column (Thermo Fisher Scientific). Muropeptide species were eluted in 0.1 M sodium phosphate, pH 2.0, with a gradient of 5–30% methanol for 155 min and detected at 206 nm.

## Labeling and imaging of *S. aureus*

Strains with *sgfp* fusions were grown overnight, diluted 1/200 in fresh medium and incubated at 37°C. 0.2 mM IPTG was added to the cultures expressing the fusions from the ectopic *spa* locus. At $OD_{600nm}$ of approximately 0.6, 1 ml of each culture was centrifuged, resuspended in phosphate-buffered saline (PBS) and 1 µl drop was placed onto a thin film of 1.2% agarose prepared in PBS mounted on a microscopy slide.

Parental and deletion mutant strains were grown overnight, diluted 1/200 in fresh medium and incubated at 37°C. At $OD_{600nm}$ of approximately 0.6, 1 ml of each culture was taken and incubated for 5 min with DNA dye Hoechst 33342 (3 µg ml$^{-1}$, Invitrogen), membrane dye Nile Red (10 µg ml$^{-1}$, Invitrogen) or cell wall dye Vancomycin (Sigma) mixed with a BODIPY FL conjugate of vancomycin (Van-FL, Molecular Probes) to a final concentration of 0.8 µg ml$^{-1}$. The cells were then pelleted, resuspended in PBS and 1 µl of this cell suspension was placed onto a thin film of 1.2% agarose prepared in PBS mounted on a microscopy slide.

To localize the sites of peptidoglycan synthesis, cells were grown in TSB to an $OD_{600nm}$ of approximately 0.6, labeled with fluorescent D-amino acid NADA or L-amino acid NALA (500 µM)[36,37] for 5 min at 37°C, 600 rpm and washed with TSB. The cells were resuspended in PBS and 1 µl drop of this cell suspension was placed onto a thin film of 1.2% agarose prepared in PBS and visualized by SIM. To compare absolute NADA fluorescence in two different strains in the same microscopy image, one of them was labeled with DNA dye Hoechst 33342. The cells were then labeled with NADA, washed and mixed prior to visualization by epifluorescence microscopy and SIM.

## Super-resolution structured illumination microscopy (SIM)

SIM imaging was performed using a Plan-Apochromat 63x/1.4 oil DIC M27 objective, in an Elyra PS.1 microscope (Zeiss). Images were obtained using either 3 or 5 grid rotations, with 34µm grating period for the 561nm laser, 28µm period for 488nm laser and 23µm period for 405nm laser. Images were acquired using a sCMOS camera and reconstructed using ZEN software (black edition, 2012, version 8.1.0.484) based on a structured illumination algorithm[38].

## Determination of cell cycle phase and cellular volume

The cell cycle phase and the cellular volume were determined based on SIM images of *S. aureus* cells labeled with the membrane dye Nile Red. As previously described, the relative number of cells in one phase of the cell cycle is proportional to the percentage of time that those cells spend in that same phase[20]. To calculate the volume of each cell, an ellipse was overlaid with the membrane dye signal and fitted to

the border limits of the cellular membrane. The shorter and longer axes of the ellipse were measured and the volume of the cell was calculated by an approximation to the volume of a prolate spheroid $V = \frac{4}{3}\pi ab^2$, where *a* and *b* correspond to the longer and shorter semi-axes, respectively. The volume was determined for a total of 60 cells in each phase of each strain.

## Fluorescence ratio determination

Cells expressing *sgfp-mreC/D* fusions and cells labeled with NADA were observed with a Zeiss Axio Observer microscope and images were taken with a Photometrics CoolSNAP HQ2 camera (Roper Scientific) using Metamorph 7.5 software (Molecular Devices). To determine the fluorescence ratio (FR), the fluorescence at the center of division septum (only from cells with closed septa) was quantified and divided by the fluorescence at the peripheral cell wall. Average background fluorescence was subtracted from both values[39]. A total of 70 cells from each strain was analyzed.

## Statistical analysis

GraphPad Prism 6 (GraphPad Software) was used to perform the statistical analysis. The differences in cellular volume between each of the mutants and the parental strain and the comparisons between NADA-labeling fluorescence ratios were evaluated by unpaired student's t-tests. *p* values ≤ 0.05 were considered significant for all analysis performed and were indicated with asterisks: **p* ≤ 0.05, ***p* ≤ 0.01 and ****p* ≤ 0.001.

# RESULTS AND DISCUSSION

## MreC and MreD are not required for *S. aureus* growth

MreC and MreD are essential for viability in the elongated bacteria studied so far and their absence results in growth arrest and lysis[5,10,12,15]. In order to test if *mreC* and *mreD* genes were also essential for the survival of spherical *S. aureus* cells, the *mreCD* operon was placed under control of the IPTG-inducible promoter P*spac*, by integration of the non-replicative plasmid pMutin4MreCt into the Methicillin Resistant *S. aureus* (MRSA) strain COL genome. To increase promoter repression in the absence of the inducer, the P*spac* repressor LacI was expressed both from the integrated pMUTIN4 vector and the multicopy plasmid pMGPII[27]. We confirmed that expression of *mreC* in the resulting strain COL*mreCD*i was dependent on the presence of the inducer IPTG, although MreC protein levels were always below those of the parental strain COL (Fig. 1). COL*mreCD*i had a similar growth rate, in rich TSB medium, in the presence and in the absence of the inducer (Fig. 2a), suggesting that MreC and MreD are not essential proteins in *S. aureus* COL strain.

To confirm that *mreC* and *mreD* are not essential for *S. aureus* survival, we constructed *mreC*, *mreD* and *mreCD* deletion mutants in MRSA COL and in Methicillin Susceptible *S. aureus* (MSSA) strain NCTC8325-4, leaving the upstream and downstream regions of these genes intact and leaving no antibiotic marker. We were not able to delete the complete *mreD* gene from the genomes, even when an extra copy of *mreD* was expressed from the ectopic *spa* locus under the control of P*spac* promotor. This may be due to polar effects on the expression of *rplU*, an essential gene[40] encoding the 50S ribosomal protein L21, which is located 166 bp downstream of *mreD* and oriented in the same direction. However, we could delete 374 bp (from nucleotide 7 to 380)

of *mreD* (531 bp long) leaving the final 151 bp out of frame with the start codon, which resulted in strains COLΔ*mreD* and NCTCΔ*mreD*. Furthermore, we constructed strains COLΔ*mreCD* and NCTCΔ*mreCD* by deleting *mreC* and the first 380 nucleotides of *mreD*.
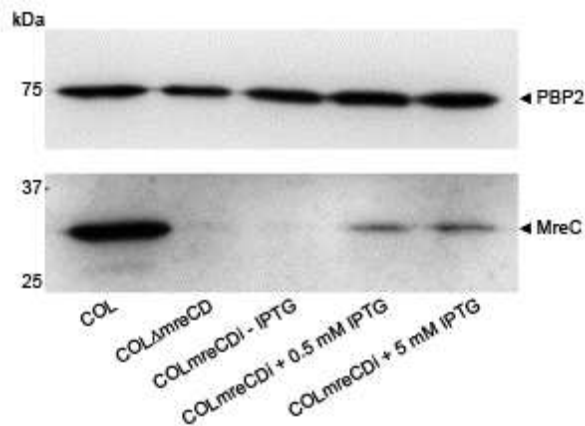


**Figure 1. Detection of MreC in COL*mreCD*i inducible mutant.** Western blot analysis of total protein extracts of COL, COLΔ*mreCD* and COL*mreCD*i grown in the absence or presence of IPTG inducer, using an MreC-specific antibody. In the inducible COL*mreCD*i mutant, MreC protein is not detected in the absence of the inducer and is detected in its presence, albeit in lower concentration than in the parental strain, even when an excess of IPTG is used. Detection of PBP2 (upper panel) was used as internal loading control.

The *mreC*, *mreD* and *mreCD* mutants were viable both in TSB rich medium and in SSM9PR minimal medium, and had similar growth rates relative to the COL and NCTC8325-4 parental strains (Fig. 2b-e). Importantly, although we did not see a growth defect for *mreCD* mutants, these genes are expressed in the laboratory conditions used, as shown by Western blotting of whole cell extracts of COL parental strain, grown in TSB rich medium, using an antibody against MreC (Fig. 3). We were not able to obtain an antibody against MreD, but the expression of an *mreD-sgfp* fusion from the native locus and controlled by the native promoter confirmed the expression of *mreD* gene (see below).
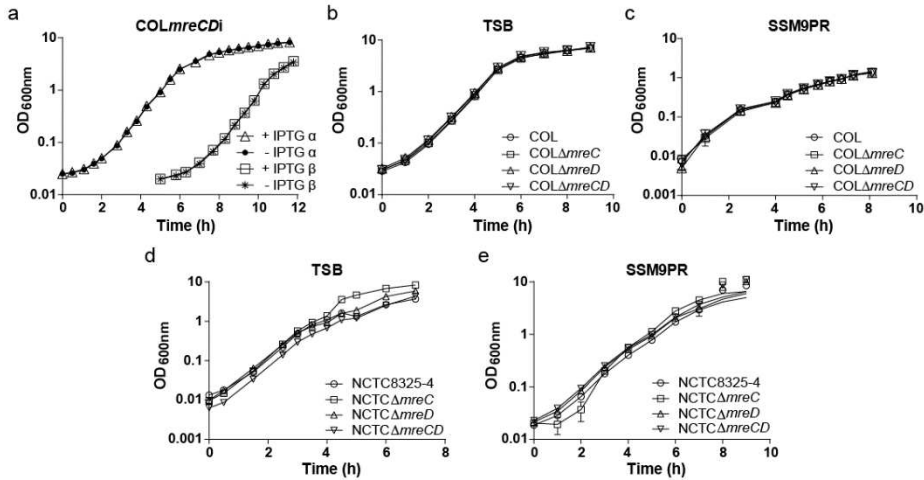
**Figure 2. Depletion of MreC or MreD does not impair *S. aureus* growth**. **a**, Growth curves for inducible mutant COL*mreCD*i in TSB medium in the presence (Δ) and absence (●) of 0.5 mM IPTG (α). When the culture without IPTG reached $OD_{600nm} \approx 1$, a sample was used to inoculate fresh media (β) with (□) and without (✱) 0.5 mM IPTG. **b, c**, Growth curves for COL, COLΔ*mreC*, COLΔ*mreD* and COLΔ*mreCD* in TSB rich medium (**b**) and SSM9PR minimal medium (**c**). Mutant strains have a growth rate similar to the parental strain, with a duplication time of approximately 41 min in TSB and 81 min in SSM9PR. **d, e**, Growth curves for NCTC8325-4, NCTCΔ*mreC*, NCTCΔ*mreD* and NCTCΔ*mreCD* in TSB (**d**) and SSM9PR (**e**) medium.

Suppressor mutations in laboratory strain R6 of *S. pneumoniae* allow the growth of *ΔmreCD* mutants[15]. In order to discard the hypothesis that lack of a growth phenotype in *S. aureus* Δ*mreC* and Δ*mreD* mutants was due to the acquisition of suppressor mutations, the entire genomes of COLΔ*mreC*, COLΔ*mreD* and COLΔ*mreCD* were sequenced, with a genome coverage of 99.99%, 99.93% and 99.86%, respectively. Deletion of *mreC* and *mreD* genes was confirmed in the respective strains and no mutations were found in COLΔ*mreC* when compared to parental strain COL. The genome of COLΔ*mreD* had only one SNP in SACOL1829, a gene of unknown function (Table 4), which was intact in COLΔ*mreCD*. COLΔ*mreCD* had only one SNP in the

plasmid recombination enzyme (pre) encoded in pT181, a natural staphylococcal plasmid present in strain COL. This protein is involved in plasmid maintenance and is unlikely to act as suppressor of *mreC* or *mreD* deletion. Importantly, none of the *S. aureus mreCD* mutants had any SNP in genes encoding PBPs, shown to suppress lack of *mreCD* in *S. pneumoniae*[15]. Thus, our results suggest that MreC and MreD are not essential proteins and do not play an important role in maintaining cell viability in *S. aureus* batch cultures.
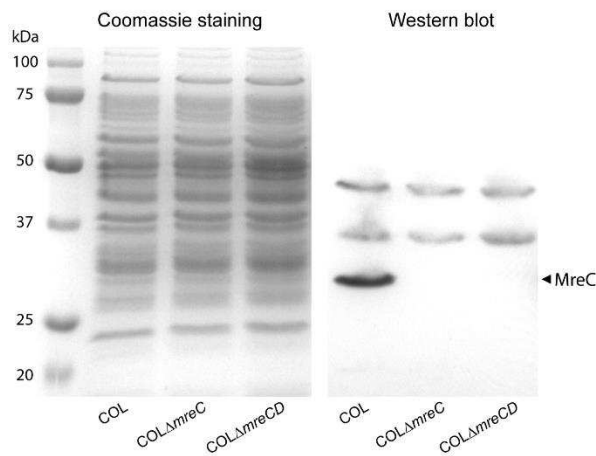


**Figure 3. MreC is present in COL but not in COLΔ*mreC* nor COLΔ*mreCD*.** Western blot analysis of total protein extracts of COL, COLΔ*mreC* and COLΔ*mreCD* using an anti MreC-specific antibody. MreC was present in the parental strain but was undetectable in the mutants.

**Table 4. Genomic mutations in COLΔ*mreD* and COLΔ*mreCD* identified by whole genome sequencing by comparison with parental strain COL.**

| Gene containing indicated mutation | Description | Nucleotide change | Amino acid change |
|---|---|---|---|
| **COLΔ*mreD*** | | | |
| SACOL_RS09375 | Hypotetical protein | C→A | Q23K |
| **COLΔ*mreCD*** | | | |
| SACOL_RS00015 | Plasmid recombination enzyme (pre) | G→A | S2F |

## MreC and MreD localize mainly at the division septum

In rod-shaped bacteria and in ovococci, MreC and MreD usually co-localize with the sidewall and peripheral cell wall synthetic machineries, respectively[6,7,13,14,16]. To study the localization of MreC and MreD in *S. aureus*, we constructed strains encoding superfast GFP (sGFP)[29] fused to the N-terminus of each protein. These fusions were expressed from an ectopic locus under control of the P*spac* promoter.

Super-resolution Structured Illumination Microscopy (SIM) and epifluorescence microscopy showed that both sGFP-MreC and sGFP-MreD localized mainly to the septa, with minor signal at the periphery of the cell (Fig. 4a,b). Septal enrichment of MreC and MreD proteins was analyzed using epifluorescence images by calculating the fluorescence ratio (FR) between the fluorescence at the center of the division septum and the fluorescence at the peripheral cell membrane in cells with a complete septum[39] (Fig. 4b). FR was 3.4 for sGFPMreC and 3.1 for sGFPMreD, confirming an enrichment of the two proteins at the division septum. In addition, *sgfp* was fused to the 3' end of *mreD* at the native locus, replacing the native copy of *mreD*. This strain showed no morphology defects relative to the wild-type parental strain and natively expressed MreD-sGFP also displayed a preferential localization at the septum (Fig. 4c).

## Deletion of *mreC* or *mreD* does not alter peptidoglycan synthesis

Localization of MreC and MreD to the septum, where peptidoglycan is mainly synthesized in *S. aureus* (reviewed in [19]), made us question about their possible role in maintaining cell wall composition. To test this, peptidoglycan from the parental strain COL and the

ΔmreCD mutants was purified and digested with mutanolysin to cleave glycan strands. The resulting muropeptides were analyzed by reverse-phase high-performance liquid chromatography (HPLC). All the strains exhibited similar profiles (Fig. 5), indicating that no significant alterations occur in peptidoglycan muropeptide composition or cross-linking in the absence of MreC and/or MreD.
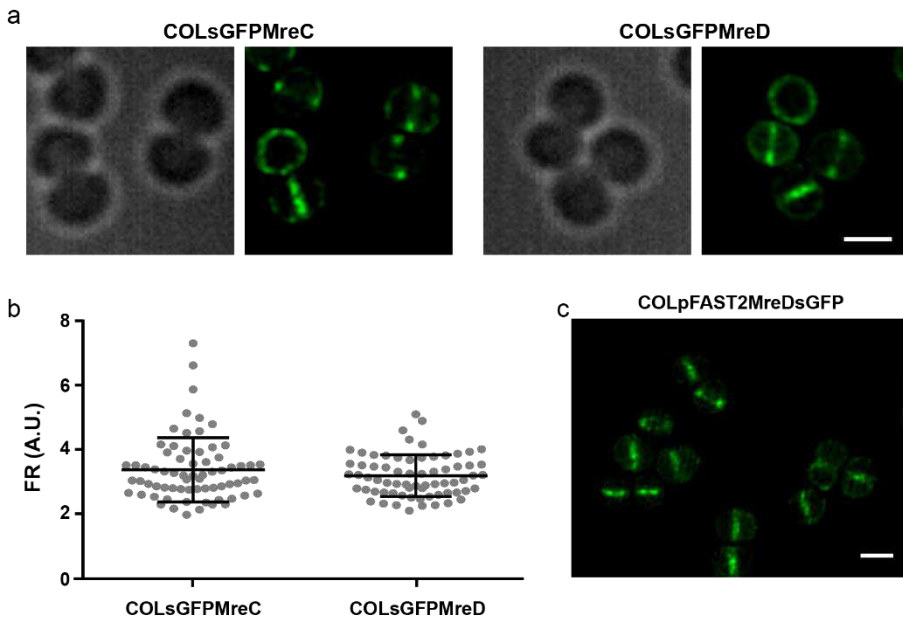


**Figure 4. MreC and MreD are enriched at the division septum**. **a**, *S. aureus* COL cells expressing sGFP fused to the N-terminal of MreC (left) or MreD (right) were grown in TSB supplemented with 0.2 mM IPTG and observed by SIM. Left panels show differential interference contrast (DIC) images and right panels show fluorescence signal of sGFP fusion proteins. **b**, Fluorescence ratio (FR) between the values quantified at the center of the division septum and the fluorescence at the peripheral cell membrane was calculated from epifluorescence microscopy images of sGFPMreC and sGFPMreD fusions. A total of 70 cells with closed septa was analyzed for each strain. An FR above two indicates protein enrichment at the septum. **c**, SIM images of COLpFAST2MreDsGFP which expresses MreD-sGFP fusion from the native locus. Scale bars, 1 µm.
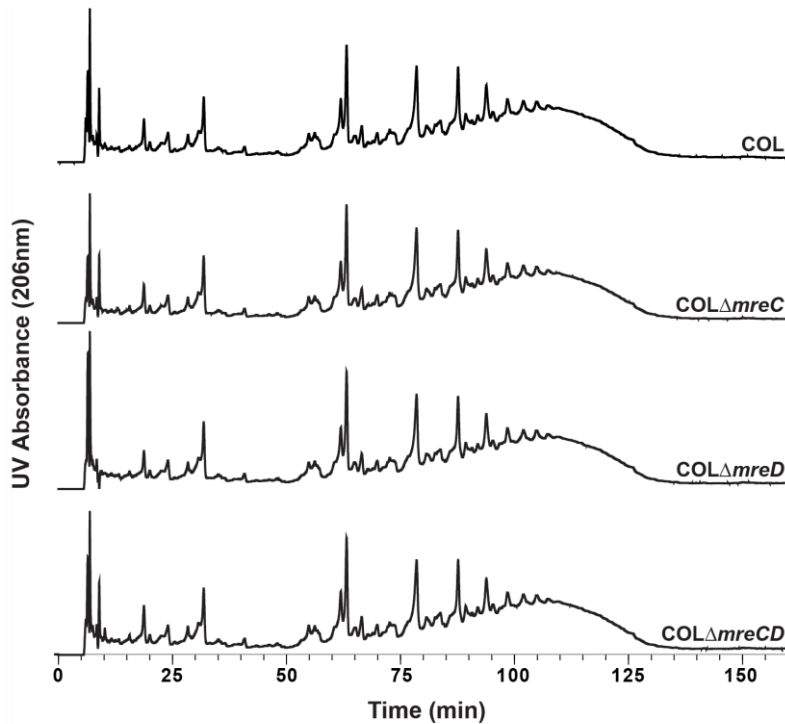
**Figure 5. Profiles of peptidoglycan muropeptides remain unaltered in the absence of MreC or MreD**. HPLC profiles of peptidoglycan muropeptides from *S. aureus* COL, COLΔ*mreC*, COLΔ*mreD* and COLΔ*mreCD*.

It has been recently shown that a small fraction of peptidoglycan synthesis in *S. aureus* occurs at the cell periphery, mediated mainly by PBP4[20,21]. Given that (i) MreC and MreD proteins are proposed to be involved in the synthesis of lateral cell wall in elongated bacteria, and (ii) we observed a small fraction of MreC and MreD localized at the cell periphery, we decided to further explore the possible role of these proteins in peripheral peptidoglycan synthesis.

For that purpose, we investigated the sites of peptidoglycan incorporation in *mreC* and *mreD* mutants, as well as in the parental strain. Cells were labelled with NADA, a green fluorescent derivative of

3-amino-D-alanine that can be incorporated in the pentapeptide chain of peptidoglycan by PBPs[36,37]. In COL parental strain, incorporation of NADA occurred mostly at the division septum, but also, at lower levels, in the peripheral wall mainly in cells that are not synthesizing the septum (Fig. 6), as it had been previously shown[20,21]. The Δ*mreC* and Δ*mreD* mutants displayed the same pattern of peptidoglycan insertion (Fig. 6). The ratio between NADA signal at the septum and the periphery of the cell was similar for all the strains (Fig. 6a), suggesting that peripheral cell wall synthesis is not dependent on MreC and/or MreD in *S. aureus*. Furthermore, COL and COLΔ*mreCD* were labeled with NADA and imaged in the same microscopy slide (previously labeling one or the other strain with DNA dye Hoechst 33342 to distinguish both strains) and fluorescence at the septum was determined. Lack of MreC and MreD did not impair septal incorporation of peptidoglycan, as values obtained for both strains were similar (Fig. 6b,c). To confirm that the observed fluorescence signal was due to NADA incorporation and not to non-specific interaction of NADA with the cell surface, we labeled parental strain and COLΔ*mreCD* mutant cells with NADA L-enantiomer NALA, which is not incorporated into the peptidoglycan[36] and no signal was detected.

## Cell volume and morphology are maintained in *mreCD* deletion and overexpression mutants

In elongated bacteria, MreC and MreD are crucial to determine cell shape and when one of these two proteins is absent, cells become shorter and wider, acquiring a more spherical shape[5,6,10,12]. To test if MreC and MreD have some role in cell morphogenesis or division in *S. aureus*, the cell wall and DNA of deletion mutants and of COL parental strain were labeled using fluorescent vancomycin and Hoechst 33342,

respectively, and imaged by SIM. The same strains were also analyzed by Scanning and Transmission Electron Microscopy (SEM and TEM).
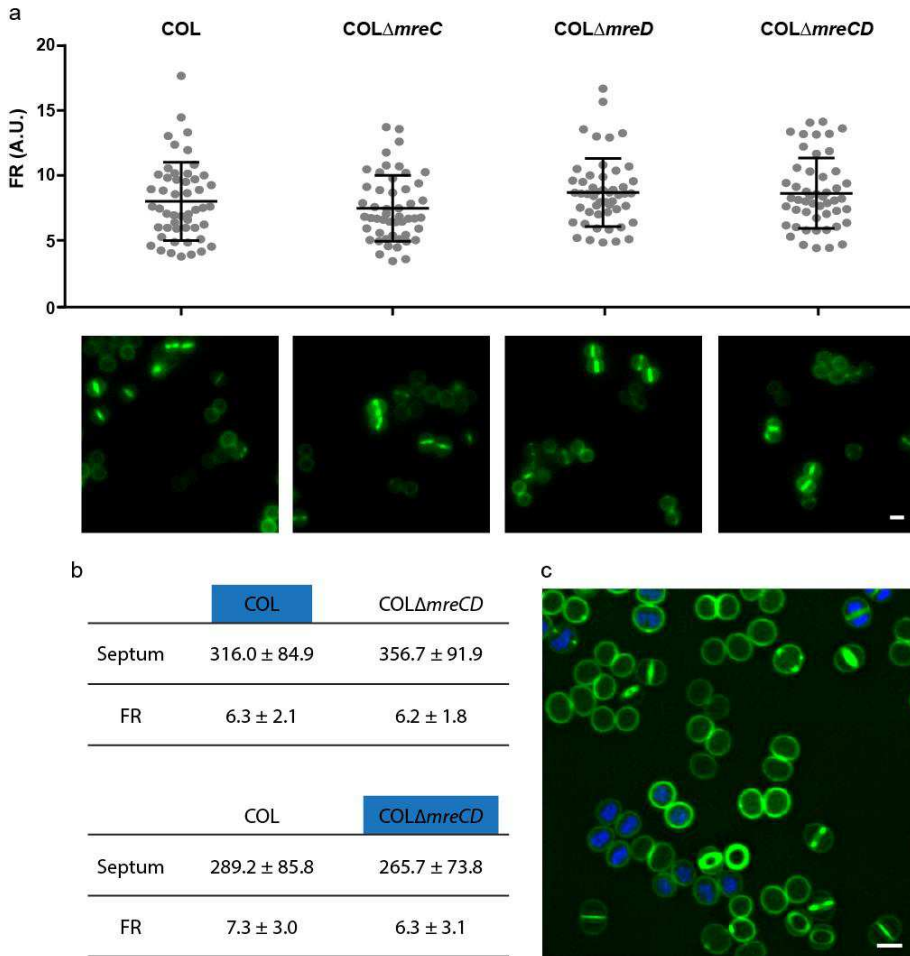


**Figure 6. Peptidoglycan incorporation pattern in *S. aureus* is not altered in the absence of MreC and MreD. a,** COL, COLΔ*mreC*, COLΔ*mreD* and COLΔ*mreCD* were imaged by epifluorescence microscopy after being labeled for 5 minutes with the fluorescent derivative of 3-amino-D-alanine, NADA. Incorporation of NADA occurs mainly at the septum but also in the peripheral cell wall. Fluorescence ratio (FR) between the values quantified at the center of the division septum and the fluorescence at the lateral cell wall was calculated. A total of 50 cells with closed septa were analyzed for each strain. The ratios were similar between COL (8.00±3.01) and the mutants Δ*mreC*

(7.47±2.54, *p* = 0.3445), Δ*mreD* (8.69±2.62, *p* = 0.2262) and Δ*mreCD* (8.63±2.71, *p* = 0.2754). Scale bar, 1 µm. **b**, Septal fluorescence (Septum) and fluorescence ratio (FR) for COL and COLΔ*mreCD*. Cells were labeled with NADA for 5 minutes, mixed together and observed by epifluorescence microscopy. To distinguish the two strains, one of them was previously labeled with the DNA dye Hoechst 33342 (shown in blue). The experiment was repeated exchanging the strain with labeled DNA to confirm that Hoechst 33342 labeling does not affect NADA fluorescence. No statistically significant differences were observed between COL parental strain and COLΔ*mreCD* mutant (*p*>0.05 for all conditions) **c**, SIM of COL parental strain (labeled with NADA and Hoechst 33342) and COLΔ*mreCD* (labeled only with NADA). Scale bar, 1 µm.

As seen in Fig. 7a, *mreC*, *mreD* and *mreCD* deletion mutants had no evident defects in DNA organization and maintained their spherical shape and surface roughness relative to the parental strain. Growth rate and cell morphology were also not affected by overexpression of MreC and MreD, as observed in strain COL harboring the replicative plasmid p*mreCD* which contains a copy of *mreCD* operon under the control of the inducible P*cad* promoter (Fig. 8).

We next measured the volume of Δ*mreC* and Δ*mreD* cells at three different phases of the cell cycle. Phase 1 is the initial stage preceding division septum formation. Phase 2 corresponds to the formation of the division septum and Phase 3 is the final stage in which *S. aureus* cells have a complete septum before splitting into two daughter cells[20]. In *S. aureus*, impairment of cell division, for example due to depletion of FtsZ protein, results in cell enlargement[41]. Only minor differences were observed in the cell volume distributions between the Δ*mreCD* mutants and the parental strain (Fig. 7c). Also, the relative time that each strain spent in each phase of the cell cycle remained approximately constant (Fig. 7b), suggesting that MreC and MreD do not influence cell cycle progression and are not critical for cell division.
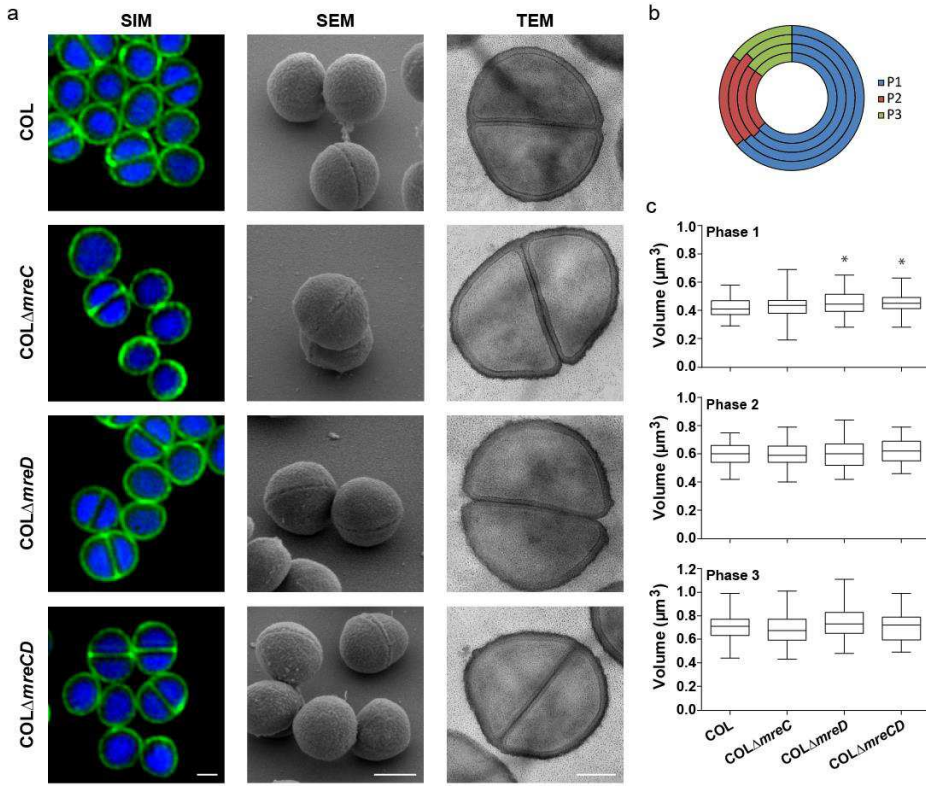
**Figure 7. Absence of MreC or MreD has no effect on cell morphology, cell dimensions or cell cycle progression**. COL, COLΔ*mreC*, COLΔ*mreD* and COLΔ*mreCD* were imaged by Super-resolution Structured Illumination Microscopy (SIM), Scanning Electron Microscopy (SEM) and Transmission Electron Microscopy (TEM). For the SIM images, cell wall and DNA were labeled with fluorescent vancomycin (Van-FL) and Hoechst 33342, respectively. Scale bars for SIM and SEM images 0.5 µm and for TEM images 0.2 µm. **b**, Fraction of the cell cycle spent in Phase 1 (blue, before initiation of septum synthesis), Phase 2 (red, septum synthesis) and Phase 3 (green, after closure of the septum, before the two daughter cells split)[20]. Cell cycle progresses clockwise. From the inner to the outer circle the values correspond to COL, COLΔ*mreC*, COLΔ*mreD* and COLΔ*mreCD*. Exponentially growing cultures were labeled with the membrane dye Nile Red and the percentage of cells in each phase of the cell cycle was determined. **c**, Cellular volume distributions during each phase of the cell cycle. Cells were labeled with Nile Red and imaged by SIM. The volume was calculated by approximation of the cellular shape to a prolate spheroid. $n$ = 60 for each phase. Statistical analysis was performed using the unpaired t test and $p$ values were >0.05 in all cases compared to the parental strain COL, except for Phase 1 COLΔ*mreD* ($p$ = 0.013) and for COLΔ*mreCD* ($p$ = 0.014).
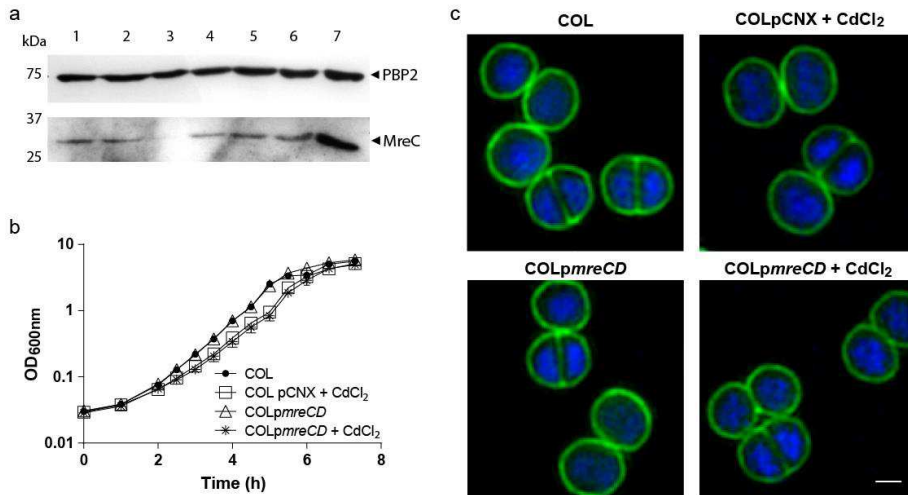
**Figure 8. Overexpression of MreC and MreD does not affect *S. aureus* COL growth or morphology. a,** Western blot analysis of total protein extracts of COL grown without (1) and with (2) 0.5 mM CdCl₂, COLΔ*mreCD* (3), COLpCNX (empty vector) grown without (4) and with (5) 0.5 mM CdCl₂ and COLp*mreCD* grown without (6) and with (7) 0.5 mM CdCl₂. MreC detection was performed using an MreC-specific antibody. Overexpression of MreC is observed in COLp*mreCD* in the presence of the inducer (lane 7). PBP2 was used as internal loading control. **b, c,** Growth curves (**b**) and SIM (**c**) of COL, COLpCNX grown with 0.5 mM CdCl₂ and COLp*mreCD* grown without and with 0.5 mM CdCl₂. Scale bar, 1 µm. Growth curves and morphology of COLpCNX (parental strain with empty vector) and COLp*mreCD* (overexpressing MreCD), both grown in the presence of cadmium, are indistinguishable.

## Susceptibility to different stress agents is not affected by *mreC* or *mreD* deletion

As we were not able to establish a link between MreC and MreD and morphogenesis or peptidoglycan synthesis in standard laboratory growth conditions, we looked for alternative functions by assessing the susceptibility of the *mreCD* mutants to different stresses. We first tested resistance against antibiotics with different cellular targets including DNA replication (nalidixic acid), protein synthesis (chloramphenicol) and several steps of cell wall synthesis (phosphomycin, bacitracin,

tunicamycin, D-cycloserine, oxacillin and vancomycin). The minimum inhibitory concentration (MIC) of Δ*mreC* and Δ*mreD* mutants to these compounds remained unaltered (Table 5). Next, osmotic, oxidative and acidic stresses were induced by adding to the medium increasing concentrations of sodium chloride, hydrogen peroxide and hydrochloric acid, respectively. Again, no differences were observed between the susceptibility of the mutants and the parental strain (Table 5). Taken together, these results indicate that MreC and MreD were not required to resist these stress conditions.

**Table 5. Susceptibility to antibiotics, osmotic, oxidative and acidic stress agents of COL, COLΔ*mreC*, COLΔ*mreD* and COLΔ*mreCD*.** Minimum Inhibitory Concentrations (MICs) of different antibiotics, sodium chloride and hydrogen peroxide and the higher acidic pH value which inhibits cell growth. The values in the table correspond to the results obtained for all the deletion mutants and the parental strain, after 24h incubation, except for oxacillin (48h).

|  | MIC |
| --- | :---: |
| **Antibiotics (µg/ml)** | |
| Oxacillin | 512 |
| Vancomycin | 2 |
| Phosphomycin * | 2000 |
| D-cycloserine | 75 |
| Nalidixic acid | 75 |
| Chloramphenicol | 3.1 |
| Bacitracin | 112.5 |
| Tunicamycin | 150 |
| **Osmotic Stress (M)** | |
| NaCl | 3 |
| **Oxidative Stress (mM)** | |
| $H_2O_2$ | 5 |
| **Acidic Stress** | |
| pH | 3 - 4 |

\* Very poor growth above 125 µg/ml

## FINAL REMARKS

The morphogenetic elements MreC and MreD are essential proteins and play a key role in sidewall elongation in various rod-shaped and ovococcoid bacteria, in cylindrical and peripheral peptidoglycan synthesis respectively. Their presence in *S. aureus*, a spherical bacterium with no dedicated elongation machinery, raised the hypothesis they could be important for septal peptidoglycan synthesis, or be involved in the recently reported minor peptidoglycan synthesis activity at the cell periphery [20,21]. In this work we showed that *mreC* and *mreD* are not essential in MRSA strain COL and in MSSA strain NCTC8325-4 and do not affect cell morphology, cell volume or cell cycle progression in the laboratory growth conditions tested, in which we have shown that MreC and MreD are expressed. Peptidoglycan muropeptide composition and peripheral peptidoglycan incorporation also remained unaltered, indicating that MreCD do not play a major role in peptidoglycan synthesis in *S. aureus*. Although the lack of an important role in *S. aureus* for these proteins was unexpected, there are precedents in nature for cocci that do not use MreCD: *Streptococcus pyogenes* and *Streptococcus agalactiae*, two ovococcus species, do not encode recognizable homologues of MreC and MreD (reviewed in [42]).

It is possible that MreCD from elongated bacteria have two functions, one in cell shape/lateral peptidoglycan synthesis and a second, non-essential unknown function, which is the one conserved in spherical bacterial. Phenotypes resulting from the lack of this second function may be visible only in conditions that were not covered in this study, which differ considerably from growth in natural environments. Further work is necessary to understand the possible roles of these two proteins in *S. aureus*.

## REFERENCES

1. Boucher, H. W. & Corey, G. R. Epidemiology of Methicillin-Resistant *Staphylococcus aureus*. *Clin. Infect. Dis.* **46**, S344–S349 (2008).
2. Silhavy, T. J., Kahne, D. & Walker, S. The Bacterial Cell Envelope. *Cold Spring Harb. Perspect. Biol.* **2**, a000414–a000414 (2010).
3. Chastanet, A. & Carballido-Lopez, R. The actin-like MreB proteins in *Bacillus subtilis*: a new turn. *Front. Biosci. (Schol. Ed).* **4**, 1582–606 (2012).
4. Carballido-López, R. & Formstone, A. Shape determination in *Bacillus subtilis*. *Curr. Opin. Microbiol.* **10**, 611–616 (2007).
5. Kruse, T., Bork-Jensen, J. & Gerdes, K. The morphogenetic MreBCD proteins of *Escherichia coli* form an essential membrane-bound complex. *Mol. Microbiol.* **55**, 78–89 (2005).
6. White, C. L., Kitich, A. & Gober, J. W. Positioning cell wall synthetic complexes by the bacterial morphogenetic proteins MreB and MreD. *Mol. Microbiol.* **76**, 616–33 (2010).
7. Van Den Ent, F. *et al.* Dimeric structure of the cell shape protein MreC and its functional implications. *Mol. Microbiol.* **62**, 1631–1642 (2006).
8. Domínguez-Escobar, J. *et al.* Processive movement of MreB-associated cell wall biosynthetic complexes in bacteria. *Science* **333**, 225–8 (2011).
9. Garner, E. C. *et al.* Coupled, circumferential motions of the cell wall synthesis machinery and MreB filaments in *B. subtilis*. *Science* **333**, 222–225 (2011).
10. Leaver, M. & Errington, J. Roles for MreC and MreD proteins in helical growth of the cylindrical cell wall in *Bacillus subtilis*. *Mol. Microbiol.* **57**, 1196–209 (2005).
11. Divakaruni, A. V., Baida, C., White, C. L. & Gober, J. W. The cell shape proteins MreB and MreC control cell morphogenesis by positioning cell wall synthetic complexes. *Mol. Microbiol.* **66**, 174–188 (2007).
12. Dye, N. A., Pincus, Z., Theriot, J. A., Shapiro, L. & Gitai, Z. Two independent spiral structures control cell shape in Caulobacter. *Proc. Natl. Acad. Sci.* **102**, 18608–18613 (2005).
13. Divakaruni, A. V, Loo, R. R. O., Xie, Y., Loo, J. A. & Gober, J. W. The cell-shape protein MreC interacts with extracytoplasmic proteins including cell wall assembly complexes in *Caulobacter crescentus*. *Proc. Nati. Acad. Sci. U S A* **102**, 18602–7 (2005).
14. El Ghachi, M. *et al.* Characterization of the elongasome core PBP2 : MreC complex of *Helicobacter pylori*. *Mol. Microbiol.* **82**, 68–86 (2011).
15. Land, A. D. & Winkler, M. E. The requirement for pneumococcal MreC and MreD is relieved by inactivation of the gene encoding PBP1a. *J. Bacteriol.* **193**, 4166–79 (2011).
16. Tsui, H. C. T. *et al.* Pbp2x localizes separately from Pbp2b and other peptidoglycan synthesis proteins during later stages of cell division of *Streptococcus pneumoniae* D39. *Mol. Microbiol.* **94**, 21–40 (2014).
17. van Opijnen, T., Bodi, K. L. & Camilli, A. Tn-seq: high-throughput parallel sequencing for fitness and genetic interaction studies in microorganisms. *Nat. Methods* **6**, 767–772 (2009).
18. Barendt, S. M. *et al.* Influences of Capsule on Cell Shape and Chain

Formation of Wild-Type and pcsB Mutants of Serotype 2 *Streptococcus pneumoniae*. *J. Bacteriol.* **191**, 3024–3040 (2009).

19. Pinho, M. G., Kjos, M. & Veening, J. W. How to get (a)round: mechanisms controlling growth and division of coccoid bacteria. *Nat. Rev. Microbiol.* **11**, 601–14 (2013).

20. Monteiro, J. M. *et al.* Cell shape dynamics during the staphylococcal cell cycle. *Nat. Commun.* **6**, 8055 (2015).

21. Gautam, S., Kim, T. & Spiegel, D. A. Chemical Probes Reveal an Extraseptal Mode of Cross-Linking in *Staphylococcus aureus*. *J. Am. Chem. Soc.* **137**, 7441–7447 (2015).

22. Formstone, A. & Errington, J. A magnesium-dependent *mreB* null mutant: implications for the role of *mreB* in *Bacillus subtilis*. *Mol. Microbiol.* **55**, 1646–1657 (2005).

23. Nicolas, P. *et al.* Condition-Dependent Transcriptome Reveals High-Level Regulatory Architecture in *Bacillus subtilis*. *Science.* **335**, 1103–1106 (2012).

24. Reed, P. *et al. Staphylococcus aureus* Survives with a Minimal Peptidoglycan Synthesis Machine but Sacrifices Virulence and Antibiotic Resistance. *PLoS Pathog.* **11**, 1–19 (2015).

25. Arnaud, M., Chastanet, A. & Débarbouillé, M. New vector for efficient allelic replacement in naturally gram-positive bacteria. *Appl. Environ. Microbiol.* **70**, 6887–6891 (2004).

26. Pereira, P. M., Veiga, H., Jorge, A. M. & Pinho, M. G. Fluorescent Reporters for Studies of Cellular Localization of Proteins in *Staphylococcus aureus*. *Appl. Environ. Microbiol.* **76**, 4346–4353 (2010).

27. Pinho, M. G., Filipe, S. R., de Lencastre, H. & Tomasz, A. Complementation of the essential peptidoglycan transpeptidase function of Penicillin-Binding Protein 2 (PBP2) by the drug resistance protein PBP2A in *Staphylococcus aureus*. *J. Bacteriol.* **183**, 6525–31 (2001).

28. Vagner, V., Dervyn, E. & Ehrlich, S. D. A vector for systematic gene inactivation in *Bacillus subtilis*. *Microbiology* **144**, 3097–3104 (1998).

29. Fisher, A. C. & DeLisa, M. P. Laboratory Evolution of Fast-Folding Green Fluorescent Protein Using Secretory Pathway Quality Control. *PLoS One* **3**, e2351 (2008).

30. Pinho, M. G. & Errington, J. A *divIVA* null mutant of *Staphylococcus aureus* undergoes normal cell division. *FEMS Microbiol. Lett.* **240**, 145–149 (2004).

31. Monk, I. R., Shah, I. M., Xu, M., Tan, M. & Foster, T. J. Transforming the untransformable: application of direct transformation to manipulate genetically *Staphylococcus aureus* and *Staphylococcus epidermidis*. *MBio.* **3**, 1–11 (2012).

32. Gill, S. R. *et al.* Insights on evolution of virulence and resistance from the complete genome analysis of an early methicillin-resistant *Staphylococcus aureus* strain and a biofilm-producing methicillin-resistant *Staphylococcus epidermidis* strain. *J. Bacteriol.* **187**, 2426–2438 (2005).

33. Oshida, T. & Tomasz, A. Isolation and characterization of a Tn551-autolysis mutant of *Staphylococcus aureus*. *J. Bacteriol.* **174**, 4952–9 (1992).

34. Arnaud, M., Chastanet, A. & Debarbouille, M. New Vector for Efficient Allelic Replacement in Naturally Nontransformable, Low-GC-Content, Gram-Positive Bacteria. *Appl. Environ. Microbiol.* **70**, 6887–6891 (2004).

35. Carvalho, F. *et al.* L-Rhamnosylation of *Listeria monocytogenes* Wall Teichoic Acids Promotes Resistance to Antimicrobial Peptides by Delaying Interaction with the Membrane. *PLOS Pathog.* **11**, e1004919 (2015).

36. Kuru, E. *et al. In Situ* Probing of Newly Synthesized Peptidoglycan in Live Bacteria with Fluorescent D-Amino Acids. *Angew. Chemie Int. Ed.* **51**, 12519–12523 (2012).

37. Kuru, E., Tekkam, S., Hall, E., Brun, Y. V & VanNieuwenhze, M. S. Synthesis of fluorescent D-amino acids (FDAAs) and their use for probing peptidoglycan synthesis and bacterial growth *in situ*. *Nat Protoc.* **10**, 33–52 (2015).

38. Heintzmann, R. & Cremer, C. G. Laterally modulated excitation microscopy: improvement of resolution by using a diffraction grating. in *SPIE 3568, Optical Biopsies and Microscopic Techniques III* (eds. Bigio, I. J., Schneckenburger, H., Slavik, J., Svanberg, K. & Viallet, P. M.) **3568**, 185–196 (International Society for Optics and Photonics, 1999).

39. Pereira, P. M., Filipe, S. R., Tomasz, A. & Pinho, M. G. Fluorescence Ratio Imaging Microscopy Shows Decreased Access of Vancomycin to Cell Wall Synthetic Sites in Vancomycin-Resistant *Staphylococcus aureus*. *Antimicrob. Agents Chemother.* **51**, 3627–3633 (2007).

40. Forsyth, R. A. *et al.* A genome-wide strategy for the identification of essential genes in *Staphylococcus aureus*. *Mol. Microbiol.* **43**, 1387–400 (2002).

41. Pinho, M. G. & Errington, J. Dispersed mode of *Staphylococcus aureus* cell wall synthesis in the absence of the division machinery. *Mol. Microbiol.* **50**, 871–881 (2003).

42. Zapun, A., Vernet, T. & Pinho, M. G. The different shapes of cocci. *FEMS Microbiol. Rev.* **32**, 345–60 (2008).

# CHAPTER III

**SEDS-bPBP pairs direct lateral and septal peptidoglycan synthesis in *Staphylococcus aureus***

**Author contributions**

**Data contained in this chapter is accepted for publication:**

# ABSTRACT

Peptidoglycan (PGN) is the major component of the bacterial cell wall, a structure essential for the physical integrity and shape of the cell. Bacteria maintain cell shape by directing PGN incorporation to distinct regions of the cell, namely through the localization of late stage PGN synthesis proteins. These include two key protein families, SEDS transglycosylases and bPBP transpeptidases, proposed to function in cognate pairs. Rod-shaped bacteria have two SEDS-bPBP pairs, involved in elongation and division. Here, we elucidate why coccoid bacteria, such as *Staphylococcus aureus,* also possess two SEDS-bPBP pairs. We determined that *S. aureus* RodA-PBP3 and FtsW-PBP1 likely constitute cognate pairs of interacting proteins. Lack of RodA-PBP3 resulted in more spherical cells due to deficient sidewall PGN synthesis, whereas depletion of FtsW-PBP1 arrested normal septal PGN incorporation. Although PBP1 is an essential protein, a mutant lacking PBP1 transpeptidase activity is viable, showing that this protein has a second function. We propose that the FtsW-PBP1 pair has a role in stabilizing the divisome at midcell. In the absence of these proteins, the divisome appears as multiple rings/arcs that drive lateral PGN incorporation, leading to cell elongation. We conclude that RodA-PBP3 and FtsW-PBP1 mediate sidewall and septal PGN incorporation, respectively, and that their activity must be balanced to maintain coccoid morphology.

## INTRODUCTION

Peptidoglycan (PGN) synthesis is an essential process that is both spatially and temporally regulated to ensure that the bacterial cell shape is maintained[1]. Rod-shaped bacteria elongate by synthesizing PGN along the length of the cell in a process directed by the cytoskeletal protein MreB[2]. In *Escherichia coli* and *Bacillus subtilis*, this protein polymerizes into short filaments that move processively around the cell diameter, and organize a multi-protein machinery, including PGN synthesis proteins, referred to as the elongasome or the Rod system[3–5]. Cell division is dependent on another cytoskeletal protein, FtsZ, which polymerizes to form the Z-ring and recruits a multi-protein complex responsible for septum synthesis, known as the divisome[6,7]. This complex directs PGN incorporation to the midcell, resulting in inward PGN synthesis, and eventually bisects the mother cell, leading to daughter cell separation.

Ovococci such as *Streptococcus pneumoniae* and *Lactococcus lactis* lack MreB, and FtsZ is proposed to coordinate both elongation and septation[8–10]. In these organisms PGN is incorporated at the midcell in two defined modes: (i) at the lateral wall, eventually increasing the length of the cell and (ii) inwards, to synthesize the septum and future cell poles. Cocci, such as *Staphylococcus aureus*, also require FtsZ for divisome assembly and lack components of the elongasome, including MreB, consistent with its spherical shape[9].

Directed PGN incorporation is accomplished by different sets of transglycosylases (TGase) and transpeptidases (TPase), the enzymes involved in the final stages of cell wall synthesis, that promote PGN polymerization and cross-linking, respectively[11]. Key proteins involved in these steps are the penicillin-binding proteins (PBPs) that can be class A PBPs (aPBPs), with both TGase and TPase activity or class B

PBPs (bPBPs) that possess only TPase activity and have a second domain of unknown function[11]. Some bacteria also have monofunctional glycosyltransferases (MGTs), enzymes with a TGase domain with homology to the TGase domain of aPBPs[11]. More recently, RodA and FtsW, members of the shape, elongation, division and sporulation (SEDS) protein family, were also shown to have TGase activity[12–14]. Together, the SEDS and bPBPs have been proposed to form TGase-TPase cognate pairs, involved in cell elongation (RodA) and cell division (FtsW) in rod-shaped bacteria[14,15]. Compared to rod-shaped bacteria, *S. aureus* encodes a small number of PBPs: one bifunctional aPBP (PBP2), two bPBPs (PBP1 and PBP3) and one low molecular weight PBP (PBP4) with transpeptidase activity[16]. However, similarly to rods, it contains two SEDS proteins (FtsW and RodA). Given the proposed roles of SEDS-bPBP pairs in elongation and division of rod-shaped bacteria, why a coccus requires two sets of these proteins has remained a long-standing question.

Although the cell shape of *S. aureus* is close to spherical, we have recently used super-resolution microscopy to show that *S. aureus* cells elongate slightly during growth[17]. Here we investigated whether SEDS-bPBP cognate pairs occur in *S. aureus* and their role in directing PGN incorporation during the cell cycle.

# MATERIALS AND METHODS

## Bacterial growth conditions

Strains and plasmids used in this study are listed in Table 1. *E. coli* strains were grown in Luria–Bertani broth (Difco) or Luria–Bertani agar (Difco) at 37°C. *S. aureus* strains were grown in tryptic soy broth (TSB, Difco) or on tryptic soy agar (TSA, Difco) at 37°C. When necessary, culture media was supplemented with antibiotics (ampicillin 100 µg ml$^{-1}$, kanamycin 50 µg ml$^{-1}$, neomycin 50 µg ml$^{-1}$, erythromycin 10 µg ml$^{-1}$ or chloramphenicol 10 µg ml$^{-1}$), with 100 µg ml$^{-1}$ 5-Bromo-4-chloro-3-indolyl β-D-galactopyranoside (X-gal, from Apollo Scientific), with 0.5 mM (ColFtsWi) or 0.01 mM (ColPBP1i) Isopropyl β-D-1-thiogalactopyranoside (IPTG, Apollo Scientific) or with 0.1 µM of cadmium chloride (Sigma-Aldrich).

**Table 1. Strains and plasmids used in this study.**

| Strains and plasmids | Description | Source or Ref. |
|---|---|---|
| *E. coli* | | |
| DC10B | Δ*dcm* in DH10B background; Dam methylation only; for cloning | [18] |
| *S. aureus* | | |
| RN4220 | restriction-negative derivative of NCTC8325-4 | [19] |
| COL | HA-MRSA | [20] |
| USA300 JE2 | CA-MRSA | [21] |
| ColΔ*rodA* | *rodA* deletion of parental strain COL tet$^S$ | This work |
| ColΔ*pbpC* | *pbpC* deletion of parental strain COL | This work |
| JE2Δ*pbpC* | *pbpC* deletion of parental strain USA300 JE2 | This work |
| ColΔ*rodA*Δ*pbpC* | *rodA* and *pbpC* deletions of parental strain COL | This work |
| JE2Δ*rodA*Δ*pbpC* | *rodA* and *pbpC* deletions of parental strain USA300 JE2 | This work |

| Strains and plasmids | Description | Source or Ref. |
|---|---|---|
| ColpMGPII | COL tet[S] with pMGPII; Cam[R] | This work |
| ColFtsWhigh | COL *spa::*P$_{spac}$*ftsW* | This work |
| ColFtsWlow | COL Δ*ftsW spa::*P$_{spac}$*ftsW* | This work |
| ColFtsWi | COL Δ*ftsW spa::*P$_{spac}$*ftsW* with pMGPII; Cam[R] | This work |
| ColFtsWiΔ*pbpD* | COL Δ*ftsW* Δ*pbpD spa::*P$_{spac}$*ftsW* with pMGPII; Cam[R] | This work |
| COL tet[S] | HA-MRSA cured of pT181; tet[S] | [22] |
| ColPBP1high | COL tet[S] *spa::*P$_{spac}$*pbpA* | This work |
| ColPBP1low | COL tet[S] Δ*pbpA spa::*P$_{spac}$*pbpA* | This work |
| ColPBP1i | COL tet[S] Δ*pbpA spa::*P$_{spac}$*pbpA* with pMGPII; Cam[R] | This work |
| ColPBP1iΔ*pbpD* | COL tet[S] Δ*pbpA* Δ*pbpD spa::*P$_{spac}$*pbpA* with pMGPII; Cam[R] | This work |
| ColPBP1TP | COL tet[S] *pbpA::pbpA*[S314A] | This work |
| ColPBP3TP | COL tet[S] *pbpC::pbpC*[S392G] | This work |
| ColFtsW-mCherry | COL *ftsW::ftsW-mCherry* | [23] |
| ColFtsW-sGFP | COL *ftsW::ftsW-sgfp* | [23] |
| ColsGFP-PBP1 | COL tet[S] *pbpA::sgfp-pbpA* | [23] |
| ColsGFP-PBP3 | COL tet[S] *pbpC::sgfp-pbpC* | [23] |
| ColMurJ-mCherry | COL *murJ::murJ-mCherry* | [23] |
| ColRodA-sGFP | COL *rodA::rodA-sgfp* | [23] |
| ColRodA-mCherry | COL *rodA::rodA-mCherry* | This work |
| ColpCNX | COL tet[S] with pCNX; Kan[R] | This work |
| ColpFtsW-mCherry | COL tet[S] with pCNX-ftsWmCh; Kan[R] | This work |
| ColpsGFP-PBP1 | COL tet[S] with pCNX-sgfppbpA; Kan[R] | This work |
| ColpsGFP-PBP3 | COL tet[S] with pCNX-sgfppbpC; Kan[R] | This work |
| ColpRodA-mCherry | COL tet[S] with pCNX-rodAmCh; Kan[R] | This work |
| ColpmCherry-sGFP | COL tet[S] with pCNX-mChsgfp; Kan[R] | This work |
| ColpmCherry-sGFP-TM | COL tet[S] with pCNX-mChsgfpTM; Kan[R] | This work |
| ColWP1 | COL *ftsW::ftsW-mCherry pbpA::sgfp-pbpA* | This work |
| ColWP3 | COL *ftsW::ftsW-mCherry pbpC::sgfp-pbpC* | This work |
| ColP1pA | COL tet[S] *pbpA::sgfp-pbpA* pCNX-rodAmCh | This work |
| ColP3pA | COL tet[S] *pbpC::sgfp-pbpC* pCNX-rodAmCh | This work |

| Strains and plasmids | Description | Source or Ref. |
|---|---|---|
| ColpWP1 | COL tet$^S$ with pCNX-WP1; Kan$^R$ | This work |
| ColpJP1 | COL tet$^S$ with pCNX-JP1; Kan$^R$ | This work |
| ColpAP1 | COL tet$^S$ with pCNX-AP1; Kan$^R$ | This work |
| ColpAP3 | COL tet$^S$ with pCNX-AP3; Kan$^R$ | This work |
| ColFtsWiEzrA-sGFP | COL Δ*ftsW spa::*P$_{spac}$*ftsW ezrA::ezrA-sgfp* with pMGPII; Cam$^R$ | This work |
| ColFtsWiΔ*pbpD*EzrA-sGFP | COL Δ*ftsW* Δ*pbpD spa::*P$_{spac}$*ftsW ezrA::ezrA-sgfp* with pMGPII; Cam$^R$ | This work |
| ColFtsWipCNX | COL Δ*ftsW spa::*P$_{spac}$*ftsW* with pMGPII and pCNX; Cam$^R$, Kan$^R$ | This work |
| ColFtsWipFtsW-sGFP | COL Δ*ftsW spa::*P$_{spac}$*ftsW* with pMGPII and pCNX-ftsWsgfp; Cam$^R$, Kan$^R$ | This work |
| ColFtsWipFtsW$^{W121A}$-sGFP | COL Δ*ftsW spa::*P$_{spac}$*ftsW* with pMGPII and pCNX-ftsW$^{W121A}$sgfp; Cam$^R$, Kan$^R$ | This work |
| ColFtsWipFtsW$^{D287A}$-sGFP | COL Δ*ftsW spa::*P$_{spac}$*ftsW* with pMGPII and pCNX-ftsW$^{D287A}$sgfp; Cam$^R$, Kan$^R$ | This work |
| ColFtsWipFtsZ-sGFP | COL Δ*ftsW spa::*P$_{spac}$*ftsW* with pMGPII with pCN-ftsZ$^{55-56}$sGFP; Cam$^R$, Kan$^R$ | This work |
| ColPBP1iEzrA-sGFP | COL tet$^S$ Δ*pbpA spa::*P$_{spac}$*pbpA ezrA::ezrA-sgfp* with pMGPII; Cam$^R$ | This work |
| ColPBP1iΔ*pbpD*EzrA-sGFP | COL tet$^S$ Δ*pbpA* Δ*pbpD spa::*P$_{spac}$*pbpA ezrA::ezrA-sgfp* with pMGPII; Cam$^R$ | This work |
| ColPBP1iFtsW-sGFP | COL tet$^S$ Δ *pbpA spa::*P$_{spac}$*pbpA ftsW::ftsW-sgfp* with pMGPII; Cam$^R$ | This work |
| ColPBP1ipFtsZ-sGFP | COL tet$^S$ Δ*pbpA spa::*P$_{spac}$*pbpA* with pMGPII and pCN-ftsZ$^{55-56}$sGFP; Cam$^R$, Kan$^R$ | This work |
| ColPBP1iMurJ-sGFP | COL tet$^S$ Δ*pbpA spa::*P$_{spac}$*pbpA murJ::murJ-sgfp* with pMGPII; Cam$^R$ | This work |
| ColPBP1iRodA-sGFP | COL tet$^S$ Δ*pbpA spa::*P$_{spac}$*pbpA rodA::rodA-sgfp* with pMGPII; Cam$^R$ | This work |
| ColΔ*rodA*sGFP-PBP3 | COL tet$^S$ Δ*rodA pbpC::sgfp-pbpC* | This work |
| ColΔ*rodA*pRodA-sGFP | COL tet$^S$ Δ*rodA* with pCNX-rodAsgfp; Kan$^R$ | This work |
| ColΔ*rodA*pRodA$^{W111A}$-sGFP | COL tet$^S$ Δ*rodA* with pCNX-rodA$^{W111A}$sgfp; Kan$^R$ | This work |
| ColΔ*rodA*pRodA$^{D286A}$-sGFP | COL tet$^S$ Δ*rodA* with pCNX-rodA$^{D286A}$sgfp; Kan$^R$ | This work |
| ColΔ*pbpC*RodA-sGFP | COL Δ*pbpC rodA::rodA-sgfp* | This work |

| Strains and plasmids | Description | Source or Ref. |
|---|---|---|
| ColΔ*pbpC*RodA-sGFPpPBP3 | COL Δ*pbpC rodA*::*rodA-sgfp* with pCNX-pbpC; Kan[R] | This work |
| ColPBP3TPRodA-sGFP | COL tet[S] *pbpC*::*pbpC*[S392G]*rodA*::*rodA-sgfp* | This work |
| ColpRodA-PBP3 | COL tet[S] with pCNX-rodA-pbpC; Kan[R] | This work |
| ColΔ*rodA*Δ*pbpC*pRodA-PBP3 | Col*ΔrodAΔpbpC with* pCNX-rodA-pbpC; Kan[R] | This work |

**Plasmids**

| | | |
|---|---|---|
| pMGPII | *S. aureus* replicative plasmid containing *lacI* gene; Amp[R], Cam[R] | [24] |
| pTRC99a-P7 | Plasmid containing *sgfp-p7* gene; Amp[R] | [25] |
| pROD17 | Plasmid containing *mCherry* gene | D. Sherratt |
| pMAD | *E. coli - S. aureus* shuttle vector with a thermosensitive origin of replication for Gram positive bacteria; Amp[R], Ery[R], *lacZ* | [26] |
| pSKP1S314A | pSK5632 vector with *pbpA*[S314A] copy; Amp[R], Cam[R] | [27] |
| pBCBAJ001 | pMAD containing the 3' end and the downstream region of ezrA; Amp[R], Ery[R] | [28] |
| pMAD-Δ*ftsW* | pMAD derivative containing up-and downstream regions of *ftsW;* Amp[R], Ery[R] | This work |
| pMAD-Δ*pbpA* | pMAD derivative containing upstream and 3' end regions of *pbpA;* Amp[R], Ery[R] | This work |
| pMAD-Δ*pbpC* | pMAD derivative containing up-and downstream regions of *pbpC;* Amp[R], Ery[R] | This work |
| pΔpbpD | pMAD derivative containing up-and downstream regions of *pbpD;* Amp[R], Ery[R] | [29] |
| pMAD-Δ*rodA* | pMAD derivative containing up-and downstream regions of *rodA;* Amp[R], Ery[R] | This work |
| pMAD-pbpATP | pMAD derivative containing P*spac* and full-length *pbpA*[S314A]*;* Amp[R], Ery[R] | This work |
| pMAD-pbpCTP | pMAD derivative containing a 1kb fragment of *pbpC*[S392G]; Amp[R], Ery[R] | This work |
| pMAD-ezrAsgfp | pMAD derivative containing an *ezrA-sgfp* fusion and the downstream region of *ezrA;* Amp[R], Ery[R] | This work |
| pMAD-ftsWsgfp | pMAD derivative containing an *ftsW-sgfp* fusion and the downstream region of *ftsW;* Amp[R], Ery[R] | [23] |

| Strains and plasmids | Description | Source or Ref. |
|---|---|---|
| pMAD-murJsgfp | pMAD derivative containing a *murJ-sgfp* fusion and the downstream region of *murJ;* Amp$^R$, Ery$^R$ | [23] |
| pMAD-sgfpPbp1 | pMAD derivative containing an *sgfp-pbpA* fusion and the upstream region of *pbpA;* Amp$^R$, Ery$^R$ | [23] |
| pMAD-sgfpPbp3 | pMAD derivative containing a *sgfp-pbpC* fusion and the upstream region of *pbpC;* Amp$^R$, Ery$^R$ | [23] |
| pMAD-rodAsgfp | pMAD derivative containing a *rodA-sgfp* fusion and the downstream region of *rodA;* Amp$^R$, Ery$^R$ | [23] |
| pMAD-rodAmCh | pMAD derivative containing a *rodA-mCherry* fusion and the downstream region of *rodA;* Amp$^R$, Ery$^R$ | This work |
| pBCB13 | pMAD derivative with up- and downstream regions of the *spa* locus and P*spac-lacI*; Amp$^R$, Ery$^R$, *lacZ* | [30] |
| pBCB13-ftsW | pBCB13 derivative containing *ftsW* gene under the control of IPTG-inducible P*spac* promoter*;* Amp$^R$,Ery$^R$ | This work |
| pBCB13-pbpA | pBCB13 derivative containing *pbpA* gene under the control of IPTG-inducible P*spac* promoter*;* Amp$^R$,Ery$^R$ | This work |
| pBCB13-sgfppbpA | pBCB13 derivative containing an *sgfp-pbpA* fusion under the control of IPTG-inducible P*spac* promoter*;* Amp$^R$, Ery$^R$ | This work |
| pCNX | Shuttle vector containing a cadmium inducible P*cad* promoter; Amp$^R$, Kan$^R$ | [17] |
| pCNX-pbpC | pCNX derivative containing *pbpC* gene; Amp$^R$, Kan$^R$ | This work |
| pCNX-rodA-pbpC | pCNX derivative containing *rodA* and *pbpC* genes; Amp$^R$, Kan$^R$ | This work |
| pCNX-ftsWsgfp | pCNX derivative containing an *ftsW-sgfp* fusion; Amp$^R$, Kan$^R$ | This work |
| pCNX-ftsW$^{W121A}$sgfp | pCNX derivative containing an *ftsW$^{W121A}$-sgfp* fusion; Amp$^R$, Kan$^R$ | This work |
| pCNX-ftsW$^{D287A}$sgfp | pCNX derivative containing an *ftsW$^{D287A}$-sgfp* fusion; Amp$^R$, Kan$^R$ | This work |
| pCNX-ftsWmCh | pCNX derivative containing an *ftsW-mCherry* fusion; Amp$^R$, Kan$^R$ | This work |
| pCN-ftsZ$^{55-56}$sGFP | pCNX derivative containing an *ftsZ-sgfp* fusion; Amp$^R$, Kan$^R$ | [23] |
| pCNX-rodAsgfp | pCNX derivative containing a *rodA-sgfp* fusion; Amp$^R$, Kan$^R$ | This work |
| pCNX-rodA$^{W111A}$sgfp | pCNX derivative containing a *rodA$^{W111A}$-sgfp* fusion; Amp$^R$, Kan$^R$ | This work |
| pCNX-rodA$^{D286A}$sgfp | pCNX derivative containing a *rodA$^{D286A}$-sgfp* fusion; Amp$^R$, Kan$^R$ | This work |

| Strains and plasmids | Description | Source or Ref. |
|---|---|---|
| pCNX-rodAmCh | pCNX derivative containing a *rodA-mCherry* fusion; Amp[R], Kan[R] | This work |
| pCNX-sgfppbpA | pCNX derivative containing an *sgfp-pbpA* fusion; Amp[R], Kan[R] | This work |
| pCNX-sgfppbpC | pCNX derivative containing an *sgfp-pbpC* fusion; Amp[R], Kan[R] | This work |
| pCNX-mChsgfp | pCNX derivative containing an *mCherry-sgfp* fusion; Amp[R], Kan[R] | This work |
| pCNX-mChsgfpTM | pCNX derivative containing an *mCherry-sgfp-TM* fusion; Amp[R], Kan[R] | This work |
| pCNX-WP1 | pCNX derivative containing an *ftsW-mCherry* and *sgfp-pbpA* fusion; Amp[R], Kan[R] | This work |
| pCNX-JP1 | pCNX derivative containing a *murJ-mCherry* and *sgfp-pbpA* fusion; Amp[R], Kan[R] | This work |
| pCNX-AP1 | pCNX derivative containing a *rodA-mCherry* and *sgfp-pbpA* fusion; Amp[R], Kan[R] | This work |
| pCNX-AP3 | pCNX derivative containing a *rodA-mCherry* and *sgfp-pbpC* fusion; Amp[R], Kan[R] | This work |

Abbreviations: Kan[R] – kanamycin resistance; Amp[R] – ampicillin resistance; Cam[R] – Chloramphenicol resistance; Ery[R] – erythromycin resistance.

## Construction of *S. aureus* strains

Primers used in this study are listed in Table 2. Plasmids were initially constructed in *E. coli,* then introduced in *S. aureus* RN4220 strain by electroporation, as previously described[31] and finally transduced to the strain of interest using phage 80α[32]. For the construction of ColFtsWi and ColPBP1i, a second copy of each gene was first introduced at the ectopic *spa* locus, under the control of an IPTG-inducible P*spac* promoter, prior to the deletion of the native loci copies. Briefly, a DNA fragment containing an RBS and the *ftsW* or *pbpA* gene was amplified by PCR from *S. aureus* strain COL with primers 4179/4180, and 4470/202, respectively. Each PCR fragment was digested with *Sma*I/*Xho*I and cloned into pBCB13, downstream of the P*spac* promoter,

giving pBCB13-ftsW and pBCB13-pbpA. Integration/excision was performed in COL or COL tet[S] as previously described[30], resulting in ColFtsWhigh and ColPBP1high.

In order to delete the native copies of *ftsW*, *rodA*, and *pbpC* (encoding PBP3), upstream and downstream regions of each gene of interest were amplified from COL using primers 3049/3050 and 3051/3052 (for *ftsW)*, 3056/3057 and 3058/3059 (for *rodA*), and 2587/2588 and 2589/2590 (for *pbpC*). In each case, the two fragments were joined by overlap PCR using primers 3049/3052, 3056/3059 and 2587/2590, respectively, digested with *Sma*I/*Bam*HI (*ftsW* and *rodA*) or *Eco*RI/*Bam*HI (*pbpC*) and cloned into pMAD, originating pMAD-Δ*ftsW*, pMAD-Δ*rodA* and pMAD-Δ*pbpC*. Integration/excision of pMAD-Δ*rodA* and pMAD-Δ*pbpC* in COL tet[S] and COL, respectively, resulted in strains ColΔ*rodA* and ColΔ*pbpC*. Plasmid pMAD-Δ*rodA* was also introduced into ColsGFP-PBP3[23] and ColΔ*pbpC*, and integration/excision generated ColΔ*rodA*sGFP-PBP3 and ColΔ*rodA*Δ*pbpC*, respectively. Whole genome sequencing of ColΔ*rodA*, ColΔ*pbpC* and ColΔ*rodA*Δ*pbpC* was performed and SNPs are shown in Supplementary Table 1. Integration/excision of pMAD-rodAsgfp in ColΔ*pbpC* resulted in ColΔ*pbpC*RodA-sGFP. Plasmid pMAD-Δ*pbpC* was also integrated/excised in *S. aureus* USA300 JE2, originating JE2Δ*pbpC.* Integration/excision of pMAD-Δ*rodA* in JE2Δ*pbpC* originated JE2Δ*rodA*Δ*pbpC* and whole genome sequencing of chromosomal DNA confirmed the absence of both genes, without the introduction of additional SNPs*.*

Despite several attempts, deletion of the full *pbpA* gene (encoding PBP1) was unsuccessful. In case we were affecting the expression of the essential *mraY* gene (290 bp downstream of *pbpA*), we instead constructed pMAD-Δ*pbpA* to include a stop codon followed by the last 340 bp of *pbpA* using primers 3806/5772 and 5773/5774.

Overlap PCR was performed with primers 3806/5774 and the full fragment was digested with *Bgl*II/*Bam*HI and cloned into pMAD, generating pMAD-Δ*pbpA*.

Plasmids pMAD-Δ*ftsW* and pMAD-Δ*pbpA* were introduced into ColFtsWhigh and ColPBP1high, and integration/excision in the presence of IPTG resulted in deletion of the native genes, originating ColFtsWlow and ColPBP1low. Plasmid pMGPII, encoding the P*spac* repressor LacI was transduced into these strains and into COL tet[S], giving rise to ColFtsWi, ColPBP1i and ColpMGPII.

For the construction of ColPBP1TP, a *pbpA* allele encoding the TPase point mutation S314A (by substitution of TCA for GCA at bases 940-942) was placed under the control of the P*spac* promoter by first amplifying the P*spac* promoter and an RBS from pBCB13 using primers 1285/4235, and the *pbpA* gene encoding for PBP1[S314A] from pSKP1S314A, using primers 4236/3490. The two fragments were joined by overlap PCR using primers 1285/3490, digested with *Eco*RI/*Bam*HI and cloned into pMAD, to give pMAD-pbpATP. Integration/excision was performed in COL tet[S] in the presence of 0.5 mM IPTG and the chromosomal DNA of the resulting ColPBP1TP was sent for whole genome sequencing, confirming the absence of SNPs with the exception of S314A.

For the construction of ColPBP3TP, base substitutions encoding the TPase point mutation S392G (TCTTCT for GGATCC at bases 1174-1179) were introduced into a 1 kb fragment of *pbpC* by amplifying 500 bp fragments from COL using primers 4980/4981 and 4982/4983. The two fragments were digested with *Bam*HI, ligated and amplified using primers 4980/4983, digested with *Eco*RI/*Sal*I and cloned into pMAD, resulting in pMAD-pbpCTP. Integration/excision of this plasmid in COL

tet$^S$ resulted in ColPBP3TP. Integration/excision of pMAD-rodAsgfp in ColPBP3TP resulted in ColPBP3TPRodA-sGFP.

For localization studies of EzrA, sGFP was amplified from pTRC99a-P7 using primers 2949/3350, digested with NheI/XhoI and cloned into pBCBAJ001, giving pMAD-ezrAsgfp, which was transduced to ColFtsWi and ColPBP1i. Integration/excision resulted in the introduction of a 3´ *sgfp* fusion to the native copy of *ezrA*, giving strains ColFtsWiEzrA-sGFP and ColPBP1iEzrA-sGFP, respectively.

For construction of *pbpD* deletion strains, plasmid pΔpbpD was transduced into ColFtsWi, ColPBP1i, ColFtsWiEzrA-sGFP and ColPBP1iEzrA-sGFP, and following integration/excision generated strains ColFtsWiΔ*pbpD*, ColPBP1iΔ*pbpD*, ColFtsWiΔ*pbpD*EzrA-sGFP and ColPBP1iΔ*pbpD*EzrA-sGFP, respectively.

For localization of FtsZ, pCN-ftsZ$^{55-56}$sGFP was transduced into ColFtsWi and ColPBP1i, generating ColFtsWipFtsZ-sGFP and ColPBP1ipFtsZ-sGFP, respectively. For localization studies in ColPBP1i, transduction and integration/excision of pMAD-ftsWsgfp, pMAD-murJsgfp and pMAD-rodAsgfp plasmids gave rise to ColPBP1iFtsW-sGFP, ColPBP1iMurJ-sGFP and ColPBP1iRodA-sGFP, respectively.

For co-localization studies with FtsW-mCherry, plasmids pMAD-sgfpPbp1 and pMAD-sgfpPbp3 were transduced into ColFtsW-mCherry and following integration/excision gave strain ColWP1 and ColWP3, respectively. For co-localization studies with RodA-mCherry, this fusion was first introduced into COL. Briefly, the final 1051 bp of the *rodA* gene, excluding the stop codon, and its downstream region were amplified using primers 2284/5665 and 5546/2287, respectively. The *mCherry* gene was amplified from pROD17 plasmid using primers 5599/5545. Fragments were joined by overlap PCR using primers 2284/2287,

digested with *Sma*I/*Bam*HI and cloned into pMAD vector, originating pMAD-rodAmCh. Integration and excision in COL gave rise to ColRodA-mCherry. The *rodA-mCherry* fusion was then amplified from ColRodA-mCherry using primers 5707/5941, digested with *Bam*HI/*Kpn*I and cloned into pCNX, resulting in pCNX-rodAmCh. This plasmid was transduced into COL tet^S, ColsGFP-PBP1 and ColsGFP-PBP3, giving ColpRodA-mCherry, ColP1pA and ColP3pA, respectively.

For inducible expression of FtsW-mCherry, *ftsW-mCherry* was amplified from strain ColFtsW-mCherry using primers 5706/5671, digested with *Bam*HI/*Eco*RI and cloned into pCNX, resulting in pCNX-ftsWmCh. This plasmid and empty pCNX vector were introduced into COL tet^S, giving ColpFtsW-mCherry and ColpCNX, respectively. For inducible expression of sGFP-PBP1, *sgfp-pbpA* was first cloned into plasmid pBCB13, before amplification and introduction into pCNX. For construction of pBCB13-sgfppbpA, a fragment containing *sgfp* was amplified from pTRC99a-P7 using primers 3112/3211 and the *pbpA* gene was amplified from COL using primers 1387/202. The two fragments were joined by overlap PCR using primers 3112/202, digested with *Sma*I/*Xho*I and cloned into pBCB13. Primers 3599/3600 were then used to amplify the *sgfp-pbpA* fragment, digested with *Bam*HI/*Eco*RI and cloned into pCNX, resulting in pCNX-sgfppbpA. This plasmid was transduced into COL tet^S, giving ColpsGFP-PBP1. For inducible expression of sGFP-PBP3, primers 6404/5668 were used to amplify *sgfp-pbpC* from ColsGFP-PBP3, introducing an RBS at the 5' end. This PCR was re-amplified using primers 5440/5668 in order to add a *Bam*HI restriction site, and following digestion with *Bam*HI/*Eco*RI, was cloned into pCNX, resulting in pCNX-sgfppbpC. Transduction of this plasmid into COL tet^S gave ColpsGFP-PBP3.

For inducible expression of PBP3, primers 5704/5668 were used to amplify *pbpC* from COL, digested with *Bam*HI/*Eco*RI, and cloned into

pCNX, resulting in pCNX-pbpC. Transduction of this plasmid into ColΔ*pbpC*RodA-sGFP generated ColΔ*pbpC*RodA-sGFPpPBP3.

For complementation experiments, sGFP fusions to wild-type and point mutants of FtsW and RodA were expressed from pCNX. Briefly, *ftsW-sgfp* and *rodA-sgfp* fragments were amplified from ColFtsW-sGFP and ColRodA-sGFP using primers 4179/5603 and 5609/4041, digested with *Sma*I/*Eco*RI or *Bam*HI/*Kpn*I and cloned into pCNX vector, originating pCNX-ftsWsgfp and pCNX-rodAsgfp. In FtsW, amino acid exchange was performed by mutating *ftsW* bases 361-363 from TGG to GCA (W121A) and bases 859-861 from GAT to GCA (D287A). Mutations were introduced by amplifying pCNX-ftsWsgfp with primers 5547/5548 or 5553/5554, originating plasmids pCNX-ftsW$^{W121A}$sgfp and pCNX-ftsW$^{D287A}$sgfp. These plasmids, along with pCNX and pCNX-ftsWsgfp were introduced into ColFtsWi, resulting in ColFtsWipFtsW$^{W121A}$-sGFP, ColFtsWipFtsW$^{D287A}$-sGFP, ColFtsWipCNX and ColFtsWipFtsW-sGFP, respectively.

For RodA, amino acid exchange was performed by altering *rodA* bases 331-333 from TGG to GCA (W111A) and bases 856-858 from GAC to GCA (D286A). Mutations were introduced by amplifying pCNX-rodAsgfp with primers 5559/5560 or 5565/5566, originating plasmids pCNX-rodA$^{W111A}$sgfp and pCNX-rodA$^{D286A}$sgfp. These plasmids, along with pCNX-rodAsgfp, were introduced into ColΔ*rodA*, resulting in ColΔ*rodA*pRodA$^{W111A}$-sGFP, ColΔ*rodA*pRodA$^{D286A}$-sGFP and ColΔ*rodA*pRodA-sGFP, respectively.

For complementation of ColΔ*rodA*Δ*pbpC* and overexpression studies, *rodA* was amplified from pCNX-AP1 (see below) using primers 6686/6682 and *pbpC* was amplified from COL using primers 6683/6692. These fragments were introduced into *Bam*HI-digested pCNX using the Gibson assembly® cloning kit (NEB), originating plasmid pCNX-rodA-

pbpC. This plasmid was introduced into COL and ColΔ*rodA*Δ*pbpC*, resulting in ColpRodA-PBP3 and ColΔ*rodA*Δ*pbpC*pRodA-PBP3.

For FLIM and seFRET experiments, plasmids co-expressing fluorescent fusions were designed. In general, mCherry fluorescent protein fusions were amplified with an RBS and flanked with *Bam*HI and *Not*I restriction sites, and sGFP fluorescent protein fusions were amplified with an RBS and flanked with *Not*I and *Eco*RI sites. Digested PCR products were ligated to *Bam*HI/*Eco*RI-digested pCNX, resulting in an RBS and mCherry fusion, followed by a second RBS and sGFP fusion placed under a cadmium inducible promoter. Specifically, *ftsW-mCherry*, *murJ-mCherry* and *rodA-mCherry* were amplified using primers 5706/6052, 5708/6052 and 5707/6052 from ColFtsW-mCherry, ColMurJ-mCherry and ColRodA-mCherry, respectively. GFP fusions *sgfp-pbpA* and *sgfp-pbpC* were amplified using primers 6053/3600 and 6053/5668 from ColsGFP-PBP1 and ColsGFP-PBP3, respectively. Digestion and ligation gave rise to plasmids pCNX-WP1, pCNX-JP1, pCNX-AP1 and pCNX-AP3, and transduction into COL tet[S] resulted in strains ColpWP1, ColpJP1, ColpAP1 and ColpAP3, respectively.

As a positive membrane control for FLIM, a fusion between *mCherry*, *sgfp* and a fragment of *pbpB* encoding its transmembrane domain (amino acids 2 to 34) was cloned into pCNX. Primers 6407/6398 were used to amplify *mCherry* from ColFtsW-mCherry, *gfp* was amplified from pTRC99a-P7 using primers 6399/3809, and the *pbpB* fragment was amplified from COL using primers 6400/5187. These three fragments were joined by overlap PCR using primers 3599/5187, digested with *Bam*HI/*Sma*I and cloned into pCNX, resulting in pCNX-mChsgfpTM. Transduction into COL tet[S] gave ColpmCherry-sGFP-TM.

To construct a positive cytoplasmic control for seFRET, an *mcherry-sgfp* fusion was cloned into pCNX. Primers 6407/6398 were

used to amplify *mCherry* from ColFtsW-mCherry and *gfp* was amplified from pTRC99a-P7 using primers 6399/4041. These two fragments were joined by overlap PCR using primers 3599/4041, digested with *Bam*HI/*Kpn*I and cloned into pCNX, resulting in pCNX-mChsgfp. Transduction into COL tet[S] gave ColpmCherry-sGFP.

**Table 2. Primers used I this study.**

| Primer No. | Primer Name | Sequence (5'-3') |
|---|---|---|
| 2590 | pPBP3-KO-P4 | AGTCGGATCCCTATGCTGCTTGAT |
| 2949 | sfGFP_Cterm_P1_NheI | GCATGGCTAGCATGAGTAAAGGAGAAGAACTTTTC |
| 3049 | P1 SACOL1122 KO | AGTCCCGGGGTCGTACTATCTAATGTTATAGG |
| 3050 | P2 SACOL1122 KO | TTGGCTAGTATTTTTTTAATATTCAGTCATCCAATTC |
| 3051 | P3 SACOL1122 KO | ATTGTAGAATTGGATGACTGAATATTAAAAAAATACTAGCC |
| 3052 | P4 SACOL1122 KO | ACTGGATCCTGCTACATCAATGATACGCTC |
| 3056 | P1 SACOL2075 KO | ATTCCCGGGCATAGAACTTGCAGCTGACAATACACC |
| 3057 | P2 SACOL2075 KO | TATTTGAAACTCAAAATAGTTTAAATTATGCAAACTCCTTTTATACTCAC |
| 3058 | P3 SACOL2075 KO | AGTATAAAAGGAGTTTGCATAATTTAAACTATTTTGAGTTTC |
| 3059 | P4 SACOL2075 KO | ATAGGATCCGTAAGTCAATTGACAGAACGC |
| 3112 | XmaI-RBS-GFP(P7) for | GCGCCCGGGAAAAAATAAGGAGGAAAAAAAATGAGTAAAGGAGAAGAACTTTTC |
| 3211 | GFP(P7)-10aa linker revx | AGAACCTCCTCCACCAGAACCTCCTCCACCGTCGACTTTGTATAGTTCATCCATG |
| 3350 | GFP(P7)-TAA-XhoI rev | CCGGCTCGAGTTATTTGTATAGTTCATCCATG |
| 3490 | PBP1-BamHI rev | GCCGGATCCTTAGTCCGACTTATCCTTGTC |
| 3599 | BamHI-RBS for | GCCGGATCCAAAAAATAAGGAGGAAAAAAAATG |
| 3600 | PBP1-EcoRI rev | GCCGAATTCTTAGTCCGACTTATCCTTGTC |

| 3806 | BglII-SACOL1192 (last183bp) for | CCGAGATCTCAGGTGTTCCAAGAATATG |
|------|-------------------------------|------------------------------|
| 3809 | GFP(P7)-10aa linker rev | AGAGCCACCTCCGCCAGAACCGCCTCCACC GTCGACTTTGTATAGTTCATCC |
| 4041 | C-GFP-KpnI Rev | CCGGTACCTTATTTGTATAGTTCATCCATGC CATGTG |
| 4179 | P1 SACO1122i_spa | ACTCCCGGGGATCATTTGAAGTATAAATTG |
| 4180 | P2 SACO1122i_spa | AGTCTCGAGATCTCGTACTAAATATTGG |
| 4235 | Pspac-RBS Rev | CATTTTTTTTCCTCCTTATTTTTTCCCGGGAA AAGCTTAATTGTTATCC |
| 4236 | RBS-pbpA For | GAAAAAATAAGGAGGAAAAAAATGGCGAAG CAAAAAATTAAAATT |
| 4470 | SmaI-RBS-pbpA For | GCGCCCGGGAAAAAATAAGGAGGAAAAAAA ATGGCGAAGCAAAAAATTAAAATT |
| 4980 | EcoRI-PBP3 (670bp) For | GCCGAATTCCACGTCTATGGATTGGGATAG |
| 4981 | PBP3S392G-BamHI Rev | CGCGGATCCTCCAACCGCAAATTGAGAAG |
| 4982 | BamHI-PBP3S392G For | CGCGGATCCGTAAAAGGTGGAACATTATTAG |
| 4983 | PBP3 (1.7kb)-SalI Rev | GCCGTCGACCTTGAGTGGACCAACCTCATC |
| 5187 | TMpbp2_Xma_Rev | TCGGTACCCGGGTTAAGCAAACAATAAGATA CTAG |
| 5440 | BamHI-RBS-ATG For | CGCGGATCCAAAAAATAAGGAGGAAAAAAAA TG |
| 5545 | 2075-mCh_P2 | ATAGTTTAAATTACTTGTACAGCTCGTCCATG |
| 5546 | 2075-mCh_P3 | GTACAAGTAATTTAAACTATTTTGAGTTTC |
| 5547 | 1122_W121A_P1 | ATATTAATGGTTCTAAAAGTGCAATAAACTTA GGATTTATGAAC |
| 5548 | 1122_W121A_P2 | TTCATAAATCCTAAGTTTATTGCACTTTTAGA ACCATTAATATC |
| 5553 | 1122_D287A_P1 | ATTTACCAGAACCACATACAGCATTTATTTTT GCAATTATTTG |
| 5554 | 1122_D287A_P2 | CAAATAATTGCAAAAATAAATGCTGTATGTGG TTCTGGTAAATAG |
| 5559 | 2075_W111A_P1 | TTATCAATGGTGCCAAAAGTGCATACACGTT TGGCCCTATCAG |
| 5560 | 2075_W111A_P2 | CTGATAGGGCCAAACGTGTATGCACTTTTGG CACCATTGATAATAG |
| 5565 | 2075_D286A_P1 | ATATACCTGAAAATCATACTGCATTTATCTTT TCAGTGATTTG |
| 5566 | 2075_D286A_P2 | CCAATCACTGAAAAGATAAATGCAGTATGAT TTTCAGGTATATAAAC |

| | | |
|---|---|---|
| **5599** | 10aa-mCh For | GGCGGTTCTGGCGGAGGTGGCTCTGCTATCATTAAAGAGTTCATGCGC |
| **5603** | GFPSTOPP2_Eco | CGCCGAATTCTTATTTGTATAGTTCATCCATGCC |
| **5609** | SACOL2075_P1_BamHI | CGCGGATCCTGAGTATAAAAGGAGTTTGC |
| **5665** | 2075-mCh_P4 | AGAGCCACCTCCGCCAGAACCGCCTCCACCATTACTTTTTGGATGGTATAAATC |
| **5668** | PBP3-EcoRI Rev | GCCGAATTCTTATTTGTCTTTGTCTTTATTTTTATC |
| **5671** | CFP-EcoRI Rev | GCCGAATTCTTACTTGTACAGCTCGTCCATGCC |
| **5704** | BamHI-RBS-PBP3 For | CGCGGATCCAAAAAATAAGGAGGAAAAAAATTGTTAAAAAGACTAAAAGAAAAATCGACTAAAAGAAAAATC |
| **5706** | BamHI-RBS-1122 For | CGCGGATCCAAAAAATAAGGAGGAAAAAAAATGAAGAATTTTAGAAGTATTTTAC |
| **5707** | BamHI-RBS-2075 For | CGCGGATCCAAAAAATAAGGAGGAAAAAAAATGAATTATTCATCTCGTCAACAG |
| **5708** | BamHI-RBS-1804 For | CGCGGATCCAAAAAATAAGGAGGAAAAAAAATGAGTGAAAGTAAAGAAATGGTG |
| **5772** | 1193-pbpA1.9kb Rev | GATTGTGCTTTTATTTAATTTTTTGCTTCGCCATTAC |
| **5773** | 1193-pbpA1.9kb For | CAAAAAATTAAATAAAAGCACAATCTATAAAAGCAG |
| **5774** | 250dwnpbpA-BamHI Rev | CGCGGATCCCCACTAATATATTATCAATTTTTC |
| **5941** | CFP-KpnI Rev | GCCGGTACCTTACTTGTACAGCTCGTCCATGCC |
| **6052** | CFP-NotI Rev | GGGGCGGCCGCTTACTTGTACAGCTCGTCCATGCC |
| **6053** | NotI-RBS For | GGGGCGGCCGCAAAAAATAAGGAGGAAAAAAAATG |
| **6398** | mCh-KRSGSGGS Rev | GGAGCCACCAGAACCAGATCTTTTCTTGTACAGCTCGTCCATGCCACC |
| **6399** | KRSGSGGS-GFP For | GAAAAGATCTGGTTCTGGTGGCTCCAGTAAAGGAGAAGAACTTTTCAC |
| **6400** | GGGSGGGGS-TM2 For | GGAGGCGGTTCTGGCGGAGGTGGCTCTACGGAAAACAAAGGATCTTCTCAG |
| **6404** | (RBS)-ATG-GFP For | GGAGGAAAAAAAATGAGTAAAGGAGAAGAACTTTTC |
| **6407** | (RBS)-ATG-mCh For | GGAGGAAAAAAAATGGCTATCATTAAAGAGTTCATG |

| 6682 | 2075-RBS_rev | CATTTTTTTTCCTCCTTATTTTTTGCGGCCGC<br>TTAATTACTTTTTGGATGGTATAAATC |
|------|--------------|--------------------------------------------------------|
| 6683 | RBS_PBP3_fw | TAAGCGGCCGCAAAAAATAAGGAGGAAAAAA<br>AATGTTAAAAAGACTAAAAGAAAAATC |
| 6686 | pCNX-RBS_Gibson_P1 | CTGCAGGTCGACTCTAGAGGATCCAAAAAAT<br>AAGGAGGAAAAAAAATG |
| 6692 | PBP3_rev_MCS | TTCGAGCTCGGTACCCGGGGATCCTTATTTG<br>TCTTTGTCTTTATTTTTATC |

## Whole genome sequencing

Chromosomal DNA was purified using a standard phenol chloroform extraction technique[33] (for strains COL and ColPBP1TP) or Wizard® Genomic DNA Purification Kit Protocol (for strains ColΔ*rodA*, ColΔ*pbpC*, Col Δ*rodA*Δ*pbpC*, JE2 and JE2Δ*pbp3*Δ*rodA*). Libraries were prepared at the Gene Expression Unit (Instituto Gulbenkian de Ciência, Oeiras, Portugal) by simultaneous fragmentation and tagging using Nextera™ DNA Library Preparation kit. Sequencing was performed on a MiSeq instrument (Illumina, Inc.) with a 2x300-cycle kit, resulting in an average raw genomic coverage superior to 100X.

The computational pipeline Breseq version 0.32.1[34] with default settings was used to map the obtained paired-end reads against the genome of parental strains COL or JE2 and to predict mutations and structural variations. The resulting percentage of mapped reads ranged from 86.6% to 99.8%. Only predicted mutational events present in at least 50% of the mapped reads were included in Table 3.

## Growth curves

Overnight cultures were back-diluted to $OD_{600nm}$ of 0.02 in TSB and grown for 8 hours with $OD_{600nm}$ measurements taken every hour. In

the case of ColFtsWi, ColPBP1i and their derivatives, overnight cultures were washed four times with TSB and back-diluted to $OD_{600nm}$ of 0.02 in TSB with or without IPTG. At $OD_{600nm}$ of approximately 1, cells were similarly washed and back-diluted to $OD_{600nm}$ of 0.05. Measurements of $OD_{600nm}$ were taken every hour.

## Minimum inhibitory concentration (MIC) assays

Moenomycin MIC was determined using broth microdilution in sterile 96-well plates, where overnight cultures were diluted to a cell density of ~$5x10^5$ CFU $ml^{-1}$ in wells containing two-fold dilutions of moenomycin. Plates were incubated aerobically for 24 hours at 37°C, and endpoint growth was assessed visually. All assays were performed in triplicate.

## HPLC analysis of muropeptides

Peptidoglycan purification from mid-exponential phase cultures was performed as previously described[35]. Preparation of muropeptides was performed by digestion with mutanolysin (Sigma) and reduction with sodium borohydride (Sigma), before analysis by reverse-phase HPLC using a Hypersil ODS column (Thermo Electron Corporation). Areas under the curve (AUC) of integrated peaks were calculated using the Shimadzu Prominence LC solution Version 1.21 SP1 software. The percentage of each peak was calculated based on the ratio of the peak AUC over the sum of AUC of all integrated peaks.

## Total protein extraction, western blot analysis and bocillin-FL binding

For protein extraction, *S. aureus* cultures were grown in 50 ml TSB to an $OD_{600nm}$ of 0.8. Cells were lysed using glass beads in a Fast Prep FP120 (Thermo Electro Corporation), separated from the glass beads by centrifugation for 1 min at 1630 x g, and centrifuged for 15 min at 16,000 x g to remove unbroken cells. Total protein content present in the supernatant was quantified using the Pierce™ BCA Protein Assay Kit (Thermo Scientific) and 50 µg of protein extract were loaded in each well of a 10 % SDS-PAGE gel and separated at 80 V for 2 hrs. For the detection of fluorescent proteins, the gel was imaged in a *FujiFilm* FLA-*5100* Fluorescent *Image* Analyser using 473 nm/LPB filter for sGFP fusions and 532 nm/LPFR filter for mCherry fusions. For western blotting, COL and ColPBP1TP samples were transferred to a Hybond-P Polyvinylidene difluoride (PVDF) membrane (GE Healthcare) using a semi-dry transfer cell (Biorad), blocked for 1 hr with 5 % milk in PBS-T (0.5 % Tween 20 in phosphate buffered saline) and incubated at 4°C with anti-PBP1[36] overnight. Washed membranes were then incubated for 1 h with HRP-conjugated goat anti-rabbit secondary antibody (GE Healthcare) and bands were visualized using the ECL Plus Western blotting detection kit (Amersham) and a Chemidoc XRS+ Imaging System (Biorad). Bocillin-FL binding was performed by incubating 100 µg of total protein extract with 100 µM Bocillin-FL for 15 min at 30°C before adding 5X SDS/PAGE sample buffer to give a 1X concentration. Following 15 min of incubation at 30°C, samples were centrifuged at 16,000 x g for 1 min and half the sample volume (equal to 50 µg of protein) was loaded on a 10 % SDS-PAGE gel and separated at 80 V for 2 hrs. Fluorescent bands were then imaged using a 532 nm laser in an FLA-5100 reader.

## *S. aureus* imaging by fluorescence microscopy

Structured Illumination Microscopy (SIM) was performed using an Elyra PS.1 microscope (Zeiss) with a Plan-Apochromat 63x/1.4 oil DIC M27 objective. SIM images were acquired using three or five grid rotations, with 34 µm grating period for the 561 nm laser (100 mW), 28 µm period for 488 nm laser (100 mW) and 23 µm period for 405 nm laser (50 mW), and captured using a Pco.edge 5.5 camera. Images were reconstructed using ZEN software (black edition, 2012, version 8.1.0.484) based on a structured illumination algorithm[37], using synthetic, channel specific optical transfer functions and noise filter settings ranging from −6 to −8.

Epifluorescence microscopy for co-localization studies and fluorescence ratio analysis was performed using a Zeiss Axio Observer microscope with a Plan-Apochromat 100x/1.4 oil Ph3 objective. Images were acquired with a Retiga R1 CCD camera (QImaging) using Metamorph 7.5 software (Molecular Devices).

For fluorescence microscopy experiments, *S. aureus* cultures were grown to mid-exponential phase ($OD_{600nm}$ of 0.6-1.0) prior to pelleting. Cells were suspended in phosphate buffer saline (PBS) and placed on a thin layer of agarose (1.2% in PBS). For time lapse microscopy, cells were suspended in TSB and spotted on 1.2% agarose in 50% TSB/PBS (COL) or 100% TSB (JE2) slide, before imaging every 3 or 5 min. In the case of ColFtsWi, ColPBP1i and their derivatives, overnight cultures were back-diluted to an $OD_{600nm}$ of 0.1 and grown for 3 hours in the presence of 0.5 mM and 0.01 mM IPTG, respectively. Cells were washed three times with TSB and grown in the presence or absence of IPTG. Cells were then harvested and prepared for microscopy as described above.

To observe the localization of peptidoglycan incorporation, *S. aureus* cells were consecutively incubated with 250 µM of fluorescent D-amino-acids HADA, NADA and TDL[38,39] for 10 min, as previously described[40]. Cells were washed with PBS, mounted on a PBS agarose pad and imaged.

To label *S. aureus* membranes, cells were stained with Nile Red (Invitrogen) at a final concentration of 5 µg ml^{-1} for 5 min at 37°C, washed with PBS and then placed on PBS agarose pads for imaging. To label *S. aureus* cell wall, cells were stained with a mixture of equal volumes of vancomycin (Sigma) and a BODIPY FL conjugate of vancomycin (Van-FL, Molecular Probes) at a final concentration of 0.8 µg ml^{-1} for 5 min at 37°C, washed with PBS and then placed on PBS agarose pads for imaging.

## Microscopy analysis

Cell axes and volumes were calculated as previously described[17]. In brief, an ellipse was first fitted to the border of Nile-Red-stained cells, overlaying the fluorescence signal. The longer and shorter axes were then measured and used to calculate the ratio of long/short axis (L/S). These axes were also used to calculate the volume based on a prolate spheroid.

Fluorescence ratio (FR) of septal to peripheral signal was measured using the 25 % brightest pixels, using in-house software, eHooke, as previously described[23].

For cell elongation analysis, the long/short cell axis ratio was calculated using eHooke[23]. For this, individual cells were segmented and the smallest box possible was fitted around each cell. The box length was considered the cell long axis and the box width was considered the

cell short axis. The percentage of cells with an axis ratio higher than 1.25 (approximately percentile 95 of COL) was then calculated for each strain.

To calculate the percentage of cells with multiple rings, 2D SIM images were analyzed for single rings (single line or two opposite foci depending on cell orientation) or multiple rings (multiple lines or more than two foci). Cells without rings were excluded from analysis.

To calculate the percentage of cells with midcell HADA in Phase 1, 100 Nile-Red-stained cells without a septum were assessed from 3 different images for each strain. Experiments were performed in triplicate.

For cell cycle distribution analysis, Nile-Red-stained cells were classified into one of three cell cycle phases, as previously described[17]. In brief, Phase 1 refers to the first stage of the cell cycle, before initiation of septum synthesis, Phase 2 is the stage of septum synthesis and Phase 3 cells have a complete septum, undergoing maturation prior to daughter cell separation. Assays were performed in triplicate.

## Transmission electron microscopy (TEM)

ColFtsWi and ColPBP1i were initially grown in the presence of IPTG before being washed and back-diluted with and without IPTG until mid-exponential phase. Sample preparation was performed essentially as previously described[28]. Briefly, cell pellets were suspended in a primary fixative solution (2.5 % glutaraldehyde + 1 % osmium tetroxide in 0.1 M PIPES buffer at pH 7.2) for 1 hr at 4°C, with gentle movement. Cells were then washed five times with MilliQ $H_2O$ to remove the fixative and suspended in 3-4 % agarose. Small sections of agarose-embedded cells were incubated overnight at 4 °C in 0.5 % uranyl acetate. The

following day, sample were washed with MilliQ $H_2O$ twice and dehydrated using 10 min steps in ethanol (30-100 %), anhydrous ice-cold acetone and anhydrous room temperature acetone. Samples were gradually shifted into 100 % Spurr's resin and polymerized for 24 hrs at 60 °C. Ultrathin sections (90 nm) were mounted on 200 mesh Cu grids and stained with Reynold's lead citrate. Excess stain was removed with degassed water and TEM imaging at 120 kV was performed on a FEI Tecnai 12 microscope, using a Gatan OneView CMOS camera with Digital Micrograph 3.0 software, at the Electron Microscopy Facility at the Instituto Gulbenkian de Ciência, Oeiras, Portugal.

## Fluorescence lifetime imaging microscopy (FLIM)

Cultures were grown to mid-exponential phase in TSB supplemented with 0.1 µM cadmium chloride. Cells were pelleted and suspended in PBS, before being spotted on a PBS agarose pad. FLIM measurements were performed by time correlated single photon counting (TCSPC) using a Leica TCS SP5 confocal microscope with a 63x apochromatic water immersion objective (NA of 1.2, Zeiss) coupled to a multiphoton Titanium-Sapphire laser (Spectra-Physics Mai Tai BB) as the excitation source. FLIM data was acquired during 120 seconds. The excitation wavelength was set to 480 nm and emission light was selected with a dichroic beam splitter with an excitation SP700 short-pass filter and an emission 525 ± 25 nm band-pass filter inserted in front of the photomultiplier. Images were acquired using a Becker and Hickl SPC 830 module. Fluorescence decays in the septum of each cell were calculated by integrating the FLIM data for all pixels of each septum. Fluorescence lifetimes were obtained by analyzing the fluorescence decays through a least square iterative re-convolution of decay functions with the instrument response function (IRF) using the software

SPCImage (Becker and Hickl). Monoexponential decays were considered in this analysis. Average FRET efficiencies ($E$) in each cell were determined from $E = 1 - \frac{\tau_{DA}}{\tau_D}$, where $\tau_{DA}$ and $\tau_D$ are the donor fluorescence lifetime in the presence and absence of acceptor, respectively.

## seFRET quantification.

COL cells expressing mCherry-sGFP (cytoplasmic tandem, E = 12 % as determined by FLIM-FRET), sGFP fusion only (donor-only), mCherry fusion only (acceptor-only), both sGFP and mCherry fusions (double), as well as COL cells containing the empty pCNX vector, were grown to mid-exponential phase. In order to obtain microscopy images with the five types of cells, a similar number of cells from each strain was mixed together, pelleted, suspended in PBS and placed on a PBS agarose slide. Imaging was performed on a Zeiss Axio Observer.Z1 microscope equipped with a Photometrics CoolSNAP HQ2 camera (Roper Scientific) and a Colibri Light Emitting Diode (LED) illumination system (Zeiss), using ZEN blue software. Slides were imaged for donor signal (300 msec, ex$_{470nm}$/em$_{502.5-537.5nm}$), FRET signal (1500 msec, ex$_{470nm}$/em$_{603.5-678.5nm}$) and acceptor signal (3000 msec, ex$_{555nm}$/em$_{603.5-678.5nm}$) sequentially. FRET efficiency was calculated as described in Chen et al.[41], by measuring the autofluorescence in each channel of ColpCNX cells, calculating correction factors for channel bleeding and cross-channel excitation using donor-only and acceptor-only cells, and calculating the ratio between sensitized acceptor emission and quenched donor emission due to FRET (G)[42], using the cytoplasmic tandem and the FRET efficiency value determined by earlier FLIM experiments. The G value[42] was used to quantify the FRET efficiency

(E) of sets of proteins, using the donor, acceptor and FRET channel measurements in double strain cells.

To perform seFRET quantification on subcellular regions, in-house developed software was used to identify single cells, as previously described[23]. The background for each cell was locally calculated and removed from each channel signal. Additionally, autofluorescence (median signal value of wild type cells) was subtracted. To define subcellular regions, the software then separated the membrane of each cell by expanding the cell outline inwards. Following membrane identification, the septum was detected using an isodata algorithm, corresponding to the inner region of the cell with the most fluorescence. After this segmentation, user input defined which cells corresponded to each strain based on the presence/absence of donor and acceptor signals. Correction factors were taken from the membrane and septum signals, and the E values were then calculated for each cell of strains expressing a pair of proteins, using septal signal only.

Github repository: https://github.com/BacterialCellBiologyLab/PyFRET

## **Statistical analysis.**

Statistical analyses were done using Excel 2010 to calculate the $p$ values using the two-tailed Mann-Whitney $U$ test. $p$ values $< 2.22 \times 10^{-16}$ could not be accurately determined and are reported as $p < 10^{-16}$. $p$ values $\leq 0.05$ were considered as significant for all analysis performed and were indicated with asterisks: *$p \leq 0.05$, **$p \leq 0.01$, ***$p \leq 0.001$ and ****$p \leq 0.0001$.

# RESULTS

## RodA-PBP3 and FtsW-PBP1 form cognate pairs in *S. aureus*

To understand if SEDS proteins and bPBPs function together in cocci such as *S. aureus*, we investigated the essentiality of SEDS proteins FtsW and RodA, and bPBPs PBP1 (encoded by *pbpA*) and PBP3 (encoded by *pbpC*). Previous data have shown that PBP1 is essential[22], while growth is unaffected in the absence of PBP3[43]. We were able to delete *rodA* from the methicillin-resistant *S. aureus* (MRSA) strain COL, but not *ftsW*. Therefore, *ftsW* was placed under the IPTG-inducible P*spac* promoter at an ectopic locus before deletion of the native copy, resulting in strain ColFtsWi. The same strategy was implemented for *pbpA*, giving rise to ColPBP1i.

Growth curves of the null RodA (ColΔ*rodA*) and PBP3 (ColΔ*pbpC*) mutants mimicked that of COL, and the growth rate was maintained even in the absence of both genes (ColΔ*rodA*Δ*pbpC*) showing that RodA and PBP3 are not essential (Fig. 1a). Similar results were obtained in the background of the community-acquired MRSA strain JE2 (Fig. 1b). Although whole genome sequencing (Table 3) showed the presence of single nucleotide polymorphisms (SNPs) in ColΔ*rodA*Δ*pbpC,* no SNPs were present in JE2Δ*rodA*Δ*pbpC*, indicating that no suppressor mutations are required for the viability of a mutant lacking RodA and PBP3.

In contrast to RodA and PBP3, depletion of FtsW or PBP1 resulted in growth inhibition, indicating that these proteins are essential for cell viability (Fig. 1c). To determine if the essential functions of FtsW and PBP1 are related to their roles in PGN synthesis, the growth of active site mutants was assessed. Conserved tryptophan and aspartic acid residues shown to abolish transglycosylase activity in *B. subtilis* RodA[14], were identified in *S. aureus* FtsW (W121 and D287) and RodA

(W111 and D286). Point mutations were introduced into sGFP fusions to FtsW, which were expressed at basal P*cad* promoter levels, from a multicopy plasmid. Unlike wild-type FtsW-sGFP, these mutated proteins could not complement the growth of ColFtsWi in the absence of IPTG, although they localized to the divisome, indicating that FtsW essentiality is dependent on its transglycosylase activity (Fig. 2). In contrast, the PBP1TP mutant carrying the S314A mutation in the transpeptidase active site (which abolished binding of the substrate analogue Bocillin-FL) was not affected in terms of growth rate, despite having decreased PGN cross-linking (Fig. 3). This suggests that PBP1 has a second role, as previously proposed[27]. Comparable results have been obtained in *B. subtilis*, where introduction of a point mutation in the TPase active site of the essential protein PBP2B, did not lead to loss of cell viability[44].

**Table 3. Whole genome sequencing results.**

| Gene containing indicated mutation | Description | Nucleotide change | Amino acid change |
|---|---|---|---|
| **COLΔ*rodA*** | | | |
| SACOL1290 | tRNA pseudouridine 55 synthase (*truB*) | A94 del. | I33* |
| **COLΔpbpC** | | | |
| SACOL_1364 | homoserine kinase (thrB) | G760A | V196I |
| SACOL_2325>IGR> SACOL_2326 | transcriptional regulator (*lysR*) > IGR > fosfomycin resistance protein (*fosB*) | GT→TC | |
| **COLΔpbpCΔ*rodA*** | | | |
| SACOL_1364 | homoserine kinase (thrB) | G760A | V196I |
| SACOL_1981 | isochorismatase family protein | N(251-271)dup. | G84-Y90dup. |
| SACOL_2057 | sigma factor B regulator protein (*rsbU*) | G4A | E2* |
| SACOL_2325>IGR> SACOL_2326 | transcriptional regulator (*lysR*) > IGR > fosfomycin resistance protein (*fosB*) | GT→TC | |

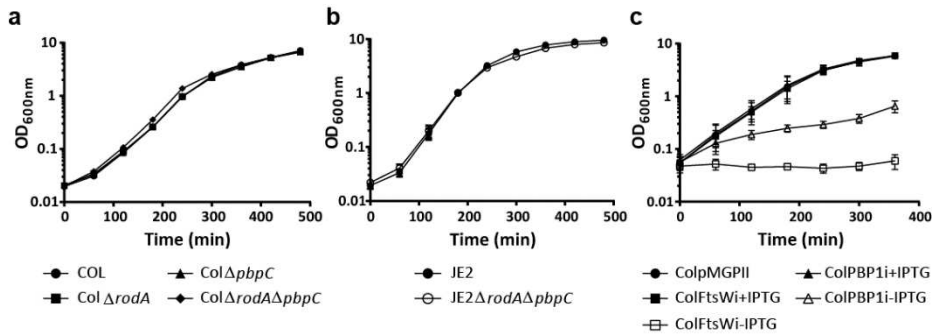dup-duplication; del-deletion; IGR-intergenic region; *- stop codon

**Figure 1. Viability of *S. aureus* cells in the absence of SEDS-bPBPs pairs.** **a**, Growth curve of parental strain COL and null mutants lacking RodA (ColΔ*rodA*), PBP3 (ColΔ*pbpC*) or both (ColΔ*rodA*Δ*pbpC*). **b**, Growth curve of parental strain JE2 and null mutant JE2Δ*rodA*Δ*pbpC* lacking RodA and PBP3. **c**, Growth curve of strains expressing IPTG inducible FtsW (ColFtsWi) or PBP1 (ColPBP1i) grown in the presence or absence of IPTG. Control strain ColpMGPII was grown in the absence of IPTG. Data represent the mean and s.d. of three independent experiments.

A recent study on the localization patterns of PGN synthesis proteins demonstrated that FtsW and PBP1 are almost exclusively septal localized and arrive at the divisome at a similar time, while RodA and PBP3 are enriched at the septum but can also be observed at the peripheral membrane[23]. Given that cognate SEDS-bPBP pairs are likely to co-localize, we decided to correlate the time of arrival of each SEDS protein with the two *S. aureus* bPBPs in co-localization studies. We observed a high percentage of co-localized FtsW-mCherry with sGFP-PBP1 (96%, *n*=577) and RodA-mCherry with sGFP-PBP3 (84%, *n*=441), while FtsW-mCherry with sGFP-PBP3 and RodA-mCherry with sGFP-PBP1 were not as temporally coordinated (57%, *n*=523 and 51%, *n*=481 of cells showed co-localization of these proteins, respectively) (Fig. 4a). In fact, cells with septal FtsW-mCherry arriving ahead of sGFP-PBP3 (22%, *n*=523) and septal sGFP-PBP1 arriving ahead of RodA-mCherry (49%, *n*=481) were identified (Fig. 4a,b, white arrows),

whereas the reverse was not observed, overall supporting the notion that FtsW/PBP1 and RodA/PBP3 may form two complexes.
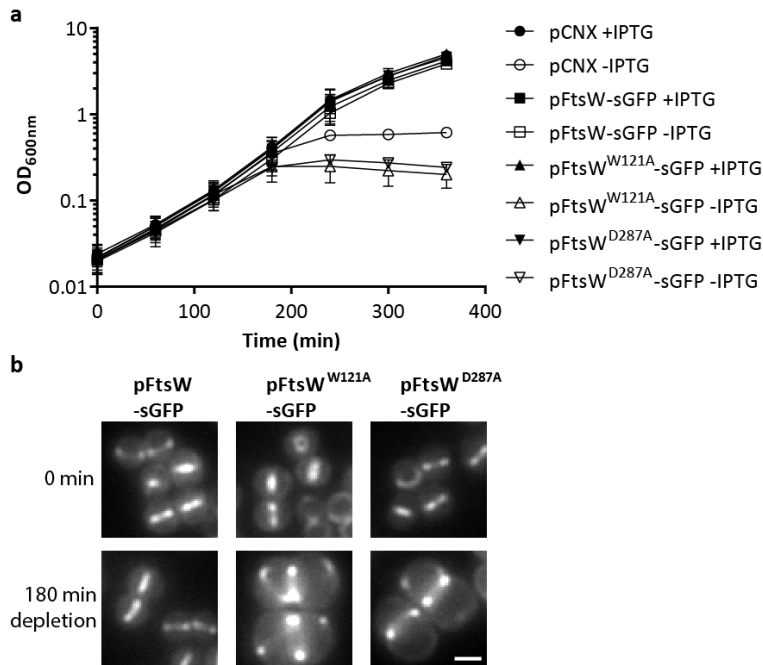


**Figure 2. FtsW^W121A and FtsW^D287A mutants are non-functional. a**, Growth curves of strain ColFtsWi encoding a chromosomal copy of *ftsW* under the control of an IPTG inducible promoter and complemented with the empty vector pCNX, the same vector encoding a sGFP derivative of native FtsW (pCNX-ftsWsgfp) or two active site mutants (pCNX-ftsW^W121Asgfp and pCNX-ftsW^D287Asgfp). FtsW fusions are expressed from a leaky cadmium inducible promoter which therefore gives rise to a detectable basal level of expression in the absence of cadmium. Strains were grown in the presence or absence of IPTG and the data represent the mean and s.d. of three independent experiments. **b**, Epifluorescence microscopy images of ColFtsWi complemented with FtsW-sGFP derivatives expressed from a plasmid (pCNX-ftsWsgfp, pCNX-ftsW^W121Asgfp and pCNX-ftsW^D287Asgfp). Images were taken before (0 min) and after (180 min) depletion of chromosomally encoded FtsW and are representative from one of the three biological repeats. Scale bar, 1 µm.

| Muropeptide Species | Content (%) | |
|---|---|---|
| | COL | ColPBP1TP |
| Monomer (5) | 2.79 | 7.35 |
| Dimer (11) | 3.66 | 6.59 |
| Trimer (15) | 4.34 | 4.85 |
| Tetramer (16) | 5.14 | 5.14 |
| Pentamer (17) | 4.16 | 1.61 |
| >Pentamer | 43.24 | 37.11 |
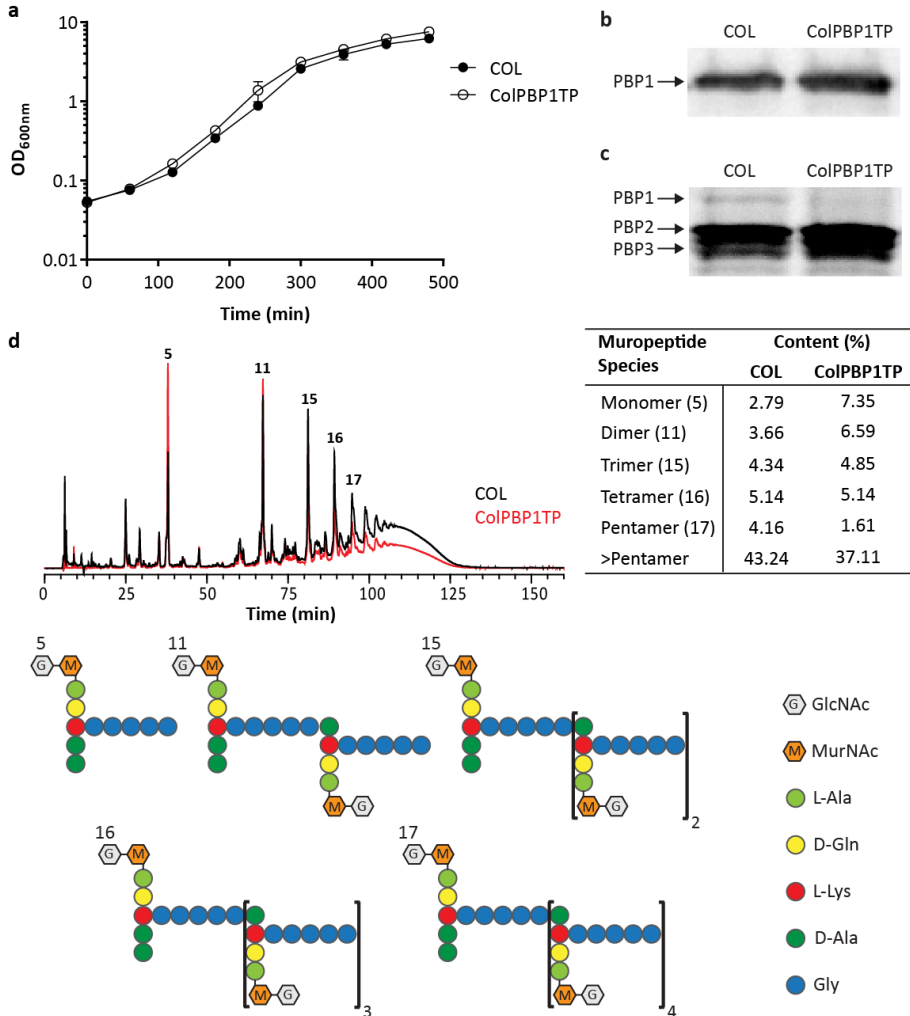
**Figure 3. PBP1 transpeptidase mutant shows reduced PGN cross-linking while maintaining normal growth rate. a**, Growth curve of parental strain COL and PBP1 S314A point mutant (ColPBP1TP) representing the mean and s.d. of three biological replicates. **b, c**, COL and ColPBP1TP total protein extracts analyzed in triplicate with similar results by western blotting with anti-PBP1 antibody (**b**) and bocillin-FL binding (**c**) demonstrating that ColPBP1TP expresses PBP1 at similar levels to COL, but can no longer bind bocillin-FL at its active site. **d**, HPLC analysis, performed in duplicate with similar results, of PGN muropeptides of COL (black) and ColPBP1TP (red) and table of quantification of peaks 5, 11, 15, 16, 17 and ≥18 (>Pentamer) confirming an increase in monomers and decrease in highly cross-linked species (>Pentamer) in ColPBP1TP compared to COL. Proposed structures of the muropeptide peaks present in the chromatogram according to de Jonge & Tomasz[45] are shown graphically below.

**Figure 4. FtsW-mCherry/GFP-PBP1 and RodA-mCherry/sGFP-PBP3 co-localize in the majority of cells. a,** Tables correlate the localization of mCherry derivatives of SEDS proteins FtsW and RodA with sGFP derivatives of bPBPs PBP1 and PBP3, in strains ColWP1 (*n*=577), ColWP3 (*n*=523), ColP1pA (*n*=481) and ColP3pA (*n*=441). Yellow squares show the percentage and s.d.

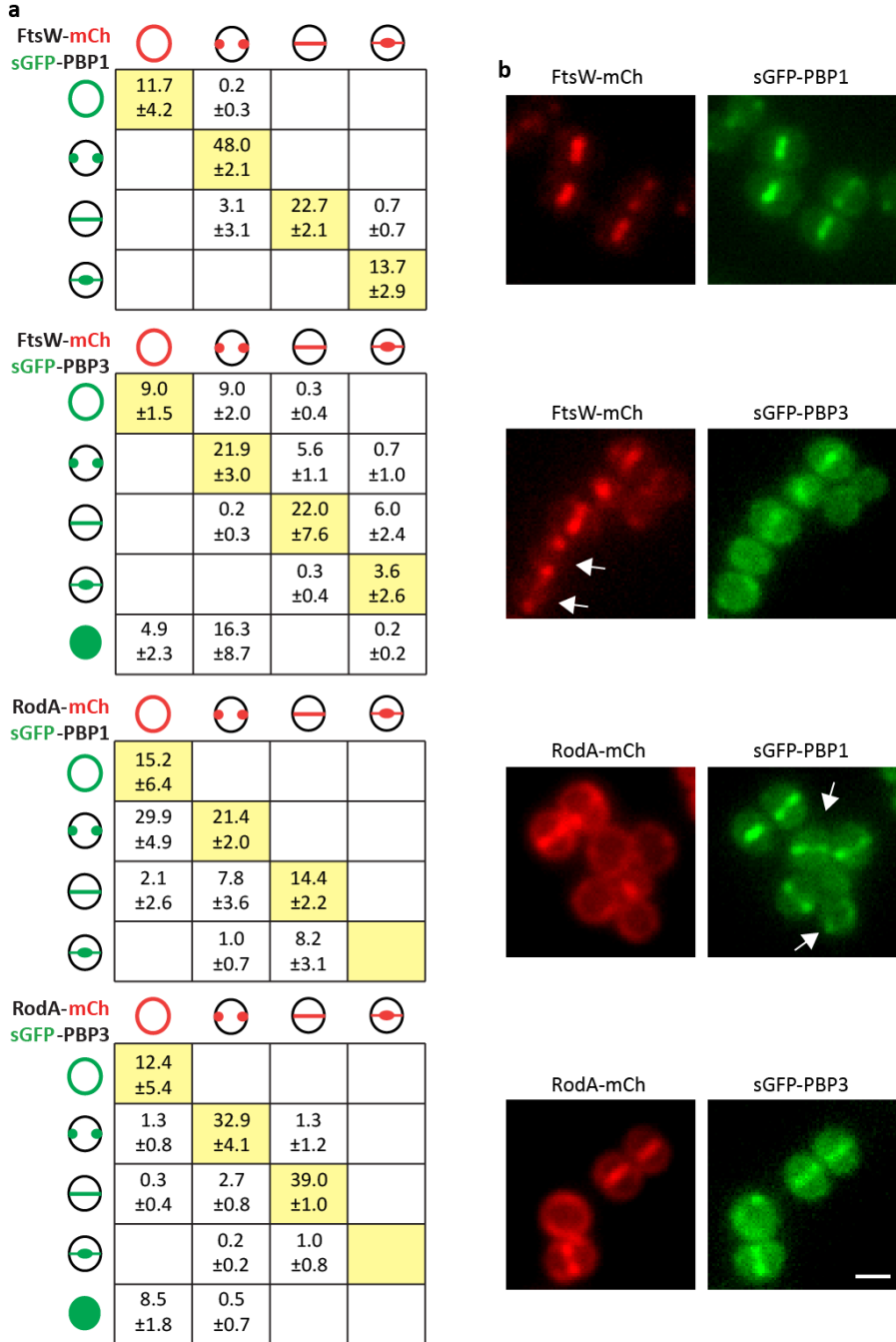of cells with co-localization of the SEDS and bPBP proteins at different stages of the cell cycle. Data suggests that PBP1 arrives to the septum before RodA (top right table) and that FtsW arrives to the septum before PBP3 (bottom left corner). **b**, Epi-fluorescence images of strains ColWP1, ColWP3, ColP1pA and ColP3pA (from top to bottom) co-expressing different combinations of SEDS and bPBPs. Scale bar, 1 μm. Images are representative of three biological replicates. Arrows highlight cells with midcell localized FtsW but not PBP3, or midcell localized PBP1 but not RodA.

Together, these results suggest that FtsW and PBP1 form an essential cognate pair that is recruited to the divisome before RodA and PBP3. To determine if these proteins directly interact, we performed Fluorescence Lifetime Imaging Microscopy - Förster Resonance Energy Transfer (FLIM-FRET) using *S. aureus* cells expressing plasmid-encoded sGFP-PBP1 fluorescent fusion and mCherry fusions to the SEDS proteins. Since PBP1 localizes to midcell, fluorescence lifetime analysis was restricted to septa. The co-expression of sGFP-PBP1 and FtsW-mCherry in *S. aureus* cells caused a drop in the average fluorescence lifetime of sGFP in comparison to the lifetime of sGFP-PBP1 expressed alone (1.80 ± 0.09 vs 1.59 ± 0.10 ns; Fig. 5c), equating to a FRET efficiency (E) of 11.5 ± 5.3% (*n*=90) (Fig. 5a). Similarly, high E values were observed for mCherry fused directly to sGFP and anchored to the membrane (tandem control mCherry-sGFP-TM, E=14.8 ± 4.8%, *n*=50), while E values for RodA-mCherry and sGFP-PBP1 were consistently lower (E=5.9 ± 5.3%, *n*=90) (Fig. 5a). These data indicate that PBP1 preferentially interacts with FtsW and not with RodA. Importantly, FLIM is independent of donor (sGFP-PBP1) concentration[46] and we have confirmed that acceptor (FtsW-mCherry or RodA-mCherry) concentrations were similar (Fig. 5d). To rule out the possibility of interactions being detected purely due to enrichment at the septum, an mCherry fusion to another almost exclusively septal localized protein, the putative lipid II flippase MurJ, was also probed for interactions with sGFP-PBP1, and was found to have low E values (4.3 ± 6.0%, *n*=90)

(Fig. 5a). Our data on PBP1/FtsW interaction agrees with the fact that PBP1 can be co-purified with an affinity-tagged FtsW when both proteins are co-expressed in *E. coli*[12].
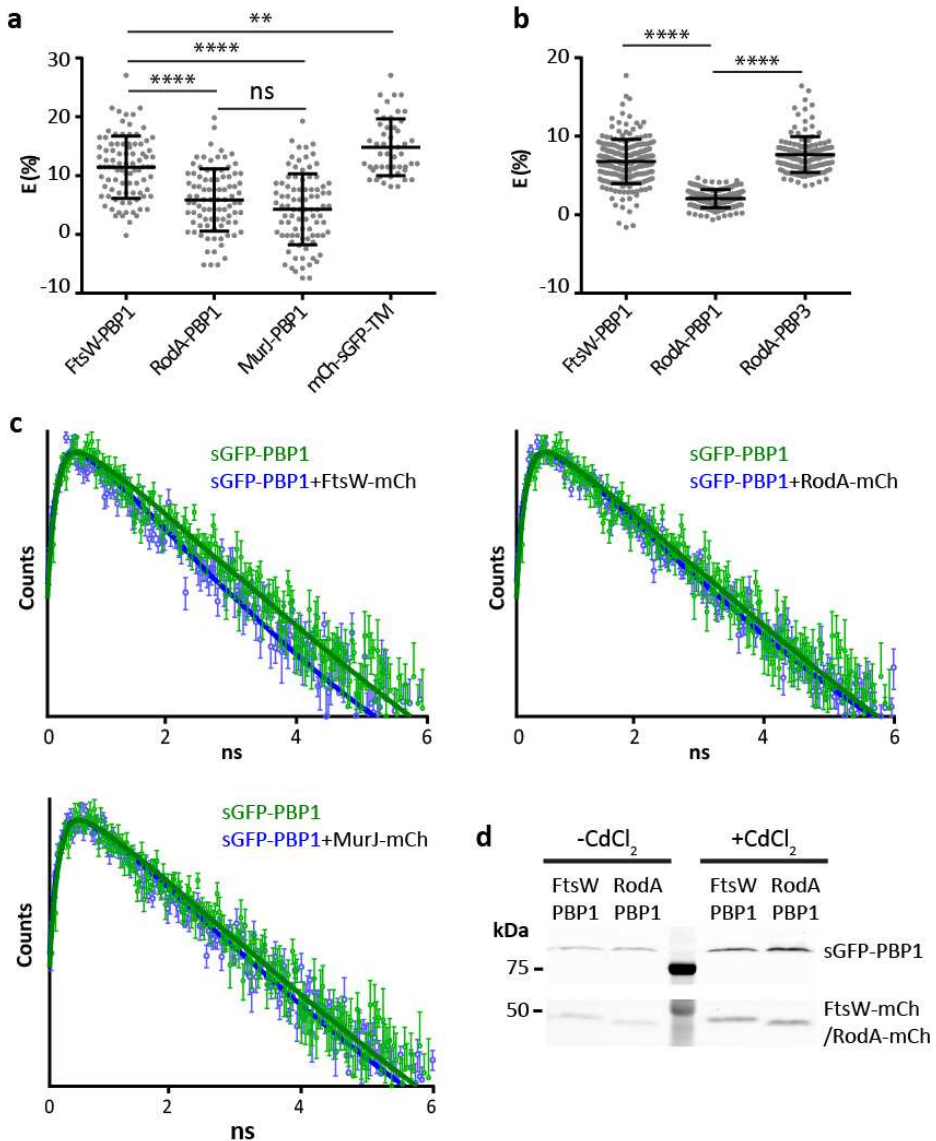


**Figure 5. *S. aureus* has two cognate SEDS-bPBPs pairs of interacting proteins, FtsW-PBP1 and RodA-PBP3. a,** FRET efficiency (E) determined by FLIM-FRET of strains ColpWP1 (*n*=90), ColpAP1 (*n*=90), ColpJP1 (*n*=90) and

ColpmCherry-sGFP-TM (*n*=50, tandem control where mCherry is linked to sGFP and anchored at the membrane). **b**, FRET efficiency (E) determined by seFRET of strains ColpWP1 (*n*=212), ColpAP1 (*n*=158) and ColpAP3 (*n*=141), performed in triplicate. Data in panels a and b are represented as scatter plots in which the middle line represents the mean and top and bottom lines are s.d.. Statistical analysis was performed using a two-sided Mann-Whitney *U* test. **\*\*p*<0.01; *\*\*\*\*p*<0.0001. **c**, Decay curves of sGFP-PBP1 (ColpsGFP-PBP1) in the absence (green) or presence (blue) of FtsW-mCherry (ColpWP1), RodA-mCherry (ColpAP1) and MurJ-mCherry (ColpJP1) (*n*=8). Data points correspond to the mean, error bars represent s.e. and lines show fits to the FLIM data. **d**, Fluorescence of total protein extracts of strains ColpWP1 (expressing FtsW-mCherry and sGFP-PBP1) and ColpAP1 (expressing RodA-mCherry and sGFP-PBP1) grown in the absence and presence of 0.1 μM $CdCl_2$ were analyzed in triplicate following SDS-PAGE and shown to express each mCherry fusion at a similar level. Predicted molecular weights were calculated: FtsW-mCherry (71.2 kDa); RodA-mCherry (70.8 kDa); sGFP-PBP1 (110.2 kDa).

Despite attempts to detect interactions with the sGFP-PBP3 fusion by FLIM-FRET, its fluorescence was too weak under the conditions used. Therefore, we decided to test protein-protein interactions by sensitized emission FRET (seFRET), allowing lower expression levels of fluorescent fusions to be examined. Using this approach, we were able to detect interactions between RodA-mCherry and sGFP-PBP3 occurring at the septum (E=7.7 ± 2.3%, *n*=141) (Fig. 5b). Furthermore, we detected a FRET efficiency of 6.8 ± 2.8% (*n*=212) for sGFP-PBP1 and FtsW-mCherry, compared to 2.0 ± 1.2% (*n*=158) for sGFP-PBP1 and RodA-mCherry (Fig. 5b), corroborating the FLIM-FRET data and providing in vivo evidence that both FtsW-PBP1 and RodA-PBP3 form cognate pairs.

## Elongation of *S. aureus* is mediated by RodA-PBP3

Having established that RodA-PBP3 and FtsW-PBP1 are the most likely *S. aureus* cognate TGase-TPase pairs, we decided to

investigate their functions. *B. subtilis* RodA was recently shown to possess TGase activity in vitro and its overexpression conferred resistance to moenomycin, an antibiotic that targets classical TGase domains, but to which SEDS proteins are insensitive[14]. Given their essentiality, moenomycin sensitivity under FtsW or PBP1 depletion conditions could not be accurately determined. However, analysis of ColΔ*rodA* demonstrated that this strain was hyper-susceptible to moenomycin, while overexpression of RodA/PBP3 (ColpRodA-PBP3) led to an increase in moenomycin resistance (Fig. 6a). Introduction of TGase active site point mutations W111A and D286A was sufficient to cause a decrease in minimum inhibitory concentration (MIC) without decreasing RodA-sGFP septal localization (Fig. 6a,b). Although moenomycin does not inhibit TPase activity, ColΔ*pbpC* had increased moenomycin susceptibility (Fig. 6a), indicating that RodA activity may be impaired in the absence of PBP3. Accordingly, we saw that RodA-sGFP requires PBP3 for correct septal localization (independently of its transpeptidase activity), while the opposite was not observed (Fig. 6b).

Previous analysis of the cell shape of *S. aureus* has revealed that these cocci are slightly eccentric and elongate prior to septum synthesis[17]. We therefore evaluated whether an *S. aureus* SEDS-bPBP pair was responsible for this slight elongation. Although lack of RodA and/or PBP3 did not alter progression of the cell cycle (Fig. 7a,b), the double mutant was consistently enlarged, and cells were less elongated when compared to wild-type, both in the COL background (Fig. 7c,d) and in the JE2 background (Fig. 8a), pointing to a role of the RodA-PBP3 pair in generating the slightly elliptical shape of *S. aureus*. Lack of either PBP3 or RodA was sufficient to generate more spherical COL cells and elongated cell shape was restored upon complementation of ColΔ*rodA*Δ*pbpC* with plasmid encoded RodA and PBP3 (Fig. 8b,c).

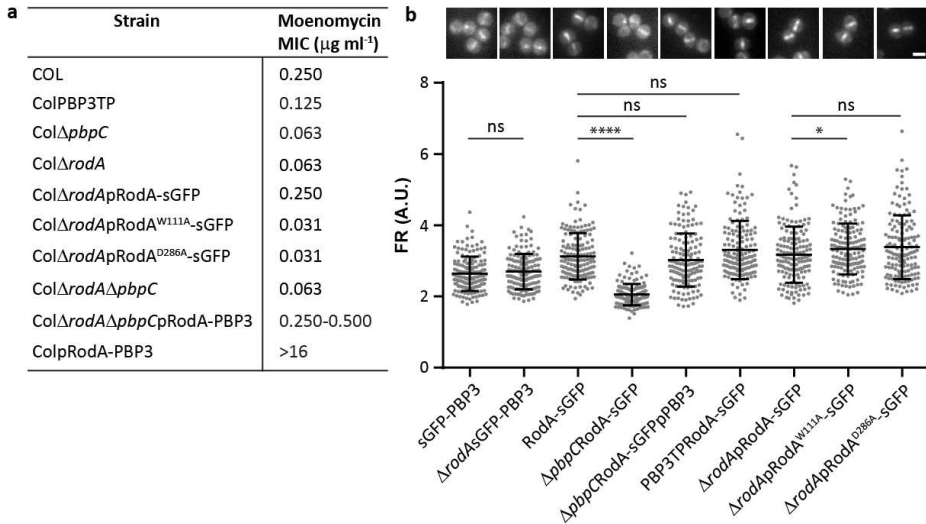| Strain | Moenomycin MIC ($\mu$g ml$^{-1}$) |
|---|---|
| COL | 0.250 |
| ColPBP3TP | 0.125 |
| Col$\Delta pbpC$ | 0.063 |
| Col$\Delta rodA$ | 0.063 |
| Col$\Delta rodA$pRodA-sGFP | 0.250 |
| Col$\Delta rodA$pRodA$^{W111A}$-sGFP | 0.031 |
| Col$\Delta rodA$pRodA$^{D286A}$-sGFP | 0.031 |
| Col$\Delta rodA\Delta pbpC$ | 0.063 |
| Col$\Delta rodA\Delta pbpC$pRodA-PBP3 | 0.250-0.500 |
| ColpRodA-PBP3 | >16 |

**Figure 6. RodA localization is dependent on the presence of PBP3. a**, Minimum Inhibitory Concentration (MIC) of moenomycin for (top to bottom) parental strain COL, PBP3 S392G mutant (ColPBP3TP), null mutants lacking PBP3 or RodA, *rodA* null mutant complemented with sGFP derivatives of native or inactive RodA, double mutant lacking PBP3/RodA, double mutant complemented with plasmid expressing PBP3/RodA and COL strain overexpressing PBP3/RodA. **b**, Representative epifluorescence images (top) and fluorescence ratios values (FR, bottom) for septal/peripheral signal in strains ColsGFP-PBP3, Col$\Delta rodA$sGFP-PBP3, ColRodA-sGFP, Col$\Delta pbpC$RodA-sGFP, Col$\Delta pbpC$RodA-sGFPpPBP3, ColPBP3TPRodA-sGFP, Col$\Delta rodA$pRodA-sGFP, Col$\Delta rodA$pRodA$^{W111A}$-sGFP and Col$\Delta rodA$pRodA$^{D286A}$-sGFP (*n*=150 for all strains). Statistical analysis was performed using a two-sided Mann-Whitney *U* test. *\*p*<0.05; \*\*\*\**p*<0.0001. Scale bar, 1 μm.

For cell elongation to occur, PGN must be incorporated into defined regions of the cell. In rod-shaped bacteria, PGN synthesis is directed to the long axis by MreB, while ovococci (which lack MreB) incorporate PGN at the midcell along the lateral wall. To understand where PGN insertion takes place for *S. aureus* elongation, we used fluorescent D-amino acids (FDAAs)[38] to label PGN synthesis. We found that 15 ± 3% (*n*=900) of the wild type cells had enriched HADA incorporation at midcell prior to any visible membrane invagination (Fig. 9, asterisks), indicating that *S. aureus* elongation may occur through a

process analogous to ovococci. Importantly, in the absence of PBP3 and RodA, the number of cells with this sidewall HADA incorporation was reduced to less than 2 ± 3% (*n*=900), strengthening the notion that RodA-PBP3 mediates elongation of *S. aureus* by directing PGN synthesis to the sidewall at midcell. Altogether, these data support a model whereby PBP3 recruits RodA to midcell and modulates its activity, and together this protein pair directs the side-wall insertion of PGN that leads to slight elongation of the *S. aureus* cell.
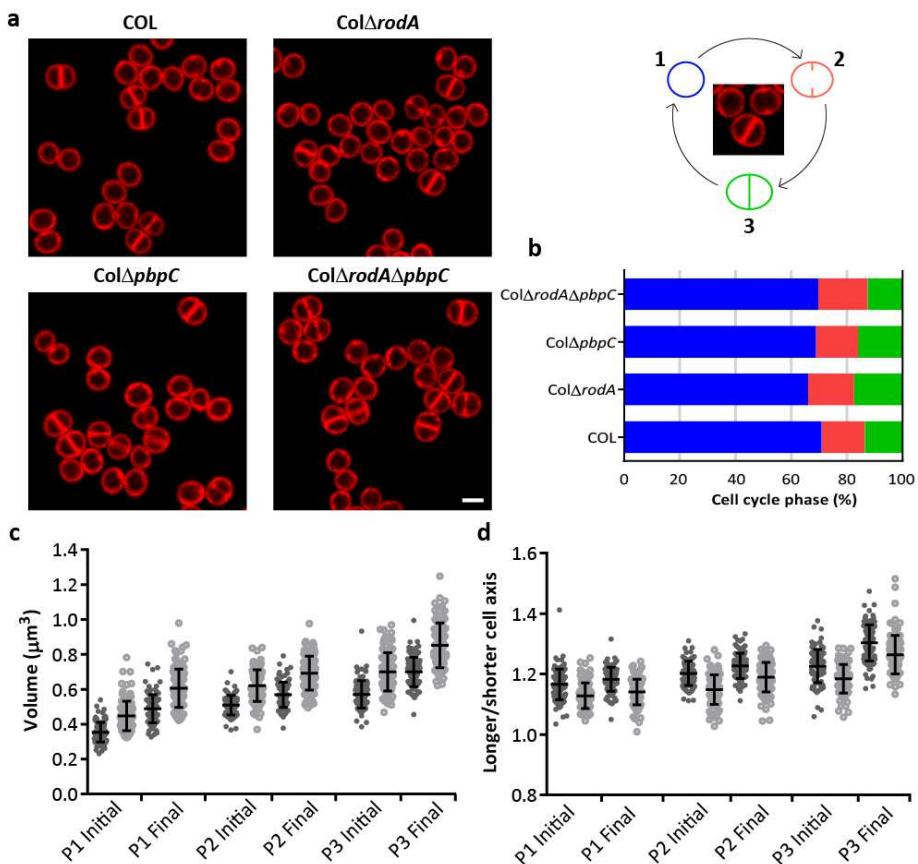


**Figure 7. RodA-PBP3 have a role in cell elongation. a**, SIM images of mid-exponential phase cells of COL, Col∆*rodA*, Col∆*pbpC* and Col∆*rodA*∆*pbpC* stained with Nile Red. Scale bar, 1 μm. The diagram to the top right shows examples of cells in each of the three cell cycle phases. **b**, Percentage of cells in cell cycle phase 1 (cells with no septum, blue), phase 2 (cells undergoing

septum synthesis, red) and phase 3 (cells with a complete septum, green), determined from SIM images of Nile Red stained cells of COL (*n*=1100), Col*ΔrodA* (*n*=900), Col*ΔpbpC* (n=1035) and Col*ΔrodAΔpbpC* (*n*=900). The mean of three independent experiments is shown in the graph and corresponds to the fraction of the cell cycle spent in each phase. **c, d,** Cell volume (**c**) and cell axis ratios (**d**) of strain COL (filled dark grey circles) and Col*ΔrodAΔpbpC* (open light grey circles) at the beginning and end of the cell cycle three phases (*n*=100). Volume fold changes of Col*ΔrodAΔpbpC* compared to COL vary between 1.22 and 1.27 for each cell cycle stage and cell axis ratio fold changes of Col*ΔrodAΔpbpC* compared to COL vary from 1.03 to 1.05. Data are represented as scatterplots where the middle line represents the mean and top and bottom lines show the s.d.. Experiments were performed in triplicate. Statistical analysis was performed using a two-tailed Mann-Whitney *U* test. ****\**p*<0.0001 for all compared pairs.
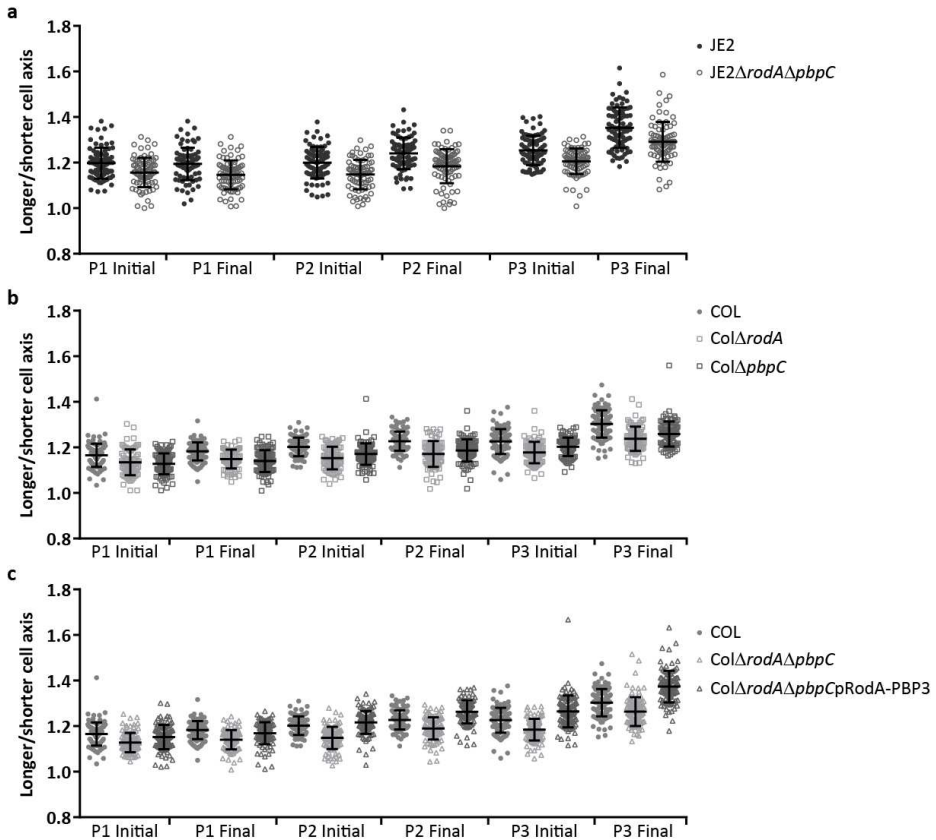


**Figure 8. Absence of RodA and PBP3 causes *S. aureus* cells to become more spherical. a**, **b**, **c**, Cell axis ratios at the beginning and end of the three phases of *S. aureus* cell cycle of parental strain JE2 (*n*=80, 80, 80) and null mutant JE2*ΔrodAΔpbpC* (*n*=80, 80, 80) (**a**), COL (*n*=100, 100, 100), Col*ΔrodA*

(*n*=81, 86, 85) and Col*ΔpbpC* (*n*=100, 100, 96) (**b**), COL (*n*=100, 100, 100), Col*ΔrodAΔpbpC* (*n*=100, 100, 100) and the complemented strain Col*ΔrodAΔpbpC*pRodA-PBP3 (*n*=100, 100, 100) (**c**). The absence of either RodA or PBP3 causes a decrease in cell axis ratio, while complementation of Col*ΔrodAΔpbpC* with plasmid expressed RodA and PBP3 restores cell elongation. *p* values comparing cell axis ratio fold change for the beginning and end of each cell cycle phase were always ****$p<0.0001$, except for JE2 vs. JE2*ΔrodAΔpbpC* P1 initial (***$p<0.001$), COL vs. Col*ΔpbpC* P3 initial (***$p<0.001$) and COL vs. Col*ΔrodAΔpbpC*pRodA-PBP3 P3 initial (*$p<0.05$). Data are represented as scatter plots, where the middle line represents the mean and the top and bottom lines show the s.d. Experiment was performed in triplicate. Statistical analysis was performed using a two-sided Mann-Whitney *U* test.



| Strain | Midcell HADA in Phase 1 (%) |
|---|---|
| COL | 15 ± 3 |
| Col*ΔrodA* | 2 ± 1 |
| Col*ΔpbpC* | 1 ± 2 |
| Col*ΔrodAΔpbpC* | 2 ± 2 |
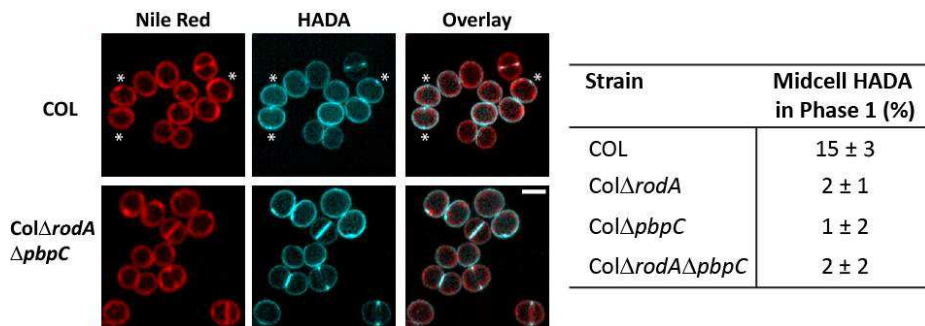
**Figure 9. RodA-PBP3 direct PGN synthesis to the sidewall.** Structured Illumination Microscopy (SIM) images of COL and Col*ΔrodAΔpbpC* stained with Nile Red (membrane) and HADA (PGN incorporation). Asterisks indicate cells with midcell HADA signal but no visible membrane invagination. Scale bar, 1 μm. Quantification of percentage of Phase 1 cells (cells with no septum) with midcell HADA signal in strains COL, Col*ΔrodA*, Col*ΔpbpC* and Col*ΔrodAΔpbpC* (*n*=900 cells). Data correspond to mean ± s.d. The *p* values were calculated for COL vs mutants and ****$p<0.0001$ for all compared pairs. Statistical analysis was performed using a two-tailed Mann-Whitney *U* test.

## The FtsW-PBP1 cognate pair is essential for inward PGN incorporation at the septum

To determine the function of the essential proteins FtsW and PBP1, we imaged ColFtsWi and ColPBP1i depleted of IPTG over time. Both strains became progressively enlarged and with an indentation at

midcell, clearly demonstrating a defect in cell division (Fig. 10a,b; Fig. 11a,b). Most strikingly, and contrary to RodA and PBP3 deletion mutants, lack of FtsW or PBP1 led to elongated cells (Fig. 10a,b; Fig. 11a,b) not only highlighting the key role of FtsW-PBP1 in synthesizing the septum, but also that the two cognate pairs most likely play opposing roles in defining the *S. aureus* cell shape.
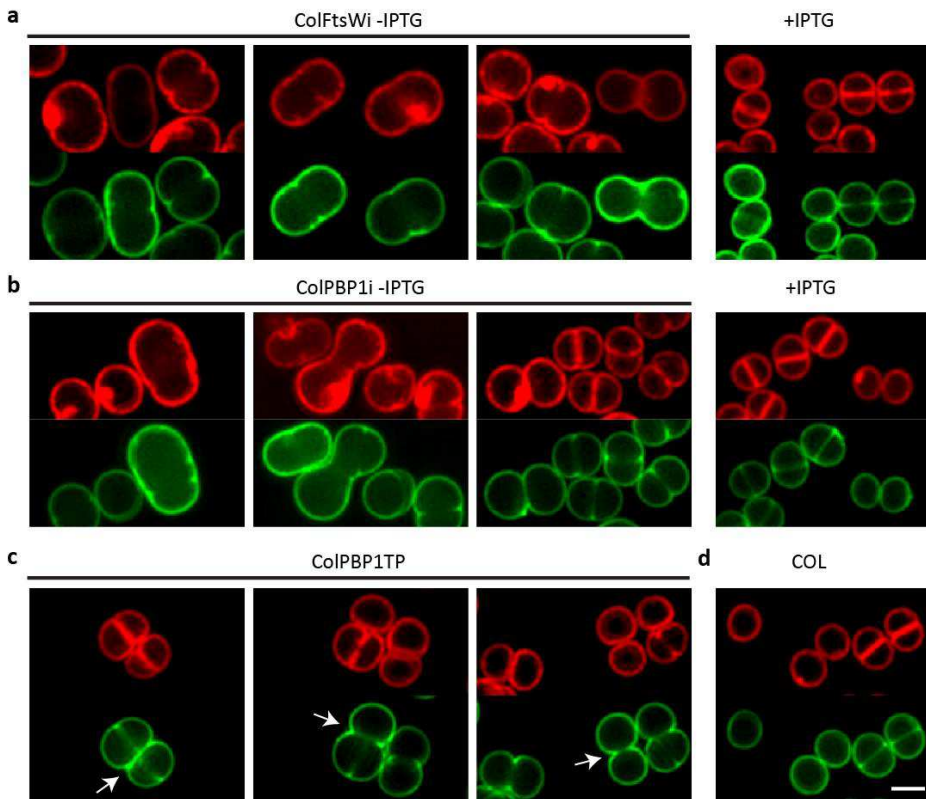


**Figure 10. FtsW-PBP1 have a role in maintaining the near-spherical shape of cocci. a, b,** SIM images of ColFtsWi (**a**) and ColPBP1i (**b**) grown for 3 hours in the absence or presence of IPTG, stained with Nile Red (membrane, Red) and Van-FL (cell wall, Green). Percentages of elongated cells (defined as cells with long/short cell axis ratio larger than 1.25) were: 38.2% (*n*=513) for ColFtsWi -IPTG vs 4.2% (*n*=505) in the presence of IPTG; 24.0% (*n*=296) for ColPBP1i -IPTG vs 7.9% (*n*=556) in the presence of IPTG. **c, d,** SIM images of PBP1 transpeptidase mutant ColPBP1TP (**c**) and parental strain COL (**d**) stained with Nile Red (membrane, Red) and Van-FL (cell wall, Green). Experiment was performed in triplicate with similar results. Arrows point to cell

separation defects, where two daughter cells remain attached to one another. Scale bar, 1 μm.
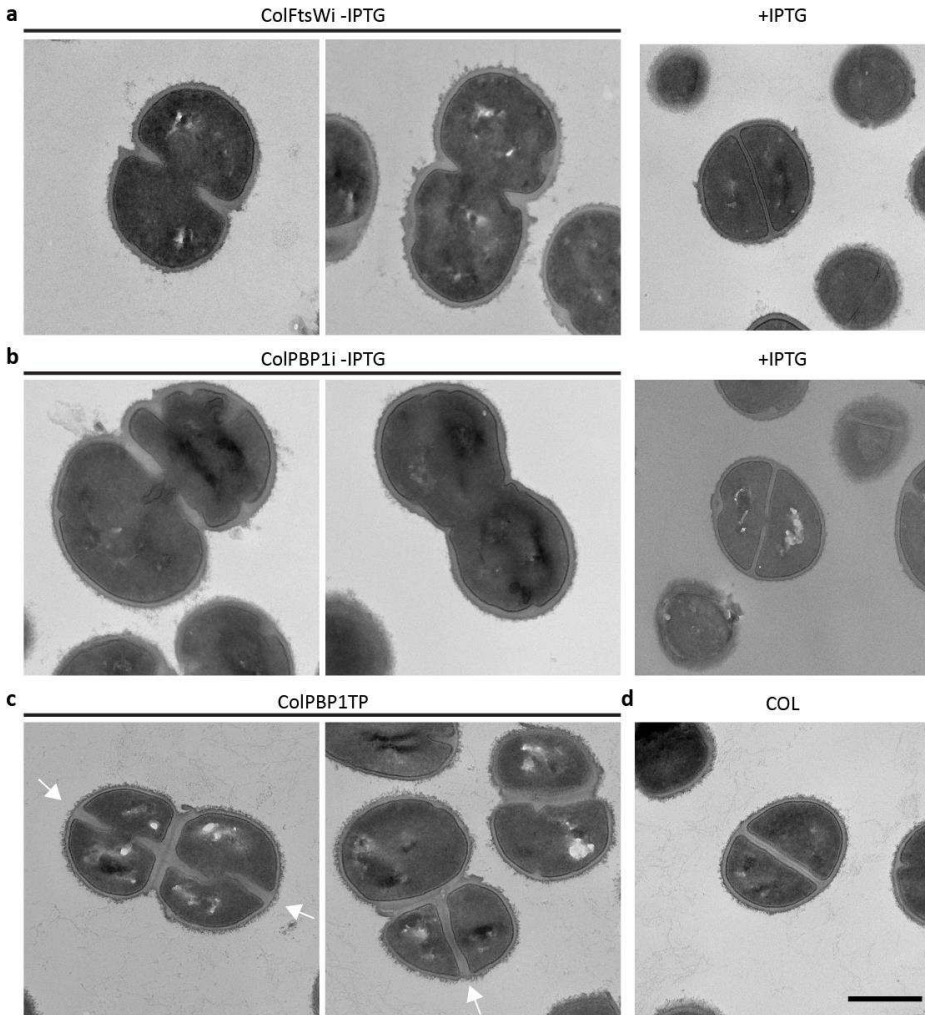


**Figure 11. Depletion of PBP1 or FtsW and mutation of transpeptidase active site of PBP1 leads to cell division defects. a, b,** Transmission Electron Microscopy (TEM) images of ColFtsWi (**a**) and ColPBP1i (**b**) grown in the absence and presence of IPTG. **c, d** TEM images of PBP1TP mutant ColPBP1TP (**c**) and parental strain COL (**d**). Arrows in (**c**) indicate division septa present prior to daughter cell separation. TEM was performed once (panels a and b) or twice (panels c and d). Scale bar, 0.5 μm.

Given that PBP1 TPase activity is not required for growth, we tested whether the morphological phenotypes of the PBP1 depleted cells were dependent on PBP1 TPase activity. Compared to the parental strain COL, ColPBP1TP cells showed cell separation defects, where daughter cells began to synthesize the future division septum while still attached (Fig. 10c,d, Fig. 11c,d, white arrows). After completion of septum synthesis, cells did not quickly pop apart, as observed with COL, but instead slowly acquired an indentation at midcell. However, the elongation phenotype characteristic of the PBP1 depleted cells was not observed in the PBP1TP mutant (Fig. 10c, Fig. 11c), reinforcing the idea that PBP1 has a second function besides its TPase activity.

A second line of evidence pointing to an early function of PBP1, separate from its role in PGN synthesis, comes from the fact that FtsW and PBP1 localize early at midcell, but inward septum synthesis is not initiated until the lipid II flippase MurJ is recruited to the divisome[23]. Given the elongation phenotype of FtsW or PBP1 depleted cells, we reasoned that this cognate pair could have an initial structural role in divisome assembly and that cell elongation could arise from destabilization of the divisome. We therefore determined the localization of FtsZ and its negative regulator EzrA[28,47] (as a proxy) upon depletion of FtsW and PBP1. Imaging of FtsZ-sGFP and EzrA-sGFP, after depletion of FtsW or PBP1, revealed the presence of multiple rings/arcs spread across the long axis of the cell, indicating that FtsW and PBP1 have a stabilizing effect on the divisome, maintaining it at midcell (Fig. 12a,b). These extraneous Z-rings appeared capable of recruiting downstream proteins of the divisome, as multiple rings were also observed for FtsW, MurJ and RodA in the absence of PBP1 (Fig. 12b). Therefore, it seemed likely that cell elongation was due to PGN incorporation organized by the mislocalized divisome.
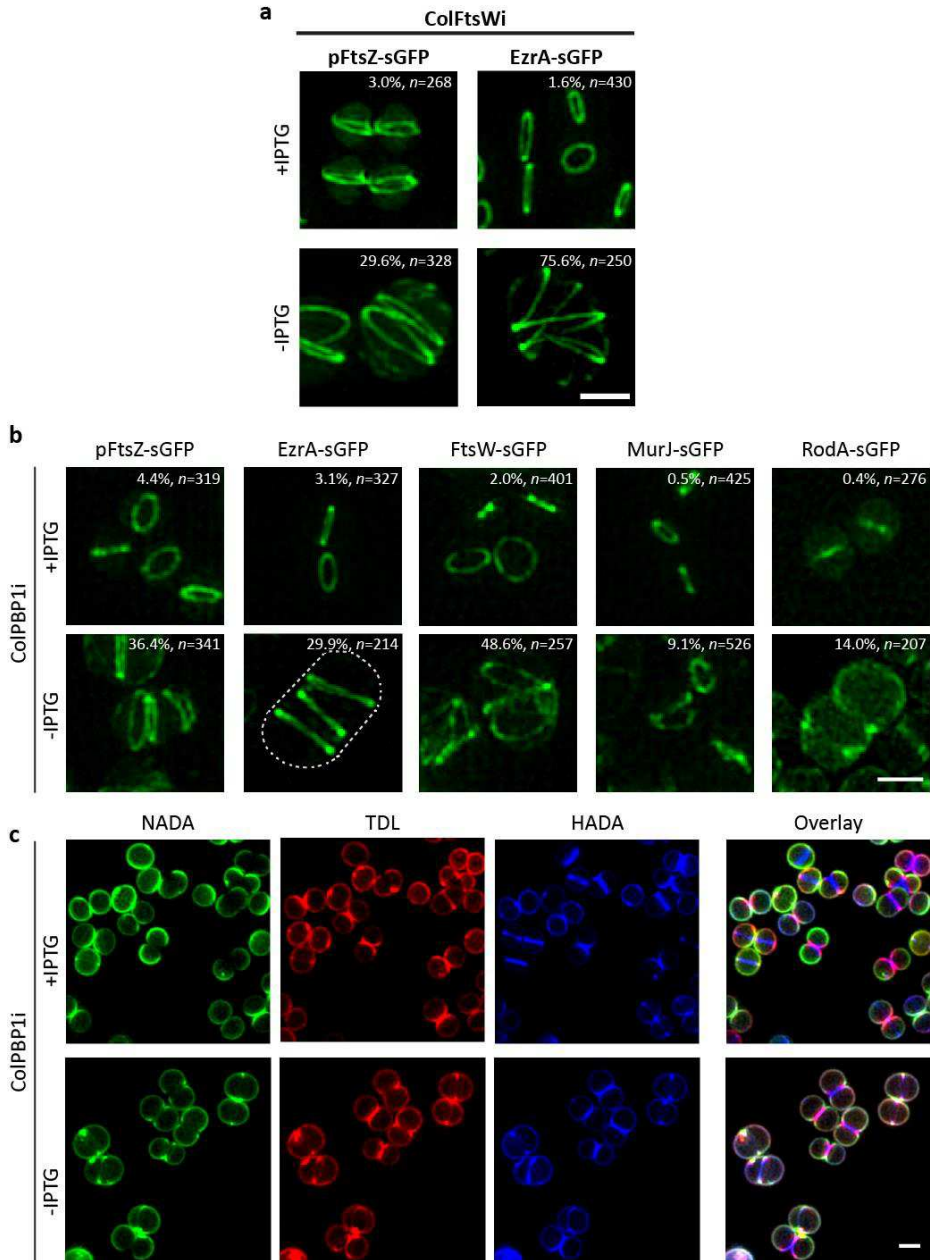
**Figure 12. FtsW/PBP1 depletion leads to multiple divisome structures. a**, FtsZ-sGFP and EzrA-sGFP localization in ColFtsWipFtsZ-sGFP and ColFtsWiEzrA-sGFP cells depleted (-IPTG) or not (+IPTG) of FtsW. **b**, Localization of FtsZ-sGFP (ColPBP1ipFtsZ-sGFP), EzrA-sGFP (ColPBP1iEzrA-sGFP), FtsW-sGFP (ColPBP1iFtsW-sGFP), MurJ-sGFP (ColPBP1iMurJ-sGFP) and RodA-sGFP (ColPBP1iRodA-sGFP) grown in the presence (+IPTG) and absence of IPTG (-IPTG) for PBP1 depletion. **c,** SIM images of strain ColPBP1i grown in the presence and absence of IPTG and

sequentially stained for 10 min (each) with fluorescent D-amino acids NADA, TDL and HADA. Scale bar, 1 μm. To evaluate the penetrance of the phenotype, percentages of cells with multiple rings were calculated and are shown in the top right of each panel. Outline of one cell is indicated with dashed line.

To test this, we observed the incorporation of FDAAs following depletion of either FtsW or PBP1. Initial imaging showed faint septal incorporation, with peripheral signal throughout the cell (Fig. 12c). Given that the low molecular weight PBP4 is responsible for the majority of peripheral FDAA incorporation in *S. aureus*[17], it was possible that a signal corresponding to divisome localization could have been masked by PBP4 activity. We therefore repeated these experiments in the absence of PBP4, and found that similarly to the divisome localization, multiple PGN incorporation rings were visible along the long axis of the mutant (Fig. 13a,b). HADA staining of these strains expressing EzrA-sGFP confirmed that the insertion of PGN was directed by the mislocalized divisome, indicating that cell elongation is caused by lateral PGN insertion at defined regions of the cell (Fig. 13c,d). Together these data support a model whereby both SEDS-bPBPs cognate pairs are responsible for maintaining the cell shape by directing PGN synthesis to the side-wall or septum during the cell cycle of *S. aureus*.
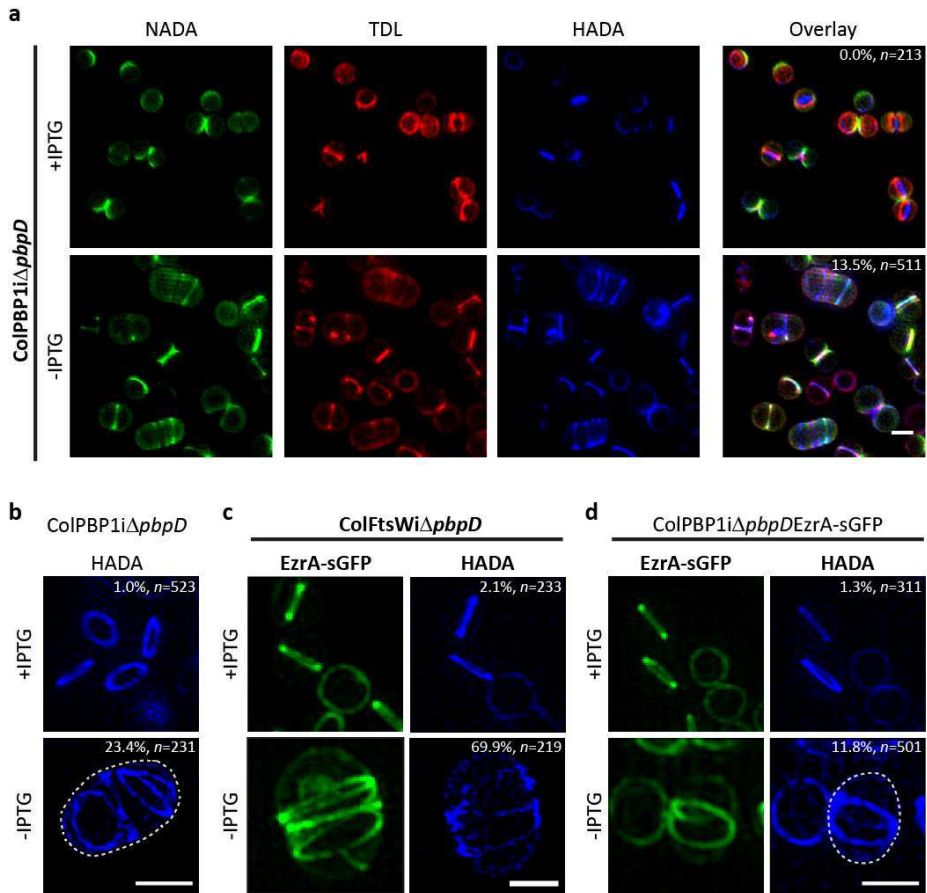
**Figure 13. Multiple divisome structures incorporate PGN at the lateral wall and elongate cells. a,** SIM images of strain ColPBP1iΔ*pbpD* grown in the presence and absence of IPTG and sequentially stained for 10 min (each) with fluorescent D-amino acids NADA, TDL and HADA. **b**, PGN insertion visualized by HADA staining in PBP4 null mutant strain ColPBP1iΔ*pbpD* depleted (-IPTG) or not (+IPTG) of PBP1. **c, d,** EzrA-sGFP (left) and PGN insertion visualized by HADA staining (right) in PBP4 null mutant ColFtsWiΔ*pbpD*EzrA-sGFP (**c**) and ColPBP1iΔ*pbpD*EzrA-sGFP (**d**) in the presence or absence of IPTG. Panels show a maximum intensity projection of a SIM Z-stack Scale bars, 1 µm. To evaluate the penetrance of the phenotype, percentages of cells with multiple rings were calculated and are shown in the top right of each panel. Outlines of some cells are indicated with dashed lines.

## DISCUSSION

In rod shaped bacteria, the elongasome (via MreB) ensures synthesis along the long axis of the cell resulting in elongation, while the divisome (via FtsZ) promotes inward synthesis of the septum[7,48]. Each of these machineries includes a specific SEDS-bPBP pair required for lateral or septal synthesis of PGN[15]. Cocci like *S. aureus* lack a canonical elongasome including an MreB protein. However, they do encode two SEDS proteins whose role was so far unknown. Given that SEDS proteins are promising targets for new antimicrobial compounds[13], it is of particular importance to study their role in bacterial pathogens such as *S. aureus.* We have now confirmed the existence of two SEDS-bPBP cognate pairs of interacting proteins in *S. aureus*. The RodA-PBP3 pair is recruited to midcell and promotes side-wall insertion of PGN, leading to slight cell elongation, in a manner reminiscent of pre-septal PGN synthesis of *E. coli*[11] or *Caulobacter crescentus*[49], or peripheral PGN synthesis responsible for cell elongation in ovococci[8], both of which are dependent on FtsZ. The second SEDS-bPBP pair, FtsW-PBP1, is essential for cell viability and is required for inward PGN synthesis at the division site. Interestingly, the essential function of PBP1 is not dependent on its transpeptidase activity, suggesting that this protein has a second function. While writing this manuscript, data from the Walker laboratory demonstrated that *S. aureus* PBP1 stimulates the essential TGase activity of FtsW, independently of its TPase active site[12], which could explain the essentiality of PBP1. This regulation of the activity of SEDS proteins and bPBPs may be essential to avoid the synthesis of uncross-linked glycans[50], which has been shown to lead to a toxic futile cycle of glycan synthesis and degradation in *E. coli*[51] (although such a cycle has not been identified in *S. aureus* so far). We now propose an additional mode of regulation of SEDS proteins by cognate bPBPs through protein localization. Our data has shown that *S. aureus* PBP3 is

required for the septal localization of RodA, and most likely modulates its activity, as lack of the transpeptidase PBP3 causes a similar increase in susceptibility to moenomycin (an inhibitor of classical transglycosylases) as the lack of RodA.

We also found that the FtsW-PBP1 pair has an additional function in stabilizing the divisome. FtsW has been previously suggested to have a role in divisome activation in *E. coli* and *C. crescentus*[52,53]. Here we showed that *S. aureus* FtsW-PBP1 pair is required to maintain the divisome at midcell, as depletion of these proteins led to multiple rings/arcs of FtsZ or EzrA present across the long axis of the cell. FtsW and PBP1 arrive early to the divisome of *S. aureus*, even before the lipid II flippase MurJ[23]. It is therefore possible that a major function of FtsW-PBP1 is to stabilize the early divisome before this SEDS-bPBP pair initiates TGase and TPase activity in the orientation perpendicular to the membrane, required to begin septum synthesis. In the absence of these proteins, the normally compact midcell divisome mislocalizes to the peripheral wall, leading to cell elongation.

In conclusion, we propose that *S. aureus* maintains its slightly ellipsoid shape through the coordinated activities of two cognate SEDS-bPBP pairs that insert new PGN in two distinct fashions at the midcell (Fig. 14). Newborn cells incorporate PGN around the entire surface[17,54]. Just before septum inward growth is initiated, RodA-PBP3 localizes at midcell and incorporates PGN at the sidewall, while FtsW-PBP1 stabilizes assembly of the divisome during initial stages of cytokinesis. Importantly, the transpeptidase activity of PBP1 is required to ensure that cell wall maturation of the closed septum concludes with rapid daughter cell separation and reshaping of the septum. Together these SEDS-bPBP pairs localize PGN incorporation and this balance between sidewall and septal PGN synthesis is crucial in conserving the *S. aureus* cell shape. Our findings suggest that cell shape development in cocci,

ovococci and rods presents more similarities than previously thought, with the three morphologies requiring protein complexes for elongation and division.
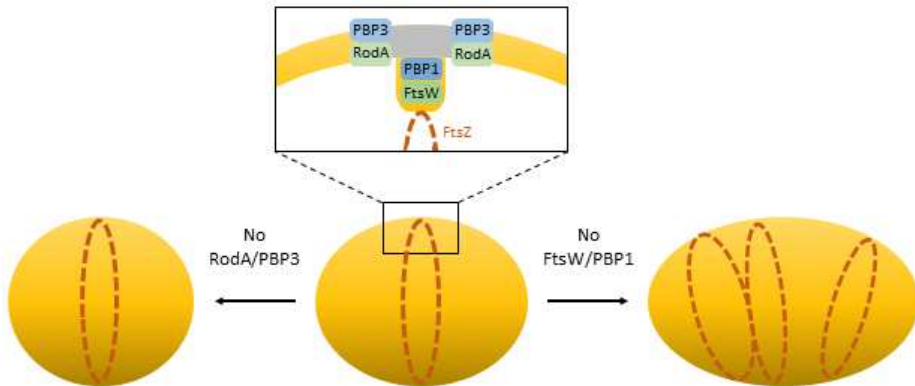


**Figure 14. Model for the role of SEDS/bPBPs in *S. aureus* morphogenesis.** *S. aureus* cells slight elongation depends on the activity of RodA/PBP3, which catalyze side-wall synthesis of PGN at the future division site (grey). In the absence of this cognate pair, staphylococcal cells become rounder. FtsW/PBP1 have a dual function during cell division. This pair is required for septal peptidoglycan synthesis, possibly to reorient the synthesis of PGN from the lateral wall to the perpendicular septum, promoting inward growth of the septum, as well as to stabilize the divisome. In the absence of FtsW/PBP1 the divisome is no longer localized exclusively at mid cell, but forms multiple rings/arcs, capable of promoting PGN synthesis, leading to cell elongation.

## REFERENCES

1. Egan, A. J. F., Cleverley, R. M., Peters, K., Lewis, R. J. & Vollmer, W. Regulation of bacterial cell wall growth. *FEBS J.* **284**, 851–867 (2017).

2. Chastanet, A. & Carballido-Lopez, R. The actin-like MreB proteins in *Bacillus subtilis*: a new turn. *Front. Biosci. (Schol. Ed).* **4**, 1582–606 (2012).

3. Domínguez-Escobar, J. *et al.* Processive movement of MreB-associated cell wall biosynthetic complexes in bacteria. *Science* **333**, 225–8 (2011).

4. Garner, E. C. *et al.* Coupled, circumferential motions of the cell wall synthesis machinery and MreB filaments in *B. subtilis*. *Science* **333**, 222–225 (2011).

5. van Teeffelen, S. *et al.* The bacterial actin MreB rotates, and rotation depends on cell-wall assembly. *Proc. Natl. Acad. Sci.* **108**, 15822–15827 (2011).

6. den Blaauwen, T., Hamoen, L. W. & Levin, P. A. The divisome at 25: the road ahead. *Curr. Opin. Microbiol.* **36**, 85–94 (2017).

7. Egan, A. J. F. & Vollmer, W. The physiology of bacterial cell division. *Ann. N. Y. Acad. Sci.* **1277**, 8–28 (2013).

8. Massidda, O., Nováková, L. & Vollmer, W. From models to pathogens: how much have we learned about *Streptococcus pneumoniae* cell division? *Environ. Microbiol.* **15**, 3133–3157 (2013).

9. Pinho, M. G., Kjos, M. & Veening, J. W. How to get (a)round: mechanisms controlling growth and division of coccoid bacteria. *Nat. Rev. Microbiol.* **11**, 601–14 (2013).

10. Perez, A. J. *et al.* Movement dynamics of divisome proteins and PBP2x:FtsW in cells of *Streptococcus pneumoniae*. *Proc. Natl. Acad. Sci. U. S. A.* **116**, 3211–3220 (2019).

11. Typas, A., Banzhaf, M., Gross, C. A. & Vollmer, W. From the regulation of peptidoglycan synthesis to bacterial growth and morphology. *Nat. Rev. Microbiol.* **10**, 123–136 (2012).

12. Taguchi, A. *et al.* FtsW is a peptidoglycan polymerase that is functional only in complex with its cognate penicillin-binding protein. *Nat. Microbiol.* **4**, 587–594 (2019).

13. Emami, K. *et al.* RodA as the missing glycosyltransferase in *Bacillus subtilis* and antibiotic discovery for the peptidoglycan polymerase pathway. *Nat. Microbiol.* **2**, 1–8 (2017).

14. Meeske, A. J. *et al.* SEDS proteins are a widespread family of bacterial cell wall polymerases. *Nature* **537**, 634–638 (2016).

15. Cho, H. *et al.* Bacterial cell wall biogenesis is mediated by SEDS and PBP polymerase families functioning semi-autonomously. *Nat. Microbiol.* **1**, 1–8 (2016).

16. Scheffers, D. J. & Pinho, M. G. Bacterial Cell Wall Synthesis : New Insights from Localization Studies. *Microbiol Mol Biol Rev.* **69**, 585–607 (2005).

17. Monteiro, J. M. *et al.* Cell shape dynamics during the staphylococcal cell cycle. *Nat. Commun.* **6**, 8055 (2015).

18. Monk, I. R., Shah, I. M., Xu, M., Tan, M. & Foster, T. J. Transforming the untransformable: application of direct transformation to manipulate

genetically *Staphylococcus aureus* and *Staphylococcus epidermidis*. *MBio.* **3**, 1–11 (2012).

19.  Nair, D. *et al.* Whole-genome sequencing of *Staphylococcus aureus* strain RN4220, a key laboratory strain used in virulence research, identifies mutations that affect not only virulence factors but also the fitness of the strain. *J. Bacteriol.* **193**, 2332–5 (2011).

20.  Gill, S. R. *et al.* Insights on evolution of virulence and resistance from the complete genome analysis of an early methicillin-resistant *Staphylococcus aureus* strain and a biofilm-producing methicillin-resistant *Staphylococcus epidermidis* strain. *J. Bacteriol.* **187**, 2426–2438 (2005).

21.  Widhelm, T. J. *et al.* A Genetic Resource for Rapid and Comprehensive Phenotype Screening of Nonessential *Staphylococcus aureus* Genes. *MBio* **4**, 1–8 (2014).

22.  Pereira, S. F. F., Henriques, A. O., Pinho, M. G., de Lencastre, H. & Tomasz, A. Role of PBP1 in cell division of *Staphylococcus aureus*. *J. Bacteriol.* **189**, 3525–31 (2007).

23.  Monteiro, J. M. *et al.* Peptidoglycan synthesis drives an FtsZ-treadmilling-independent step of cytokinesis. *Nature* **554**, 528–532 (2018).

24.  Pinho, M. G., Filipe, S. R., de Lencastre, H. & Tomasz, A. Complementation of the essential peptidoglycan transpeptidase function of Penicillin-Binding Protein 2 (PBP2) by the drug resistance protein PBP2A in *Staphylococcus aureus*. *J. Bacteriol.* **183**, 6525–31 (2001).

25.  Fisher, A. C. & DeLisa, M. P. Laboratory Evolution of Fast-Folding Green Fluorescent Protein Using Secretory Pathway Quality Control. *PLoS One* **3**, e2351 (2008).

26.  Arnaud, M., Chastanet, A. & Debarbouille, M. New Vector for Efficient Allelic Replacement in Naturally Nontransformable, Low-GC-Content, Gram-Positive Bacteria. *Appl. Environ. Microbiol.* **70**, 6887–6891 (2004).

27.  Pereira, S. F. F., Henriques, A. O., Pinho, M. G., de Lencastre, H. & Tomasz, A. Evidence for a dual role of PBP1 in the cell division and cell separation of *Staphylococcus aureus*. *Mol. Microbiol.* **72**, 895–904 (2009).

28.  Jorge, A. M., Hoiczyk, E., Gomes, J. P. & Pinho, M. G. EzrA contributes to the regulation of cell size in *Staphylococcus aureus*. *PLoS One* **6**, (2011).

29.  Atilano, M. L. *et al.* Teichoic acids are temporal and spatial regulators of peptidoglycan cross-linking in *Staphylococcus aureus*. *Proc. Nati. Acad. Sci. U S A* **107**, (2010).

30.  Pereira, P. M., Veiga, H., Jorge, A. M. & Pinho, M. G. Fluorescent Reporters for Studies of Cellular Localization of Proteins in *Staphylococcus aureus*. *Appl. Environ. Microbiol.* **76**, 4346–4353 (2010).

31.  Veiga, H. & Pinho, M. G. Inactivation of the SauI type I restriction-modification system is not sufficient to generate *Staphylococcus aureus* strains capable of efficiently accepting foreign DNA. *Appl. Environ. Microbiol.* **75**, 3034–8 (2009).

32.  Oshida, T. & Tomasz, A. Isolation and characterization of a Tn551-

autolysis mutant of *Staphylococcus aureus*. *J. Bacteriol.* **174**, 4952–9 (1992).

33. Sambrook, J., Fritsch, E. F. & Maniatis, T. *Molecular cloning: a laboratory manual*. (Cold Spring Harbor Laboratory Press, 1989).

34. Deatherage, D. E. & Barrick, J. E. Identification of Mutations in Laboratory-Evolved Microbes from Next-Generation Sequencing Data Using breseq. *Methods Mol. Biol.* **1151**, 165–188 (2014).

35. Filipe, S. R., Tomasz, A. & Ligoxygakis, P. Requirements of peptidoglycan structure that allow detection by the Drosophila Toll pathway. *EMBO Rep.* **6**, 327–333 (2005).

36. Reed, P. *et al. Staphylococcus aureus* Survives with a Minimal Peptidoglycan Synthesis Machine but Sacrifices Virulence and Antibiotic Resistance. *PLoS Pathog.* **11**, 1–19 (2015).

37. Heintzmann, R. & Cremer, C. G. Laterally modulated excitation microscopy: improvement of resolution by using a diffraction grating. in *SPIE 3568, Optical Biopsies and Microscopic Techniques III* (eds. Bigio, I. J., Schneckenburger, H., Slavik, J., Svanberg, K. & Viallet, P. M.) **3568**, 185–196 (International Society for Optics and Photonics, 1999).

38. Kuru, E. *et al. In Situ* Probing of Newly Synthesized Peptidoglycan in Live Bacteria with Fluorescent D-Amino Acids. *Angew. Chemie Int. Ed.* **51**, 12519–12523 (2012).

39. Kuru, E., Tekkam, S., Hall, E., Brun, Y. V & VanNieuwenhze, M. S. Synthesis of fluorescent D-amino acids (FDAAs) and their use for probing peptidoglycan synthesis and bacterial growth *in situ*. *Nat Protoc.* **10**, 33–52 (2015).

40. Pereira, A. R. *et al.* FtsZ-Dependent Elongation of a Coccoid Bacterium. *MBio* **7**, e00908-16 (2016).

41. Chen, H., Puhl, H. L., Koushik, S. V., Vogel, S. S. & Ikeda, S. R. Measurement of FRET Efficiency and Ratio of Donor to Acceptor Concentration in Living Cells. *Biophys. J.* **91**, L39–L41 (2006).

42. Hoppe, A., Christensen, K. & Swanson, J. A. Fluorescence Resonance Energy Transfer-Based Stoichiometry in Living Cells. *Biophys. J.* **83**, 3652–3664 (2002).

43. Pinho, M. G., de Lencastre, H. & Tomasz, A. Cloning, characterization, and inactivation of the gene *pbpC*, encoding penicillin-binding protein 3 of *Staphylococcus aureus*. *J. Bacteriol.* **182**, 1074–9 (2000).

44. Sassine, J. *et al.* Functional redundancy of division specific penicillin-binding proteins in *Bacillus subtilis*. *Mol. Microbiol.* **106**, 304–318 (2017).

45. De Jonge, B. L. M., Chang, Y. S., Gage, D. & Tomasz, A. Peptidoglycan composition of a highly methicillin-resistant *Staphylococcus aureus* strain. The role of penicillin binding protein 2A. *J. Biol. Chem.* **267**, 11248–11254 (1992).

46. Wallrabe, H. & Periasamy, A. Imaging protein molecules using FRET and FLIM microscopy. *Curr. Opin. Biotechnol.* **16**, 19–27 (2005).

47. Levin, P. A., Kurtser, I. G. & Grossman, A. D. Identification and characterization of a negative regulator of FtsZ ring formation in *Bacillus subtilis*. *Proc. Natl. Acad. Sci. U. S. A.* **96**, 9642–7 (1999).

48. Den Blaauwen, T., de Pedro, M. A., Nguyen-Distèche, M. & Ayala, J. A. Morphogenesis of rod-shaped sacculi. *FEMS Microbiol. Rev.* **32**, 321–344 (2008).

49.   Aaron, M. *et al.* The tubulin homologue FtsZ contributes to cell elongation by guiding cell wall precursor synthesis in *Caulobacter crescentus*. *Mol. Microbiol.* **64**, 938–952 (2007).
50.   Rohs, P. D. A. *et al.* A central role for PBP2 in the activation of peptidoglycan polymerization by the bacterial cell elongation machinery. *PLoS Genet.* **14**, e1007726 (2018).
51.   Cho, H., Uehara, T. & Bernhardt, T. G. Beta-lactam antibiotics induce a lethal malfunctioning of the bacterial cell wall synthesis machinery. *Cell* **159**, 1300–11 (2014).
52.   Du, S., Pichoff, S. & Lutkenhaus, J. FtsEX acts on FtsA to regulate divisome assembly and activity. *Proc. Natl. Acad. Sci.* **113**, E5052–E5061 (2016).
53.   Modell, J. W., Kambara, T. K., Perchuk, B. S. & Laub, M. T. A DNA Damage-Induced, SOS-Independent Checkpoint Regulates Cell Division in *Caulobacter crescentus*. *PLoS Biol.* **12**, e1001977 (2014).
54.   Lund, V. A. *et al.* Molecular coordination of *Staphylococcus aureus* cell division. *Elife* **7**, e32057 (2018).

# CHAPTER IV

**Lipid II flipping is dependent on the presence of MurJ**

**Author contributions**

A. C. Tavares and G. Covas performed all experiments.

# ABSTRACT

The bacterial cell wall is mainly composed of peptidoglycan (PGN), produced through polymerization and cross-linking of lipid-linked precursors at the outer leaflet of the cytoplasmic membrane. The lipid II PGN precursor is synthesized at the inner surface of the membrane and needs to be flipped to the outer surface prior to incorporation into new PGN chains. This transport has been shown to require MurJ, a member of the multidrug/oligosaccharidyl-lipid/polysaccharide (MOP) exporter superfamily, involved in PGN biosynthesis and in the maintenance of cell morphology. In *Escherichia coli*, absence of MurJ results in accumulation of lipid II precursors at the inner surface of the cytoplasmic membrane, supporting the role of MurJ as the lipid II flippase[1]. Here we show that in *Staphylococcus aureus*, MurJ is essential for cell viability and for the preservation of a proper cell shape. An accumulation of lipid II precursors in the absence of MurJ, together with a reduction of lipid II on the outer membrane leaflet and a decrease of PGN incorporation suggest an impairment in lipid II flipping, indicating that MurJ is also involved in the process of lipid II flipping in *S. aureus*.

## INTRODUCTION

Peptidoglycan (PGN) is composed of alternate units of β-1,4-linked *N*-acetyl-glucosamine (GlcNAc) and *N*-acetyl muramic acid (MurNAc) linked to a five amino acid stem peptide. In *Staphylococcus aureus*, the stem peptide consists of L-Ala$_{(1)}$–D-Glu$_{(2)}$–L-Lys$_{(3)}$–D-Ala$_{(4)}$–D-Ala$_{(5)}$, in which L-Lys$_{(3)}$ is a dibasic amino acid involved in the cross-linking of two different stem peptides, by connecting to the D-Ala in the fourth position of the second stem peptide through a five glycine cross bridge[2]. These building blocks are constructed and assembled into new PGN in three consecutive stages that occur in three different locations. The first stage occurs in the cytoplasm and includes several reactions catalyzed by GlmSMU and MurABCDEF enzymes, resulting in the synthesis of the uridine diphosphate-GlcNAc (UDP-GlcNAc) and uridine diphosphate-MurNAc (UDP-MurNAc)-pentapeptide precursors [3,4]. The second stage is the synthesis of PGN lipid-linked precursors at the inner side of the cytoplasmic membrane. In this stage, MraY links UDP-MurNAc-pentapeptide to the lipid carrier undecaprenyl phosphate, or bactoprenol, via a pyrophosphate bridge, forming lipid I[5]. Addition of UDP-GlcNAc to MurNAc by MurG leads to the synthesis of lipid II[6], which is further modified by addition of five glycines to the L-Lys$_{(3)}$ amino acid by FemXAB enzymes[7]. The D-Glu on the second position of the stem peptide of all PGN precursors liked to bactoprenol, including lipid I and lipid II, can be amidated in vitro by the GatD/MurT enzyme complex[8,9]. This amidation reaction is necessary to maintain a high degree of PGN cross-linking in *S. aureus* cell wall[8]. In the third stage, transglycosylation reactions performed by penicillin-binding proteins (PBPs), monofunctional transglycosylases and SEDS proteins, polymerize the disaccharide-pentapeptide subunits into new PGN[2,10,11], while transpeptidation reactions by PBPs cross-link them through the five glycines bridge[2].

Although most steps of PGN biosynthesis are well studied, translocation of lipid II across the cytoplasmic membrane needs further elucidation. Translocation of fluorescently 7-nitro-2,1,3-benzoxadiazol-4-yl (NBD)-labelled lipid II does not occur spontaneously in protein-free artificial membranes, but is observed in *Escherichia coli* membrane vesicles[12], indicating that lipid II translocation and re-cycling is probably performed by an enzyme. Two proteins proposed to perform this function are FtsW and MurJ. Both are membrane proteins with FtsW displaying 10 transmembrane domains[13] and belonging to the shape, elongation, division and sporulation (SEDS) family[14], while MurJ has 14 transmembrane domains and belongs to the MOPS (multidrug/ oligosaccharidyl-lipid/polysaccharide) family of exporters[15]. SEDS proteins FtsW and RodA were proposed to be lipid II flippases over 20 years ago, due to their polytopic membrane nature and their role in septal and lateral PGN synthesis[16,17]. More recently, in vitro biochemical experiments showed that FtsW can flip NBD-lipid II in model membranes and *E. coli* membrane vesicles[18]. However, this activity was later shown not to be specific for lipid II, since FtsW could also translocate different phospholipids and larger NBD-lipid II analogs[19]. Despite the in vitro results, in vivo studies failed to demonstrate FtsW translocase activity[1]. Additionally, SEDS proteins were shown to have transglycosylase activity in different organisms, suggesting a role in PGN synthesis different from lipid II flipping[10,11,20].

MurJ was initially identified in *E. coli* as the best candidate for lipid II flipping using a reductionist bioinformatics approach[21]. It is an essential protein, necessary for PGN synthesis and maintenance of cell morphology[21–24], and it is structurally similar to the MATE (Multidrug And Toxic Extrusion) proteins, the best studied members of the MOP superfamily[15]. MATE proteins usually export molecules from the bacterial cytoplasm by an antiport mechanism dependent on the

electrochemical gradient of protons or cations across the cytoplasmic membrane[25,26]. These proteins possess a V-shaped central cavity which can alternate its conformation to open to the inner or outer side of the cytoplasmic membrane, binding and releasing its cargo, respectively[25–27]. Wzx, another member of MOP superfamily, displays a similar central cavity and mode of action to transport Und-PP-oligosaccharide molecules[28]. In *E. coli* and *Thermosipho africanus* a similar V-shaped cavity was identified in MurJ, probably capable of accommodating the lipid II head group[15,29]. In fact, biochemical assays in *E. coli* showed that MurJ can form a stable complex with lipid II and that its affinity is much higher than that of FtsW[30]. A combination of crystallography and sequence co-evolution analysis showed that *E. coli* MurJ can adopt two distinct conformations, inward-open and outward-open, supporting a rocker-switch model for the transport of lipid II[31]. Agreeing with this model, in vivo studies in *E. coli* and *Bacillus subtilis* showed that upon MurJ inactivation there is an accumulation of lipid-linked PGN precursors in the cytoplasmic membrane, a reduction in PGN synthesis and an asymmetrical swelling of the cells[1,21–23]. A relevant study by Sham and colleges developed a method for distinguishing lipid II accumulation on the inner or outer leaflet of *E. coli* cytoplasmic membrane, using protein toxin colicin M (ColM)[1]. Exogenous ColM is translocated across the *E. coli* outer membrane into the periplasmic space, where it cleaves lipid II into bactoprenol and 1-pyrophospho-MurNAc(pentapeptide)-GlcNAc. Since ColM is unable to cross the cytoplasmic membrane, lipid II on the inner side of the cytoplasmic membrane is not cleaved in the presence of this enzyme. Treatment of *E. coli* cells with ColM, followed by the purification of soluble and lipid-linked radiolabeled PGN precursors allows the quantification of lipid II on the outer and inner leaflet of the cytoplasmic membrane, respectively. This method revealed an accumulation of lipid II at the inner leaflet of *E. coli* cytoplasmic membrane upon MurJ inactivation[1].

The same strategy was used in *B. subtilis* to show that MurJ and Amj, another predicted lipid II flippase, had flipping activity[23]. Together, these results strongly indicate that MurJ is a lipid II flippase.

In *S. aureus*, MurJ is an essential protein and its inhibition leads to a defective cell wall synthesis and accumulation of PGN precursors[24,32]. MurJ was recently shown to localize to the division septum and to be responsible for directing PGN synthesis to midcell[33]. Here we show that absence of MurJ leads to an enlargement of the cells, a decrease of PGN incorporation and an accumulation of lipid II precursors, likely at the inner side of the cytoplasmic membrane, suggesting a role for this protein in lipid II flipping in *S. aureus*.

## MATERIALS AND METHODS

## Bacterial growth conditions

Strains and plasmids used in this study are listed in Table 1. *E. coli* strains were grown in Luria–Bertani broth (LB, VWR) or Luria–Bertani agar (LA, VWR) at 37°C. *S. aureus* strains were grown in Tryptic Soy Broth (TSB, Difco) or on Tryptic Soy Agar (TSA, Difco) at 37°C. When necessary, culture media was supplemented with antibiotics [ampicillin 100 $\mu g\,ml^{-1}$ (Apollo Scientific), erythromycin 10 $\mu g\,ml^{-1}$ (Apollo Scientific) or CDFI 8 $\mu g\,ml^{-1}$ (gift from Merck)], with 0.5 mM Isopropyl β-D-1-thiogalactopyranoside (IPTG, Apollo Scientific) or with 0.125 M D-serine (Sigma).

## Construction and growth of a MurJ inducible strain

A fragment containing the ribosome-binding site and the initial 636 bp of *murJ* gene was amplified by PCR using primers 1525/1526 (Table 2). The resulting fragment was digested with *Hind*III/*Bam*HI restriction enzymes and cloned into pMUTIN4, generating plasmid pMutMurJi. Transduction of this plasmid, using phage $80\alpha$[34], into COL generated strain ColpMurJi, which has the native *murJ* gene under the control of IPTG-inducible P*spac* promoter and a truncated *murJ* gene under the control of the native promoter.

ColpMurJi overnight cultures grown in the presence of IPTG 0.5 mM were back-diluted to an $OD_{600nm}$ of 0.1 and grown until $OD_{600nm}$ of approximately 1 in the presence of IPTG 0.5 mM. Cells were washed three times with TSB, back-diluted to $OD_{600nm}=0.05$ and grown in the presence or absence of IPTG 0.5 mM for 3h.

## Growth curves

Overnight cultures of ColpMurJi grown with IPTG 0.5 mM were washed three times with TSB and back-diluted to $OD_{600nm}$ of 0.02 in 20 mL TSB with or without IPTG 0.5 mM. $OD_{600nm}$ measurements were taken every hour. Growth curve was performed in triplicate.

## *S. aureus* imaging by fluorescence microscopy

*S. aureus* cells were labelled for 5 minutes at 37°C with membrane dye Nile Red (5 µg ml$^{-1}$, Invitrogen), washed with phosphate buffered saline (PBS) and placed on pads of 1.2% agarose in PBS, for imaging.

The localization of peptidoglycan incorporation was evaluated using fluorescent D-amino acid NADA[35,36]. To compare absolute fluorescence of incorporated NADA in two different strains in the same microscopy image, one of them was labeled with DNA dye Hoechst 33342 (1 µg mL$^{-1}$, Invitrogen). The cells were then labeled with 250 µM of NADA for 5 min, washed and mixed 1:1 prior to imaging.

To label recently flipped lipid II, *S. aureus* overnight cultures grown in TSB containing an excess of D-serine (0.125 M) were diluted to $OD_{600nm}$=0.1 in TSB with D-serine 0.125 M and grown until $DO_{600nm}$ of approximately 0.5. Samples of 1 mL were then centrifuged and resuspended in 1ml of TSB, TSB with D-serine 0.125 M or TSB with CDFI 8 µg ml$^{-1}$. Samples were incubated at 37°C for 25 min, labelled for 5 min with a mixture of equal volumes of vancomycin (Sigma) and a BODIPY FL conjugate of vancomycin (Van-FL, Molecular Probes) at a final concentration of 0.8 µg ml$^{-1}$, and analyzed by fluorescence microscopy.

Structured Illumination Microscopy (SIM) imaging was performed using an Elyra PS.1 microscope (Zeiss) with a Plan-Apochromat 63x/1.4 oil DIC M27 objective. SIM images were acquired using five grid rotations, with 34 µm grating period for the 561 nm laser (100 mW), 28 µm period for 488 nm laser (100 mW) and 23 µm period for 405 nm laser (50 mW), and captured using a Pco.edge 5.5 camera. Images were reconstructed using ZEN software (black edition, 2012, version 8.1.0.484) based on a structured illumination algorithm[37].

Epifluorescence microscopy was performed using a Zeiss Axio Observer microscope with a Plan-Apochromat 100x/1.4 oil Ph3 objective. Images were acquired with a Retiga R1 CCD camera (QImaging) using Metamorph 7.5 software (Molecular Devices).

## Microscopy analysis

Cell volume and elongation, septum median fluorescence and peripheral cell wall median fluorescence were measured using our in-house software, eHooke, as previously described[33]. Fluorescence ratio (FR) of septal to membrane signal was measured by eHooke taking in consideration only the 25% brightest pixels.

## Copper-catalyzed click-reaction

A culture of *S. aureus* COL was grown until $OD_{600nm}$ of approximately 1.2, split in two and labelled for 1 hour with 4 mM of the unnatural D-Ala-D-Pra dipeptide 2[38] and with or without 8 µg ml$^{-1}$ of CDFI (2xMIC). Samples of 1 ml were washed 3 times with PBS with or without 8 µg ml$^{-1}$ of CDFI and resuspended in 0.2 ml click-reaction solution [$CuSO_4.5H_2O$ 1 mM, Tris(3-hydroxypropyltriazolylmethyl)amine

(THPTA) 250 µM, Ascorbic Acid 1.2 mM; Sigma] with 100 µM of AF488-azide (Jena Bioscience) probe and with or without 8 µg ml$^{-1}$ of CDFI. After a 15 min incubation at 37°C, cells were washed with PBS and placed on pads of 1.2% agarose in PBS, for imaging.

## ColM protein purification

Plasmid pMLD237[39] encoding His$_6$-ColM was introduced into *E. coli* BL21(DE3). Cultures were incubated at 30°C until an OD$_{600nm}$ of 0.4-0.6, and protein expression was induced with 0.5 mM IPTG for 3h at 30°C. ColM purification was performed as previously described[1]. Briefly, cells were harvested, resuspended in buffer A (Tris-HCl 20 mM pH 7.4, NaCl 0.5 M, Imidazole 20 mM) containing protease inhibitor cocktail III (EMD Millipore) and broken in a French press, twice at 15000 pounds/square inch. After centrifugation at 17100 *g* at 4°C, the solubilized protein was mixed with Ni-NTA agarose (QIAGEN), incubated for 1h at 4°C with gentle shaking and then transferred to a gravity flow column (BioRad). After two wash steps with Buffer A, protein was eluted in Buffer B (Tris-HCl 20 mM pH 7.4, NaCl 0.5 M, Imidazole 300 mM) and dialyzed overnight against 1X PBS, 10% glycerol. A final protein concentration of 25 mg ml$^{-1}$ was determined by Pierce™ BCA Protein Assay Kit (Thermo Scientific) and protein purity was assessed by SDS–PAGE electrophoresis.

## ColM antibacterial activity

*Disc Diffusion Assay*. *E. coli* and *S. aureus* cultures were grown in LB or TSB liquid medium, respectively, until OD$_{600nm}$ of 0.6. Aliquots of 1 ml were centrifuged and cells were plated onto LA, TSA or TSA with tunicamycin 0.4 µg ml$^{-1}$ plates. Sterile 6mm-diameter paper discs

(Quilaban) were placed on the agar surface and were loaded with 50 µg of purified ColM protein. A control with sterile water was performed. Growth inhibition was observed after 24h of incubation at 37°C.

*Colony Forming Units (CFUs) determination and cell imaging. E. coli* and *S. aureus* cultures were grown in LB or TSB liquid medium, respectively. When $OD_{600nm}≈0.6$, cultures were divided and 0 µg ml$^{-1}$, 10 µg ml$^{-1}$ or 100 µg ml$^{-1}$ of ColM was added. Cells were incubated at 37°C for 1h and 3h, after which they were imaged by phase contrast microscopy. 100 µl samples from 10$^{-5}$ or 10$^{-6}$ dilutions (*S. aureus* strains) were plated on TSA or TSA with tunicamycin 0.4 µg ml$^{-1}$ plates. 100 µl samples from 10$^{-2}$, 10$^{-5}$ or 10$^{-6}$ dilutions (*E. coli* K12) were plated on LA plates. Values of CFUs/ml for each condition were determined after 24h.

## Extraction of cellular-linked PGN precursors and UHPLC analysis

ColpMurJi was grown as described above. COL overnight cultures were back-diluted to an $OD_{600nm}$ of approximately 0.05 and grown until $OD_{600nm}$ of 0.6-0.8. Lipid II precursors were purified as previously described[40]. Briefly, the cells were harvested, resuspended in a 1:1:2 PBS:CHCl$_3$:MeOH mixture and disrupted with glass beads in a FastPrep-24™ 5G Homogeniser for 3 sets of 2 cycles of 45 seconds at 4.5 RPM with a 5-minute interval on ice between cycles. Cell debris were removed by centrifugation at 4000 x *g* for 10 min at 4°C. The resulting sample was added to 2 ml of CHCl$_3$ and 1.5 ml PBS, vortexed for 10 min and centrifuged for 10 minutes at 4000 x *g* at RT to ease phase separations. The fraction containing the interface and organic phase was collected and dried in a speedvac at 30°C.

The lipid extracts were resuspended in 200 µl of MilliQ $H_2O$ and homogenized in a FastPrep-24™ 5G Homogeniser for 45 seconds at 4.5 RPM. Samples were hydrolysed to a muropeptide-like structure by incubation in 0.1 M HCl for 15 minutes at 95°C without shaking. This step hydrolyses the pyrophosphate bond that connects bactoprenol to the glycopeptide moiety. The resulting samples were then reduced by incubation with $NaBH_4$ at pH 9.0 in 0.5 M Borate Buffer for 2 hours at room temperature. The reduction reaction was stopped by lowering the pH to 2.0 with o-phosphoric acid and the samples resolved by UHPLC using a Waters Acquity CSH C18 2.1x100mm with 1.7µm particle size with a linear gradient from 5% (v/v) MeOH to 24% (v/v) MeOH in 100 mM Sodium Phosphate Buffer at pH 2.0 over 21.5 minutes, followed by a linear step at 24% (v/v) MeOH until 22.2 minutes (adapted from [41]). Profiles were compared to the *S. aureus* COL profile of muropeptides.

## Statistical analysis.

Statistical analyses were done using GraphPad Prism 6 (GraphPad Software) using the two-tailed Mann-Whitney *U* test. *p* values ≤ 0.05 were considered as significant for all analysis performed and were indicated with asterisks: *$p$ ≤ 0.05, **$p$ ≤ 0.01, ***$p$ ≤ 0.001 and ****$p$ ≤ 0.0001.

**Table 1 – Strains and plasmids used in this study**

| Strains and plasmids | Description | Reference |
|---|---|---|
| *E. coli* | | |
| DC10B | Δ*dcm* in DH10B background; Dam methylation only; for cloning | [42] |
| K12 | | FFUL laboratory stock |

| Strains and plasmids | Description | Reference |
|---|---|---|
| *S. aureus* | | |
| RN4220 | restriction-negative derivative of NCTC8325-4 | [43] |
| COL | HA-MRSA strain | [44] |
| ColpMurJi | COL with *murJ* gene under P*spac* control in the chromosome | This Work |
| COLΔ*pbpD* | COL *pbpD* (PBP4) null mutant | [45] |
| NCTC 8325-4 | MSSA strain | |
| NCTCΔt*agO* | NCTC8325-4 *tagO* null mutant | [46] |
| | | |
| **Plasmids** | | |
| pMutMurJi | *S. aureus* integrative vector including the IPTG-inducible P*spac* promoter and *lacI* gene; Amp$^R$; Ery$^R$ | This work |
| pMLD237 | pET2430 encoding His6-ColM. Kan$^R$ | [39] |

Abbreviations: Kan$^R$ – kanamycin resistance; Amp$^R$ – ampicillin resistance; Ery$^R$ – erythromycin resistance.

## Table 2 – Oligonucleotides used in this study

| Primer No | Primer Name | Sequence (5'-3') |
|---|---|---|
| 1525 | 1804P1HindIII | cgcaagcttacatgagatagggagattcg |
| 1526 | 1804P2BamHI | ataggatccaataatcgcaccaactgctg |

## RESULTS AND DISCUSSION

### MurJ is essential for *S. aureus* viability

Lipid II flipping is an essential process for the synthesis of bacterial cell wall and consequently cell division, and MurJ has been previously suggested to be necessary for *S. aureus* growth[24,32]. We confirmed the essentiality of MurJ in *S. aureus* cells by constructing a conditional *murJ* mutant, ColpMurJi, in which expression of *murJ* gene was placed under the control of the IPTG-inducible P*spac* promoter in the native locus.

In the presence of 0.5 mM IPTG inducer, ColpMurJi cells were viable, showing a growth rate similar to the parental strain COL (Fig. 1). However, in the absence of IPTG, bacterial growth almost ceased, indicating that MurJ is necessary for normal cell proliferation, as previously predicted[24,32].
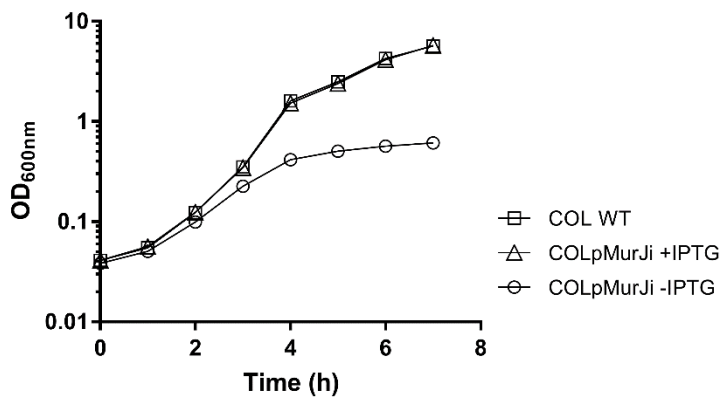


**Figure 1. MurJ is essential for *S. aureus* viability**. Growth curve of parental strain COL (□) and inducible mutant ColpMurJi with (Δ) or without (o) IPTG. Data represent the mean and s.d. of three independent experiments.

## MurJ depletion leads to an increase in cell size

Previous studies in both *B. subtilis* and *E. coli* have revealed that cells lacking MurJ become asymmetrically swollen before lysis[21–23]. We therefore evaluated if MurJ depletion in *S. aureus* could lead to alterations in cell morphology.
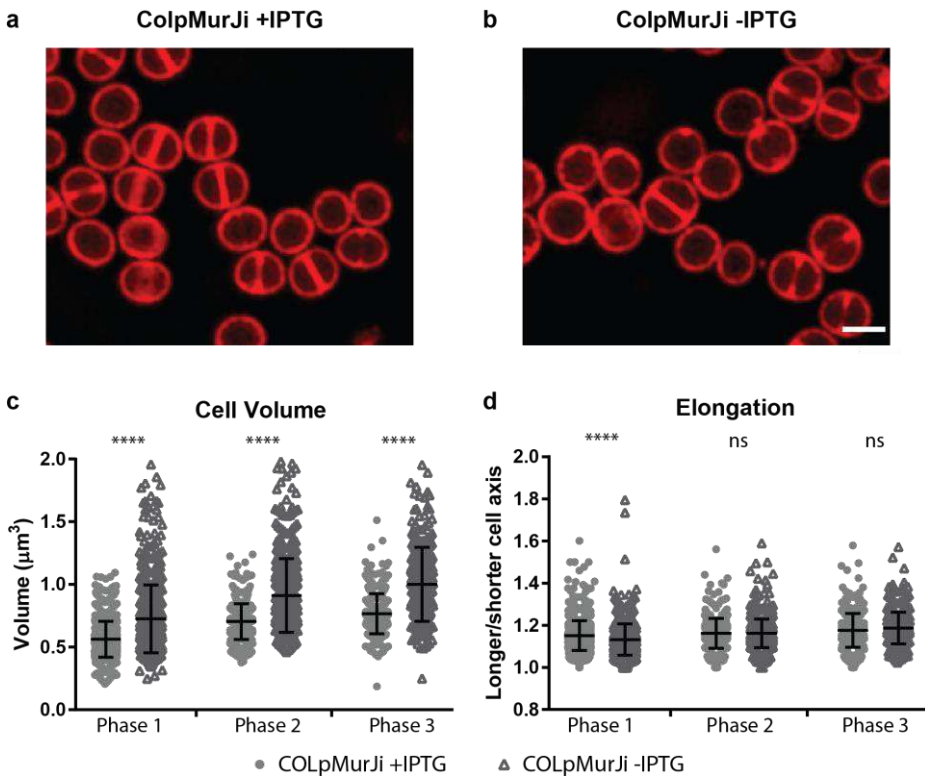


**Figure 2. MurJ depletion causes cell enlargement. a, b**, Structured Illumination Microscopy (SIM) images of ColpMurJi with (**a**) or without (**b**) IPTG stained with Nile Red (membrane). Scale bar, 1 μm. **c, d**, Cell volume (**c**) and ratio of longer/shorter cell axis (**d**) of ColpMurJi with (●) or without (△) IPTG during each of the three cell cycle phases (*n*>300). Data is represented as scatter plots in which the middle line represents the mean and top and bottom lines are s.d. Volume fold changes of ColpMurJi -IPTG compared to +IPTG is 1.3 across the entire cell cycle. Statistical analysis was performed using a Mann-Whitney *U* test. ****$p<0.0001$.

Examination by SIM microscopy of ColpMurJi cells during depletion revealed larger cells but with normal shape (Fig. 2a,b). Using eHooke, an inhouse developed software[33], we detected an increase in cell volume in all phases of the cell cycle. This increase corresponds to approximatelly 30% of normal cell volume and remains constant throughout the cell cycle (Fig. 2c). No biologically relevant difference was observed for the long/short axis ratios, indicating no alteration in the cell elongation process (Fig. 2d).

## MurJ is necessary for peptidoglycan incorporation

In order to determine if PGN synthesis was affected in the absence of MurJ, we evaluated the incorporation of NADA, a fluorescent D-amino acid, that can be incorporated in the last position of the PGN stem peptide and label regions of PGN insertion[35,36]. A general decrease of fluorescence occurred throughout the cell after MurJ depletion, suggesting a reduction in PGN incorporation both at the septum and peripheral cell wall (Fig. 3a,c,d). A decrease in septum/periphery fluorescence ratio (FR) indicates that this fluorescence decrease was more pronounced at the septum than at the cell periphery (Fig. 3b), possibly due to delocalization of PGN synthesis. The fact that septal and peripheral PGN incorporation in *S. aureus* are performed by different enzymes[47], and that both processes are affected by MurJ depletion, suggests that the role of MurJ is not related to an individual synthetic machinery but rather to a process common to PGN incorporation in general.

Parallel studies in our laboratory suggested that the arrival of MurJ to the septum directs PGN incorporation to midcell, leading to fast cytokinesis, independent of FtsZ treadmilling activity[33]. Altogether, these

results suggest the involvement of MurJ in PGN synthesis, as previously proposed[21,22,24,32].
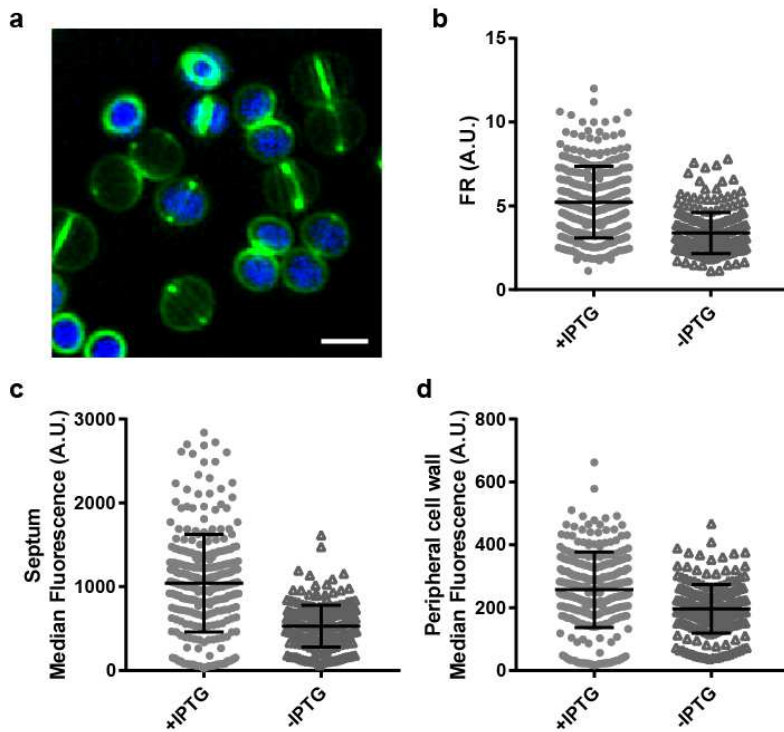


**Figure 3. PGN incorporation is decreased in the absence of MurJ. a**, Structured Illumination Microscopy (SIM) images of ColpMurJi grown in the presence or absence of IPTG 0.5 mM, stained with NADA for 5 minutes. DNA of cells grown with IPTG was also stained with Hoechst 33342 prior mixing of the cells, to allow distinction from cells grown in the absence of IPTG. Scale bar, 1 μm. **b, c, d**, Fluorescence ratio (FR) between the septum and peripheral cell wall values (**b**), fluorescence at the septum (**c**) and at the peripheral cell wall (**d**) in ColpMurJi cells grown with or without IPTG (n>200 cells). In b, c, d, analysis were performed using epifluorescence images. Data is represented as scatter plots in which the middle line represents the mean and top and bottom lines are s.d. Statistical analysis was performed using a Mann-Whitney *U* test. ****$p$<0.0001.

## **Lipid II precursors accumulate in the absence of MurJ**

To understand if the role of MurJ in PGN incorporation was related to lipid II flipping we started by evaluating alterations in total amount of lipid II in the absence of MurJ. ColpMurJi cells were grown in the presence of IPTG inducer for 3h, then washed and incubated with or without IPTG. After 3 hours of MurJ depletion, the lipid II precursors were purified and bactoprenol was removed by hydrolysis of the pyrophosphate bond with HCl. The resulting samples were resolved by UHPLC and compared to the profile of *S. aureus* COL muropeptides. Preliminary results showed an accumulation of four peaks, eluted approximately at 3.3, 3.6, 4.9 and 5.6 minutes. The peaks at 3.3 min and 5.6 minutes co-elute with muropeptide peaks 1 and 5, respectively, according to the muropeptides profile published by de Jonge and collegues[41] (Fig. 4). Furthermore, mass spectrometry (MS) analysis of the peak with 5.6 minutes of retention time showed that the major species found has a mass compatible to that of peak 5, corresponding to GlcNAc β-(1→4) MurNAc-[L-Ala-D-Glu-L-Lys(Gly5)-D-Ala-D-Ala], the glycopeptide moiety of the expected product of the final stage of lipid II synthesis. This result indicates that the blockage of PGN synthesis due to MurJ depletion occurs after the action of FemB, and of complete synthesis of lipid II precursor. MS analysis of the peak eluting at 3.6 minutes shows a mass compatible with a non-amidated MurNAc-[L-Ala-D-Glu-L-Lys-D-Ala-D-Ala], the structure of Lipid I glycopeptide moiety.

Considering the decrease of new PGN synthesis showed in the previous section, this accumulation of lipid II precursors at the membrane in the absence of MurJ confirms a role for this protein between lipid II synthesis and its incorporation into new PGN, compatible with the hypothesis of MurJ being a lipid II flippase.
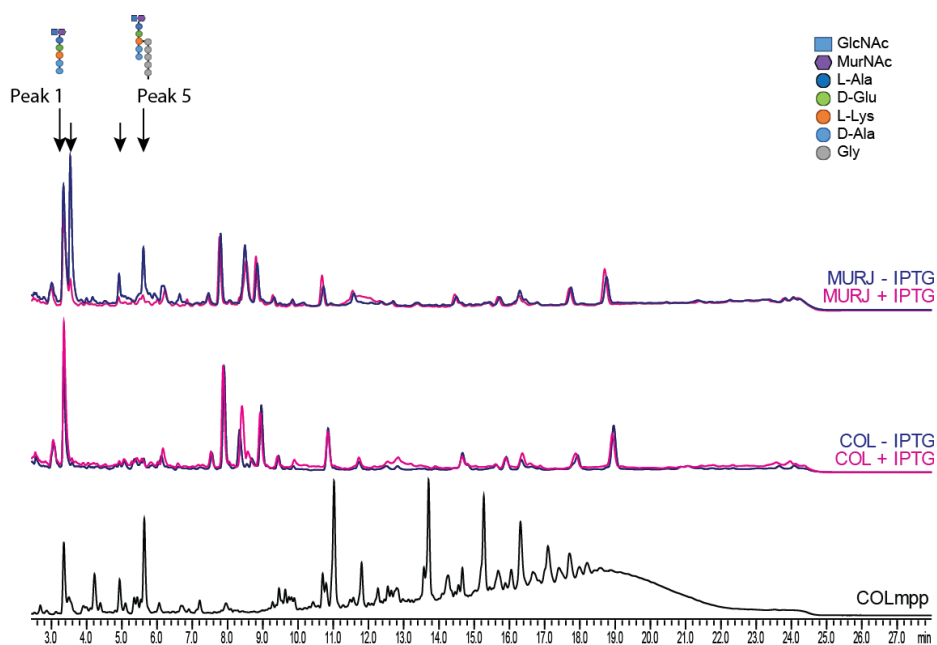
**Figure 4. Lipid II precursors accumulate in the absence of MurJ**. UHPLC analysis of COL muropeptides (COLmpp) and of the glycopeptide moiety of lipid II precursors extracted from COL and COLpMurJi in the presence (pink) or absence (blue) of IPTG 0.5 mM. Experiment performed in triplicate with similar results. In COLpMurJi, peaks accumulated in the absence of IPTG are indicated by arrows. Graphical representation of muropeptides corresponding to peaks 1 and 5, according to [41], is shown.

## MurJ inhibition reduces lipid II on the outer leaflet of the cytoplasmic membrane

Having observed the accumulation of lipid II precursors at the cytoplasmic membrane, the next step was to understand if this accumulation occurred in the inner or outer leaflet of the membrane. For that we decided to use the protein toxin colicin M (ColM), an enzyme known to cleave Lipid II into C55-OH and 1-pyrophospho-MurNAc (pentapeptide)-GlcNAc in *E. coli,* and previously used as a tool to evaluate the amount of lipid II on both sides of the cytoplasmic membrane[1].

To determine if ColM is also active against *S. aureus* cells, we started by purifying His₆-ColM protein and testing its activity against Methicillin-Resistant *S. aureus* (MRSA) strain COL and Methicillin-Sensitive *S. aureus* (MSSA) strain NCTC8325-4, as well as *E. coli* K12 as a control. Disc diffusion assay using 50 µg of purified ColM showed an inhibition zone in plates inoculated with *E. coli* K12, confirming ColM activity. However, no inhibition zone was observed in plates inoculated with *S. aureus* strains, indicating that these strains are not affected by the presence of ColM (Fig. 5a).
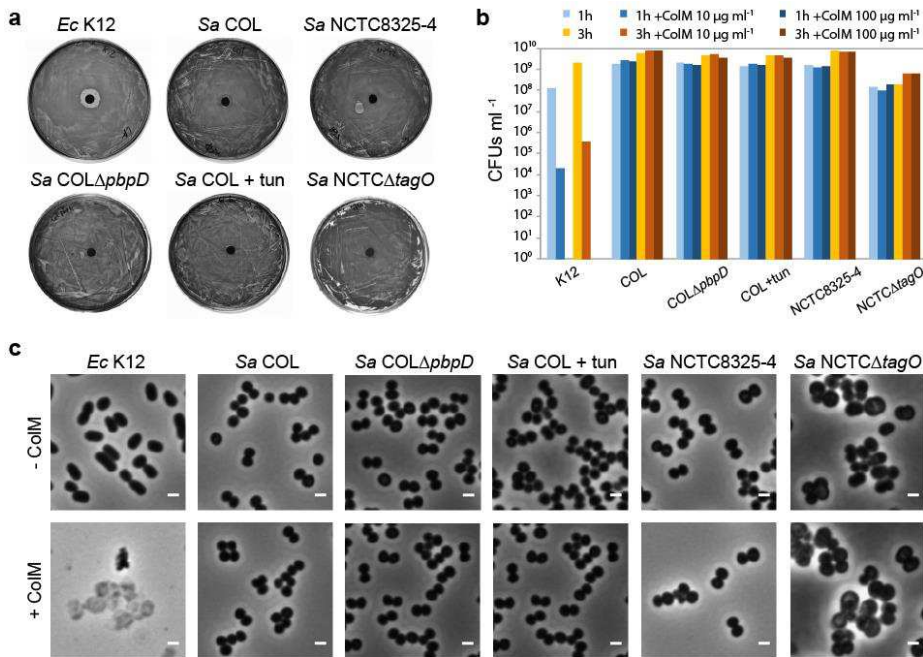


**Figure 5.** ***S. aureus* cells are not affected by ColM activity. a**, Disk diffusion assay using 50 µg of purified ColM, against *E. coli* K12, *S. aureus* COL, COL*ΔpbpD*, NCTC8325-4 and NCTC*ΔtagO*. The assay was performed on LA plates (*E. coli*), TSA plates (*S. aureus*) and TSA with 0.4 µg ml⁻¹ tunicamycin (*S. aureus*, COL+tun). **b**, **c**, Colony Forming Units (CFUs) per ml after 1h and 3h incubation with 10 µg ml⁻¹ and 100 µg ml⁻¹ of ColM (**b**) and phase contrast images after a 3h incubation with 10 µg ml⁻¹ (*E. coli*) or 100 µg ml⁻¹ (*S. aureus*) of ColM (**c**) of *E. coli* K12, *S. aureus* COL, NCTC8325-4, COL*ΔpbpD* and

NCTC$\Delta$*tagO*. Cells were grown in LB (*E. coli*), TSB (*S. aureus*) or TSB with 0.4 µg ml$^{-1}$ tunicamycin (*S. aureus*, COL+tun).

To confirm these results, *E. coli* and *S. aureus* were grown in the presence of 10 µg ml$^{-1}$ and 100 µg ml$^{-1}$ of ColM. After 1h and 3h, cells were imaged by phase contrast microscopy and the number of colony forming units (CFUs) was determined. In *E. coli* K12, both the decrease of CFUs in the presence of ColM and the high percentage of lysed cells observed indicate a reduction in the cell viability (Fig. 5b,c). On the contrary, in *S. aureus* strains the CFUs increased during the 3h incubation with ColM, and no cell lysis was observed by phase contrast microscopy (Fig. 5b,c). This confirms that ColM has no effect on the viability of *S. aureus* strains, probably indicating that lipid II is not being cleaved.

One possible explanation for this reduced susceptibility of *S. aureus* strains could be the difficulty of ColM to reach its substrate due to the thick cell wall layer surrounding *S. aureus* cells or to the presence of wall teichoic acids (WTAs), anionic glycopolymers anchored to PGN[46]. We therefore tested ColM activity against COL$\Delta$*pbpD*, a PBP4 mutant strain with a reduced level of PGN cross-linking. We also tested ColM activity against COL grown in the presence of tunicamycin 0.4 µg ml-$^{1}$, which is known to inhibit teichoic acid synthesis, and NCTC$\Delta$*tagO*, a strain without WTAs. In all of these cases, *S. aureus* cells were able to grow normally, showing an increasing number of CFUs over time and no visible cell lysis in the presence of ColM (Fig. 5). We then concluded that ColM is not active against *S. aureus* in the laboratory conditions tested.

A different strategy to understand if Lipid II accumulation occurs at the inner or outer membrane leaflet was performed by labelling the recently flipped lipid II with Van-FL, which naturally binds D-Ala-D-Ala

residues in the last two positions of PGN stem peptides. In the presence of high concentrations of D-serine in the culture media, *S. aureus* cells can incorporate this amino acid instead of D-alanine, in the fifth position of the stem peptide[48], leading to a reduced efficiency of vancomycin binding[49]. By growing the cells in the presence of an excess of D-serine, a reduction of Van-FL signal is expected. The transfer of these cells to culture media without D-serine will allow the incorporation of normal D-alanine in lipid II, which, after flipping across the cytoplasmic membrane, can be bound by Van-FL, increasing fluorescence signal. Therefore, cells were grown overnight and diluted during the day with an excess of D-serine (0.125 M) and then centrifuged and resuspended in TSB or in TSB supplemented with D-serine or with the MurJ inhibitor CDFI[24], for 30 min prior to Van-FL labelling.

As expected, cells resuspended in TSB show a higher Van-FL fluorescence signal at the septum than cells resuspended in TSB with D-serine (Fig. 6). When resuspended in TSB with CDFI, a significant reduction in the septal fluorescence was observed, in comparison to the cells resuspended in TSB (Fig. 6c), presumably due to inhibition of lipid II flipping. Similarly to what was observed for NADA incorporation, this reduction results from a general decrease of the fluorescent signal, although more pronounced at the septum than the peripheral wall (Fig. 6).

To further confirm these results, we used a different approach based on the ability of *S. aureus* to incorporate different dipeptides in the two last positions of lipid II pentapeptide. For this, we grew the cells in the presence of D-Ala-D-Pra, an unnatural dipeptide with an alkyl group able to covalently bind compounds with azide groups by a copper-catalyzed click-reaction[38]. By using both permeable and impermeable fluorescent probes with azide groups we were expecting to distinguish between lipid II on the outer membrane leaflet and total lipid II. Binding

of the impermeable probe (AF488-Azide) in the parental strain showed a visible fluorescent signal, which almost disappeared when MurJ was inhibited with CDFI (Fig. 7). This again suggests that an active MurJ is necessary for lipid II to be flipped and that the accumulation of lipid II precursors previously observed, probably occurs at the inner surface of the cytoplasmic membrane. Unfortunately, the results using the cell permeable probe 5-TAMRA Azide were similar, with almost no signal detected after MurJ inhibition. This is probably due to the impermeability of the cells to the copper ion necessary for copper-catalyzed click reaction, even after several attempts to permeabilize the cells.
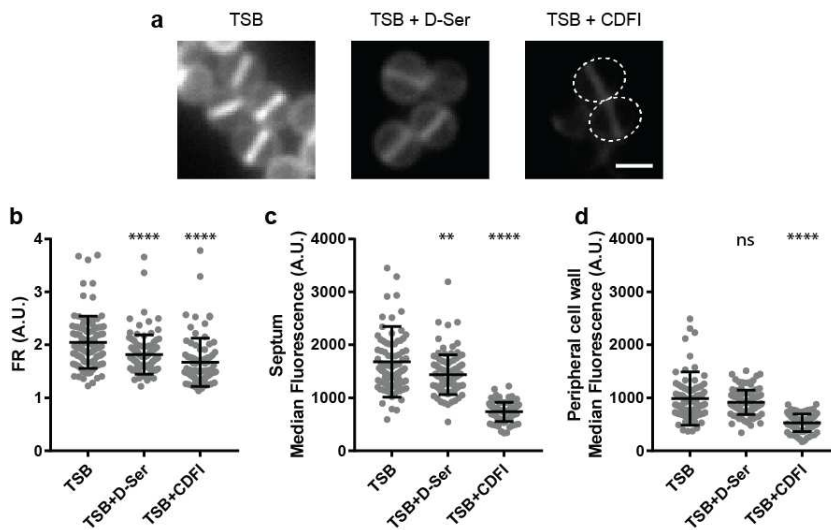


**Figure 6 – Active MurJ is necessary for lipid II flipping**. Epifluorescence images (**a**), fluorescence ratio (FR) between the septum and peripheral cell wall values (**b**), fluorescence at the septum (**c**) and at the peripheral cell wall (**d**) of *S. aureus* COL cells grown in TSB with D-serine and resuspended in TSB, TSB with D-serine or TSB with CDFI (n>80). Data is represented as scatter plots in which the middle line represents the mean and top and bottom lines are s.d.. Statistical analysis was performed using a two-sided Mann-Whitney *U* test. **$p$<0.01; ****$p$<0.0001. Experiment performed in triplicate with similar results. Scale bar, 1 μm. Outlines of two cells are indicated with a dashed line.
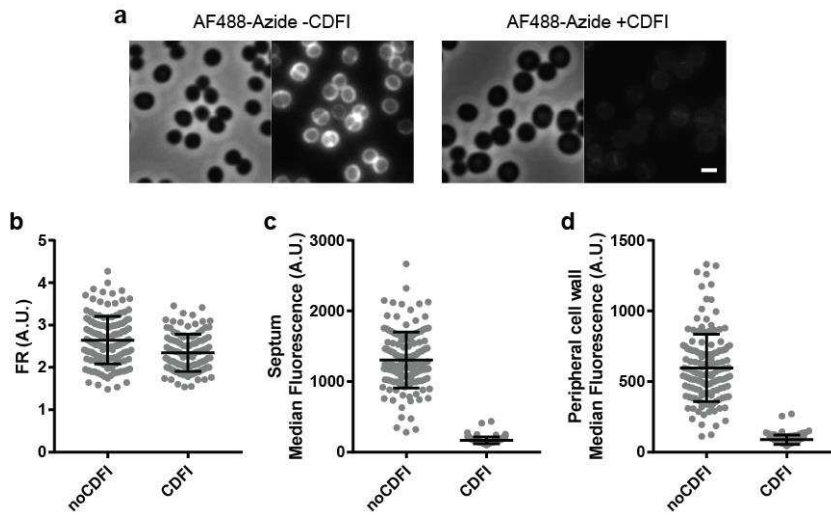
**Figure 7 – MurJ inhibition reduces lipid II at the outer membrane leaflet**. Phase contrast (left) and epifluorescence (right) images (**a**)**,** Fluorescence ratio (FR) between the septum and peripheral cell wall values (**b**), fluorescence at the septum (**c**) and at the peripheral cell wall (**d**) of cells incubated for 30 min with D-Ala-D-Pra dipeptide and with or without CDFI, and further labelled by AF488-Azide fluorescent dye through a copper-catalyzed click-reaction (n>100). Statistical analysis was performed using a two-sided Mann-Whitney *U* test. ****$p$<0.0001 for all comparisons. Experiment performed in triplicate with similar results. Scale bar, 1 μm.

## FINAL REMARKS

Lipid II flipping is an essential process for the synthesis of the bacterial cell wall and the inhibition of this step was shown to impair cell growth and division in different bacteria, including *S. aureus*[21–24,32]. Although several proteins have been proposed as the lipid II flippase, leading to a debate among the scientific community, MurJ is generally accepted as the main candidate at the moment. In this work we showed that MurJ is necessary for maintaining the size and viability of *S. aureus* COL cells. Its absence led to a reduction of PGN synthesis and to accumulation of lipid II precursors at the cytoplasmic membrane. Our results also evidenced that this accumulation does not occur at the outer leaflet of the membrane and suggest that upon inactivation of MurJ, lipid II accumulates at the inner side of the membrane, probably due to a blockage on the flipping process. Together with recent work from our laboratory showing that MurJ is the main responsible for driving PGN synthesis to the septum[33], these results indicate that MurJ activity is involved in lipid II flipping in *Staphylococcus aureus*.

## REFERENCES

1.  Sham, L. T. *et al.* MurJ is the flippase of lipid-linked precursors for peptidoglycan biogenesis. *Science* **345**, 220–222 (2014).
2.  Scheffers, D. J. & Pinho, M. G. Bacterial Cell Wall Synthesis : New Insights from Localization Studies. *Microbiol Mol Biol Rev.* **69**, 585–607 (2005).
3.  van Heijenoort, J. Assembly of the monomer unit of bacterial peptidoglycan. *Cell. Mol. Life Sci. C.* **54**, 300–304 (1998).
4.  Kotnik, M., Anderluh, P. S. & Prezelj, A. Development of novel inhibitors targeting intracellular steps of peptidoglycan biosynthesis. *Curr. Pharm. Des.* **13**, 2283–309 (2007).
5.  Neuhaus, F. C. Initial Translocation Reaction in the Biosynthesis of Peptidoglycan by Bacterial Membranes. *Acc. Chem. Res.* **4**, 297–303 (1971).
6.  Mengin-Lecreulx, D., Texier, L., Rousseau, M. & van Heijenoort, J. The *murG* gene of *Escherichia coli* codes for the UDP-N-acetylglucosamine: N-acetylmuramyl-(pentapeptide) pyrophosphoryl-undecaprenol N-acetylglucosamine transferase involved in the membrane steps of peptidoglycan synthesis. *J. Bacteriol.* **173**, 4625–36 (1991).
7.  Schneider, T. *et al.* In vitro assembly of a complete, pentaglycine interpeptide bridge containing cell wall precursor (lipid II-Gly5) of *Staphylococcus aureus*. *Mol. Microbiol.* **53**, 675–685 (2004).
8.  Münch, D. *et al.* Identification and in vitro Analysis of the GatD/MurT Enzyme-Complex Catalyzing Lipid II Amidation in *Staphylococcus aureus*. *PLoS Pathog.* **8**, e1002509 (2012).
9.  Figueiredo, T. A. *et al.* Identification of Genetic Determinants and Enzymes Involved with the Amidation of Glutamic Acid Residues in the Peptidoglycan of *Staphylococcus aureus*. *PLoS Pathog.* **8**, e1002508 (2012).
10. Meeske, A. J. *et al.* SEDS proteins are a widespread family of bacterial cell wall polymerases. *Nature* **537**, 634–638 (2016).
11. Emami, K. *et al.* RodA as the missing glycosyltransferase in *Bacillus subtilis* and antibiotic discovery for the peptidoglycan polymerase pathway. *Nat. Microbiol.* **2**, 1–8 (2017).
12. van Dam, V. *et al.* Transmembrane transport of peptidoglycan precursors across model and bacterial membranes. *Mol. Microbiol.* **64**, 1105–1114 (2007).
13. Lara, B. & Ayala, J. A. Topological characterization of the essential *Escherichia coli* cell division protein FtsW. *FEMS Microbiol. Lett.* **216**, 23–32 (2002).
14. Henriques, A. O., Glaser, P., Piggot, P. J. & Moran, C. P. Control of cell shape and elongation by the *rodA* gene in *Bacillus subtilis*. *Mol. Microbiol.* **28**, 235–247 (1998).
15. Butler, E. K., Davis, R. M., Bari, V., Nicholson, P. A. & Ruiz, N. Structure-function analysis of MurJ reveals a solvent-exposed cavity containing residues essential for peptidoglycan biogenesis in *Escherichia coli*. *J. Bacteriol.* **195**, 4639–4649 (2013).
16. Höltje, J. V. Growth of the stress-bearing and shape-maintaining murein sacculus of *Escherichia coli*. *Microbiol. Mol. Biol. Rev.* **62**, 181–203

(1998).

17.  Matsuhashi, M. Utilization of lipid-linked precursors and the formation of peptidoglycan in the process of cell growth and division: membrane enzymes involved in the final steps of peptidoglycan synthesis and the mechanism of their regulation. in *Bacterial cell wall* (eds. Ghuysen, J. M. & Hakenbeck, R.) **27**, 55–71 (Elsevier Biochemical Press, 1994).

18.  Mohammadi, T. *et al.* Identification of FtsW as a transporter of lipid-linked cell wall precursors across the membrane. *EMBO J.* **30**, 1425–1432 (2011).

19.  Mohammadi, T. *et al.* Specificity of the transport of lipid II by FtsW in *Escherichia coli*. *J. Biol. Chem.* **289**, 14707–14718 (2014).

20.  Taguchi, A. *et al.* FtsW is a peptidoglycan polymerase that is functional only in complex with its cognate penicillin-binding protein. *Nat. Microbiol.* **4**, 587–594 (2019).

21.  Ruiz, N. Bioinformatics identification of MurJ (MviN) as the peptidoglycan lipid II flippase in *Escherichia coli*. *Proc. Natl. Acad. Sci.* **105**, 15553–15557 (2008).

22.  Inoue, A. *et al.* Involvement of an essential gene, *mviN*, in murein synthesis in *Escherichia coli*. *J. Bacteriol.* **190**, 7298–7301 (2008).

23.  Meeske, A. J. *et al.* MurJ and a novel lipid II flippase are required for cell wall biogenesis in *Bacillus subtilis*. *Proc. Natl. Acad. Sci.* **112**, 6437–6442 (2015).

24.  Huber, J. *et al.* Chemical Genetic Identification of Peptidoglycan Inhibitors Potentiating Carbapenem Activity against Methicillin-Resistant *Staphylococcus aureus*. *Chem. Biol.* **16**, 837–848 (2009).

25.  Lu, M., Radchenko, M., Symersky, J., Nie, R. & Guo, Y. Structural insights into H⁺-coupled multidrug extrusion by a MATE transporter. *Nat. Struct. Mol. Biol.* **20**, 1310–1317 (2013).

26.  Lu, M. *et al.* Structures of a Na⁺-coupled, substrate-bound MATE multidrug transporter. *Proc. Natl. Acad. Sci. U. S. A.* **110**, 2099–104 (2013).

27.  Tanaka, Y. *et al.* Structural basis for the drug extrusion mechanism by a MATE multidrug transporter. *Nature* **496**, 247–251 (2013).

28.  Islam, S. T. *et al.* A cationic lumen in the Wzx flippase mediates anionic O-antigen subunit translocation in *Pseudomonas aeruginosa* PAO1. *Mol. Microbiol.* **84**, 1165–1176 (2012).

29.  Kuk, A. C. Y., Mashalidis, E. H. & Lee, S. Crystal structure of the MOP flippase MurJ in an inward-facing conformation. *Nat Struct Mol Biol* **24**, 171–176 (2017).

30.  Bolla, J. R. *et al.* Direct observation of the influence of cardiolipin and antibiotics on lipid II binding to MurJ. *Nat. Chem.* **10**, 363–371 (2018).

31.  Zheng, S. *et al.* Structure and mutagenic analysis of the lipid II flippase MurJ from *Escherichia coli*. *Proc. Natl. Acad. Sci.* **115**, 6709–6714 (2018).

32.  Mott, J. E. *et al.* Resistance mapping and mode of action of a novel class of antibacterial anthranilic acids: evidence for disruption of cell wall biosynthesis. *J. Antimicrob. Chemother.* **62**, 720–729 (2008).

33.  Monteiro, J. M. *et al.* Peptidoglycan synthesis drives an FtsZ-treadmilling-independent step of cytokinesis. *Nature* **554**, 528–532 (2018).

34.  Oshida, T. & Tomasz, A. Isolation and characterization of a Tn551-

autolysis mutant of *Staphylococcus aureus*. *J. Bacteriol.* **174**, 4952–9 (1992).

35. Kuru, E. *et al. In Situ* Probing of Newly Synthesized Peptidoglycan in Live Bacteria with Fluorescent D-Amino Acids. *Angew. Chemie Int. Ed.* **51**, 12519–12523 (2012).

36. Kuru, E., Tekkam, S., Hall, E., Brun, Y. V & VanNieuwenhze, M. S. Synthesis of fluorescent D-amino acids (FDAAs) and their use for probing peptidoglycan synthesis and bacterial growth *in situ*. *Nat Protoc.* **10**, 33–52 (2015).

37. Heintzmann, R. & Cremer, C. G. Laterally modulated excitation microscopy: improvement of resolution by using a diffraction grating. in *SPIE 3568, Optical Biopsies and Microscopic Techniques III* (eds. Bigio, I. J., Schneckenburger, H., Slavik, J., Svanberg, K. & Viallet, P. M.) **3568**, 185–196 (International Society for Optics and Photonics, 1999).

38. Sarkar, S., Libby, E. A., Pidgeon, S. E., Dworkin, J. & Pires, M. M. *In Vivo* Probe of Lipid II-Interacting Proteins. *Angew. Chemie Int. Ed.* **55**, 8401–8404 (2016).

39. Barreteau, H. *et al.* Deciphering the Catalytic Domain of Colicin M, a Peptidoglycan Lipid II-degrading Enzyme. *J. Biol. Chem.* **285**, 12378–12389 (2010).

40. Qiao, Y. *et al.* Detection of lipid-linked peptidoglycan precursors by exploiting an unexpected transpeptidase reaction. *J. Am. Chem. Soc.* **136**, 14678–14681 (2014).

41. De Jonge, B. L. M., Chang, Y. S., Gage, D. & Tomasz, A. Peptidoglycan composition of a highly methicillin-resistant *Staphylococcus aureus* strain. The role of penicillin binding protein 2A. *J. Biol. Chem.* **267**, 11248–11254 (1992).

42. Monk, I. R., Shah, I. M., Xu, M., Tan, M. & Foster, T. J. Transforming the untransformable: application of direct transformation to manipulate genetically *Staphylococcus aureus* and *Staphylococcus epidermidis*. *MBio.* **3**, 1–11 (2012).

43. Nair, D. *et al.* Whole-genome sequencing of *Staphylococcus aureus* strain RN4220, a key laboratory strain used in virulence research, identifies mutations that affect not only virulence factors but also the fitness of the strain. *J. Bacteriol.* **193**, 2332–5 (2011).

44. Gill, S. R. *et al.* Insights on evolution of virulence and resistance from the complete genome analysis of an early methicillin-resistant *Staphylococcus aureus* strain and a biofilm-producing methicillin-resistant *Staphylococcus epidermidis* strain. *J. Bacteriol.* **187**, 2426–2438 (2005).

45. Memmi, G., Filipe, S. R., Pinho, M. G., Fu, Z. & Cheung, A. *Staphylococcus aureus* PBP4 Is Essential for beta-Lactam Resistance in Community-Acquired Methicillin-Resistant Strains. *Antimicrob. Agents Chemother.* **52**, 3955–3966 (2008).

46. Atilano, M. L. *et al.* Teichoic acids are temporal and spatial regulators of peptidoglycan cross-linking in *Staphylococcus aureus*. *Proc. Nati. Acad. Sci. U S A* **107**, (2010).

47. Monteiro, J. M. *et al.* Cell shape dynamics during the staphylococcal cell cycle. *Nat. Commun.* **6**, 8055 (2015).

48. De Jonge, B. L. M., Gage, D. & Xu, N. The carboxyl terminus of peptidoglycan stem peptides is a determinant for methicillin resistance

in *Staphylococcus aureus*. *Antimicrob. Agents Chemother.* **46**, 3151–3155 (2002).

49. Pereira, P. M., Filipe, S. R., Tomasz, A. & Pinho, M. G. Fluorescence Ratio Imaging Microscopy Shows Decreased Access of Vancomycin to Cell Wall Synthetic Sites in Vancomycin-Resistant *Staphylococcus aureus*. *Antimicrob. Agents Chemother.* **51**, 3627–3633 (2007).

# CHAPTER V

**General Discussion**

**and Conclusions**

*Staphylococcus aureus* is a coccoid bacteria able to colonize the nasopharynx mucosa of humans and capable of causing severe illness. Its spherical shape facilitates the escape from the human innate immune system, contributing for the high infection rate of this species[1]. To maintain a spherical shape with a constant size over generations, *S. aureus* cells need to increase their volume during each cell cycle, prior to cell division. Recent work from our laboratory has identified 3 phases in the cell cycle: phase 1, when cells have not yet started the synthesis of the division septum; phase 2, during which the septum is synthesized and phase 3, when the septum is complete and is undergoing maturation before cells divide to originate two daughter cells[2]. An increase in cell volume is observed mainly during phases 1 and 3 and is accompanied by a slight increase in cell lenght[2].

## The elongation mechanism in *S. aureus*

The protein complex involved in cell elongation (elongasome) is composed of different elements, including peptidoglycan (PGN) synthases from both the SEDS and PBPs family, cytoskeletal proteins and other morphogenetic elements that can act as scaffolds or stabilizers of the complex. In rod-shaped bacteria like *Bacillus subtilis* or *Escherichia coli,* the elongasome is dependent on the MreB cytoskeleton and incorporates PGN along the lateral wall[3]. Ovococcoid bacteria, like *Streptococcus pneumoniae*, lack MreB homologues and their elongasome incorporates PGN at midcell probably in a manner dependent on FtsZ[4,5]. Although no MreB homologues nor elongation complex had been identified in *S. aureus*, it was intriguing that several genes encoding proteins associated with rod elongation were present in its genome, including *mreC*, *mreD* and *rodA*.

MreC and MreD have been associated with cell elongation in both rod-shaped and ovococcoid bacteria. In *B. subtilis*[6], *E. coli*[7] and *S. pneumoniae*[8], deletion of *mreC* or *mreD* genes leads to severe morphologic alterations, as the cells become round and eventually lyse. In this study, we determined that lack of MreC or MreD in Methicillin-Resistant *S. aureus* (MRSA) strain COL or in Methicillin-Sensitive *S. aureus* (MSSA) strain NCTC8325-4, does not alter the volume of the cells, the surface roughness or the PGN composition. A parallel study by Garcia-Lara and colleagues suggested a patterned distribution for MreD in the *S. aureus* membrane, similar to the one observed for PlsY and CdsA, two proteins involved in lipid metabolism[9]. MreD was shown to interact with both proteins and they were proposed to form a supramolecular structure involved in the large-scale organization of protein complexes across the cell surface[9]. In our work we observed that sGFP fusions of MreC and MreD were enriched at the division septum. Despite this preferential septal localization, both MreC and MreD could also be found, although in much lower amounts, around the cell periphery. However, no obvious patterned distribution was observed both by epifluorescence or Super-Resolution Structured Illumination Microscopy (SIM). This localization mainly at the septum and, in lower amounts, at the periphery, matches the pattern of septal and peripheral PGN incorporation in *S. aureus*[2]. The coordination of MreC and MreD localization with PGN synthesis has been previously described in both *B. subtilis*[10] and *E. coli*[11]. Also, in *S. pneumoniae* both MreC and MreD localize to the current and future septal regions, areas of active PGN synthesis[8].

Besides MreC and MreD, different pairs of SEDS and class B PBPs (bPBPs) play a role in elongation[12–15] and division[16–19] of different bacteria. In *S. aureus* cells two SEDS proteins, FtsW and RodA, and two bPBPs, PBP1 and PBP3, are present. We have shown that RodA

interacts with PBP3, forming a complex involved in the maintenance of cell size and shape. Septal RodA localization was not dependent on its transglycosylase (TGase) activity but both localization and TGase activity required the presence of PBP3. In the absence of PBP3, RodA delocalized from the septum to the cell periphery and susceptibility to moenomycin (inhibitor of PBP-like TGase domains[20]) increased to values similar to those in a strain lacking RodA, evidencing the dependency between both proteins and suggesting a new mode of regulation of PGN synthesis in *S. aureus*. Similar SEDS-bPBP complexes have been identified in other bacteria, with RodA being associated to PBP2 in *E. coli*[12], PBP2A/PbpH in *B. subtilis*[14] and PBP2b in *S. pneumoniae*[13]. Agreeing with our results, activities of PBP2 and RodA in *E. coli* have been shown to depend on each other[21] and PBP2 has recently been proposed to stimulate RodA polymerase activity[22]. This regulatory process avoids the synthesis of uncrosslinked glycan chains, which leads to a cytotoxic futile cycle of PGN synthesis and degradation[23]. Although no such cycle has been identified in *S. aureus* so far, we can speculate a similar consequence in this organism.

RodA-bPBP cognate pairs are involved in the elongation of rod-shaped[12,24] and ovococcoid[13,25] cells, as cells become rounder in their absence. In line with this idea, we observed that RodA and PBP3 are responsible for the slight elongation of *S. aureus* cells, since cells depleted of both proteins had a lower longer to shorter axis ratio, becoming more spherical. Both RodA and PBP3 are recruited to the future division site, where they incorporate PGN in the *S. aureus* side-wall, with consequent elongation of the cells. This peripheral PGN incorporation could be observed in cells in phase 1 of the division cycle, indicating that it is independent from septal PGN synthesis and starts slightly before cell division. This elongation mode resembles pre-septal elongation in *E. coli*[26,27] and *Caulobacter crescentus*[28] or peripheral

synthesis in *S. pneumoniae*[4,5], both of which resulting in growth of the cell envelope probably dependent on FtsZ. The role of RodA-PBP3 pair in *S. aureus* cell elongation is the first evidence for the existence of an elongation machinery in spherical cocci.

## Septal peptidoglycan synthesis and divisome stabilization

Given that RodA and PBP3 form a complex involved in *S. aureus* elongation, we hypothesized that FtsW and PBP1 had a role in cell division. Our results showed that FtsW and PBP1 are essential for *S. aureus* viability and form a SEDS-bPBP interacting pair. The identification of this functional pair in *S. aureus* is in agreement with the existence of similar pairs in other bacteria like FtsW-PBP3 in *E. coli*[29] and FtsW-PBP2x in *S. pneumoniae*[19], as well as with the *S. aureus* FtsW-PBP1 interaction recently observed in vitro by Taguchi and colleagues[30]. This latter study also showed the essential TGase activity of FtsW when coupled with PBP1, even in the absence of PBP1 TP activity[30]. We determined that this TGase activity was not necessary for FtsW localization to PGN incorporation sites, but constituted an essential function of this protein, since FtsW mutants lacking TGase activity were not able to complement FtsW-depleted strains. Interestingly, the essentiality of PBP1 was not due to its TPase activity, as the inactivation of that activity did not prevent cell viability.

Cell division occurs through inward incorporation of PGN at midcell in an FtsZ-dependent manner[31]. In ovococcoid bacteria, inactivation of PBP2x, involved in septal PGN synthesis, results in cell elongation and enlargement in *S. pneumoniae*[32,33] or filamentation in *Lactococcus lactis*[34], evidencing septation problems. Our results are in accordance with these observations, as depletion of *S. aureus* FtsW or

PBP1 resulted in a blockage of inward septal PGN incorporation and consequently of cell division, and an increase in cell elongation. FtsW and PBP1 were previously shown to localize to the division septum at early stages of the cell cycle, before septal recruitment of MurJ, the putative lipid II flipase[35], suggesting a second role of these two proteins, besides their TGase-TPase activity. Agreeing with this idea, FtsW-PBP1 pair displays an early function in divisome stabilization, being responsible for maintaining septal PGN synthesis at midcell. Early division proteins, like FtsZ or EzrA, localize to the future division site and recruit later divisome proteins responsible for PGN incorporation. Mislocalization of FtsZ prevents the correct placement of the divisome at midcell and leads to alterations in PGN incorporation pattern[36,37]. In fact, *S. aureus* FtsZ mutants that form arcs or helical-like FtsZ filaments incorporate PGN in similar helical-like patterns, leading to an abnormal elongation of the cells[36]. In the absence of FtsW or PBP1, we showed that both FtsZ and EzrA were mislocalized, forming multiple rings or arcs. Despite the altered localization, these structures were still able to recruit other divisome proteins and to incorporate PGN. As a consequence, elongated cells that are unable to efficiently close the division septum appeared. The role of FtsW and its cognate bPBP in early divisome stabilization has been previously proposed, with FtsZ correct assembly being dependent on FtsW in *B. subtilis*[38] or on FtsW and FtsI (FtsW cognate bPBP) in *Streptomyces coelicolor*[39]. Additionally, FtsW was shown to be involved in divisome activation in *E. coli*[40] and *C. crescentus*[41]. Agreeing with these observations, our work has shown the importance of FtsW and PBP1 in early stages of divisome assembly in *S. aureus.*

## Cell division and elongation - Two peptidoglycan incorporation machineries in *S. aureus*

Until now, only one PGN synthesis machinery had been identified in *S. aureus*, responsible for the incorporation of PGN both at the septum and at the cell periphery[2,4]. Taken together, our data suggest the existence of two different PGN incorporation complexes, responsible for cell division and cell elongation. Their coordinated activities allow the establishment of the coccoid morphology and its maintenance over generations. The existence of these two systems indicates that the regulation of PGN incorporation mechanisms in coccoid bacterial cells is more complex than previously thought.

During cell division, PGN is inserted inwards to form the division septum, an activity that depends on the tubulin homologue FtsZ. On the other hand, cell elongation occurs by incorporation of PGN in the peripheral cell wall, in a mechanism directed by actin homologue MreB in rod-shaped bacteria or by FtsZ in ovococcoid and possibly, according to our work, in coccoid cells. Each of these cytoplasmic cytoskeletal proteins, FtsZ and MreB, interacts with membrane proteins that connect them to proteins on the outer surface of the cytoplasmic membrane, including PBPs, forming large PGN synthesis complexes. However, the mechanisms that regulate and coordinate both division and elongation mechanisms in different cell morphologies remain elusive.

In ovococcoid *S. pneumoniae*, septal and peripheral PGN synthesis complexes are temporally and spatially coordinated and are probably both dependent on FtsZ. Since MreC and MreD in *B. subtilis* are believed to couple the internal MreB cytoskeleton to the PBPs on the outer surface of the membrane, and that their absence in *S. pneumoniae* leads to cell rounding, they were also proposed to be responsible for directing peripheral synthesis. The ability of MreC to

physically or functionally interact with different PBPs in different species, including elongation-related PBP2 in *E. coli*[42], PBP2 in *C. crescentus*[43] and PBP2 in *Helicobacter pylori*[44], but also division-related PBPs, like PBP1 in *B. subtilis*[45], suggests that MreC might be involved in the coordination of cell elongation and division. Agreeing with this idea, MreC and MreD localization in predivisional *E. coli* cells alters from the lateral wall to ring structures near midcell and MreC localization is necessary for PBP2 localization both to midcell and lateral wall[42]. A similar septal and lateral MreCD localization is observed in *B. subtilis*[6], evidencing a connection between cell elongation and cell division. In *S. aureus,* the identification of an elongation mechanism made us speculate that MreCD could also function as a scaffold for elongation proteins in this organism, directing RodA-PBP3 activity and coordinating it with cell division. This made us revisit the work on MreC and MreD described in chapter 2 and analyse a possible relationship with RodA-PBP3 complex. Preliminary experiments on the effects of MreCD depletion on cell elongation showed a small reduction on longer to shorter cell axis ratio, although less significant than in the absence of RodA-PBP3. Additionally, *mreCD* null mutants showed an increase in moenomycin susceptibility, albeit not as high as in the *rodA* and *pbpC* (PBP3) null mutants, with the MIC decreasing from 0.250 µg ml$^{-1}$ in the parental strain COL to 0.063-0.125 µg ml$^{-1}$ in the double *mreCD* mutant. These initial data may suggest a functional interaction between MreCD and RodA-PBP3 in *S. aureus* cells, strengthening the hypothesis of the existence of a larger elongation complex. Moreover, a possible interaction between MreC and EzrA was identified by bacterial two-hybrid (preliminary data, not shown), although further confirmation with different techniques is still required. This observation suggests a possible coordination of this elongation complex with cell division.

Another possibility for the coordination of cell division and elongation is the activity of serine/threonine kinases/phosphatases (STKs/STPs), which are proposed to act as molecular switches between the two types of synthesis[46–48]. Stk1/Stp1 is the only STK/STP pair identified in *S. aureus*. Stk1, also known as PknB, contains three extracellular PASTA domains and has been associated to cell wall metabolism, virulence and drug resistance[49–52]. In fact, mutants lacking Stk1 or Stp1 display problems in the synthesis of cell wall precursor metabolites[51,52] and mutants lacking both proteins show several cell division and morphology defects, including multiple and incomplete septa, increased cell size and thicker cell walls[49]. These observations make Stk1/Stp1 good candidates for the regulation of PGN synthesis processes in *S. aureus* and it would be very interesting to evaluate in which extent they affect both RodA-PBP3 and FtsW-PBP1 activities.

An essential step for the different modes of PGN synthesis is lipid II flipping across the cytoplasmic membrane. The debate on whether FtsW or MurJ could perform this task, motivated us to pursue this question in *S. aureus*. Recent results from our laboratory showed that FtsW localizes early to the division site and that only a small percentage of the cells with septal FtsW and peripheral MurJ were able to incorporate a fluorescent D-amino acid at midcell[35]. On the contrary, the majority of the cells with septal MurJ showed septal incorporation, indicating that MurJ is more likely than FtsW to be the *S. aureus* lipid II flippase[35]. MurJ recruitment to midcell was also identified as the molecular trigger for the transition from peripheral to septal PGN synthesis[35]. Our results showed that FtsW depletion did not impair the incorporation of fluorescent D-amino acids, as the resulting fluorescent signal was visible around the cell periphery and in multiple rings. On the contrary, this incorporation depended on MurJ activity and was strongly

decreased after MurJ depletion or specific drug-mediated inhibition, presumably due to the reduction of lipid II pool on the outer surface of the cytoplasmic membrane. Accumulation of lipid II precursors observed upon MurJ depletion probably occurred on the inner leaflet of the membrane and resulted from a blockage on the flipping process. Preliminary results showed that FtsW depletion did not cause any detectable alteration on lipid II precursors profile, contributing to the idea that MurJ is in fact the major lipid II flippase in *S. aureus*.

The fact that MurJ is responsible for the majority of lipid II membrane translocation does not exclude the possibility of FtsW having a low level activity of lipid II flipping. Actually, FtsW flipping activity in *E. coli* was shown to take place in vitro[53], although it was not specific for lipid II[54] nor reproducible in vivo[55]. Additionally, FtsW and PBP1 localize to the division septum before MurJ, raising the possibility of FtsW being able to translocate its own substrate, lipid II, across the cytoplasmic membrane.

This work increased our knowledge about some of the fundamental biological processes in the important pathogen *S. aureus,* including how it translocates lipid precursors across the cytoplasmic membrane for the synthesis of PGN and how it establishes and maintains its cell morphology over generations. We now know that the development of cell shape in spherical cocci is not as different from rods or ovococci as we could initially imagine. A myriad of exciting questions has now appeared and the search for a coccoid elongasome is launched. What other proteins are involved in cell elongation, how are elongation and division regulated and coordinated and what is the relevance of elongation for *S. aureus* cells are just some of the questions we hope to answer in the future.

# REFERENCES

1. Yang, D. C., Blair, K. M. & Salama, N. R. Staying in Shape: the Impact of Cell Shape on Bacterial Survival in Diverse Environments. *Microbiol. Mol. Biol. Rev.* **80**, 187–203 (2016).

2. Monteiro, J. M. *et al.* Cell shape dynamics during the staphylococcal cell cycle. *Nat. Commun.* **6**, 8055 (2015).

3. Den Blaauwen, T., de Pedro, M. A., Nguyen-Distèche, M. & Ayala, J. A. Morphogenesis of rod-shaped sacculi. *FEMS Microbiol. Rev.* **32**, 321–344 (2008).

4. Pinho, M. G., Kjos, M. & Veening, J. W. How to get (a)round: mechanisms controlling growth and division of coccoid bacteria. *Nat. Rev. Microbiol.* **11**, 601–14 (2013).

5. Massidda, O., Nováková, L. & Vollmer, W. From models to pathogens: how much have we learned about *Streptococcus pneumoniae* cell division? *Environ. Microbiol.* **15**, 3133–3157 (2013).

6. Leaver, M. & Errington, J. Roles for MreC and MreD proteins in helical growth of the cylindrical cell wall in *Bacillus subtilis*. *Mol. Microbiol.* **57**, 1196–209 (2005).

7. Kruse, T., Bork-Jensen, J. & Gerdes, K. The morphogenetic MreBCD proteins of *Escherichia coli* form an essential membrane-bound complex. *Mol. Microbiol.* **55**, 78–89 (2004).

8. Land, A. D. & Winkler, M. E. The requirement for pneumococcal MreC and MreD is relieved by inactivation of the gene encoding PBP1a. *J. Bacteriol.* **193**, 4166–79 (2011).

9. García-Lara, J. *et al.* Supramolecular structure in the membrane of *Staphylococcus aureus*. *Proc. Natl. Acad. Sci.* **112**, 201509557 (2015).

10. Errington, J., Daniel, R. A. & Scheffers, D. J. Cytokinesis in bacteria. *Microbiol. Mol. Biol. Rev.* **67**, 52–65, table of contents (2003).

11. Ursell, T. S. *et al.* Rod-like bacterial shape is maintained by feedback between cell curvature and cytoskeletal localization. *Proc. Natl. Acad. Sci.* **111**, E1025–E1034 (2014).

12. Cho, H. *et al.* Bacterial cell wall biogenesis is mediated by SEDS and PBP polymerase families functioning semi-autonomously. *Nat. Microbiol.* **1**, 1–8 (2016).

13. Philippe, J., Vernet, T. & Zapun, A. The Elongation of Ovococci. *Microb. Drug Resist.* **20**, 215–221 (2014).

14. Domínguez-Escobar, J. *et al.* Processive movement of MreB-associated cell wall biosynthetic complexes in bacteria. *Science* **333**, 225–8 (2011).

15. Garner, E. C. *et al.* Coupled, circumferential motions of the cell wall synthesis machinery and MreB filaments in *B. subtilis*. *Science* **333**, 222–225 (2011).

16. Weiss, D. S. *et al.* Localization of the *Escherichia coli* cell division protein FtsI (PBP3) to the division site and cell pole. *Mol. Microbiol.* **25**, 671–81 (1997).

17. Daniel, R. A., Williams, A. M. & Errington, J. A complex four-gene operon containing essential cell division gene *pbpB* in *Bacillus subtilis*. *J. Bacteriol.* **178**, 2343–50 (1996).

18. Gamba, P., Veening, J. W., Saunders, N. J., Hamoen, L. W. & Daniel,

R. A. Two-Step Assembly Dynamics of the *Bacillus subtilis* Divisome. *J. Bacteriol.* **191**, 4186–4194 (2009).

19. Perez, A. J. *et al.* Movement dynamics of divisome proteins and PBP2x:FtsW in cells of *Streptococcus pneumoniae*. *Proc. Natl. Acad. Sci. U. S. A.* **116**, 3211–3220 (2019).

20. Huber, G. & Nesemann, G. Moenomycin, an inhibitor of cell wall synthesis. *Biochem. Biophys. Res. Commun.* **30**, 7–13 (1968).

21. Ishino, F. *et al.* Peptidoglycan synthetic activities in membranes of *Escherichia coli* caused by overproduction of Penicillin-binding protein 2 and RodA protein. *J. Biol. Chem.* **261**, 7024–31 (1986).

22. Rohs, P. D. A. *et al.* A central role for PBP2 in the activation of peptidoglycan polymerization by the bacterial cell elongation machinery. *PLoS Genet.* **14**, e1007726 (2018).

23. Cho, H., Uehara, T. & Bernhardt, T. G. Beta-lactam antibiotics induce a lethal malfunctioning of the bacterial cell wall synthesis machinery. *Cell* **159**, 1300–11 (2014).

24. Meeske, A. J. *et al.* SEDS proteins are a widespread family of bacterial cell wall polymerases. *Nature* **537**, 634–638 (2016).

25. Thibessard, A., Fernandez, A., Gintz, B., Leblond-Bourget, N. & Decaris, B. Effects of *rodA* and *pbp2b* disruption on cell morphology and oxidative stress response of *Streptococcus thermophilus* CNRZ368. *J. Bacteriol.* **184**, 2821–6 (2002).

26. Potluri, L. P., Kannan, S. & Young, K. D. ZipA Is Required for FtsZ-Dependent Preseptal Peptidoglycan Synthesis prior to Invagination during Cell Division. *J. Bacteriol.* **194**, 5334–5342 (2012).

27. de Pedro, M. A., Quintela, J. C., Höltje, J. V & Schwarz, H. Murein segregation in *Escherichia coli*. *J. Bacteriol.* **179**, 2823–34 (1997).

28. Aaron, M. *et al.* The tubulin homologue FtsZ contributes to cell elongation by guiding cell wall precursor synthesis in *Caulobacter crescentus*. *Mol. Microbiol.* **64**, 938–952 (2007).

29. Fraipont, C. *et al.* The integral membrane FtsW protein and peptidoglycan synthase PBP3 form a subcomplex in *Escherichia coli*. *Microbiology* **157**, 251–259 (2011).

30. Taguchi, A. *et al.* FtsW is a peptidoglycan polymerase that is functional only in complex with its cognate penicillin-binding protein. *Nat. Microbiol.* **4**, 587–594 (2019).

31. Margolin, W. FtsZ and the division of prokaryotic cells and organelles. *Nat. Rev. Mol. Cell Biol.* **6**, 862–871 (2005).

32. Berg, K. H., Stamsas, G. A., Straume, D. & Havarstein, L. S. Effects of Low PBP2b Levels on Cell Morphology and Peptidoglycan Composition in *Streptococcus pneumoniae* R6. *J. Bacteriol.* **195**, 4342–4354 (2013).

33. Peters, K. *et al. Streptococcus pneumoniae* PBP2x mid-cell localization requires the C-terminal PASTA domains and is essential for cell shape maintenance. *Mol. Microbiol.* **92**, 733–755 (2014).

34. Pérez-Núñez, D. *et al.* A new morphogenesis pathway in bacteria: unbalanced activity of cell wall synthesis machineries leads to coccus-to-rod transition and filamentation in ovococci. *Mol. Microbiol.* **79**, 759–771 (2011).

35. Monteiro, J. M. *et al.* Peptidoglycan synthesis drives an FtsZ-treadmilling-independent step of cytokinesis. *Nature* **554**, 528–532 (2018).

36. Pereira, A. R. *et al.* FtsZ-Dependent Elongation of a Coccoid Bacterium. *MBio* **7**, e00908-16 (2016).

37. Pinho, M. G. & Errington, J. Dispersed mode of *Staphylococcus aureus* cell wall synthesis in the absence of the division machinery. *Mol. Microbiol.* **50**, 871–881 (2003).

38. Gamba, P., Hamoen, L. W. & Daniel, R. A. Cooperative Recruitment of FtsW to the Division Site of *Bacillus subtilis*. *Front. Microbiol.* **7**, (2016).

39. Mistry, B. V, Del Sol, R., Wright, C., Findlay, K. & Dyson, P. FtsW is a dispensable cell division protein required for Z-ring stabilization during sporulation septation in *Streptomyces coelicolor*. *J. Bacteriol.* **190**, 5555–66 (2008).

40. Du, S., Pichoff, S. & Lutkenhaus, J. FtsEX acts on FtsA to regulate divisome assembly and activity. *Proc. Natl. Acad. Sci.* **113**, E5052–E5061 (2016).

41. Modell, J. W., Kambara, T. K., Perchuk, B. S. & Laub, M. T. A DNA Damage-Induced, SOS-Independent Checkpoint Regulates Cell Division in *Caulobacter crescentus*. *PLoS Biol.* **12**, e1001977 (2014).

42. Vats, P., Shih, Y. L. & Rothfield, L. Assembly of the MreB-associated cytoskeletal ring of *Escherichia coli*. *Mol. Microbiol.* **72**, 170–182 (2009).

43. Divakaruni, A. V, Loo, R. R. O., Xie, Y., Loo, J. A. & Gober, J. W. The cell-shape protein MreC interacts with extracytoplasmic proteins including cell wall assembly complexes in *Caulobacter crescentus*. *Proc. Nati. Acad. Sci. U S A* **102**, 18602–7 (2005).

44. El Ghachi, M. *et al.* Characterization of the elongasome core PBP2 : MreC complex of *Helicobacter pylori*. *Mol. Microbiol.* **82**, 68–86 (2011).

45. Claessen, D. *et al.* Control of the cell elongation–division cycle by shuttling of PBP1 protein in *Bacillus subtilis*. *Mol. Microbiol.* **68**, 1029–1046 (2008).

46. Fiuza, M. *et al.* From the characterization of the four serine/threonine protein kinases (PknA/B/G/L) of *Corynebacterium glutamicum* toward the role of PknA and PknB in cell division. *J. Biol. Chem.* **283**, 18099–112 (2008).

47. Kang, C. M. *et al.* The *Mycobacterium tuberculosis* serine/threonine kinases PknA and PknB: substrate identification and regulation of cell shape. *Genes Dev.* **19**, 1692–704 (2005).

48. Beilharz, K. *et al.* Control of cell division in *Streptococcus pneumoniae* by the conserved Ser/Thr protein kinase StkP. *Proc. Natl. Acad. Sci.* **109**, E905–E913 (2012).

49. Beltramini, A. M., Mukhopadhyay, C. D. & Pancholi, V. Modulation of cell wall structure and antimicrobial susceptibility by a *Staphylococcus aureus* eukaryote-like serine/threonine kinase and phosphatase. *Infect. Immun.* **77**, 1406–16 (2009).

50. Débarbouillé, M. *et al.* Characterization of a serine/threonine kinase involved in virulence of *Staphylococcus aureus*. *J. Bacteriol.* **191**, 4070–81 (2009).

51. Donat, S. *et al.* Transcriptome and Functional Analysis of the Eukaryotic-Type Serine/Threonine Kinase PknB in *Staphylococcus aureus*. *J. Bacteriol.* **191**, 4056–4069 (2009).

52. Liebeke, M., Meyer, H., Donat, S., Ohlsen, K. & Lalk, M. A Metabolomic View of *Staphylococcus aureus* and Its Ser/Thr Kinase and Phosphatase Deletion Mutants: Involvement in Cell Wall Biosynthesis.

*Chem. Biol.* **17**, 820–830 (2010).

53.     Mohammadi, T. *et al.* Identification of FtsW as a transporter of lipid-linked cell wall precursors across the membrane. *EMBO J.* **30**, 1425–1432 (2011).

54.     Mohammadi, T. *et al.* Specificity of the transport of lipid II by FtsW in *Escherichia coli*. *J. Biol. Chem.* **289**, 14707–14718 (2014).

55.     Sham, L. T. *et al.* MurJ is the flippase of lipid-linked precursors for peptidoglycan biogenesis. *Science* **345**, 220–222 (2014).

+351 964834011
andreia.f.c.tavares@gmail.com

linkedin.com/in/andreiactavares
orcid.org/0000-0002-8260-0776

# Curriculum Vitae

## Andreia Filipa Campos Tavares

### Professional Summary

- PhD on *Staphylococcus aureus* cell morphology and division at ITQB-NOVA. As part of an international collaboration project, I spent 6 months working in the Micalis unit at INRA (France).
- Scientific Expertise on Bacterial Cell Biology, Molecular Biology, Fluorescence and Super-Resolution Microscopy, Biochemical techniques
- Communication and Data Presentation Skills developed through several oral, poster and written science communications, Science Communication courses, improvisation theatre sessions and organization of scientific events.
- Business and Management Skills developed through Bioentrepreneurship, Project management and Research Skills Development (RSD) courses

### Work Experience

PhD student                                        2014 - 2019

- Instituto de Tecnologia Química e Biológica António Xavier – ITQB NOVA. Laboratory of Bacterial Cell Biology. International collaboration with the Micalis unit at INRA (France).
- Title of the thesis: Determination of cell shape in *Staphylococcus aureus*
- Science communication and Bioentrepreneurship units

Graduate Research Fellow                          2013 –2014

- Instituto de Tecnologia Química e Biológica António Xavier – ITQB NOVA. Laboratory of Bacterial Cell Biology

+351 964834011                          linkedin.com/in/andreiactavares
andreia.f.c.tavares@gmail.com           orcid.org/0000-0002-8260-0776

Undergraduate Research Integration Fellow            2009 – 2010

- Instituto de Tecnologia Química e Biológica António Xavier – ITQB NOVA. Laboratory of Bacterial Cell Biology. Final Classification: 19 (in 20)

## EDUCATION

Postgraduation in Clinical Trials Monitoring                    2019
- Escola de Ciências e Tecnologias da Saúde – Lusófona University
- Training in:
    - Clinical Trials Methodologies
    - Good Clinical Practice
    - Monitoring Techniques
    - Risc management in Clinical Research
    - Data Analysis in Clinical Trials

University Extension Course - Scientific Research Training C  2013 – 2014
- Instituto de Tecnologia Química e Biológica António Xavier – ITQB NOVA.
- Laboratory of Bacterial Cell Biology. Final Classification: 19 (in 20).

MSc on Cell Biology and Biotechnology              2010 – 2012
- Faculdade de Ciências - University of Lisbon
- Dissertation developed at Instituto Superior Técnico on the Biological relevance of mucoid *vs*. nonmucoid morphotype variation by *Burkholderia cepacia* complex. Final Classification: 18.4 (in 20)

BSc on Cell and Molecular Biology                  2007 – 2010
- Faculdade de Ciências e Tecnologia - New University of Lisbon
- Final Classification: 17.4 (in 20)
- Two Merit Scholarships for the 2008-2009 and 2009-2010 academic years.

+351 964834011

andreia.f.c.tavares@gmail.com

linkedin.com/in/andreiactavares

orcid.org/0000-0002-8260-0776

**PUBLICATIONS**

Papers

- Reichmann NT*, **Tavares AC***, Saraiva BM, Jousselin A, Reed P, Pereira AR, Monteiro JM, Sobral RG, VanNieuwenhze MS, Fernandes F, Pinho MG. 2019. SEDS-bPBP pairs direct lateral and septal peptidoglycan synthesis in *Staphylococcus aureus*. Nat Microbiol. doi: 10.1038/s41564-019-0437-2.
- Monteiro JM*, Pereira AR*, Reichmann NT, Saraiva B, Fernandes PB, Veiga H, **Tavares AC**, Santos M, Ferreira MT, Macário V, VanNieuwenhze MS, Pinho MG. 2017. Recruitment of peptidoglycan synthesis to midcell drives cell envelope constriction independent of FtsZ treadmilling. Nature. 554(7693):528-532. doi: 10.1038/nature25506
- Silva IN, Ramires MJ, Azevedo LA, Guerreiro AR, **Tavares AC**, Becker JD, Moreira LM. 2017. Regulator LdhR and d-Lactate dehydrogenase LdhA of *Burkholderia multivorans* play roles in carbon overflow and in planktonic cellular aggregate formation. Appl Environ Microbiol. 83(19). pii: e01343-17. doi: 10.1128/AEM.01343-17.
- Pereira AR, Hsin J, Król E, **Tavares AC**, Flores P, Hoiczyk E, Ng N, Dajkovic A, Brun YV, VanNieuwenhze MS, Roemer T, Carballido-Lopez R, Scheffers D, Huang KC, Pinho MG. 2016. FtsZ-dependent elongation of a coccoid bacterium. mBio 7(5):e00908-16. doi:10.1128/mBio.00908-16.
- **Tavares AC**, Fernandes PB, Carballido-López R, Pinho MG. 2015. MreC and MreD Proteins Are Not Required for Growth of *Staphylococcus aureus*. PLoS ONE 10(10): e0140523. doi:10.1371/journal.pone.0140523.
- Monteiro JM*, Fernandes PB*, Vaz F, Pereira AR, **Tavares AC**, Ferreira MT, Pereira PM, Veiga H, Kuru E, VanNieuwenhze MS, Brun YV, Filipe SR, Pinho MG. 2015. Cell shape dynamics during the staphylococcal cell cycle. Nat Commun 6:8055. doi: 10.1038/ncomms9055
- Silva IN, **Tavares AC**, Ferreira AS, Moreira LM. 2013. Stress conditions triggering mucoid morphotype variation in *Burkholderia* species and effect on virulence in *Galleria mellonella* and biofilm formation in vitro. PLoS One. 8(12):e82522. doi: 10.1371/journal.pone.0082522.

* These authors contributed equally

+351 964834011                    linkedin.com/in/andreiactavares
andreia.f.c.tavares@gmail.com     orcid.org/0000-0002-8260-0776

Posters

- **Tavares AC***, Reichmann NT*, Saraiva BM, Jousselin A, Reed P, Pereira AR, Montero JM, VanNieuwenhze MS, Fernandes F, Pinho, MG. 2019. (July 8-10). Directed peptidoglycan synthesis maintains the cell shape of *Staphylococcus aureus*. Poster presented at Ciência'19 meeting, Lisboa, Portugal.
- **Tavares AC**, Ferreira MJ, Carballido-López R, Pinho MG. 2017 (Sep 24-27). Identification of MreC and MreD interaction partners in *Staphylococcus aureus*. Poster presented at the 5th Great Wall Symposium, Albufeira, Portugal.
- **Tavares AC**, Fernandes PB, Carballido-López R, Pinho MG. 2015 (Sep 21-23). MreC and MreD proteins are not required for growth of *Staphylococcus aureus*. Poster presented at the 4th Great Wall Symposium, Florence, Italy.
- **Tavares AC**, Silva IN, Becker JD, Ferreira AS, Moreira LM. 2012 (Nov 23-24). Mucoid morphotype variation of *Burkholderia* isolates under stress conditions: Effects on gene expression, phenotypic properties and virulence. Poster presented in the IV Symposium on Bioengineering, Faculty of Engineering, University of Porto, Porto, Portugal.
- Silva IN, **Tavares AF**, Ferreira AS, Moreira LM. 2012 (Sep 04-09). Mucoid morphotype variation of *Burkholderia multivorans*: adaptation to cystic fibrosis lung environment. *In Genomics and Proteomics*. Poster presented at 22nd IUBMB - 37th FEBS congress – From single molecules to systems biology, Sevilla, Spain.
- **Tavares AC**, Silva IN, Becker JD, Ferreira AS, Moreira LM. 2012 (May 28-30). Effect of mucoid morphotype variation of *Burkholderia* isolates on gene expression, resistance to antimicrobials and virulence. *In Genetic disorders and health*. Poster presented at XXXVII Portuguese Genetics Conference, Lisbon, Portugal.
- Silva IN, Ferreira AS, **Tavares AC**, Moreira LM. 2011 (Dec 01-03). Mucoid morphotype variation of *Burkholderia multivorans* during chronic persistence in the airways of cystic fibrosis patients. *In Cellular Microbiology and Pathogenesis*. Poster presented at Microbiotec'11 - portuguese society for microbiology, Braga, Portugal.

* These authors contributed equally

+351 964834011

andreia.f.c.tavares@gmail.com

linkedin.com/in/andreiactavares

orcid.org/0000-0002-8260-0776

## COURSES

- Project management - NOVA Doctoral School, Lisbon. 6th edition. October 13-15, 2016
- Bioentrepreneurship unit by NOVA Buisness School, integrated in MolBioS doctoral program. Nova SBE, Lisbon. October 26-November 6, 2015.
- Science Communication unit, integrated on MolBioS PhD Program. June 15-19 2015
- Research Skills Development (RSD) – NOVA Doctoral School. Convento da Arrábida. 8th edition. April 25-28, 2014
- IMPROV: improvisation theatre sessions at Science Gulbenkian Institute (IGC).

## SCIENCE OUTREACH ACTIVITIES

- April 2017. ITQB-NOVA representative at POCH (Educational program integrated on Portugal 2020 project) stand at Futuralia (biggest national exhibition on education offers and vocation training), >79000 visitors. http://futuralia.fil.pt/en/
- November 2016. Organization of the 7th ITQB-NOVA PhD Students' Meeting. http://www.itqb.unl.pt/education/7th-itqb-phd-students-meeting
- April 2016. Organization of Gut Thinking – How your Microbes Influence your Life. AR events from Champalimaud foundation. http://events.ar.fchampalimaud.org/gut-thinking/
- 2011, 2015. Volunteer in the organization of ITQB NOVA open day (scientific day for the public at Instituto de Tecnologia Química e Biológica António Xavier– ITQB NOVA, ~1000-2000 people)

## LANGUAGES

- Portuguese. Native or bilingual proficiency.
- English. Full professional proficiency

+351 964834011

andreia.f.c.tavares@gmail.com

linkedin.com/in/andreiactavares

orcid.org/0000-0002-8260-0776

# CURRICULUM VITAE
Andreia Filipa Campos Tavares

## PROFESSIONAL SUMMARY

- PhD on *Staphylococcus aureus* cell morphology and division at ITQB-NOVA. As part of an international collaboration project, I spent 6 months working in the Micalis unit at INRA (France).
- Scientific Expertise on Bacterial Cell Biology, Molecular Biology, Fluorescence and Super-Resolution Microscopy, Biochemical techniques
- Communication and Data Presentation Skills developed through several oral, poster and written science communications, Science Communication courses, improvisation theatre sessions and organization of scientific events.
- Business and Management Skills developed through Bioentrepreneurship, Project management and Research Skills Development (RSD) courses

## WORK EXPERIENCE

PhD                                                                                          2014 - 2019
- Instituto de Tecnologia Química e Biológica António Xavier – ITQB NOVA. Laboratory of Bacterial Cell Biology. International collaboration with the Micalis unit at INRA (France).
- Title of the thesis: Determination of cell shape in *Staphylococcus aureus*
- Science communication and Bioentrepreneurship units

Graduate Research Fellow                                                                  2013 –2014
- Instituto de Tecnologia Química e Biológica António Xavier – ITQB NOVA. Laboratory of Bacterial Cell Biology

Undergraduate Research Integration Fellow                                           2009 – 2010
- Instituto de Tecnologia Química e Biológica António Xavier – ITQB NOVA. Laboratory of Bacterial Cell Biology. Final Classification: 19 (in 20)

## EDUCATION

Postgraduation in Clinical Trials Monitoring                                        2019 - Presente
- Escola de Ciências e Tecnologias da Saúde – Lusófona University
- Training in:
  - Clinical Trials Methodologies
  - Good Clinical Practice
  - Monitoring Techniques
  - Risc management in Clinical Research
  - Data Analysis in Clinical Trials

+351 964834011
andreia.f.c.tavares@gmail.com

linkedin.com/in/andreiactavares
orcid.org/0000-0002-8260-0776

University Extension Course - Scientific Research Training C          2013 – 2014
- Instituto de Tecnologia Química e Biológica António Xavier – ITQB NOVA.
- Laboratory of Bacterial Cell Biology. Final Classification: 19 (in 20).

MSc on Cell Biology and Biotechnology          2010 – 2012
- Faculdade de Ciências - University of Lisbon
- Dissertation developed at Instituto Superior Técnico on the Biological relevance of mucoid *vs*. nonmucoid morphotype variation by *Burkholderia cepacia* complex. Final Classification: 18.4 (in 20)

BSc on Cell and Molecular Biology          2007 – 2010
- Faculdade de Ciências e Tecnologia - New University of Lisbon
- Final Classification: 17.4 (in 20)
- Two Merit Scholarships for the 2008-2009 and 2009-2010 academic years.

**PUBLICATIONS**

Papers

- Reichmann NT*, **Tavares AC***, Saraiva BM, Jousselin A, Reed P, Pereira AR, Monteiro JM, Sobral RG, VanNieuwenhze MS, Fernandes F, Pinho MG. 2019. SEDS-bPBP pairs direct lateral and septal peptidoglycan synthesis in *Staphylococcus aureus*. Nat Microbiol. doi: 10.1038/s41564-019-0437-2.
- Monteiro JM*, Pereira AR*, Reichmann NT, Saraiva B, Fernandes PB, Veiga H, **Tavares AC**, Santos M, Ferreira MT, Macário V, VanNieuwenhze MS, Pinho MG. 2017. Recruitment of peptidoglycan synthesis to midcell drives cell envelope constriction independent of FtsZ treadmilling. Nature. 554(7693):528-532. doi: 10.1038/nature25506
- Silva IN, Ramires MJ, Azevedo LA, Guerreiro AR, **Tavares AC**, Becker JD, Moreira LM. 2017. Regulator LdhR and d-Lactate dehydrogenase LdhA of *Burkholderia multivorans* play roles in carbon overflow and in planktonic cellular aggregate formation. Appl Environ Microbiol. 83(19). pii: e01343-17. doi: 10.1128/AEM.01343-17.
- Pereira AR, Hsin J, Król E, **Tavares AC**, Flores P, Hoiczyk E, Ng N, Dajkovic A, Brun YV, VanNieuwenhze MS, Roemer T, Carballido-Lopez R, Scheffers D, Huang KC, Pinho MG. 2016. FtsZ-dependent elongation of a coccoid bacterium. mBio 7(5):e00908-16. doi:10.1128/mBio.00908-16.
- **Tavares AC**, Fernandes PB, Carballido-López R, Pinho MG. 2015. MreC and MreD Proteins Are Not Required for Growth of *Staphylococcus aureus*. PLoS ONE 10(10): e0140523. doi:10.1371/journal.pone.0140523.

- Monteiro JM*, Fernandes PB*, Vaz F, Pereira AR, **Tavares AC**, Ferreira MT, Pereira PM, Veiga H, Kuru E, VanNieuwenhze MS, Brun YV, Filipe SR, Pinho MG. 2015. Cell shape dynamics during the staphylococcal cell cycle. Nat Commun 6:8055. doi: 10.1038/ncomms9055
- Silva IN, **Tavares AC**, Ferreira AS, Moreira LM. 2013. Stress conditions triggering mucoid morphotype variation in *Burkholderia* species and effect on virulence in *Galleria mellonella* and biofilm formation in vitro. PLoS One. 8(12):e82522. doi: 10.1371/journal.pone.0082522.

* These authors contributed equally

+351 964834011
andreia.f.c.tavares@gmail.com

linkedin.com/in/andreiactavares
orcid.org/0000-0002-8260-0776

Posters

- **Tavares AC**\*, Reichmann NT\*, Saraiva BM, Jousselin A, Reed P, Pereira AR, Montero JM, VanNieuwenhze MS, Fernandes F, Pinho, MG. 2019. (July 8-10). Directed peptidoglycan synthesis maintains the cell shape of *Staphylococcus aureus*. Poster presented at Ciência'19 meeting, Lisboa, Portugal.
- **Tavares AC**, Ferreira MJ, Carballido-López R, Pinho MG. 2017 (Sep 24-27). Identification of MreC and MreD interaction partners in *Staphylococcus aureus*. Poster presented at the 5th Great Wall Symposium, Albufeira, Portugal.
- **Tavares AC**, Fernandes PB, Carballido-López R, Pinho MG. 2015 (Sep 21-23). MreC and MreD proteins are not required for growth of *Staphylococcus aureus*. Poster presented at the 4th Great Wall Symposium, Florence, Italy.
- **Tavares AC**, Silva IN, Becker JD, Ferreira AS, Moreira LM. 2012 (Nov 23-24). Mucoid morphotype variation of *Burkholderia* isolates under stress conditions: Effects on gene expression, phenotypic properties and virulence. Poster presented in the IV Symposium on Bioengineering, Faculty of Engineering, University of Porto, Porto, Portugal.
- Silva IN, **Tavares AF**, Ferreira AS, Moreira LM. 2012 (Sep 04-09). Mucoid morphotype variation of *Burkholderia multivorans*: adaptation to cystic fibrosis lung environment. *In Genomics and Proteomics*. Poster presented at 22nd IUBMB - 37th FEBS congress – From single molecules to systems biology, Sevilla, Spain.
- **Tavares AC**, Silva IN, Becker JD, Ferreira AS, Moreira LM. 2012 (May 28-30). Effect of mucoid morphotype variation of *Burkholderia* isolates on gene expression, resistance to antimicrobials and virulence. *In Genetic disorders and health*. Poster presented at XXXVII Portuguese Genetics Conference, Lisbon, Portugal.
- Silva IN, Ferreira AS, **Tavares AC**, Moreira LM. 2011 (Dec 01-03). Mucoid morphotype variation of *Burkholderia multivorans* during chronic persistence in the airways of cystic fibrosis patients. *In Cellular Microbiology and Pathogenesis*. Poster presented at Microbiotec'11 - portuguese society for microbiology, Braga, Portugal.

\* These authors contributed equally

**COURSES**

- Project management - NOVA Doctoral School, Lisbon. 6th edition. October 13-15, 2016
- Bioentrepreneurship unit by NOVA Buisness School, integrated in MolBioS doctoral program. Nova SBE, Lisbon. October 26-November 6, 2015.
- Science Communication unit, integrated on MolBioS PhD Program. June 15-19 2015
- Research Skills Development (RSD) – NOVA Doctoral School. Convento da Arrábida. 8th edition. April 25-28, 2014
- IMPROV: improvisation theatre sessions at Science Gulbenkian Institute (IGC).

+351 964834011

andreia.f.c.tavares@gmail.com

linkedin.com/in/andreiactavares

orcid.org/0000-0002-8260-0776

### SCIENCE OUTREACH ACTIVITIES

- April 2017. ITQB-NOVA representative at POCH (Educational program integrated on Portugal 2020 project) stand at Futuralia (biggest national exhibition on education offers and vocation training), >79000 visitors. http://futuralia.fil.pt/en/
- November 2016. Organization of the 7th ITQB-NOVA PhD Students' Meeting. http://www.itqb.unl.pt/education/7th-itqb-phd-students-meeting
- April 2016. Organization of Gut Thinking – How your Microbes Influence your Life. AR events from Champalimaud foundation. http://events.ar.fchampalimaud.org/gut-thinking/
- 2011, 2015. Volunteer in the organization of ITQB NOVA open day (scientific day for the public at Instituto de Tecnologia Química e Biológica António Xavier– ITQB NOVA, ~1000-2000 people)

### LANGUAGES

- Portuguese. Native or bilingual proficiency.
- English. Full professional proficiency